LUND UNIVERSITY

Modeling and Performance Analysis of Alternative Heat Exchangers for Heavy Vehicles

Lin, Wamei

2014

[Link to publication](#)

Department of Energy Sciences
Division of Heat Transfer

Modeling and Performance Analysis of Alternative Heat Exchangers for Heavy Vehicles

Wamei Lin

AKADEMISK AVHANDLING/DOCTORAL DISSERTATION

Organization LUND UNIVERSITY	Document name DOCTORAL DISSERTATION
Division of Heat Transfer Department of Energy Sciences PO Box 118, SE-221 00 LUND, Sweden	Date of issue June 10, 2014
	ISRN LUTMDN/TMHP-14/1103-SE
Author(s) Wamei Lin	Sponsoring organization Swedish Energy Agency

Title and subtitle
Modeling and Performance Analysis of Alternative Heat Exchangers for Heavy Vehicles

Abstract

Cross flow heat exchangers made from aluminum are common as radiators in vehicles. However, due to the increasing power requirement and the limited available space in vehicles, it is extremely difficult to increase the size of heat exchangers (HEXs) placed in the front of vehicles. Placing the heat exchanger on the roof or at the underbody of vehicles might offer opportunity to increase the size of the heat exchangers. A new configuration of heat exchangers has to be developed to accommodate the position change. In this study, a countercurrent heat exchanger is proposed for the position on the roof of the vehicle compartment. Furthermore, a new material, graphite foam having high thermal conductivity (1700 W/(m·K)) and low density (0.2 to 0.6 g/cm^3), is introduced as a potential material for those heat exchangers in vehicles.

In order to find an appropriate configuration of fins with high thermal performance and low pressure loss on the air side for a countercurrent flow HEX, the main-flow enhancement and the secondary-flow enhancement methods are employed to analyze different configurations of fins. The main-flow enhancement cases included are (1) aluminum: louver-, wavy-, and pin fin; (2) graphite foam: corrugated-, wavy corrugated-, pin-finned-, and baffle fin. The secondary-flow enhancement cases included are graphite foam: rectangular fin, rectangular fin with one-side dimples, and rectangular fin with two-side dimples. The computational fluid dynamics (CFD) approach is applied for the comparative studies by using the ANSYS FLUENT software. Moreover, the simulation results are verified by experimental results from literature.

After comparing the performance among different configurations of fin, it is found that the aluminum louver fin shows better performance than the wavy fin and pin fin. Also the graphite foam wavy corrugated fin presents higher heat transfer performance and lower pressure drop than the corrugated-, pin-finned-, and baffle fin. On the other hand, the graphite foam rectangular fin with two-side dimples exhibits better performance than the fin with one-side dimples.

The cross flow HEX (made from aluminum) is compared with countercurrent flow HEXs (made from aluminum or graphite foam), in terms of the coefficient of performance (COP), power density (PD), compactness factor (CF), and energy saving efficiency. Due to the high power density and high compactness factor in the countercurrent flow HEXs, the overall size and weight of the countercurrent flow HEXs are much lower than those of the cross flow HEX. Moreover, the graphite foam wavy corrugated fin provides higher power density and higher compactness factor than an aluminum louver fin because of the high thermal conductivity and low density of the graphite foam. Furthermore, a graphite foam fin with two-side dimples exhibits higher coefficient of performance than an aluminum louver fin, and it becomes very efficient in energy saving. However, due to the high pressure loss in the graphite foam wavy corrugated fin, the air pumping power for the countercurrent flow graphite foam wavy corrugated fin HEX is much higher than that of the cross flow aluminum louver fin HEX.

Based on the presented studies, useful recommendations are highlighted to promote the development of countercurrent flow HEXs and the graphite foam HEXs in vehicles.

Key words
Countercurrent flow, Graphite foam, Heat exchanger, Thermal performance, Computational fluid dynamics

Classification system and/or index terms (if any)

Supplementary bibliographical information	Language English
ISSN and key title 0282-1990	ISBN 978-91-7473-919-0 (print) 978-91-7473-920-6 (pdf)
Recipient´s notes	Number of pages	Price
	Security classification	

Distribution by (name and address)

I, the undersigned, being the copyright owner of the abstract of the above-mentioned dissertation, hereby grant to all reference sources permission to publish and disseminate the abstract of the above-mentioned dissertation.

Signature _____*Wamei Lin*_____   Date ___May 05, 2014___

Modeling and Performance Analysis of Alternative Heat Exchangers for Heavy Vehicles

Doctoral Dissertation

Wamei Lin

Division of Heat Transfer, Department of Energy Sciences
Faculty of Engineering LTH, Lund University
22100 Lund, Sweden

LUND UNIVERSITY

Popular Science

Low fuel consumption, and reduced exhaust emissions, as well as improved performance and durability become much more important than before for the vehicle industry. These requirements lead to a number of additional equipment installed in the vehicles. All these efforts increase the operating temperature in the engine compartment and reduce the available free space in the vehicle. In order to keep the engine working at its optimal condition, a huge amount of heat has to be removed from the engine to the surrounding air. In modern heavy vehicles, this heat is so huge that a conventional heat exchanger (HEX) cannot handle it easily. In addition, more and more electric powertrains are introduced to heavy vehicles. Because of the increased demand in cooling power, a larger heat exchanger size with a huge cooling surface area is required for the vehicle cooling system. However, the space in such vehicles is limited. It is impossible to increase the size of the conventional HEX to dissipate the required amount of heat from the vehicle. All these factors imply a need for a revolution of the HEX design in vehicles.

Based on literature review, there are two ideas available for developing an alternative heat exchanger for heavy vehicles:
1) Changing the position of heat exchangers: Moving the HEX from the front of the vehicles to the roof of the driver compartment, which might increase the possibility to increase the size of the HEX. Based on the air flowing direction and the engine coolant direction, a countercurrent flow HEX is introduced at the roof position instead of a cross flow HEX.
2) Introducing new materials: Using graphite foam as a thermal material for HEXs in vehicles. Nowadays aluminum HEXs are very common in the vehicle industry. Due to the increasing cooling power and the space limitation in vehicles, a highly compact HEX is required. Graphite foam has even higher thermal conductivity, large specific surface area, and low density. These characteristics imply that graphite foam is a potentially good thermal material for HEXs (instead of the conventional aluminum HEX). However, due to its porous structure, the flow resistance of graphite foam is very high.

In order to find an appropriate fin configuration with good performance in the HEX, a computational method is applied to simulate the performance of the HEX with different fin configurations. The numerical model is verified by experimental results from literature.

The analysis of the results shows:

1) The overall size and weight of a countercurrent flow HEX can be reduced compared to the cross flow HEX because of the high power density and high compactness factor achieved by the countercurrent flow HEX.
2) Because of the high thermal conductivity and low density of the graphite foam, the graphite foam wavy corrugated fin provides higher power density and higher compactness factor than an aluminum louver fin. A graphite foam fin with two-side dimples exhibits higher coefficient of performance (COP) than an aluminum louver fin, and it becomes very efficient in energy saving. Thus, the graphite foam has a very high potential as an alternative material for heat exchanger applications.

The countercurrent flow HEXs made from graphite foam can be designed to be much lighter and smaller than the convectional cross flow aluminum HEXs. A light and compact HEX is not only good for the thermal management of the vehicle, but also it reduces the weight of the vehicle which has an effect on the fuel consumption and overall cost.

Abstract

Cross flow heat exchangers made from aluminum are common as radiators in vehicles. However, due to the increasing power requirement and the limited available space in vehicles, it is extremely difficult to increase the size of heat exchangers (HEXs) placed in the front of vehicles. Placing the heat exchanger on the roof or at the underbody of vehicles might offer opportunity to increase the size of the heat exchangers. A new configuration of heat exchangers has to be developed to accommodate the position change. In this study, a countercurrent heat exchanger is proposed for the position on the roof of the vehicle compartment. Furthermore, a new material, graphite foam having high thermal conductivity (1700 W/(m·K)) and low density (0.2 to 0.6 g/cm^3), is introduced as a potential material for those heat exchangers in vehicles.

In order to find an appropriate configuration of fins with high thermal performance and low pressure loss on the air side for a countercurrent flow HEX, the main-flow enhancement and the secondary-flow enhancement methods are employed to analyze different configurations of fins. The main-flow enhancement cases included are (1) aluminum: louver-, wavy-, and pin fin; (2) graphite foam: corrugated-, wavy corrugated-, pin-finned-, and baffle fin. The secondary-flow enhancement cases included are graphite foam: rectangular fin, rectangular fin with one-side dimples, and rectangular fin with two-side dimples. The computational fluid dynamics (CFD) approach is applied for the comparative studies by using the ANSYS FLUENT software. Moreover, the simulation results are verified by experimental results from literature.

After comparing the performance among different configurations of fin, it is found that the aluminum louver fin shows better performance than the wavy fin and pin fin. Also the graphite foam wavy corrugated fin presents higher heat transfer performance and lower pressure drop than the corrugated-, pin-finned-, and baffle fin. On the other hand, the graphite foam rectangular fin with two-side dimples exhibits better performance than the fin with one-side dimples.

The cross flow HEX (made from aluminum) is compared with countercurrent flow HEXs (made from aluminum or graphite foam), in terms of the coefficient of performance (COP), power density (PD), compactness factor (CF), and energy saving efficiency. Due to the high power density and high compactness factor in the countercurrent flow HEXs, the overall size and weight of the countercurrent flow HEXs are much lower than those of the cross flow HEX. Moreover, the graphite foam wavy corrugated fin provides higher power density and higher compactness factor than an aluminum louver fin because of the high thermal conductivity and low density of the graphite foam. Furthermore, a graphite foam fin with two-side dimples exhibits higher coefficient of performance than an aluminum louver fin, and it becomes very efficient in energy saving. However, due to the high pressure loss in the graphite foam wavy

corrugated fin, the air pumping power for the countercurrent flow graphite foam wavy corrugated fin HEX is much higher than that of the cross flow aluminum louver fin HEX.

Based on the presented studies, useful recommendations are highlighted to promote the development of countercurrent flow HEXs and the graphite foam HEXs in vehicles.

Acknowledgements

I would like to express my great appreciation to my supervisor Professor Bengt Sundén for giving me this wonderful opportunity to pursue my postgraduate study in Lund University. I also thank him for his helpful support, guidance, encouragement and kindness over the past five years. Meanwhile, I would like to thank Professor Jinliang Yuan and Professor Gongnan Xie (Northwestern Polytechnical University, Xi'an, China), for their fruitful supports and discussion during my PhD work.

Also I thank Professor Lennart Löfdahl (Chalmers University of Technology) and Erik Dahl (Volvo Truck) for suggestions about my PhD studies. Thanks to Lisa Henriksson for sharing her knowledge of fluid dynamics of vehicles.

In addition, I would like to give my many thanks to my current colleagues in Department of Energy Sciences: Dr. Lei Wang, Professor Christoffer Norberg, Dr. Martin Andersson, Dr. Teresa Hankala-Janiec, Dr. Zan Wu, Dr. Toru Yamada, Dr. Helgi Fridriksson, Dr. Zahra Ghorbani-Tari, Chenglong Wang, Jiatang Wang, Ali Alhelfi, Mayken Espinoza Andaluz, Henrik Hofgren, Erik Johansson, Maria Navasa, Gengzhao Zheng and other colleguges and friends (Mengqin Shen, Professor Xuesong Bai, Dr. Rixin Yu, Cheng Gong, and others). Having had their help and support, my Ph.D. study period was full of colors and happiness. Also I would like to thank our helpful and nice administrators: Catarina Lindén, Maj-Lis Roos, and Elna Andersson.

Finally, I would like to thank my parents for teaching and guiding me patiently and supporting my choices and study for more than 30 years without any words of trouble. Thanks to my husband (Sebastian) supporting me completely through my PhD study. Last but not least, thanks to my lovely son (Derek) shining my life.

List of papers

Publications included in this thesis:

1. **Wamei Lin**, Bengt Sundén, 2010, "Vehicle Cooling Systems for Reducing Fuel Consumption and Carbon Dioxide: Literature Survey", SAE Technical Paper 2010-01-0157.

2. **Wamei Lin**, Jinliang Yuan, Bengt Sundén, 2011, "Review on Graphite Foam as Thermal Material for Heat Exchangers", World Renewable Energy Congress 2011, May 8-11, 2011, Linköping, Sweden. (Paper No. 0263 EEE)

3. **Wamei Lin**, Bengt Sundén, Jinliang Yuan, 2013, "A Performance Analysis of Porous Graphite Foam Heat Exchangers in Vehicles", Applied Thermal Engineering, **50**, pp. 1201-1210.

4. **Wamei Lin**, Jinliang Yuan, Bengt Sundén, 2012, "Performance Analysis of a Countercurrent Flow Heat Exchanger Placed on the Truck Compartment Roof", ASME Journal of Thermal Science and Engineering Applications, **4**, pp. 041004-1 - 041004-7.

5. **Wamei Lin**, Jinliang Yuan, Bengt Sundén, 2014, "Performance Analysis of Aluminum and Graphite Foam Heat Exchangers under Countercurrent Arrangement", Heat Transfer Engineering, **35** (6-8), pp. 730-737.

6. **Wamei Lin**, Gongnan Xie, Bengt Sundén, Qiuwang Wang, 2014, "Flow and Thermal Performance of Graphite Foam Dimpled Fin Heat Exchangers", to appear in Proceedings of the 15th International Heat Transfer Conference, August 10-15, 2014, Kyoto, Japan. (Paper No. IHTC15-8536)

7. **Wamei Lin**, Gongnan Xie, Jinliang Yuan, Bengt Sundén, "Comparison and Analysis of Heat Transfer in Aluminum Foam using Local Thermal Equilibrium or Non-equilibrium Model", recommended for publication in Heat Transfer Engineering.

Publications not included in this thesis:

1. **Wamei Lin**, Bengt Sundén, 2011, "Graphite Foam Heat Exchanger for Vehicles", Vehicle Thermal Management Systems Conference & Exhibition 2011 (VTMS 10), May 15-19, 2011, Heritage Motor Centre, Gaydon, Warwickshire, UK.

2. **Wamei Lin**, Bengt Sundén, 2010, "A Review of Cooling Systems in Electric/Hybrid Vehicles", ASME 2010 International Mechanical Engineering Congress & Exposition (ICMEC 2010), November 12-18, 2010, Vancouver, British Columbia, Canada.

3. **Wamei Lin**, Jinliang Yuan, Bengt Sundén, 2010, "Waste Heat Recovery System for Fuel Cell System", International Green Energy Conference (IGEC 2010), June 1-3, 2010, Waterloo, Ontario Canada.

4. **Wamei Lin**, Jinliang Yuan, and Bengt Sundén, 2011, "Performance Analysis and Comparison between Aluminum and Graphite Foam Heat Exchangers under Countercurrent Flow Conditions", 2011 International Workshop on Heat Transfer Advances for Energy Conservation and Pollution Control (IWHT2011-101), October 17-20, 2011, Xi'an, China.

5. **Wamei Lin**, Jinliang Yuan, and Bengt Sundén, 2011, "Performance Analysis of a Countercurrent Flow Heat Exchanger Placed on the Truck Compartment Roof", Proceeding of the ASME 2011 International Mechanical Engineering Congress & Exposition (IMECE2011-62520), November 11-17, 2011, Denver, Colorado, USA.

6. **Wamei Lin**, Gongnan Xie, Jinliang Yuan, Bengt Sundén, 2013, "Comparison and Analysis of Heat Transfer in a Porous Aluminum Foam Using Local Thermal Equilibrium and Local Thermal Non-equilibrium Models", 2nd International Workshop on Heat Transfer Advances for Energy Conservation and Pollution Control, October 18-21, 2013, Xi'an, China.

Contents

Nomenclature

Latin Characters

A_c	minimum free-flow area [m^2]
A_o	total heat transfer surface area on the air side [m^2]
a	specific surface area [m^{-1}]
C	wetted perimeter of the minimum free-flow channel [m]
C_F	Forchheimer coefficient [-]
c_p	specific heat [J·kg^{-1}·K^{-1}]
D	dimple print diameter [m]
D_h	hydraulic diameter [m]
d_p	pore diameter [m]
F_1	blending function [-]
f	friction factor [-]
G_k	generation of turbulent kinetic energy [m^2.s^{-2}]
h	heat transfer coefficient [W·m^{-2}·K^{-1}]
k	turbulent kinetic energy [m^2·s^{-2}]
m	mass [kg]
Nu	Nusselt number [-]
P	spacing between every second dimple row [m]
Pe	Péclet number [-]
Pr	Prandtl number [-]
p	pressure [Pa]
Q	total amount of heat dissipated to air [W]
R	radius [m]
Re	Reynolds number [-]
S	spacing of adjacent dimple rows [m]
St	Stanton number [-]
T	temperature [K]
u, v, w	velocity components in x, y and z directions, respectively [m·s^{-1}]
u_i'	fluctuation from the mean velocity u_i [m·s^{-1}]
V	volume [m^3]
Δp	pressure drop [Pa]
ΔT	logarithmic mean temperature difference [K]

Greek symbols

α	permeability [m^2]
γ	area to volume ratio [m^2·m^{-3}]

δ	dimple depth [m]
ε	rate of energy dissipation [-]
λ	thermal conductivity [$W \cdot m^{-1} \cdot K^{-1}$]
μ	dynamic viscosity of fluid [Pa·s]
v	kinematic viscosity of fluid [$m^2 \cdot s^{-1}$]
ρ	density [$kg \cdot m^{-3}$]
τ	tortuosity [-]
φ	porosity [-]
ω	specific dissipation rate [-]

Subscripts

b	bulk
eff	effective
f	fluid
HEX	heat exchanger
in	inlet
i, j	coordinate indices
max	maximum
out	outlet
s	solid
t	turbulence
w	wall
0	referenced

Abbreviations

Al	aluminum
CC	countercurrent flow
CF	compactness factor
CO	carbon monoxide
CO_2	carbon dioxide
COP	coefficient of performance
CR	cross flow
DNS	direct numerical simulation
FVM	finite volume method
GF	graphite foam
H	height
HC	hydrocarbon
HEX	heat exchanger
L	length
LMTD	logarithmic mean temperature difference
LTE	local thermal equilibrium
LTNE	local thermal non-equilibrium
ORNL	Oak Ridge National Laboratory
PCM	phase change material

PD   power density
RNG   renormalization group
SIMPLE   Semi-Implicit Method for Pressure Linked Equations
SST   shear-stress transport
W   width

Chapter 1 Introduction

The present work is based on a research project "Development of new cooling systems for heavy vehicles - for reduced fuel consumption and lower carbon dioxide emission", which has been financially supported partly by the Swedish Energy Agency. There were two major parts in this project. One part was the heat exchanger design for a heavy vehicle, which was implemented by the Lund University. The other part was the flow field analysis around a heavy vehicle, which was carried out by the Chalmers University of Technology.

This work is focused on the heat exchanger design for heavy vehicles, which includes modeling, simulation and analysis of heat transfer and fluid flow in a new (graphite foam) heat exchanger. The developed models are validated by experimental data from the literature. The heat exchanger should be optimized in terms of thermal performance and flow resistance.

1.1 Background

In recent years the number of vehicles being used has constantly increased. For instance, the number of registered trucks and buses in the world increased from 138 million to 274 million between 1990 and 2008. The increased number of vehicles causes more energy/fuel to be consumed and more carbon dioxide (CO_2) to be released to the environment. As shown in Fig. 1.1, around 33 % of the total energy in Europe was consumed by the transportation sector in 2011, and 22 % of CO_2 emission was from the transportation sector in 2006 [1]. A similar situation happened in USA. Around 29.2 % of the total energy in the USA was consumed by the transportation sector (medium/heavy trucks used 18.7 % of energy in transportation) in 2008. Furthermore, 31.2 % of CO_2 emission was from the transportation sector (in which 67.9 % of 31.2 % from medium/heavy trucks and buses) [2]. Furthermore, the oil price has increased all the time. Strong legislation on emissions has been introduced as well. All these factors require innovations achieving high performance in the vehicle industry.

Many technical developments have been introduced to meet the requirements on low fuel consumption and CO_2 emission in vehicles. Concerning the energy distribution (as shown in Fig. 1.2) in the vehicle, only around 35 % of the total fuel energy finally becomes mechanical work which is used for driving the vehicle. However, 30 % of the total energy input is brought away by the coolant of the engine cooling system, and another 35 % of the energy is lost to the exhaust gases. If one could optimize the energy wasted in the coolant or the exhaust gases, the fuel consumption and the CO_2 emission (being also proportional to the fuel consumption) could be reduced correspondingly.
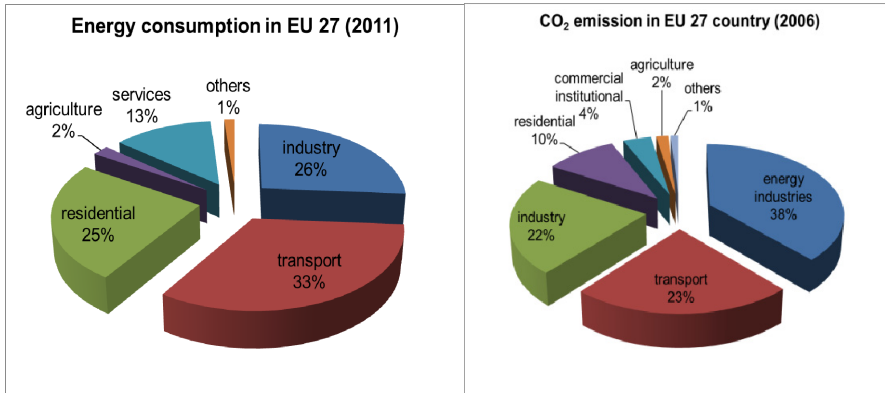
Fig. 1.1 Energy consumption and CO_2 emission in EU 27 countries [1].
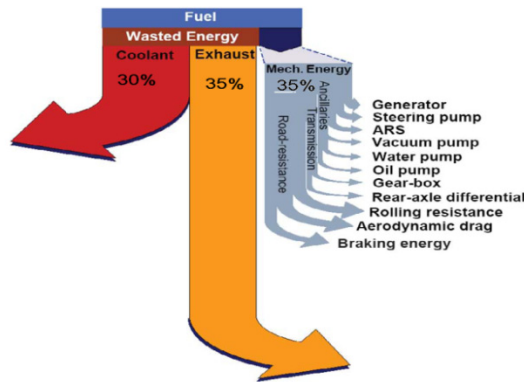
Fig. 1.2 Energy distribution in a vehicle [3].

One third of the supplied energy is lost to the exhaust gases. When the exhaust gases enter into the surroundings directly, they not only waste energy but also cause heat pollution of the environment. Reusing the waste heat of the exhaust gas has a great potential for reducing the fuel consumption of vehicles. There are several methods to reuse the energy of the exhaust gases. These methods include:

(1) The waste heat from exhaust gases is reused to generate electricity by using a thermoelectric device (3 - 8 % fuel saving is offered by a thermoelectric generator [4]);
(2) The waste heat can be used in absorption cooling, which is attractive for the tractor-trailer refrigeration or the bus air conditioning systems;
(3) The waste heat is used to heat the passenger compartment in the winter.

However, with the promotion of electric or hybrid electric vehicles and fuel cell vehicles in transportation, less and less exhaust gases are dissipated from the vehicle. If the engine efficiency is assumed to be the same as a combustion engine, then more heat

has to be brought away by the engine cooling system than before. On the other hand, the working temperature of batteries (electric vehicles) is around 55 ℃ [5], and the operating temperature of Polymer Electrolyte Membrane Fuel Cells (used for fuel cell vehicles) is around 65 ℃ [6]. These working temperatures of electric vehicles or fuel cell vehicles are much lower than those of a combustion engine vehicle (where the engine coolant temperature is around 90 ℃). Therefore the temperature difference between the engine coolant temperature and the ambient temperature is reduced. If the amount of the dissipated heat is constant, then the surface area for heat transfer has to be increased. However, there is space limitation in vehicles. It is difficult to increase the size of the heat exchanger. Thus, the cooling issues become more serious than before.

Furthermore, if the engine cooling system is not efficient, the temperature of the engine components would be higher and the engine cannot work at its optimal operational condition. More fuel would be consumed and the life time of the engine would be reduced due to its high working temperature. Contrarily, a good engine cooling system can reduce the time of the engine start and warm up processes, in which the engine reaches its optimal working temperature [7]. More hydrocarbon (HC) and carbon monoxide (CO) are produced during the starting and warming up period [8]. Thus, an efficient engine cooling system is of significant importance for the fuel consumption and the improved performance of vehicles.

1.2 Aim of the present work

The overall aim of this study is to contribute to a theoretical analysis and modeling method development identifying a new and efficient cooling system to satisfy the increasing cooling power in vehicles. In order to dissipate the huge amount of cooling power, a new compact heat exchanger is developed. There are two main ideas applied for the new compact heat exchanger in the vehicle.

1) Changing the position of heat exchangers: Due to the space limitation in vehicles, it is extremely difficult to increase the size of the heat exchangers (HEXs) to bring away the increased heat from the vehicles. Moving the HEX from the front of the vehicles to the roof of vehicles, might increase the possibility to increase the size of the HEX. When the HEX is placed at the roof, a new configuration of the HEX has to be introduced to accommodate the HEX position change. Based on the air flow direction and the engine coolant direction, a countercurrent flow HEX is introduced at the roof position, to replace a cross flow HEX.

2) Introducing alternative materials: Using graphite foam as a thermal material for HEXs in vehicles. Nowadays aluminum HEXs are very common in the vehicle industry. Due to the increasing cooling power demand and the critical space limitation in vehicles, a highly compact HEX has to be developed. Graphite foam has a high thermal conductivity (solid thermal conductivity is around 1700 W/m·K), large specific surface area (5000-50000 m^2/m^3), and low density (0.2-0.6 g/cm^3). These characteristics imply that graphite foam is a good

potential thermal material for HEXs (instead of the conventional aluminum HEX). However, due to the involved porous structure, the flow resistance is very high in the graphite foam. Finding an appropriate fin design is an important issue for the graphite foam HEX.

1.3 Methodology

A literature survey was carried out to review the performed research and analysis method for the engine cooling system, thermal management of vehicles, and the heat exchanger or radiator in the vehicles. Based on the review work, the study was focused on the design of a countercurrent flow HEX made from aluminum or graphite foam. The main-flow enhancement and the secondary-flow enhancement methods were employed to analyze different configurations of fins. The main-flow enhancement cases being included were (1) aluminum: louver-, wavy-, and pin fin; (2) graphite foam: corrugated-, wavy corrugated-, pin-finned-, and baffle fin. The secondary-flow enhancement cases included for the graphite foam were: rectangular fin, rectangular fin with one-side dimples, and rectangular fin with two-side dimples.

In order to simplify the analysis, only a core of the HEX has been considered in this work. The symmetry or periodic boundary condition has been applied to represent the operating condition of the whole HEX. Furthermore, a finite volume method (FVM) is adopted to convert the governing equations to algebraic equations in the modeling domains. The Semi-Implicit Method for Pressure Linked Equations (SIMPLE) algorithm was used to couple pressure and velocity, as implemented in the commercial software ANSYS FLUENT. The simulation models were validated by the experimental results from the literature.

The thermal performance and the pressure loss are the two important factors in heat exchanger design. In order to develop a high performance countercurrent flow HEXs, the thermal performance and pressure loss are evaluated and compared for different configurations of fins on the air side of a HEX. Moreover, the coefficient of performance (COP), power density (PD), compactness factor (CF), and energy saving efficiency are estimated for the aluminum HEX and the graphite foam HEX, to evaluate the overall performance enhancement of the graphite foam HEX.

1.4 Outline of thesis

After the introduction in Chapter 1, a literature survey is presented in Chapter 2, in which the research work on vehicle cooling systems (including different methods of thermal management in vehicles), thermal performance and flow characteristics of graphite foam are reviewed. Furthermore, the technology development of heat exchangers in the vehicles is included in Chapter 2. The physical model and numerical methods are provided in Chapter 3, in which the governing equations, the corresponding boundary conditions, together with solution methods and meshing technique are

presented. The simulation results are summarized and discussed in Chapter 4. In addition, the model validation is also carried out in Chapter 4. The conclusion and suggestion based on this study are drawn and highlighted in Chapter 5. Finally, an outlook for future work is conceived in Chapter 6.

Chapter 2 Literature Survey

The purpose of this chapter is to review different research and technology development on vehicle cooling systems. In the first part of this chapter, basic information about engine cooling systems is presented. The methods for improving the thermal management of the engine cooling are reviewed in the second part. In the third part, different methods to increase the thermal performance of heat exchangers/radiators are summarized.

2.1 Engine cooling systems

There are two major types of engine cooling systems. One is the air cooling system; another is the liquid cooling system. Nowadays the direct air cooling is only used in older cars or some modern motorcycles. The liquid cooling system plays an important role in the most automobiles. For the air cooling system, the heat is directly released to the air flow through the engine compartment, while, the liquid cooling is an indirect air cooling system. A typical engine cooling system is shown in Fig. 2.1. There are two major heat exchangers:

1) **Engine water jacket cooler (radiator)**: It is important to operate the engine at an appropriate temperature for good performance. If the engine always works at extremely high temperature, it will lead to a bad combustion process, which causes the aging of the lubricant oil and breaking down of engine material. However, if it works at low temperature, the engine will be less efficient and emit more pollution. Thus, there has to be a water jacket around the engine to keep the engine working at an optimal temperature. The engine coolant brings the redundant heat from the engine water jacket to a radiator. Then the radiator dissipates the heat to the ambient air. The coolant will return to the water jacket to continue the next cooling cycle.

2) **Charged air cooler (internal cooler)**: Fresh air firstly passes a turbocharger to increase the pressure and increase the density of the air. In this case, more air can enter into the engine to achieve a sufficient combustion process. However, after the turbocharger, the temperature of the fresh air is increased as well. The high temperature reduces the density of oxygen in the fresh air. The low density of oxygen leads to an inadequate combustion process. Thus, an internal cooler is introduced to cool the fresh air after the turbocharger to increase the density of oxygen. A condenser for the air-conditioning system may also be

placed at the front, but its front area might be less than the radiator area. However, the condenser is not considered in this work.
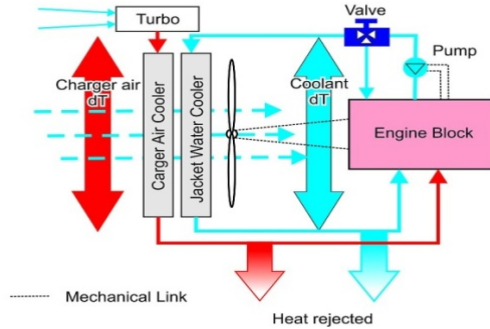
Fig. 2.1 A schematic of an engine cooling system [9].

2.2 Thermal management improvements

A good thermal management by an effective engine cooling system may extend the life time of both the engine and other components in the vehicle. A good thermal management also has an impact on the fuel consumption and CO_2 emissions. Electronic control of the cooling fan or pump, using new materials, or rearranging the position of the heat exchangers may significantly improve the performance of the engine cooling system.

2.2.1 Electronic control of cooling system components

In a combustion engine, the engine not only gives power to speed up the vehicle, but also gives power to the cooling fan and the water pump. Thus, the speed of the cooling fan and the water pump may be directly controlled by the engine speed by a mechanical connection. This method is not efficient for the cooling performance and the fuel consumption in vehicles. If the cooling fan or water pump is controlled by a separate system, then the efficiency of the cooling fan or water pump might be optimized. Staunton et al. [9] analyzed several advanced thermal management system topologies. A thermal management system with an array of small electrical fans was installed instead of a mechanical fan. When the engine cooling system was fully electrified, 17 kW was saved in a micro-hybrid vehicle, and 14.5 kW was saved in a standard diesel vehicle. Cho et al. [10] demonstrated that more than 87 % of the pumping power could be saved by using an electric pump instead of a purely mechanical one. Moreover, the radiator size could also be reduced by more than 27 % as an electric pump was used. Thus, the electrical cooling fan or water pump in the engine cooling system has a great importance in reducing the power consumption in vehicles.

2.2.2 New materials (nanofluid, phase change material)

New materials development and application promote better thermal management system in vehicles. The nanotechnology might be used to improve the thermal conductivity of the engine coolant, because of the high thermal conductivity in "nanofluids" (due to the high thermal conductivity of nanoparticles and the diffusion of the nanoparticles) [11]. Leong et al. [12] showed that 3.8 % of heat transfer enhancement could be achieved with the addition of 2 % copper particles in an engine coolant. Additionally that study showed a reduction of 18.7 % reduction of the air frontal area. However, the pumping power of the coolant increased by 12.13 %. Furthermore, Kulkarni et al. [13] analyzed nanofluids as coolants in a diesel generator. The HEX efficiency was increased with increasing nanoparticle concentration, while the specific heat of the nanofluids was reduced.

Another new material, so-called phase change material (PCM), improves the thermal management especially for electric vehicles [14]. The principle of PCM is that the state of the PCM is changed from solid to liquid after absorbing the heat from batteries (electric vehicles). Due to its high thermal capacity, the PCM will remain at solid-liquid mixture state, and the temperature of the PCM around the batteries will remain constant. On the other hand, the heat stored in the PCM will be transferred to the ambient. Thus, the PCM should be chosen based on the condition that its functional temperature is higher than the surrounding one, but could not be higher than the working temperature of the batteries.
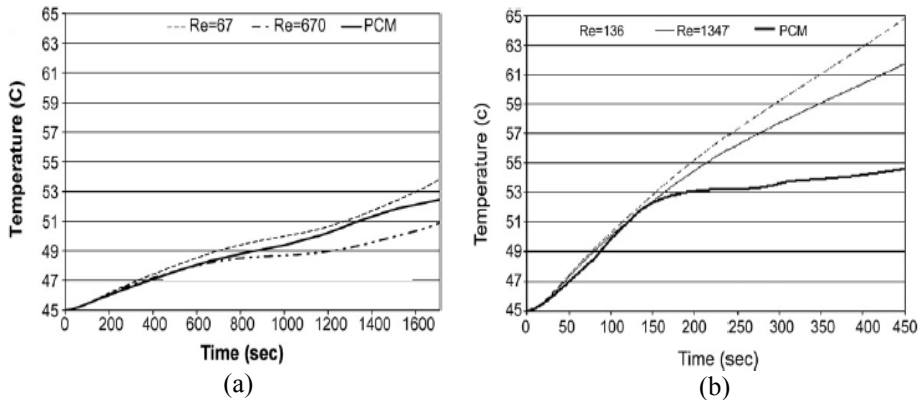
Fig. 2.2 Cooling systems based on volume averaged cell temperature at (a) 3 A; (b) 10 A [15].

Sabbah et al. [15] compared the passive cooling method by using PCM with the active cooling one by forced air in a compact Li-ion battery pack. In the passive cooling case, a micro-composite graphite-PCM matrix was used to surround the cells of the battery. In the active cooling case, air was blown through the gaps between the cells. When the ambient temperature was 45 ℃ and the current of battery was 3 A, both the active (with Re = 67 or 670) and passive cooling could keep the battery under the limiting

temperature 55 ℃, as shown in Fig. 2.2 (a). However, when the operating current of the battery was increased to 10 A, the active cooling system could not keep the battery below 55 ℃ even at higher Reynolds numbers (Re = 136 or 1347). Contrarily, the passive cooling method was able to keep the battery below 55 ℃, as shown in Fig. 2.2 (b). Furthermore, by using the passive cooling method, it was easy to get a uniform temperature distribution in the battery cells. Kizilel et al. [16] found that a failure of an individual cell might spread to the others, as the active cooling system was used. However, by using the PCM, the failure of an individual cell would not trigger the other cells to fail. Contrarily, the temperature of the cells returned to a near-ambient value in the latter case. Thus PCM is a good solution for battery cooling in vehicles.

The PCM is not only useful for cooling the batteries in electric vehicles, but also used in a combustion engine vehicle cooling system. For the diesel engine vehicle, the PCM is a good option to store the excessive heat load occurring sporadically, to reduce the size of radiator. Kim et al. [17] designed a radiator based on the average cooling power instead of the maximum one. At maximum cooling power peaks, a heat accumulator containing PCM absorbs the heat which the small radiator cannot dissipate. In this case, the small size of the radiator and cooling fan led to a reduction of the air drag force as well as the compartment weight/volume. Meanwhile, the volume of the coolant could be reduced by 30 %. Additionally the warm up time of the cold start was reduced as well.

2.2.3 Rearrangement of HEXs position

In modern heavy vehicles, the amount of energy removed from the engine compartment is so large that conventional radiators and oil coolers cannot handle it. Moreover, there is always a limit of available space in the vehicle. It is extremely difficult to further increase the size of the radiator to dissipate huge amounts of heat from the engine compartment. The position of the HEX in vehicles has to be rearranged to get a chance to dissipate more heat.

Recently, the Centro Ricerche Fiat [18] tried to use some parts of the vehicle body panels as HEXs to reduce the radiator size in the light duty vehicles, as shown in Fig. 2.3. Two roll bond HEXs installed on the engine hood and below the engine could dissipate 60 % of heat from the engine in all the test's conditions. On the other hand, in [19] two levels of cooling systems (high temperature system (engine radiator) and low temperature system) were introduced to a car. The intercooler and condenser were cooled by a liquid instead of air. After that, the liquid was cooled by air in the low temperature system. In this case, the intercooler and condenser can be moved from the front of the vehicles to any other suitable places. By introducing two levels of cooling systems, the fuel consumption in the vehicle can be reduced by 4 %.

Furthermore, in [20] the thickness of the cooling package (including a radiator, a condenser, and a sub-radiator) was reduced by placing the sub-radiator on the top (instead of the front) of the condenser. Due to the slim cooling package, the cooling fan power was reduced and the fuel consumption was reduced 3-5 %. Khaled et al. [21] compared the in-rank configuration of the HEXs (the HEXs are positioned differently,

i.e., one is behind the other) and the in-plane configuration HEXs (the different HEXs are parallel in the flow direction). It was found that the in-plane configuration HEXs can increase the overall thermal performance by 4.4 %, and 0.9 % of the pressure losses was eliminated.

Fig. 2.3 Different positions of HEXs in a vehicle [18].
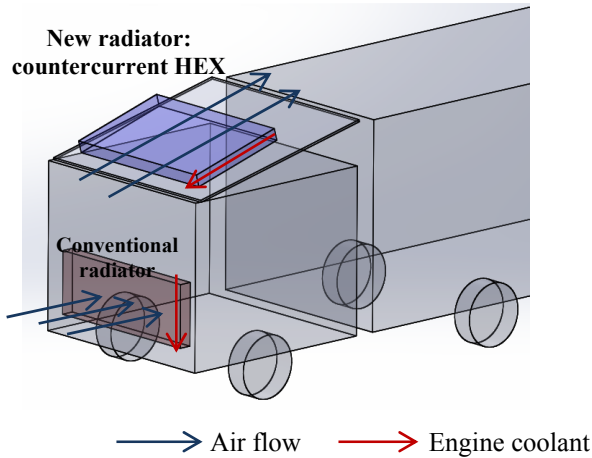
Fig. 2.4 Schematics of the positions of a radiator in trucks.

2.2.4 Idea of rearranging the position of the HEXs

Based on the literature review, it was found that the fuel consumption could be reduced by rearranging the positions of the HEXs in vehicles. The conventional radiator for heavy vehicles is always placed in the front, as shown in Fig. 2.4. If the radiator is placed at the underbody or the roof of the vehicle, it might increase the possibility to increase the radiator size for meeting the critical cooling requirement. A new configuration of the heat exchangers has to be developed to accommodate the position change. As shown in Fig. 2.4, the engine coolant flow and the air flow directions are

opposite, as the radiator is placed on the roof of the driver compartment. This is a typical principle of a countercurrent flow HEX. In the vehicle industry, the engine radiator is mostly a cross flow HEX. However, a countercurrent flow HEX generally has better thermal performance than a cross flow one. Thus, placing a countercurrent flow HEX at the roof of the heavy vehicle driver compartment might be a good option for the engine radiator.

2.3 Heat exchanger/radiator developments

If the coolant was the blood, then the radiator would be the heart of the engine cooling system. This is to illustrate that the radiator plays a significant role in the engine cooling system. There are two methods to increase the thermal performance of HEXs [22]. One is the passive technique, which includes special surface geometries and fluid additives. Another one is the active technique, in which external power is required (such as electric or acoustic fields and surface vibration). However, due to the cost, noise, safety or reliability being concerned, the active techniques are not as popular as the passive ones in the HEX commercial markets. Concerning the passive techniques, following methods are used: coated surfaces, rough surfaces, extended surfaces, displaced inserts, swirl flow, coiled tubes, surface tension, additives for liquids, and additives for gases, etc.

2.3.1 Configurations of heat exchanger/radiator

2.3.1.1 Extended surfaces

The extended surfaces will lead to high compactness (area/volume) in HEXs, which is favorable for the vehicle industries. Based on [22-23], different compact surfaces (as shown in Fig. 2.5) are included in the plate-fin HEXs, as follows:
  a) Rectangular/triangular fins: long uninterrupted flow passages are characterized.
  b) Pin fins: the high heat transfer coefficient is achieved by maintaining thin boundary layers on the pin fins.
  c) Wavy fins: due to the shape of the fins, the flow direction would be changed and the boundary-layer would be separated, which causes high thermal performance.
  d) Strip fins (or offset fins): the short sections of fins are aligned entirely with the flow direction. Due to the short flow-length fins, the boundary layer never becomes thick. Thus there is a high heat transfer coefficient.
  e) Perforated fins: the cut holes in perforated fins interrupt the boundary layer. Thus, the thermal performance is high with the perforated fins.
  f) Louvered fins: fins are cut and bent out into the flow stream at frequent intervals, to break the boundary layers and achieve high thermal performance.
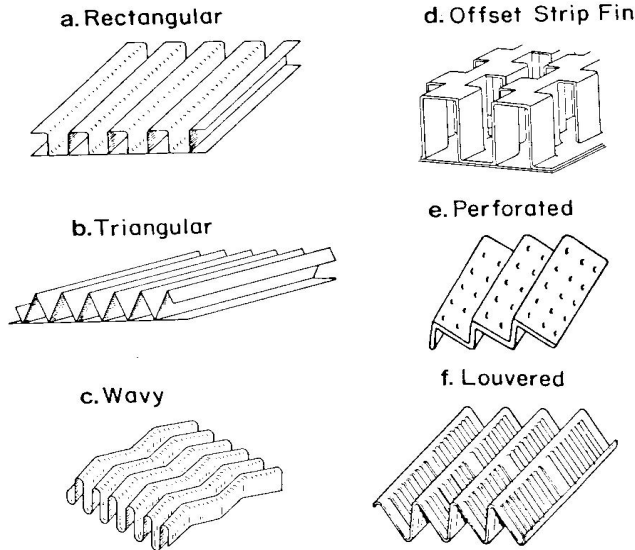
Fig. 2.5 Different configuration of fins in plate-fin HEXs [22].

Because of the low heat transfer coefficient on the air side of the radiator, extended surfaces like fins are placed on the air side to compensate for the low heat transfer coefficient. Nowadays, louvered fins are favorable for the air side of a radiator. This kind of fin enormously increases the heat transfer coefficient and keeps a low pressure drop on the air side, especially at high Reynolds numbers of the air. Oliet et al. [24] used numerical methods to carry out parametric studies for automotive radiators. The influence of some geometrical parameters (fin spacing, louver angle and so on) and the importance of coolant flow lay-out on the radiator global performance were investigated. Furthermore, Carluccio et al. [25] carried out a numerical study including a thermo-fluid-dynamic analysis for an air-oil compact cross flow HEX, which was used in ground vehicles. For the oil side, the geometry of the offset fins did not cause a high level of turbulence, but increased the surface area. On the air side, wavy fins may enhance the heat transfer coefficient twice, compared to straight triangular fins.

2.3.1.2 Rough surfaces

Rough surfaces might be arranged by placing a "roughness" adjacent to the surface. Integral roughness is formed by machining, or "restructuring" the surface. For single-phase flow, the configuration is generally chosen to promote mixing in the boundary layer near the surface, rather than to increase the heat transfer surface area. Compared to the method of extended surfaces, which enhances the heat transfer mainly by the area increase, the rough surfaces mainly enhance the heat transfer by the secondary flow enhancement.

The dimple could be an attractive rough surface for HEXs due to its high heat transfer performance and low flow resistance [26-29]. Mahmood et al. [30] experimentally tested the local heat transfer and flow characteristics above a dimpled surface in a channel. The heat transfer was enhanced by the vortex pairs and vertical fluid flow near the dimple. However, different parameters affect the thermal performance of dimple surfaces [31-34]. When the ratio of dimple depth to dimple print diameter is reduced, the vortex pairs become stronger and the local Nusselt number is increased [31]. Furthermore, Moon et al. [32] analyzed the thermal performance in the dimple passage for different channel heights. The heat transfer was enhanced by around 2.1 times compared to the channel without dimples. On the other hand, Ligrani et al. [35] found that a dimple with protrusions on opposite walls led to additional vertical, secondary flow and strong flow mixing compared to the one with flat surface. The heat transfer enhancement was achieved by adding the protrusion in the dimple channel, but the friction factors were also increased, 2.0-2.7 times compared to a channel with dimples and flat top surface. Combining the increased form drag and channel friction factors, the thermal performance factors in the channel with dimples and protrusion on the top surface were lower than those in the flat top surface channel [36].

2.3.2 New materials for heat exchangers

Another efficient method to increase the thermal performance of HEXs is the utilization of microcellular foam materials, such as metal or graphite foams. The heat transfer is enhanced by the huge fluid-solid contact surface area and the fluid mixing. Aluminum or copper heat exchangers have become common in vehicles, because of their high thermal conductivity. However, a porous medium, e.g., graphite foam developed by Oak Ridge National Laboratory (ORNL) [37], has extremely high thermal conductivity. Inside the graphite foam, there are many spherical pores with small dimensions. These pores are three-dimensionally interconnected, as shown in Fig. 2.6.
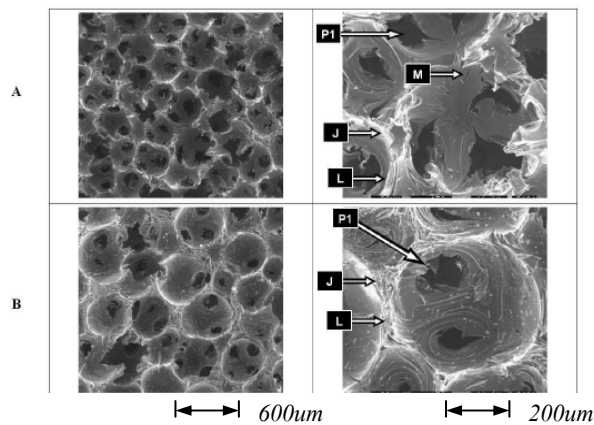
Fig. 2.6 Photomicrographs of the foams produced from Mitsubishi ARA 24 pitch at different densities, A < B (P1: opening pore; M: microcrack; J: junction; L: ligament) [38].

Because of the special structures, there are several prominent thermal properties in the graphite foam. The graphite foam made by the ORNL process exhibits high effective thermal conductivity (up to 182 W/(m·K)) and low density (0.2 - 0.6 g/cm^3). On the other hand, the data in Table 2.1 shows that the thermal conductivity in the z – plane is much larger than the one in the x – y plane. It implies that a high thermal conductivity of the graphite foam only exists in a certain direction. This is a disadvantage of the graphite foam. Klett et al. [38] found out that the heat inside the graphite lattice was transferred down the graphite lattice fast, because of the very stiff nature of the covalent bonds (as shown in Fig. 2.7). Moreover, the position and vibration of atoms in the neighboring planes may impede the vibration of atoms in the plane of interest. The crystal perfection controls the thermal performance. In order to achieve high thermal conductivity in the graphite crystal, the structure must be composed of aligned, straight graphene planes, and so on.

Table 2.1 Properties of various graphite foams made by the ORNL method compared to POCOFoam [38].

	Graphitiza-tion rate (℃/min)	Average bulk density (g/cm^3)	z-Plane thermal conductivity λ_z (W/(m·K))	x-y Plane thermal conductivity λ_{xy} (W/(m·K))
ORNL graphite foam (1)	10	0.45	125	41
ORNL graphite foam (2)	1	0.59	181	60
POCOFoam^{TM}	-	0.61	182	65
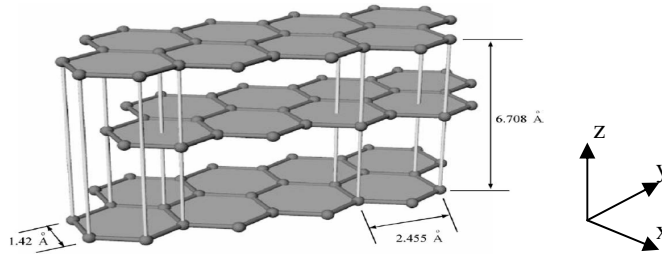
Fig. 2.7 Planar structure of hexagonal graphite [38].

Several research works about the characteristics of graphite foams have been carried out [38-40]. In summary, the characteristics of graphite foams are as follows:
1) Advantages:
   a) High thermal conductivity: The effective thermal conductivity of graphite foam is between 40 and 150 W/(m·K) [38], which is much higher than that of an aluminum foam (between 2 and 26 W/(m·K) [41]).
   b) Low density: The density of graphite foam ranges from 0.2 to 0.6 g/cm^3, which is about 20 % of the density of aluminum.

    c) Large specific surface area: Because of the open space and inter-connected void structure, the specific surface area of graphite foam is between 5000 and 50000 m^2/m^3.

2) Disadvantages:

    a) Weak mechanical properties: The tensile strength of graphite foam is much lower than that of the metal foam.

    b) Path dependency: High thermal conductivity only exists in a certain direction.

Based on these characteristics, graphite foam is a potential material for heat exchangers. Klett et al. [42] designed a radiator with carbon foam. The cross section of the automotive radiator was reduced from 48 cm × 69 cm to 20 cm × 20 cm. The reduced size could decrease the overall weight, cost and volume of the system. Yu et al. [43] proved that the thermal performance of a carbon foam finned tube radiator could be improved by 15 %, compared to a conventional aluminum finned tube radiator, without changing the frontal area, or the air flow rate and pressure drop. Furthermore, Garrity et al. [44] carried out an experimental comparison between the carbon foam heat exchanger and the multilouvered fin heat exchanger. When the volume of the heat exchangers was the same, the carbon foam samples removed more heat than the multilouvered fin.

Even though there is a huge heat transfer enhancement in the graphite foam, the high pressure drop is the major issue facing to the graphite foam, due to the large hydrodynamic loss associated with the cell windows connecting the pores [45]. In order to reduce the pressure drop, six different configurations of graphite foam heat exchangers were presented in [46]. The solid foam had the highest pressure drop, and the finned configuration had the lowest value. On the other hand, Leong et al. [47] found that the baffle foam presented the lowest pressure drop among the four configurations of graphite foams, at the same heat transfer rate. Lin et al. [48] proved that a corrugated foam could reduce the pressure drop while maintaining a high heat transfer coefficient, compared to a solid foam. Thus, the configuration has an important effect on the pressure drop through the graphite foam.

2.3.3 Idea of graphite foam HEXs

Due to the excellent thermal characteristics of graphite foam, graphite foam HEXs are considered for the vehicle cooling system in the present work. Because of the high flow resistance in the graphite foam, two enhancement techniques are applied to graphite foam HEXs: (1) main-flow enhancement (extended surfaces method): four different configurations [46-48] (corrugated, wavy corrugated, pin-finned, and baffle) of the graphite foam fins are analyzed, to find out which configuration of graphite foam fin will achieve low pressure loss and high thermal performance; (2) secondary-flow enhancement (rough surfaces method): the graphite foam rectangular fins with one-side dimples or two-side dimples are also analyzed in the graphite foam heat exchanger.

Chapter 3 Modeling and numerical simulation method evaluating HEX performance

Experimental or numerical methods have been employed to investigate which design of a radiator or HEX is economic and efficient. However, because of the high cost and the complexity of experiments, a numerical method is adopted in the present work to analyze the performance of HEXs. The physical model of the HEX has to be simplified and certain assumptions have to be set up. Meanwhile the governing equations and corresponding boundary conditions are introduced for the simulation model. On the other hand, the grid independence is carried out to ensure the accuracy and validity of the numerical models. At the end, several important parameters are defined for the analysis of thermal performance and pressure loss in HEXs.

3.1 Physical models and assumption

Simplified configurations of some plate-fin HEXs are shown in Figs. 3.1(a) and (b) (A cross flow HEX is shown in Fig. 3.1 (a), and a countercurrent one in Fig. 3.1 (b)). The engine coolant flows inside the flat tubes, and the air flows through fins. The heat is transmitted through the tube wall and the fins and finally dissipated to the ambient air.

Because of the high flow resistance in the graphite foam, two enhancement techniques are applied to graphite foam HEXs:

(1) Main-flow enhancement (extended surfaces method): four different configurations [46-48] (corrugated-, wavy corrugated-, pin-finned-, and baffle fin) of the graphite foam HEXs are analyzed**.** They will be compared with the aluminum HEX with wavy-, pin- and louver fin. In order to simplify the simulation model and save computational time, only a core of the HEX is adopted, as shown in Fig. 3.1 (c-d). Based on the literature survey, the overall size of the core of the graphite foam fin is: 45 mm × 12 mm × 50 mm (width (W) × height (H) × length (L), and the one of the core of aluminum fin is: 2.31 mm x 6.85 mm x 70 mm (W x H x L) [23].   The various properties of the aluminum fins and graphite foam fins are shown in Table 3.1 and Fig. 3.2, respectively.

water tubes

fins

(a)

(b)

Air direction

Coolant direction

(1) corrugated

(2) wavy corrugated

(3) pin-finned

(4) baffle

(c) (d)

(1) louver fin

(2) wavy fin

(3) pin fin

Fig. 3.1 Schematics of (a) the cross flow HEX, (b) the countercurrent flow HEX, and a core of (c) graphite foam fin and (d) aluminum fin with different structures to be studied.

(1) Corrugated

(2) Wavy corrugated

(3) Pin-finned

(4) Baffle

Fig. 3.2 Geometries of various graphite foams (cm).

Table 3.1 Geometry parameters of aluminum fins (mm).

Louver fin [23]	Fin pitch	Fin thickness	Louver spacing	Louver angle (degree)
	2.31	0.152	4.76	17.06
Wavy fin	Fin pitch	Fin thickness	Wave length	Wave amplitude
	2.23	0.152	8.9	1
Pin fin	Pin pattern	Pin diameter	Transverse spacing	Longitudinal spacing
	In-line	0.79	2.3	3.18

Table 3.2 Physical properties of graphite foam characteristics [45].

Graphite foam	Porosity (φ)	Density (ρ) (kg/m^3)	Area to volume ratio (a_{sf}) (m^2/m^3)	Effective thermal conductivity (λ_{eff}) (W/m·K)	Permeability (α) (m^2)	Forchheimer coefficient (C_F)
POCO	0.82	500	5240	120	6.13×10^{-10}	0.4457

(2) secondary-flow enhancement (rough surfaces method): the graphite foam rectangular fins with one-side dimples or two-side dimples are also analyzed in the graphite foam heat exchanger (Fig. 3.3). Three cases of graphite foam fins are analysed: rectangular fin without dimple (Case 1); rectangular fin with one-side dimples (Case 2); rectangular fin with two-side dimples (Case 3). Note that the fin thickness of the three cases is kept the same. According to research work about the graphite foam fin [23], the optimal thickness of the graphite foam fin is between 3 mm to 5 mm in terms of thermal performance. Accordingly, the thickness of the graphite foam fin is selected to be 5 mm in this study. The pitch of the fins in the height direction (z-direction) is 15 mm, and the width of fins is 64 mm.
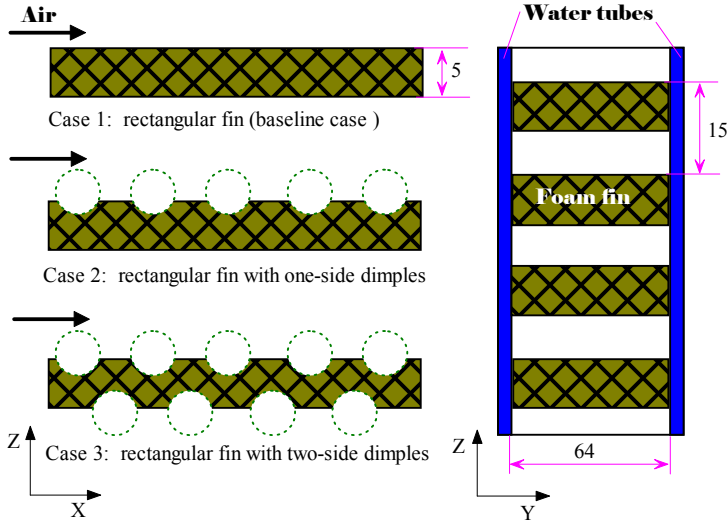
Fig. 3.3 Schematic pictures of physical model: plate fin heat exchangers (dimensions are given in mm).

The detailed geometry of the dimple fin is shown in Fig. 3.4. An array of circular-shaped dimples is positioned on the surface in a staggered arrangement, as shown in Fig. 3.4 (a). The spacing of adjacent dimple rows (S) is 8 mm, and the spacing of every other dimple row (P) is 16 mm. The dimple print diameter (D) is 5.08 mm, and the dimple depth (δ) is 1.02 mm. Due to the periodic structure, a core of graphite foam fin is chosen with only two rows of dimples (x-direction) and half of the fin width, the overall size of the core is: 16 mm×32 mm×15 mm (x×y×z), as shown in Fig. 3.4 (c). A periodic condition is applied to the flow inlet and outlet.

The assumptions in this study are as follows:
   (1) The air is assumed to be incompressible with constant properties and in steady-state.
   (2) The connection between the tube wall and the graphite foam fin is assumed perfect without any air gap between. Thus, the thermal resistance at the interface between the tube wall and the graphite foam is neglected.

(3) The porosity through the dimple finned graphite foam is constant.
(4) The thermal conductivity of the graphite foam is assumed to be isotropic.

P = 16.00,
S = 8.00,
W = 64.00.

(b)Individual dimple geometry

(c) Core of dimple fin for simulation

(a) Overall dimple fin geometry
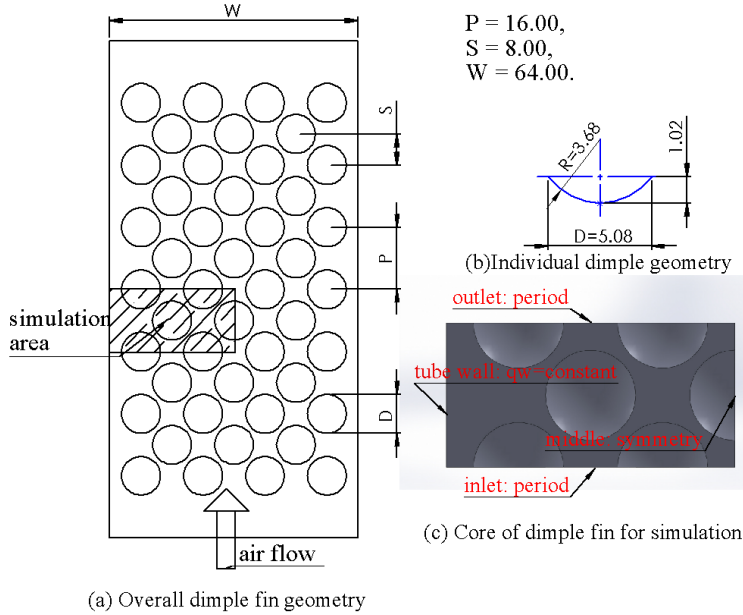
Fig. 3.4 Schematic figures of the dimple fin geometry. All dimensions are given in mm.

3.2 Adoption of flow model

In this part, a computation model (laminar or turbulent) for the flow is presented. Based on the speed of heavy vehicles, the air inlet velocity of the countercurrent flow HEX in the study is about 50 to 70 km/h. In this case, the Reynolds number (based on the hydraulic diameter of the channel and the mean velocity) on the air side is ranging from 2300 to 13152. Thus, low Reynolds number turbulent flow prevails on the air side. In order to capture the low Reynolds characteristics of the turbulent flow, the "renormalization group" (RNG) k-ε turbulence model is adopted [49-50] on the air side for the cases of graphite foam fins: corrugated, wavy corrugated, pin-finned, and baffle configurations; aluminum fins: louver fin, wavy fin, and pin fin.

On the other hand, in order to capture the effect of the vortex pairs and vertical fluid near the dimple fins, the k-ω turbulence model is considered in the regions near the dimple walls to predict the location of flow separation and the displacement effect associated with it. However, the k-ω model has a very strong sensitivity to the free stream outside the boundary layer, and the k-ω model can not accurately represent the k and ε distribution in agreement with direct numerical simulation (DNS) data. Thus in the free stream far from the boundary walls, the k-ε turbulent model is used, due to its good agreement with DNS data by employing different damping functions. Therefore in

this study the shear-stress transport (SST) *k-ω* model [51], combining the effect of *k-ω* model and the *k-ε* model, has been applied to capture the turbulent flow characteristics for the graphite foam rectangular fin with one-side or two-side dimples.

Furthermore, because the porous structure and high flow resistance in the graphite foam region, the air velocity inside the foam is very low. The Reynolds number based on the pore diameter and the air velocity inside the pores is lower than 10, which is lower than the transition region value of 100. So laminar flow is considered inside the graphite foam region. Furthermore, laminar flow is considered on the water side as well, based on the inlet velocity of the engine coolant.

3.3 Governing equations

Based on the above mentioned assumptions, the governing equations for continuity, momentum and energy can be expressed as follows:

1 Air/water zone governing equations

Continuity equation:

$$\frac{\partial\left(\rho_f u_i\right)}{\partial x_i} = 0 \tag{3.1}$$

Momentum equation:

$$\frac{\partial\left(\rho_f u_i u_j\right)}{\partial x_j} = -\frac{\partial p}{\partial x_i} + \frac{\partial}{\partial x_j}\left(\left(\mu_f + \xi\mu_t\right)\left(\frac{\partial u_i}{\partial x_j} + \frac{\partial u_j}{\partial x_i}\right)\right) \tag{3.1}$$

Energy equation:

$$\frac{\partial\left(\rho_f u_j T\right)}{\partial x_j} = \frac{\partial}{\partial x_j}\left(\left(\frac{\mu_f}{\mathrm{Pr}_f} + \xi\frac{\mu_t}{\mathrm{Pr}_t}\right)\frac{\partial T}{\partial x_j}\right) \tag{3.2}$$

When laminar flow (the water side) prevails, $\xi=0$; When turbulent flow (the air side) prevails, $\xi=1$.

a.   The RNG *k- ε* turbulence model: the equations for the turbulent kinetic energy *k* and the rate of energy dissipation *ε* are:

(1) Turbulent kinetic energy *k* equation:

$$u_j \frac{\partial k}{\partial x_j} = -\overline{u_i' u_j'} \frac{\partial u_i}{\partial x_j} + \frac{\partial}{\partial x_j}\left(\frac{K_m}{\sigma_k} \frac{\partial k}{\partial x_j} \right) - \varepsilon \tag{3.3}$$

(2) Rate of energy dissipation ε equation:

$$u_j \frac{\partial \varepsilon}{\partial x_j} = -C_{\varepsilon 1} \frac{\varepsilon}{k} \overline{u_i' u_j'} \frac{\partial u_i}{\partial x_j} + \frac{\partial}{\partial x_j}\left(\frac{K_m}{\sigma_\varepsilon} \frac{\partial \varepsilon}{\partial x_j} \right) - C_{\varepsilon 2} \frac{\varepsilon^2}{k} - R \tag{3.4}$$

where, $R = \dfrac{C_\mu \eta^3 (1-\eta\eta_0)\varepsilon^2}{(1+\beta_0 \eta^3)k}$, $\quad \mu_t = \rho C_\mu \dfrac{k^2}{\varepsilon}$,

$$\eta = \frac{k}{\varepsilon}\left[\left(\frac{\partial u_i}{\partial x_j} + \frac{\partial u_j}{\partial x_i} \right) \frac{\partial u_i}{\partial x_j} \right]^{0.5},$$

$$K_m = v\left[1 + \left(\frac{C_\mu}{v} \right)^{0.5} \frac{k}{\varepsilon^{0.5}} \right]^2,$$

and v is the kinematic viscosity of air; u_i' is the fluctuation of the mean velocity u_i.

The values of the constants are as follows:

$C_\mu = 0.0845; \sigma_k = 0.7179; \sigma_\varepsilon = 0.7179;$

$C_{\varepsilon 1} = 1.42; C_{\varepsilon 2} = 1.68; \beta_0 = 0.012; \eta_0 = 4.377.$

b. The SST k-ω turbulence model: the equations for the turbulent kinetic energy k and the specific dissipation rate ω are:

(1) Turbulent kinetic energy k:

$$\frac{\partial (\rho_{air} u_j k)}{\partial x_j} = \frac{\partial}{\partial x_j}\left[\left(\mu_{air} + \frac{\mu_t}{\sigma_k} \right) \frac{\partial k}{\partial x_j} \right] + G_k - \rho_{air} \beta^* k \omega \tag{3.6}$$

(2) Specific dissipation rate ω:

$$\frac{\partial (\rho_{air} u_j \omega)}{\partial x_j} = \frac{\partial}{\partial x_j}\left[\left(\mu + \frac{\mu_t}{\sigma_\omega} \right) \frac{\partial \omega}{\partial x_j} \right] + \frac{\eta}{v_t} G_k - \rho_{air} \beta_t \omega^2$$

$$+2(1-F_1)\rho_{air} \sigma_{\omega 2} \frac{1}{\omega} \frac{\partial k}{\partial x_j} \frac{\partial \omega}{\partial x_j} \tag{3.7}$$

where, G_k is generation of turbulent kinetic energy, F_1 blending function, $\beta^*=0.09$, $\sigma_\omega=0.5$, $\sigma_{\omega2}=0.856$, $\beta_t=0.0828$.

2 Graphite foam zone governing equations (laminar flow)

The graphite foam is a porous medium. The Forchheimer extended Darcy law has been applied for the air pressure drop through the porous media. Thus,

$$-\frac{\partial p}{\partial x_i} = \left(\frac{\mu_{air}}{\alpha} u_i + \frac{\rho_{air} C_F}{\sqrt{\alpha}} |u| u_i \right) \tag{3.8}$$

where, p is the pore pressure, μ_{air} the air viscosity, α the permeability, calculated as $\alpha = \varphi^3 d_p^2 / (c(1-\varphi)^2)$, where, c is a constant to parameterize the microscopic geometry of the porous materials; φ the porosity of porous media; d_p the pore diameter inside the porous foam. ρ_{air} stands for the air density, C_F the Forchheimer coefficient, calculated as $C_F = b / \sqrt{c\varphi^3}$, where, b is a constant to parameterize the microscopic geometry of the porous materials. u is the air velocity inside the graphite foam pores.

There are two major models for the heat transfer of the graphite foam (porous medium) [52]. One is the local thermal equilibrium model. Another one is the local thermal non-equilibrium model (two-equation model). Their characteristics are as follows:

1) The local thermal equilibrium model (LTE) assumes a local thermal equilibrium between fluid and solid phases. The effective thermal conductivity (λ_{eff}) has to be chosen or calculated correctly, to ensure the accuracy of the simulation model. There are two limiting values for λ_{eff}:

$$\lambda_{eff} = \varphi\lambda_f + (1-\varphi)\lambda_s \text{ and } \lambda_{eff} = \frac{1}{\dfrac{\varphi}{\lambda_f} + \dfrac{1-\varphi}{\lambda_s}} \tag{3.9}$$

The first one presents the higher limiting value of the effective thermal conductivity for the solid and fluid phases in parallel to the direction of the heat flow path. The second one is the lower limiting value for the two phases in series. For a random porous medium, the effective thermal conductivity might be a combination of these two limiting values:

$$\lambda_{eff} = c(\varphi\lambda_f + (1-\varphi)\lambda_s) + \frac{1-c}{\dfrac{\varphi}{\lambda_f} + \dfrac{1-\varphi}{\lambda_s}} \tag{3.10}$$

This equation could reach both limits: (1) $\varphi = 0$, solid; (2) $\varphi =1$, fluid. The value c is constant to parameterize the microscopic geometry of the porous materials. There are many different formulas of λ_{eff} based on experimental work or theoretical analyses [53-58].

2) The local thermal non-equilibrium (LTNE) is considered when there is a temperature difference between the fluid phase and the solid phase. The heat conduction in the fluid and solid phases has to be considered separately. The interfacial heat transfer (calculated as: $q_{sf} = h_{sf} a_{sf}(T_s - T_f)$) connects the heat transfer between the fluid and solid phases. Here, the estimation of λ_{eff} is eliminated. However, another important issue is to get a reasonable value for the interfacial heat transfer coefficient h_{sf}. There exist various correlations to estimate the h_{sf} in different porous structures [59-61].

A temperature difference between the solid phase and the fluid phase is assumed mostly because of the large difference of the thermal conductivity between the solid phase and fluid phase inside the porous foam [62]. This is the main reason why there are several research works on graphite foams using the LTNE model to analyze the heat transfer inside graphite foams [63-67]. Furthermore, some researchers tried to evaluate the accuracy of the LTNE model by comparing it with the LTE model. Amiri et al. [68] presented the validity of the LTE condition, and presented comprehensive error maps of the LTE based on the numerical results. Lee et al. [69] also investigated the validity of the LTE model, and presented a conceptual assessment of solid and fluid temperature differences. The error by using the LTE model was increased when the difference of the thermal conductivity between solid phase and fluid phase was increased. Meanwhile, Calmidi et al. [59] used experimental and numerical methods to quantify the thermal non-equilibrium effects in metal foams.

However, due to the high interfacial heat transfer coefficient and the large specific surface area, the graphite foam and the fluid could be in a near "thermal equilibrium" state when the fluid velocity is very high. According to [61], it was found that the solid and fluid phases inside the metal foam were in near thermal equilibrium when the air mean velocity was larger than 3 m/s. On the other hand, Kim et al. [70] obtained analytical solutions of the temperature distribution in a micro-channel heat sink (whose characteristics of fluid and thermal fields were similar to those in a porous media) by using both the LTE and LTNE model. It was shown that the LTE model could be practically used in micro-channel heat sinks with high porosity. Futhermore, Jeng et al. [71] applied the fin theory and the concept of thermal network to estimate the heat transfer of a porous heat sink. Based on the results, local thermal equilibrium may occur at a large height of the porous heat sink and high Reynolds number.

In the present study, the LTE model is used for the main-flow enhancement case (corrugated-, wavy corrugated-, pin-finned-, and baffle fin in the graphite foam HEXs). The effective thermal conductivity of the graphite foam (λ_{eff}) is based on experimental results in the literature [45]. However, the major part of air is bypassing the graphite foam fin with dimples and a very low air velocity prevails inside the graphite foam. That is why the LTNE model is adapted to the secondary-flow enhancement case: graphite foam fin with dimples. The interfacial heat transfer coefficient h_{sf} for graphite foams needs to be specified for the energy equations. After a comparison of the different formulas, the following one is used in this study [72]:

$$Nu_{sf} = a_{sf} h_{sf} d_p^2 / \lambda_f \tag{3.11}$$

$$(1) \ Pe_d \prec 40, \ Nu_{sf} = (33.3 + 0.51 Pe_d^{0.85})(1-\varphi)^{0.42} \tag{3.12}$$

$$(2) \ Pe_d \succ 40, \ Nu_{sf} = (32.0 \, \text{Pr}_f^{0.077} + 1.18 \, \text{Re}_d^{0.68} \, \text{Pr}_f^{0.38})(1-\varphi)^{0.42} \tag{3.13}$$

where, $Pe_d = \text{Re}_d \, \text{Pr}_f = \dfrac{u_p d_p}{\nu_f} \, \text{Pr}_f$

Moreover, because the effective thermal conductivity of the graphite foam is dominated by the thermal conductivity of the graphite, the thermal dispersion is ignored in the energy governing equation. Thus, the governing equations for the graphite foam are as follows:

Continuity equation:

$$\frac{\partial\left(\rho_f u_i\right)}{\partial x_i . \varphi} = 0 \tag{3.14}$$

Momentum equations:

$$\frac{\partial\left(\rho_f u_i u_j\right)}{\partial x_j} = -\varphi \frac{\partial p}{\partial x_i} + \frac{\partial}{\partial x_j}\left(\mu_f\left(\frac{\partial u_i}{\partial x_j} + \frac{\partial u_j}{\partial x_i}\right)\right)$$
$$-\varphi\left(\frac{\mu_f}{\alpha} u_i + \frac{\rho_f C_F}{\sqrt{\alpha}}|u|u_i\right) \tag{3.15}$$

Energy equation:
   a.   LTE case

$$\varphi \frac{\partial\left(\rho_f c_{p.f} u_j T\right)}{\partial x_j} = \lambda_{eff} \frac{\partial}{\partial x_j}\left(\frac{\partial T}{\partial x_j}\right) \tag{3.16}$$

   b.   LTNE case
for fluid:

$$\varphi \frac{\partial\left(\rho_f c_{p.f} u_j T_f\right)}{\partial x_j} = \lambda_{fe} \frac{\partial}{\partial x_j}\left(\frac{\partial T_f}{\partial x_j}\right) + h_{sf} a_{sf}(T_s - T_f) \tag{3.17}$$

for solid:

$$0 = \lambda_{se} \frac{\partial}{\partial x_j}\left(\frac{\partial T_s}{\partial x_j}\right) - h_{sf} a_{sf}(T_s - T_f) \tag{3.18}$$

where, $\lambda_{fe} = \lambda_f \varphi / \tau, \lambda_{se} = \lambda_s(1-\varphi)/\tau,$. The value of τ is adopted from the experimental work in [61]. φ is the porosity of the porous graphite foam; α the permeability of the porous graphite foam (m^2); a_{sf} the specific surface area between solid and fluid phases (m^{-1}); C_F the Forchheimer coefficient.

3.4 Boundary conditions and computational domain

The momentum and energy transport equations are calculated simultaneously in the air and the graphite foam zones. The boundaries on the graphite foam walls are set up as "interior surfaces" or interfaces. Thus, the solution in the momentum and energy transport on the interfaces between the air and graphite foam zones are not required. The necessary boundary conditions at the external walls are as follows.

3.4.1 Main-flow enhancement cases (extended surface cases)

Only one half of the fin height is simulated, due to the symmetry in the fin height direction (y-direction). Similarly, only half of the water tube is simulated in the height direction. Moreover, in order to eliminate the effect of the entrance, the computational domain is extended in the direction upstream twice the length of the HEX. Similarly, the downstream region of the HEX is extended twice the heat exchanger length, to eliminate the effect of the outlet on the flow inside the HEX. Thus, the total length of the computational domain is five times the length of the HEX, as shown in Fig. 3.5.
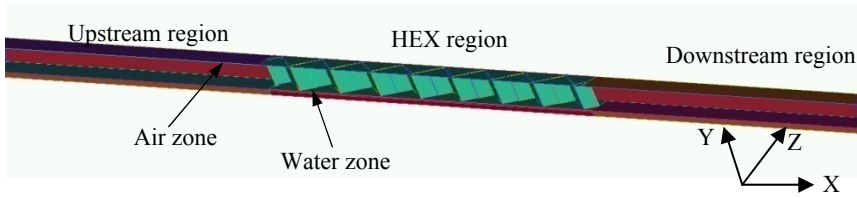
Fig. 3.5 Computational domain.

Because there are air and water zones in the simulation, the boundary conditions should be specified in the different zones separately.

1) Air zone ($H_{water} \leq Y < H$)
   a) Upstream and downstream regions ($0 \leq X < 2L,\ 3L < X \leq 5L$):
   - Z = 0 and Z = W: $\dfrac{\partial u}{\partial y} = \dfrac{\partial v}{\partial y} = 0, w = 0, \dfrac{\partial T}{\partial y} = 0;$ ·
   - Y = H: $\dfrac{\partial u}{\partial z} = \dfrac{\partial w}{\partial z} = 0, v = 0, \dfrac{\partial T}{\partial z} = 0;$
   - Y = H$_{water}$: $u = v = w = 0, T_w = const;$
   - X = 0: $u = 12 \sim 20$ m/s, $T = 300\,K, v = w = 0.$
   - X = 5L: $\dfrac{\partial u}{\partial x} = \dfrac{\partial v}{\partial x} = \dfrac{\partial w}{\partial x} = \dfrac{\partial T}{\partial x} = 0.$
   b) HEX region ($2L \leq X \leq 3L$):
   - Z = 0 and Z = W: (1) $u_{Z=0} = u_{Z=W}, v_{Z=0} = v_{Z=W},$

$w_{Z=0} = w_{Z=W}, T_{Z=0} = T_{Z=W}$. (The geometry of the louver fin and the wavy fin is not symmetric, and periodic condition is applied.)

(2) $\dfrac{\partial u}{\partial y} = \dfrac{\partial v}{\partial y} = 0, w = 0, \dfrac{\partial T}{\partial y} = 0$; (other fins)

- Y = H: $\dfrac{\partial u}{\partial z} = \dfrac{\partial w}{\partial z} = 0, v = 0, \dfrac{\partial T}{\partial z} = 0$;

- Y = H$_{water}$: $u = v = w = 0, T_w = const.$

- between aluminum fins and air walls are present, while between the graphite foam fins and the air, interior surfaces appear.

2) Water zone ($0 \le Y < H_{water}$)

    c) Upstream and downstream regions ($0 \le X < 2L$, and $3L < X \le 5L$):

- Z = 0 and Z = W: $\dfrac{\partial u}{\partial y} = \dfrac{\partial v}{\partial y} = 0, w = 0, \dfrac{\partial T}{\partial y} = 0$;

- Y = 0: $\dfrac{\partial u}{\partial z} = \dfrac{\partial w}{\partial z} = 0, v = 0, \dfrac{\partial T}{\partial z} = 0$;

- Y = H$_{water}$: $u = v = w = 0, T_w = const$;

- X = 0: $\dfrac{\partial u}{\partial x} = \dfrac{\partial v}{\partial x} = \dfrac{\partial w}{\partial x} = \dfrac{\partial T}{\partial x} = 0$ (outlet)

- X = 5L: $u = 0.5$ m/s, $T = 350\,K$, $v = w = 0$.

    d) HEX region ($2L \le X \le 3L$):

- Z = 0 and Z = W: $\dfrac{\partial u}{\partial y} = \dfrac{\partial v}{\partial y} = 0, w = 0, \dfrac{\partial T}{\partial y} = 0$;

- Y = 0: $\dfrac{\partial u}{\partial z} = \dfrac{\partial w}{\partial z} = 0, v = 0, \dfrac{\partial T}{\partial z} = 0$;

- X = 0: $u = v = w = 0, T_w = const.$

3.4.2 Secondary-flow enhancement cases (rough surface cases)

Due to the periodic structure, a core of graphite foam fin is chosen with only two rows of dimples (x-direction) and half of the fin width (y-direction), as shown in Fig. 3.6. A periodic condition is applied to the flow inlet and flow outlet. The boundary conditions are as follows:
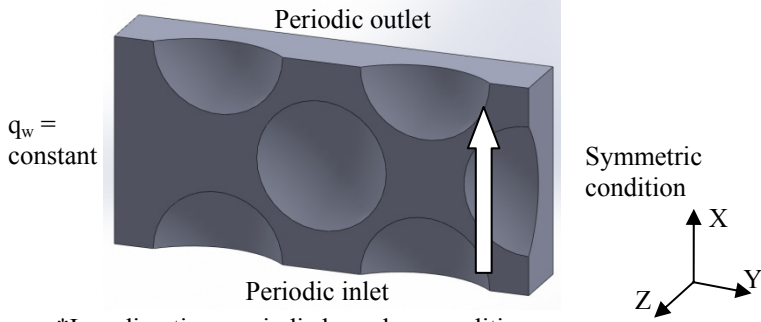
(1) X=0 and X=P (16 mm):

$$u_{X=0} = u_{X=P}, v_{X=0} = v_{X=P}, w_{X=0} = w_{X=P}, T_{X=0} = T_{X=P}, \dot{m}_x = const.$$

(2) Y=0: $q_w = const; u_{Y=0} = v_{Y=0} = w_{Y=0} = 0$.

Y= W/2 (32 mm): $\dfrac{\partial u}{\partial z} = \dfrac{\partial w}{\partial z} = 0, v = 0, \dfrac{\partial T}{\partial z} = 0$.

(3) Z=0 and Z=H (15 mm):

$$u_{Z=0} = u_{Z=H}, v_{Z=0} = v_{Z=H}, w_{Z=0} = w_{Z=H}, T_{Z=0} = T_{Z=H}.$$

*In z-direction: periodic boundary condition

Fig. 3.6 Boundary conditions of the core of graphite foam dimple fin (Case 2).

3.5 Numerical methods

The commercial code ANSYS FLUENT 14.0 is used for the numerical solutions. The finite volume method (FVM) is adopted to convert the governing equations to algebraic equations, so that they can be solved numerically [73]. The Semi-Implicit Method for Pressure Linked Equations (SIMPLE) algorithm is used to couple pressure and velocity. A second-order upwind scheme is used for the space discretization of the momentum, energy and turbulence equations in the simulations. The convergence criterion for continuity, momentum, k, ε and ω equations is that the residual should be below 10^{-3}. However, for convergence of the energy equations the energy balance between the air zone and the water zone under the countercurrent flow condition has to be guaranteed. Accordingly, the convergence criterion for the energy equations is that the residual should be below 10^{-8}.
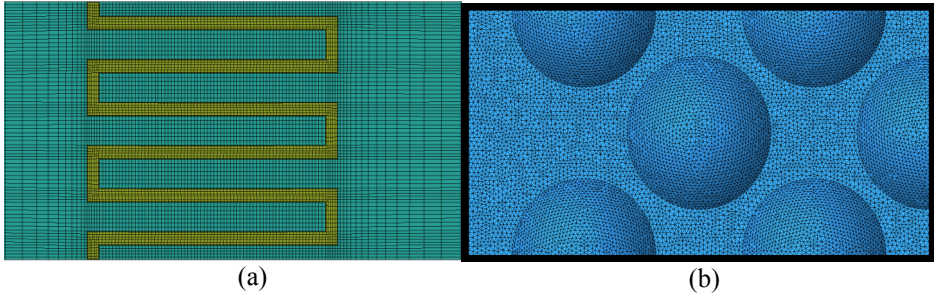

(a) (b)

Fig. 3.7 Meshing for the computations: (a) graphite foam corrugated fin; (b) graphite foam fin with dimples.

The mesh generation is carried out by the preprocessor-software ICEM. There are two major techniques in the mesh generation. One is the blocking technique, which is used

to build structure meshing or Hexa meshing, as shown in Fig. 3.7 (a). Another one is the auto meshing technique for unstructured meshing in complex geometries, shown in Fig. 3.7 (b).

To ensure the accuracy and validity of the numerical models, a careful check of the grid dependence of the numerical solutions has been carried out by considering three grid systems to the aluminum HEX and the graphite foam HEX. For instance, three sets of mesh size (11×81×49, 11×81×75, 19×81×75) were selected for the heat exchanger region to find out the grid independence of the graphite foam corrugated fin. It is found that the variation of the pressure drop is between 0.3 - 2.2 %, and the variation of the Nusselt number is between 1.4 - 3.0 %. Based on this, a mesh size of 11×81×75 was adopted for the graphite foam corrugated fin simulations. The same method was adopted to find out the grid independence of the other cases. The final mesh numbers chosen for the different fins are listed in Table 3.3.

Table 3.3 Mesh numbers for different cases (GF: graphite foam; Al: aluminum) (L×W×H)

Fin types	Mesh	Fin types	Mesh
Pin-finned (GF)	93×79×19	Two-side dimple (GF)	54×108×54
Corrugated (GF)	75×81×11	No dimple (GF)	41×81×41
Wavy corrugated (GF)	139×100×21	Wavy fin (Al)	337×21×33
Baffle (GF)	99×83×17	Louver fin (Al)	350×17×12
One-side dimple (GF)	41×81×41	Pin fin (Al)	313×29×25

3.6 Definition of parameters

Before analyzing and comparing the fluid flow and heat transfer characteristics for the different configurations of the HEX (graphite foam HEX, aluminum HEX), several parameters have to be defined. The thermal performance can be characterized by the Nusselt number (Nu), the averaged Nusselt number ($\overline{Nu}$) or the Stanton number (St) [74]. The definitions are as follows:

$$Re = \frac{\rho_f u_{max} D_h}{\mu_f} \tag{3.19}$$

$$h_f = \frac{Q}{A_0 \Delta T} \tag{3.20}$$

$$Nu = h_f \frac{D_h}{\lambda_f} = \frac{D_h Q_w}{\lambda_f A_0 \Delta T} \tag{3.21}$$

$$\overline{Nu} = \frac{h_f D_h}{\lambda_{air}} = \frac{D_h Q_w}{\lambda_{air} A_w \overline{\Delta T}} = \frac{D_h q_w}{\lambda_{air} (\overline{T_w} - \overline{T_{air}})} \tag{3.22}$$

$$St = \frac{h_f}{\rho_f u_{max} c_p} \tag{3.23}$$

Q is the total amount of heat dissipated to air (W); A_0 the fin surface area (m^2), for the graphite foam $A_0 = a_{sf}V$ (a_{sf} is specific surface area, m^{-1}; V the volume of graphite foam, m^3); $\triangle T$ the logarithmic mean temperature difference, LMTD (K); and D_h the hydraulic diameter (m), for the graphite foam it is the diameter of the foam (d_p). These are defined as follows:

$$Q_w = Q = m c_p (T_{out} - T_{in}) \tag{3.24}$$

$$\Delta T = \frac{(\Delta T_{max} - \Delta T_{min})}{\ln \dfrac{\Delta T_{max}}{\Delta T_{min}}} \tag{3.25}$$

$$\Delta T_{max} = \max(T_{out}^{water} - T_{in}^{air}, T_{in}^{water} - T_{out}^{air}) \tag{3.26}$$

$$\Delta T_{min} = \min(T_{out}^{water} - T_{in}^{air}, T_{in}^{water} - T_{out}^{air}) \tag{3.27}$$

$$\overline{T_w} = \frac{\int_{A_w} T_w dA}{A_w} \tag{3.28}$$

$$\overline{T_{air}} = \frac{\int_{V_{air}} T_{air} dV}{V_{air}} \tag{3.29}$$

$$D_h = \frac{4 A_c}{C} \tag{3.30}$$

where, T_{in} and T_{out} are the bulk temperatures at the inlet and outlet section of the HEX region, respectively, (K); A_c the minimum free-flow area (m^2); A_w the heat source surface area (m^2); V_{air} the volume of air fluid (m^3); C the wetted perimeter of the minimum free-flow channel, (m).

The fluid flow characteristics can be evaluated by the pressure drop ($\varDelta p$) and friction factor (f).

$$\Delta p = p_{in} - p_{out} \tag{3.31}$$

$$f = \frac{A_c}{A_0} \frac{2\Delta p}{\rho_{air}(u_b)^2} = \frac{\Delta p D_h}{2 L \rho_{air}(u_b)^2} \tag{3.32}$$

where, p_{in} and p_{out} are the bulk pressure at the inlet and outlet section of the HEX region, respectively, (Pa); u_b the air mean/bulk velocity (m/s).

Another method to evaluate the performance of the graphite foam dimple fin is to normalize the averaged Nusselt number and the friction factor with the corresponding values in a fully developed rectangular channel without any fin enhancement. The values for $\overline{Nu}_0$ and f_0 for fully developed channel flow are defined as follows [75]:

$$\overline{Nu}_0 = \frac{(f_0/2)(\mathrm{Re}-1000)\,\mathrm{Pr}_{air}}{1.0+12.7\sqrt{f_0/2}\left(\mathrm{Pr}_{air}^{2/3}-1\right)} \tag{3.32}$$

$$f_0 = \left(0.79\ln\mathrm{Re}-1.64\right)^{-2}/4 \tag{3.33}$$

Chapter 4 Results and discussion

The thermal performance and the pressure loss are the two important parameters in the heat exchanger design. In order to develop a high performance countercurrent flow HEX, different configurations of fins (aluminum HEX: louver-, wavy- and pin fin; graphite foam HEX: corrugated-, wavy corrugated-, pin-finned-, baffle fin; rectangular fin with one-side dimples, or two-side dimples) are simulated on the air side. Flat tubes are used on the water side. The thermal performance and the pressure loss are predicted by using ANSYS FLUENT. In addition, an overall performance comparison is carried out between the countercurrent flow (made from graphite foam or aluminum) and the cross flow aluminum HEXs, in terms of coefficient of performance (COP), compactness factor (CF), power density (PD), and energy saving efficiency.

4.1 Validation of models

Prior to presenting the simulation results, it is important to validate the computational models. There are two models in the present work: the graphite foam fin model and the aluminum fin model.

4.1.1 Validation of the graphite foam fin model

There are two models to predict the thermal performance of the graphite foam fin. One is the local thermal equilibrium model, the other one is the local thermal non-equilibrium model. By employing different models, the validation of the graphite foam fin is as follows:

(1) Local thermal equilibrium model: In order to compare the simulation results with experimental data, a block graphite foam with the size of 6 mm (width) x 50 mm (height) x 50 mm (length) is simulated. However, the coolant passing through the graphite foam block is water instead of air (in the air zone), and a constant temperature is specified at the base of the graphite foam block. The pressure drop (Δp) and Nusselt number were compared with the experimental results in [45], as shown in Table 4.1. It is found that the largest deviation of the Nusselt number between the simulation (laminar flow: the frontal velocity was chosen based on the one in the experimental work [45]) and the experimental result is less than 7.1 %, and the lowest deviation is around 1.9 %. The deviation of the pressure drops between the simulation and the experimental data is less than 3 %. It should be noted that no information on the experimental uncertainty of the Nusselt number was supplied in the experimental work [45]. Based on the maximum deviation (7.1 % in the Nusselt number, 3 % in the pressure drop), it is assumed that the

present model is sufficiently accurate and applicable to further estimate the graphite foam pressure drop and the thermal performance.

Table 4.1 Deviation between the simulations and the experimental data (graphite foam)

Frontal velocity (m/s)	Nu number in [45]	Nu number predicted in this study	Δp in [45] (kPa)	Δp predicted (kPa)
0.009	40	38 (5 %)	1.0	1.029 (2.9 %)
0.03	100	101.9 (1.9 %)	3.5	3.41 (2.6 %)
0.048	122	130 (6.5 %)	7.0	6.9 (1.4 %)
0.069	140	150 (7.1 %)	11.2	10.9 (2.7 %)

(2) Local thermal non-equilibrium model: The pressure drop (Δp) and the top surface (x = 0.5 H) temperature are calculated and compared with experimental data in [61]. Figure 4.1 (a) shows the pressure drop of the simulation results and the experimental data. The maximum pressure drop deviation between the simulation and the experimental data is less than 0.9 %. Thus, this simulation model is satisfactory by taking into account the fluid characteristics. A comparison of the top surface temperature on the porous foam is shown in Figure 4.1 (b). There is a relatively large deviation between the simulation results and the experimental ones at low velocity, i.e., 0.7 m/s. However, the deviation is gradually reduced as the air velocity is increased. Typically, quite good agreement between the simulation results and the experimental data is obtained when the air velocity is larger than 1 m/s. Thus, it is believed that the present model is satisfactory and can be applied to further estimate the pressure drop and the thermal performance for the porous foam.

(a)   (b)
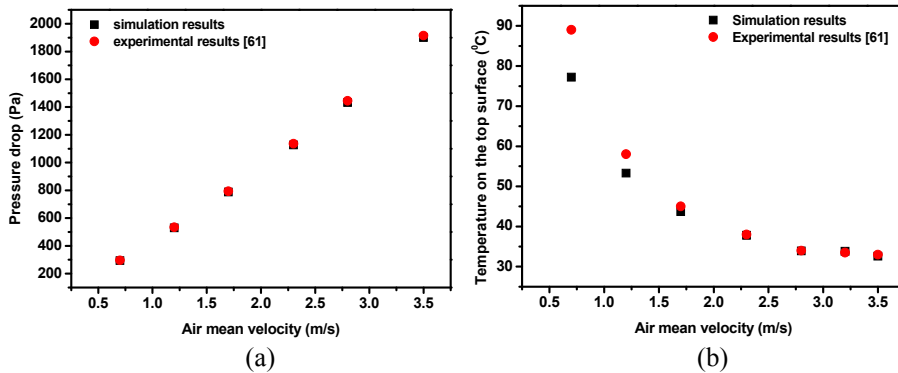
*The internal heat transfer coeffcient h_{sf} is changed as the velocity is changed.

Fig. 4.1 Validation of LTNE model: (a) Pressure drop (L=0.1524 m); (b) Temperature of 0.5H.

4.1.2 Validation of the aluminum fin model

The louver fin is adopted in the validation of the aluminum fin model. In order to compare the simulation results of the louver fin with the experimental data in [23], which was obtained for cross flow conditions, the water zone in the simulation is

assumed to be at a constant temperature. The comparison of $StPr^{2/3}$ and the friction factor f between the simulation and the experimental results is shown in Table 4.2. The deviation of the $StPr^{2/3}$ between the simulations by the RNG k-ε turbulence model and the experimental data is less than 5.4 %, and the deviation of the friction factor f is less than 4.1 %. In the experimental work by Kays [23], the experimental uncertainty of the $StPr^{2/3}$ value was ± 5.0 %, and the one in the friction factor f ± 5.0 %. Thus, there is a good agreement between the simulation and the experiment, in terms of thermal performance and pressure loss.

Table 4.2 Deviation between the prediction and the experimental data (aluminum louver fin).

Re	$StPr^{2/3}$ in [23]	Simulation $StPr^{2/3}$	f in [23]	Simulation f
2837	0.0092	0.0097 *(5.4 %)*	0.0435	0.044 *(1.1 %)*
3392	0.0087	0.0086 *(1.2 %)*	0.041	0.04 *(2.4 %)*
3769	0.0082	0.0081 *(1.2 %)*	0.0398	0.0382 *(4.1 %)*

4.2 Performance comparison of LTNE and LTE models
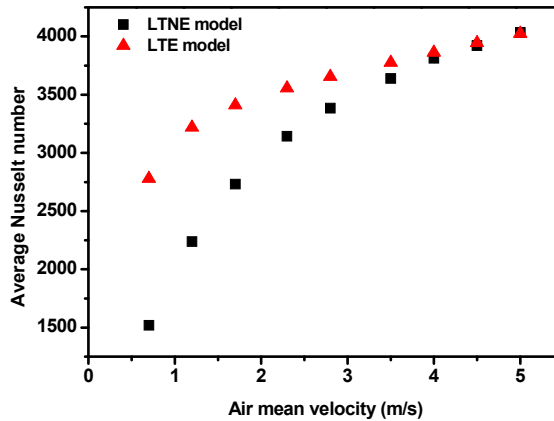
*The internal heat transfer coeffcient h_{sf} is changed as the velocity is changed.

Fig. 4.2 Average Nusselt number for the LTNE and LTE models.

In order to compare the heat transfer performance by using the LTNE model and LTE models, the average Nusselt number is analyzed. Figure 4.2 shows that the average Nu predicted by both models increases as the air velocity is increased. When the air velocity is low, the average Nu by the LTE model is higher than that by the LTNE model at a fixed velocity. This means that the LTE model over-predicts the heat transfer performance compared to the LTNE model at low velocity. However, the difference in average Nu is gradually reduced as the air velocity is increased due to increased internal heat transfer coefficient h_{sf}. When the velocity is larger than 4 m/s, the average Nu by the LTE model is similar to that by the LTNE model. This indicates that the aluminum

foam is predicted to have a similar heat transfer performance for the LTNE and LTE models at high velocity. In other words, the porous foam is in a near thermal equilibrium state at high velocities. This is mostly because the high velocity produces high convective heat transfer coefficients, and thereby might lead to that the thermal resistance in the fluid phase is of the same order of magnitude as that of the solid phase. In this sense, the fluid phase and the solid phase might have a very similar temperature distribution when the fluid velocity is sufficiently high, as shown in Fig. 4.3.
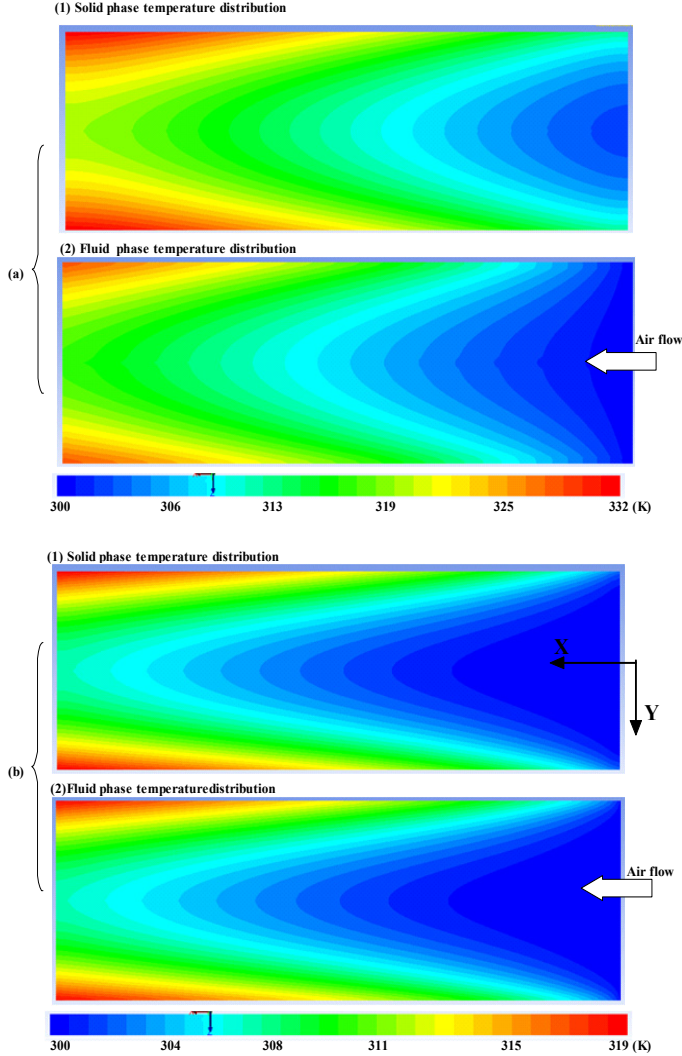

Fig. 4.3 Solid and fluid temperature distributions inside the porous foam by LTNE model: (a) u = 2.3 m/s (h_{sf} = 37.68 W/m²·K); (b) u = 4.5 m/s (h_{sf} = 68 W/m²·K).

By applying the LTNE model, the temperature difference between the solid phase and the fluid phase can easily be seen as the air velocity is 2.3 m/s, as depicted in Fig. 4.3 (a). This means that the porous foam is in a local thermal non-equilibrium state when the air velocity is 2.3 m/s. Moreover, as the thermal resistance in the solid phase is smaller than the one in the fluid phase, the temperature of the solid phase is higher than that in the fluid phase. However, as the air velocity is increased to 4.5 m/s, the temperature distribution in the solid phase becomes similar to the one in the fluid phase, as shown in Fig. 4.3 (b). This is mostly because the high air velocity leads to a high interfacial heat transfer coefficient, which reduces the thermal resistance in the fluid phase. Thus, the temperature difference between the solid phase and the fluid phase is very small. In this case, the porous foam is in a near local thermal equilibrium state. It is suggested that the LTE model can be applied for the high velocity case.

4.3 Main-flow enhancement (extended surface method) fins

4.3.1 Performance comparison among different graphite foam fins

Due to the high thermal conductivity and low density, the graphite foam is a good material for HEX. However, the high pressure loss is the major issue preventing the development of graphite foam HEXs. In order to find an appropriate configuration for the graphite foam fin, the main-flow enhancement (extended surface method) is used. Four different configurations (corrugated-, wavy corrugated-, pin-finned-, and baffle fin) of graphite foam fins are considered in the present work. To simplify the simulation in the graphite foam HEXs, only the air zone is considered. A constant temperature is set on the base of the graphite foam fin. The pressure loss and the thermal performance of different configurations of graphite foam fins are analyzed and discussed in this part.

1 Pressure loss

The extra pressure loss through the graphite foam is based on the Forchheimer extended Darcy's equation (Eq. 3.8). The extra pressure drop through the graphite foam is increased by increasing frontal velocity, as shown in Fig. 4.4. However, the pressure drop through the baffle fin increases faster than the other cases, as the frontal air velocity is increased. Furthermore, the pressure drop through the baffle fin is approximately 10 times higher than for the other cases. This implies that the baffle configuration has much higher flow resistance than the other cases.

All the air has to pass through the corrugated fin and the wavy corrugated fin. However, due to the short flow length (the flow length inside the corrugated foam is 2.5 mm, the one inside the wavy corrugated fin is 3 mm), the pressure drop through the wavy corrugated foam fin or the corrugated foam fin is low. On the other hand, the major amount of air bypasses the baffle fin and the pin-finned fin, instead of passing through them. Because the flow path around the pin-fins (in Fig. 4.6 (1.a)) is much smoother than the one around the baffle fins (in Fig. 4.6 (1.b)), the pressure drop of the pin-finned fin is much less than that for the baffle fins. Furthermore, due to the complex air flow path of the baffle fins, a large amount of air is forced to pass through the baffle graphite

foam fins. Thus, a high flow resistance is produced in the baffle fins, compared to the other configurations of the fin. In other words, the baffle fin presents the highest flow resistance among the considered four configurations.
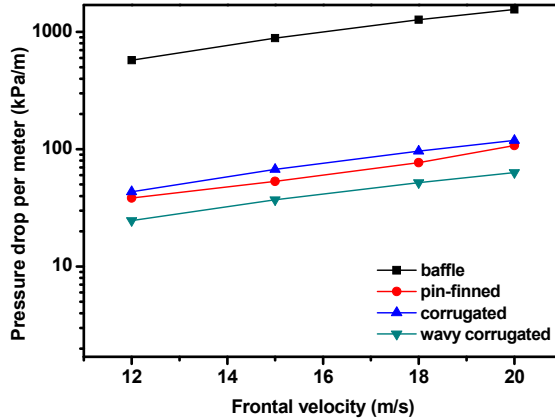

Fig. 4.4 Pressure drop through four configurations of finned foam.

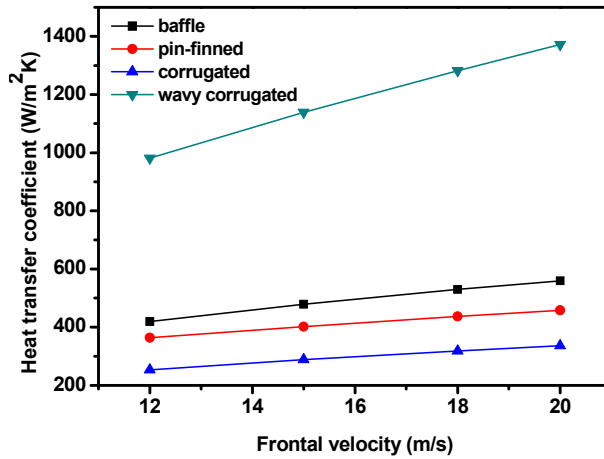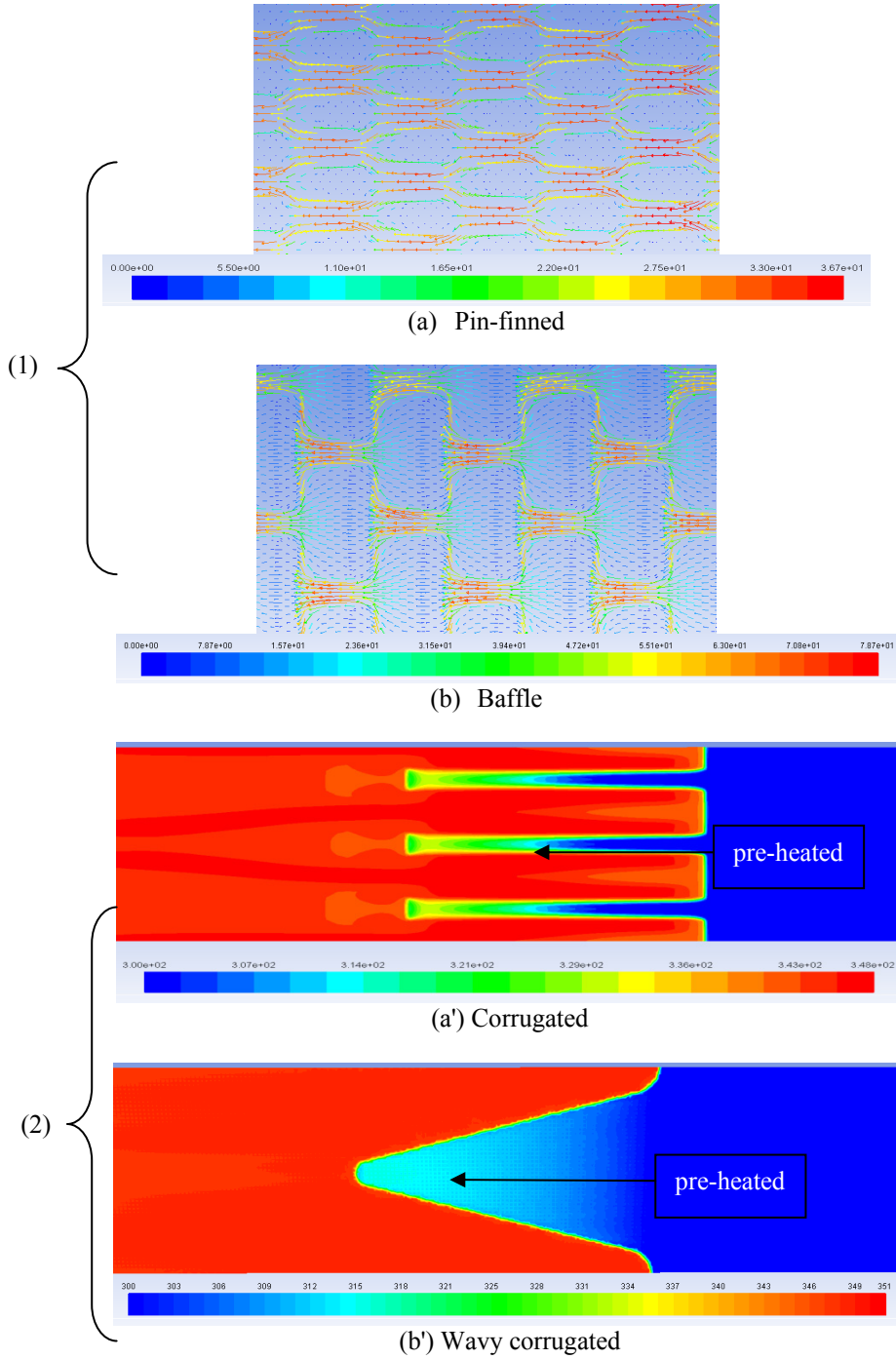**Fig. 4.5** Heat transfer coefficients of four configurations of the finned foam.

(a) Pin-finned

(b) Baffle

(a') Corrugated

(b') Wavy corrugated

Fig. 4.6 (1) Velocity vectors and (2) temperature distribution (K) at 12 m/s inlet velocity (m/s).

2 Thermal performances

The heat transfer coefficients predicted for the four configurations of graphite foam fins are shown in Fig. 4.5. The heat transfer coefficient is correlated with the frontal velocity of air. Among these four configurations, the wavy corrugated fin provides much higher heat transfer coefficient than the other configurations. In addition, the heat transfer coefficient is increased much faster for the wavy corrugated fin than for the other fins, as the air frontal velocity increases.

By taking into account Fig. 4.6, an in-depth understanding of the thermal performance among these two extreme graphite foam fins may be obtained. Figs. 4.6 (2.a') and (2.b') show that the fresh air is pre-heated before it reaches the graphite foam fin due to the heat transported from the nearby fins. The space between two adjacent fins is much larger in the wavy corrugated fin than the one in the corrugated fin. Thus, the pre-heating effect is minor in the wavy corrugated fin compared to that in the corrugated fin. Due to the pre-heating effect, the temperature difference between the fin and the air is reduced in the corrugated fin. The reduced temperature difference decreases the thermal performance of the corrugated fin. Thus, the heat transfer coefficient inside the corrugated fin is much lower than that of the wavy corrugated fin.

On the other hand, due to the different flow path appearing in the pin-finned fin and the baffle fin (see Figs. 4.6 (1.a) and (1.b)), the air is mixed better in the baffle fin than in the pin-finned fin. Thus, the thermal performance of the baffle foam is a little better than that of the pin-finned foam as shown in Fig. 4.5. However, there is a higher flow resistance in the baffle fin than in the wavy corrugated fin, as discussed previously. The high flow resistance leads to a low velocity which causes a low internal heat transfer coefficient in the baffle fin. Overall it seems that the thermal performance of the wavy corrugated foam is the best, see Fig. 4.5.

4.3.2 Performance comparison among aluminum fins

In the present work, a countercurrent flow HEX is proposed to accommodate with the change of HEX position (the radiator is moved and placed at the roof of the driver compartment). Three different configurations (pin-, wavy- and louver fin) of aluminum fin are analyzed in terms of pressure loss and thermal performance, to evaluate which configuration may achieve a good performance.

1 Pressure loss

The pressure drop through the three configurations of fins (louver-, wavy- and pin fin) varies with frontal air velocity, as shown in Fig. 4.7 (a). As expected, the pressure drops increase with increasing air velocity. Among the three configurations of the fins, the louver fin shows the lowest pressure drop. It implies that the flow resistance of the louver fin is lower than that of the wavy- and the pin fins. Moreover, in terms of a dimensionless parameter, the friction factor (f) is reduced with increasing Reynolds number. The louver fin has the lowest value of the friction factor f among the three cases (as shown in Fig. 4.7 (b)), due to the low flow resistance of the louver fin.

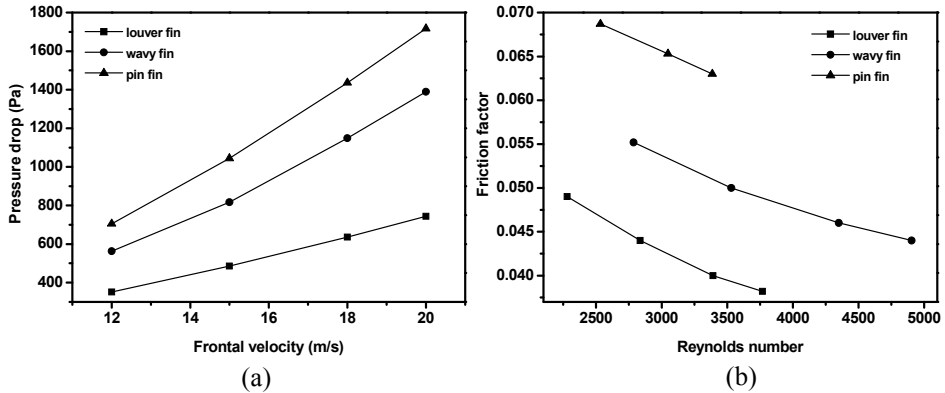(a)   (b)

**Fig. 4.7** (a) Pressure drop vs. frontal velocity; (b) Friction factor vs. Reynolds number.

Based on Fig. 4.8 (a), the flow through the louver fins becomes parallel to the louvers at high velocity. In this case, the louver fins behave like a flat plate, and the air flow path is smooth due to the "flat plate". Thus, the flow resistance is very low in this configuration. However, the flow has to change its direction, due to the structure of the wavy fin (as shown in Fig. 4.8 (b)). This effect leads to a high flow resistance for the wavy fins. On the other hand, Fig. 4.8 (c) shows that the flow has to go around the pin fins, because of the round shape of the pin fins. A high flow resistance is presented for the pin fin as well. Furthermore, it is found that the velocity is more uniform for the louver fin (Fig. 4.8 (a)) than for the wavy fin (Fig. 4.8 (b)) or the pin fin (Fig. 4.8 (c)). This means that the kinetic energy does not change significantly for the louver fin. Thus, the pressure variation is small in the louver fin configuration, compared to the wavy- and the pin fin configurations. In other words, the pressure drop through the louver fin is much smaller than those of the wavy fin and the pin fin.

2 Thermal performances

The heat transfer coefficients predicted for the three configurations of the fin are shown in Fig. 4.9 (a), correlated with the frontal velocity of air. Among these three configurations of the fins, the louver- and pin fins present higher heat transfer coefficients than the wavy fin. The boundary layers have significant effect on the thermal performance of different configurations. As shown in Fig. 4.8 (a), the boundary layer is developed along the louver fins. However, at the end of the fins, the developed boundary layer is broken by the vacancy of fins. Thus, the boundary layer in the louver fins never becomes thick at the high air velocity. This leads to a high heat transfer coefficient around the louver fin. On the other hand, the boundary layer is developed from point *a* to *b* on the pin fin (as shown in Fig. 4.8 (c)). After point *b*, the boundary layer separates from the pin fin. In this case, the boundary layer is thin. Thus, a high heat transfer coefficient is revealed around the pin fin as well. For the wavy fin configuration, the boundary layer is developing along the wavy fins. Due to the wavy configuration, the thickness of the boundary layer is reduced on one side of the fin after point *c* (Fig. 4.8 (b)). However, the boundary layer becomes thick on the other side of the fin at the same time. Thus, the total thickness of the boundary layer around the wavy

fin is kept almost constant. In this case, the heat transfer coefficient is not enhanced as much as in other configurations of the louver and pin fins (as shown in Fig. 4.9 (a)).

Parallel flow   Boundary layer broken

(a)

Boundary layer thickness is constant.
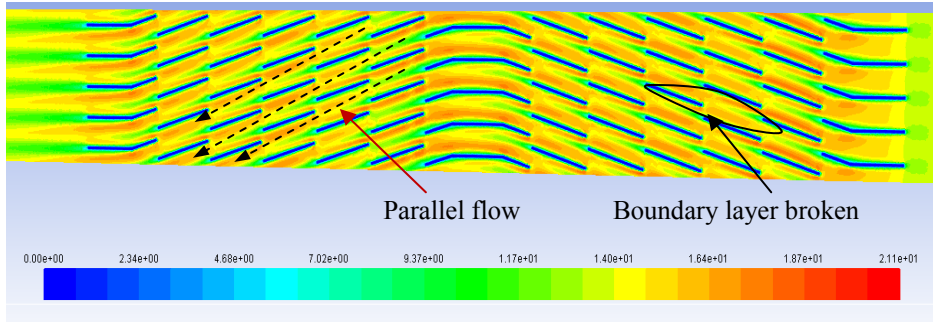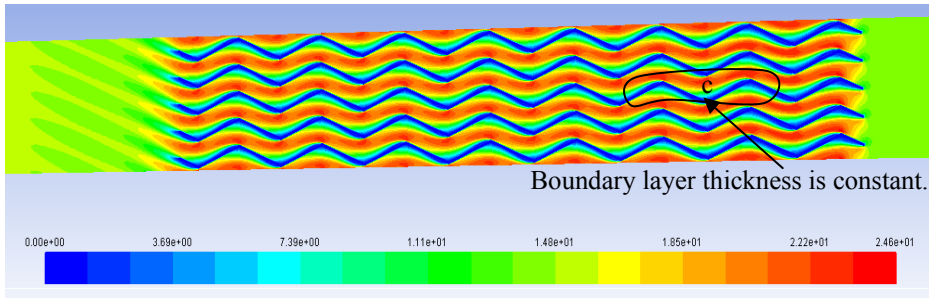
(b)
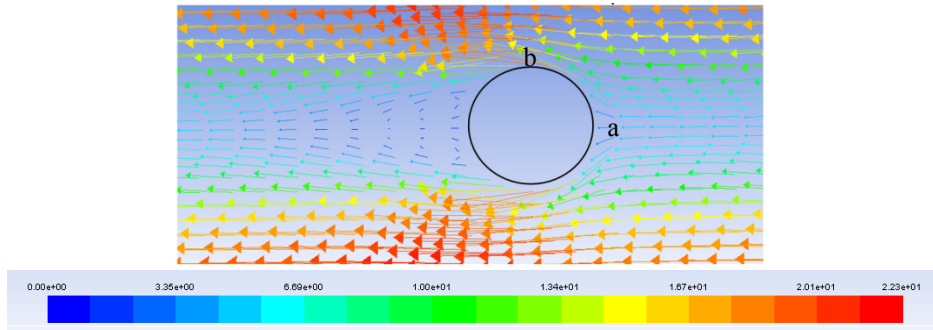
(c)

Fig. 4.8 Velocity predicted for: (a) louver fin; (b) wavy fin; and (c) around a pin fin. (at air inlet velocity of 12 m/s)

The dimensionless parameters (Nu number and Re number) are introduced to analyze the heat exchanger performance, in order to eliminate the effect of different sizes of the fins. Figure 4.9 (b) illuminates the relationship between the Nu number and the Re number among the wavy-, pin- and louver fins. The louver fin shows a higher Nu number than the wavy and the pin fins at the same Re number. Even though the heat transfer coefficients are similar for the pin fin and the louver fin (Fig. 4.9 (a)), due to the

in-line fin pattern and the small hydraulic diameter in the pin fin, the Nu number is much lower for the pin fin than for the louver fin. Based on Fig. 4.9, it is revealed that the louver fin provides better thermal performance than the wavy fin and the pin fin.

(a)   (b)
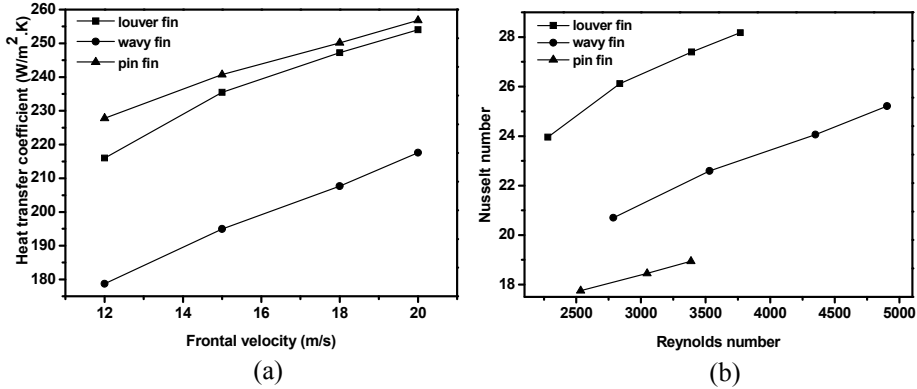
Fig. 4.9 (a) Heat transfer coefficient vs. frontal velocity; (b) Nusselt number vs. Reynolds number.

4.4 Secondary-flow enhancement (dimpled fin)

Another important method to increase the thermal performance and reduce the pressure drop in the graphite foam fin is to employ secondary-flow enhancement, i.e., a dimpled fin. In order to evaluate the heat transfer performance of the graphite foam fin with dimples, the surface averaged Nusselt number is considered. Figure 4.10 (a) shows that the averaged Nusselt numbers in the graphite foam fin with one-side dimples or with two-side dimples are higher than the one in the graphite foam fin without dimples. This is because the dimples can enhance the heat transfer by the effect of vortex pairs, vertical fluid flow, secondary flow and strong flow mixing. This effect is much clearer on the fin with two-side dimples. Moreover, as the flow structure is different between the two sides of the fin for the case of two-side dimples, some part of the fluid penetrates through the graphite foam. This penetration process also increases the heat transfer. Because of these two main reasons, the averaged Nusselt number in the graphite foam fin with one-side dimples is around 1.5 times higher than the one in the graphite foam flat fin, and the one in the graphite foam fin with two-side dimples is around 2.0 times higher than the one in the flat fin.

The flow characteristics are expressed by the pressure drop, as shown in Fig. 4.10 (b). The pressure drop of the fin with one-side dimples is around 1.5 times higher than that of the flat fin, while the fin with two-side dimples produces about 2.2 times higher pressure drop than the flat fin. This is mostly because of strong flow mixing inside the dimple and the penetration through the graphite foam. The flow mixing inside the dimple becomes more intensive as the Reynolds number is increased. Based on this reason, the pressure drops of the fin with one- or two-side dimples are increased faster than that of the flat fin. Compared to the flat fin, the pressure drop of the fin with one- or two-side dimples is 1.9 and 2.8 times higher, at high Reynolds number, respectively.

(a) Averaged Nusselt numbers   (b) Pressure drop (Pa/m)
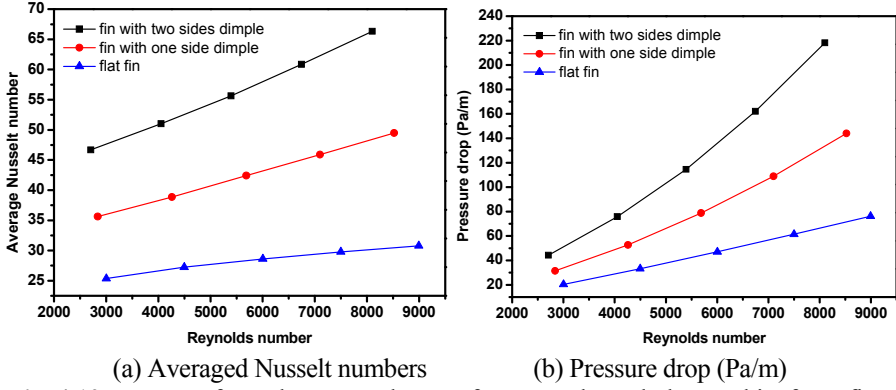
Fig. 4.10 Heat transfer and pressure drop performance through the graphite foam fins.

(a) Normalized Nusselt number   (b) Normalized friction factor
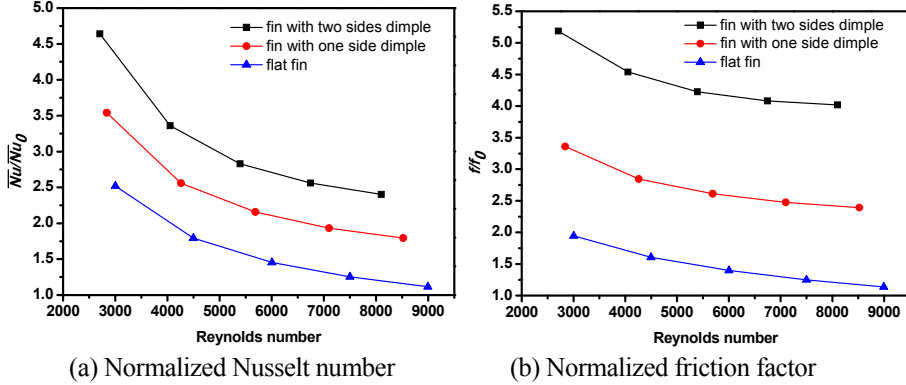
Fig. 4.11 Normalized Nusselt number and friction factor over the fully-developed flow case.

Another method to evaluate the performance of the graphite foam fin with dimples is to normalize the averaged Nusselt number and the friction factor with the corresponding values in a fully developed rectangular channel without any fin enhancement. The values for $\overline{Nu}_0$ and f_0 are for the fully developed channel flow without any fin enhancement, as defined by Eqs. 3.32 and 3.33 already.

Figure 4.11 shows that the values of $\overline{Nu}/\overline{Nu}_0$ and f/f_0 decrease by increasing Reynolds number. Due to the effect of the graphite foam fin, there is heat transfer enhancement based on the values of $\overline{Nu}/\overline{Nu}_0$ (larger than 1.0). The heat transfer enhancement of the graphite foam fin with two-side dimples is best among the three cases based on the values of $\overline{Nu}/\overline{Nu}_0$, which is between 4.6 and 2.4. On the other hand, due to the high flow resistance inside the graphite foam, more and more fluid prefers to flow through the empty channel instead of penetrating through the graphite foam as the Reynolds number is increasing. Accordingly, the effect of porous graphite foam is slowly eliminated as the Reynolds number is increased. This is the reason why the heat transfer enhancement of the graphite

foam flat fin compared to the fully-developed channel flow is reduced from 2.5 to 1.14 (nearly 1.0) as the Reynolds number is increased, and the friction factor increase in the flat fin is also reduced closed to 1 at high Reynolds number. Furthermore, due to the weakening of the porous graphite foam as the Reynolds number is increased, the reduction of the ratios of $\overline{Nu} / \overline{Nu}_0$ and f/f_0 is similar for all three cases.

From the foregoing analysis of the computed results, it is found that the heat transfer enhancement is the best for the graphite foam fin with two-side dimples. However, this case also presents the highest flow resistance. In order to combine the heat transfer performance and the flow characteristics, the overall performance of the graphite foam fin is presented.

The overall performance criterion is the value of $\overline{Nu} / \overline{Nu}_0 /(f/f_0)^{1/3}$, which was proposed by Gee et al. [76]. This performance parameter provides a heat transfer augmentation quantity at a certain input pumping power and a certain heat transfer duty condition. This parameter considers both the heat transfer augmentation and the friction loss increase. Figure 4.12 shows that, among the three cases the graphite foam fin with two-side dimples provides the highest value of $\overline{Nu} / \overline{Nu}_0 /(f/f_0)^{1/3}$, which is between 1.5 and 2.7. This implies that the graphite foam fin with two-side dimples can enhance the heat transfer as much as 2.7 times for the same input pumping power and the same heat transfer duty compared with the other two cases. Therefore, the graphite foam fin with two-side dimples exhibits good performance.
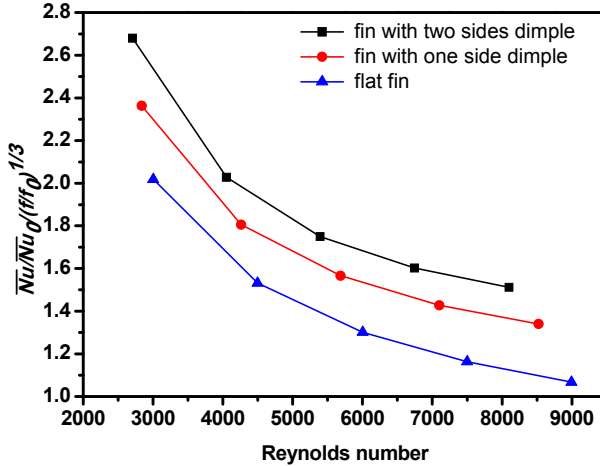

Fig. 4.12 Overall thermal performances of the three foam fins.

4.5 Overall performance comparison of different HEXs

By the comparison of various configurations, it is found that the louver fin presents higher thermal performance and lower pressure loss than the pin fin and wavy fin. On the other hand, the wavy corrugated fin configuration presents better thermal performance and lower flow resistance than the baffle-, pin-finned- and corrugated fins in the graphite foam fin, based on the main-flow enhancement method. Moreover, according to the secondary-flow enhancement method, the graphite foam rectangular fin with two-side dimples presents better performance than that with one-side dimples. Thus, based on the main-flow enhancement, the louver fin is chosen as the fin configuration for the aluminum HEX, and the wavy corrugated fin is adopted as the fin configuration in the graphite foam HEX. On the other hand, the graphite foam rectangular fin with two-side dimples is employed as the secondary-flow enhancement.

In order to evaluate the overall performance of the aluminum or the graphite foam HEX under the countercurrent flow condition, a cross flow aluminum louver fin HEX (the same louver fin as the countercurrent flow HEX) is set as the base. The performance of the graphite foam HEX and aluminum HEX under the countercurrent flow condition is investigated by using the ANSYS FLUENT software. The performance of the aluminum HEX for cross flow condition is based on the experimental data from [23]. The comparison of overall performance is carried out to analyze: (1) coefficient of performance; (2) power density; (3) compactness factor, and (4) energy saving efficiency.

1) Coefficient of performance (COP): defined as how much heat can be dissipated by a certain input pumping power;

$$COP = \frac{Q_{removed}}{u_{in} A_{in} \Delta p} \tag{4.1}$$

2) Power density (PD): defined as how much heat can be dissipated by a certain mass of fins;

$$PD = \frac{Q_{removed}}{1000 \cdot m_{HEX}} \tag{4.2}$$

3) Compactness factor (CF): defined as how much heat can be dissipated in a certain volume;

$$CF = \frac{Q_{removed}}{1000 \cdot V_{HEX}} \tag{4.3}$$

Coefficient of performance (COP)

In order to compare the graphite foam fin with the aluminum louver fin by an appropriate method, the coefficient of performance (COP) is employed to consider the enhanced thermal performance together with the required pumping power to push air through the HEX. As shown in Fig. 4.13, the COP values are reduced when the velocity is increased. It is noted that the COP value of the graphite foam dimple fin is higher than the other cases. However, one of the graphite foam wavy corrugated fins has a lower COP than the other cases. This is mostly because of the extremely high flow resistance in the graphite foam wavy corrugated fin, which counteracts the high thermal performance of the graphite foam fin design. From this point, the pressure drop or the flow resistance is the most important issue for the graphite foam HEX design. An appropriate design of the graphite foam fin may lead to a higher COP value than for the aluminum fin, like the dimple fin case. On the other hand, the countercurrent flow aluminum HEX has higher COP value than the cross flow aluminum HEX, because of the high heat transfer coefficient in the countercurrent flow aluminum HEX.
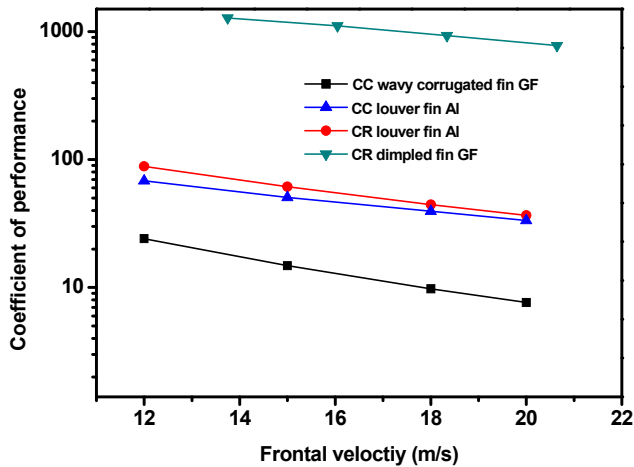
Fig. 4.13 Coefficient of performance (COP) between aluminum and graphite foam HEXs (CC: countercurrent flow; CR: cross flow; GF: graphite foam; Al: aluminum).

Power density (PD)

The mass/weight of the HEX is very important for the vehicle application. Applying the light HEXs, the total weight of the vehicle is reduced, which will lead to less fuel consumption in the vehicle. Thus, the power density of the HEX needs to be considered in the vehicle application. Figure 4.14 shows that the countercurrent flow graphite foam wavy corrugated fin HEX provides much higher PD value than the other cases. Moreover, the PD superiority of the countercurrent flow graphite foam HEX becomes more and more evident as the velocity is increased. The higher the PD value is, the lighter the HEX is. Thus, the countercurrent flow graphite foam wavy corrugated fin HEX is much lighter than the other cases, as the dissipated heat is the same. This is mainly attributed to the small density of the graphite foam. However, the graphite foam

dimple fin presents a similar PD value as the aluminum louver fin, even though the density of the graphite foam is much smaller than the aluminum. That is mostly because of the weak mechanical properties, the thickness of graphite foam dimple fin has to be big. The volume of the graphite foam dimple fin is much larger than the aluminum fin. So the graphite foam dimpled fin still needs to be optimized in terms of fin thickness, fin pitch and so on.

Fig. 4.14 Power density (PD) of corrugated and pin-finned foams and louver fin.

Fig. 4.15 Compactness factor (CF) for corrugated and pin-finned foams and louver fin.

Compactness factor (CF)

The heat exchanger with high compactness is very favorable in vehicle cooling systems, due to the space limitation in vehicles. Thus, the compactness factor is analyzed. Figure

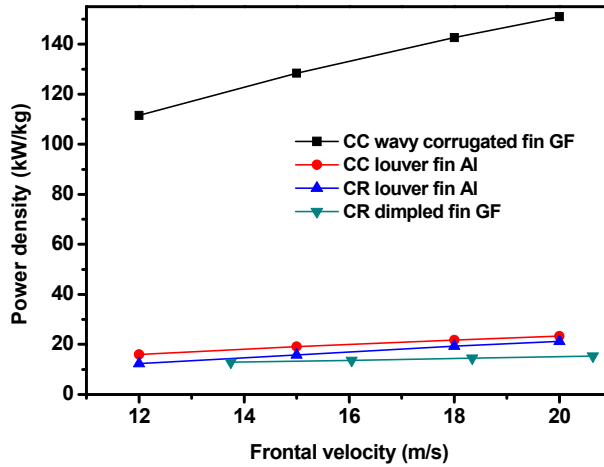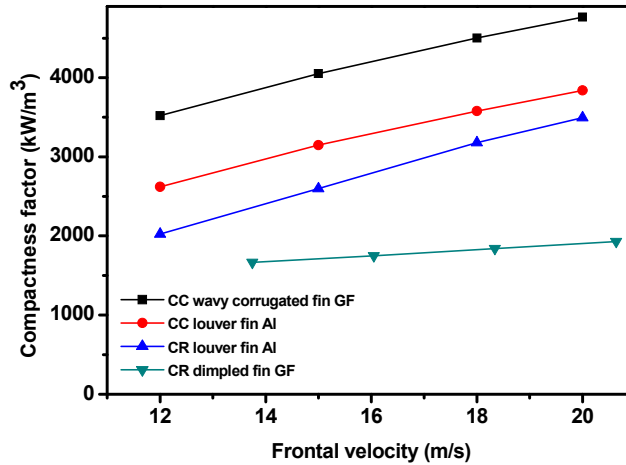4.15 reveals that the compactness factor (CF) of the countercurrent flow HEX is higher than that of the cross flow HEX. Furthermore, the countercurrent flow graphite foam wavy corrugated fin HEX has higher CF value than the countercurrent flow aluminum louver fin HEX. This implies that the volume of the countercurrent flow graphite foam HEX with wavy corrugated fin is the smallest one among these four cases, as the dissipated heat is the same. The graphite foam wavy corrugated fin can provide much larger heat transfer surface area than the alumnium louver fin HEX, due to many open cells in the graphite foam. Meanwhile, the thermal conductivity of the graphite foam is much higher than that of the aluminum. Thus, the volume of the graphite foam wavy corrugated fin HEX can be reduced significantly. However, due to the weak mechanical properties of the graphite foam, the thickness of the graphite foam dimple fin has to be big. This leads to a high volume of the HEX and a low CF value. Thus, an appropriate design of graphite foam dimpled fin is important to achieve a high CF value.

Energy saving efficiency

Another important overall performance criterion is applied to compare the graphite foam fin and the aluminum fin HEXs. The criterion is based on energy saving to compare the effectiveness of the different enhancement techniques [77]. The ratios of heat transfer enhancement ($\overline{Nu}/\overline{Nu_0}$) and friction factor increase (f/f_0) are employed as the coordinates in this evaluation. When the two coordinates are both greater than 1.0, the plot is divided into four different regions based on the energy saving effect, as shown in Fig. 4.16. If a working point of an enhancement technique is located in Region 1, the consumption of one unit pumping power will lead to a less heat transfer rate compared with that of the reference case. Thus for energy-saving purposes the working point should be located outside Region 1.
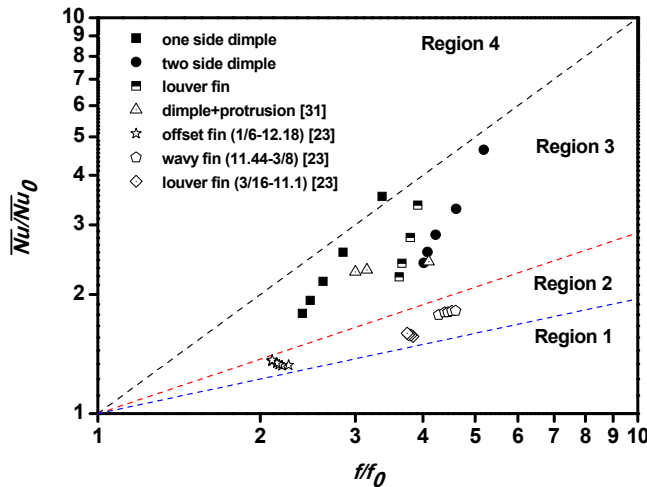

Fig. 4.16 Energy saving performance among the graphite foam fins and the aluminum fins.

The reference data of the aluminum offset fin, wavy fin and louver fin comes from the experimental data in the book by Kays and London [23]. Moreover, other reference data

concerning a channel with dimples and protrusion from the research work [31] are also included in Fig. 4.16. All of the working points are for turbulent flow condition. It is found that the working points of the aluminum offset fin, wavy fin and louver fin from [23] are all located in Region 2, in which heat transfer is enhanced based on identical pumping power but deteriorated based on identical pressure drop. The working points of the graphite foam fin with one- or two-side dimples in the present study are all in Region 3. This means that heat transfer is enhanced based on identical pressure drop but the increase in friction factor is larger than the enhancement of heat transfer at identical flow rate. Furthermore, the working points of the aluminum louver fin in this work are also in Region 3. From the energy saving point of view, the dimpled- and the louver fin are better than the aluminum offset fin, wavy fin and louver fin in [23]. However, due to the high flow resistance in the graphite foam wavy corrugated fin, the working point of this fin is located in Region 1. Thus the graphite foam wavy corrugated fin is not efficient concerning energy saving. On the other hand, the slope of the graphite foam fin with one-side dimples is very large compared to the other cases. The larger the basic line slope of a working point is, the better is its energy-saving effectiveness. From the foregoing analysis of Fig. 4.16, the graphite foam fin with one-side dimples is in the best in terms of energy saving efficiency, and the aluminum louver fin is the second best.

4.5 A case study

In order to evaluate the performance of a countercurrent flow HEX and compare it with a cross flow HEX, a typical truck with 400 kW cooling power is considered. The operating data is shown in Table 4.3.

Table 4.3 Assumed operating data of a truck.

Cooling power (kW)	400	
Truck speed (km/h)	65	
Radiator (water side)	$T_{in} = 90\ °C$	$T_{out} = 85\ °C$
Radiator (air side)	$T_{in} = 30\ °C$	$T_{out} = 50\ °C$

Based on the thermal performance and the flow resistance presented earlier, the comparative results of the size, weight, and pumping power for different HEXs are listed in Table 4.4. Due to the low CF value of the countercurrent flow aluminum louver fin HEX and the countercurrent flow graphite foam wavy corrugated fin HEX, the volume of these two designs are reduced by 5.6 % and 29 %, respectively, compared to the cross flow aluminum louver fin HEX. Moreover, because of the low PD value in the countercurrent flow aluminum louver fin HEX and the countercurrent flow graphite foam wavy corrugated fin HEX, the weight of these two HEXs are reduced by 11.1 % and 86.0 %, respectively, compared to the cross flow aluminum louver fin HEX. However, the power for forcing the air through the countercurrent flow graphite foam wavy corrugated fin HEX is approximately 3 times higher than that for the cross flow aluminum louver fin HEX. This is mostly because of the high flow resistance in the graphite foam. If the graphite foam fin is designed properly, the pumping power for air

going through the graphite foam dimple fin HEX is reduced around 96 % compared to the one for the cross flow aluminum louver fin HEX.

Table 4.4 Comparison between the cross flow HEX and the countercurrent flow HEX.

	Cross flow aluminum louver fin HEX	Cross flow graphite foam dimple fin HEX	Countercurrent flow aluminum louver fin HEX	Countercurrent flow graphite foam wavy corrugated fin HEX
Total cooling surface area (m^2)	39.06 (base)	34.9 (-11 %)	34.36 (-12 %)	20.86 (-46.6 %)
Overall size (W×H×L) (mm×mm×mm)	1000×1000×125	1000×1000×222	1000×944×125	1000×710×125
Total volume (m^3)	0.125 (base)	0.222 (+77 %)	0.118 (-5.6 %)	0.089 (-29 %)
Weight of fins (kg)	20.7 (base)	27.6 (+33 %)	18.4 (-11.1 %)	2.8 (-86.0 %)
Air pumping power (W)	10132 (base)	430 (-96 %)	9005 (-11.1 %)	40900 (+304 %)
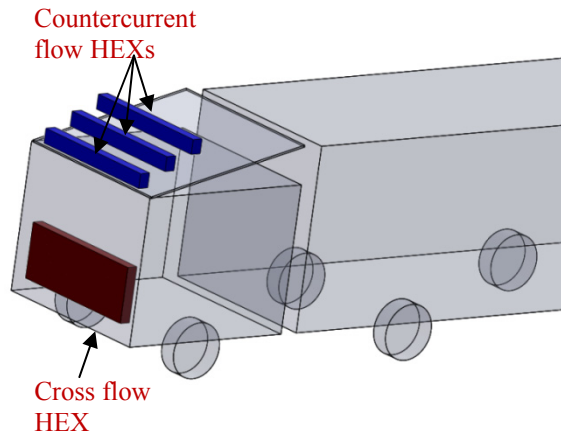
Fig. 4.17 Countercurrent flow HEX and cross flow HEX in a heavy duty truck.

The height of the countercurrent flow HEX is 944 or 710 mm, which may destroy the streamlines of the flow field of the heavy vehicle and cause a huge flow resistance to the vehicle. In order to reduce the flow resistance and optimize the performance of the countercurrent flow HEX, the countercurrent flow HEX (1000×944×125 mm or 1000×710×125 mm) is splitted up into three small countercurrent flow HEXs (the size of each one is: 1000×315×125 mm or 1000×237×125 mm). These three countercurrent

flow HEXs are placed in the slanting part of the roof of the vehicle as a staircase to reduce the effect of the flow field on the vehicle, as shown in Fig. 4.17.

Based on the comparison with the cross flow HEX, the advantages and disadvantages of the countercurrent flow HEX can be summarized as follows:

- Advantages:
    (1) The heat transfer coefficient is higher in the countercurrent flow HEX than in the cross flow HEX. Moreover, the graphite foam even further increases the heat transfer coefficient of the HEX;
    (2) The overall size of the countercurrent flow HEX is smaller than that of the cross flow HEX, when the dissipated heat is the same;
    (3) The countercurrent flow HEX has higher PD and CF than the cross flow HEX. This leads to a light and compact HEX in the vehicle.
- Disadvantages:
    (1) The countercurrent flow HEX placed on the roof of the vehicle may destroy the streamlines of the flow field around the vehicle. The co-location of the countercurrent flow HEX should be optimized.
    (2) The cooling air through the countercurrent flow HEX is driven by the movement of vehicles. When the vehicle climbs on a mountain, the speed of the vehicle is low. However, the engine cooling power is high at this time. Thus, in future work this problem should be analyzed.

Chapter 5 Conclusions

With the increasing cooling requirement in vehicles, advanced heat exchangers have to be developed for the vehicle industry. However, due to the space limitation in vehicles, placing a heat exchanger at a new place on the vehicle, or using new materials might be favorable in the design of advanced heat exchangers. In this study, a countercurrent flow aluminum HEX is designed for placement on the roof of the driver compartment. Furthermore, due to the high thermal conductivity and low density of graphite foam, a graphite foam HEX is proposed and evaluated under the countercurrent flow condition.

The present work has been carried out by the ANSYS FLUENT software. The simulation models (an aluminum HEX model and a graphite foam HEX model) were validated by experimental results from the literature. A performance comparison between the countercurrent flow HEX (made from aluminum and graphite foam) and the cross flow HEX (made from aluminum) was carried out. The major results are as follows:

1) Based on the main-flow enhancement method, the louver fin presents better thermal performance and lower pressure drop compared to the wavy fin and the pin fin in the aluminum HEX. Meanwhile, the wavy corrugated fin shows a higher heat transfer coefficient and smaller pressure loss than the corrugated -, pin-finned -, and baffle fin in the graphite foam HEX.

2) According to the secondary-flow enhancement method, the graphite foam rectangular fin with two-side dimples enhances the heat transfer as much as 2.7 times at the same input pumping power and the same heat transfer duty, compared with the graphite foam rectangular fin and the rectangular fin with one side dimples. Therefore, the graphite foam rectangular fin with two-side dimples exhibits much better performance.

3) In the overall performance comparison of different HEXs, the coefficient of performance (COP), the power density (PD) the compactness factor (CF), and the energy saving efficiency are taken into account. It is found that the countercurrent flow HEX presents higher values of PD and CF than the cross flow HEX. This implies that the countercurrent flow HEX can be much lighter and compacter than the cross flow HEX.

4) Due to the low flow resistance of the dimple fin, the graphite foam fin with two-side dimples exhibits higher coefficient of performance (COP) than the aluminum louver fin, and it is very efficient for saving energy. On the other hand, because of the high thermal conductivity and low density of the graphite

foam, the graphite foam wavy corrugated fin performs higher power density and higher compactness factor than the aluminum louver fin. Thus the graphite foam is a very good potential material for heat exchanger applications.

5) By comparing the average Nusselt numbers and the temperature in the solid phase and fluid phase, it is found that the local thermal equilibrium model can predict the heat transfer performance of a metal or graphite foam as accurately as the local thermal non-equilibrium model at high flow velocities.

Nevertheless, there are still several issues and concerns facing the further application of the countercurrent flow HEX in vehicles.

a) Due to the complex intern porous structure of the graphite foam, the pressure loss in the graphite foam wavy corrugated fin is much higher than that in the aluminum louver fin. This leads to a very low COP for the graphite foam wavy corrugated fin. Thus, appropriate configurations of the graphite foam have to be developed to reduce the pressure drop. The dimple fin might be a good choice to reduce the flow resistance of the graphite foam HEX.

b) Nowadays, the manufacturing technology for graphite foam HEX is not mature, compared to that for aluminum HEX. Furthermore, the mechanical properties of the graphite foam are not as good as those of aluminum.

Thus, much effort has to be devoted to the development of countercurrent flow HEXs in vehicles. Especially, much research work has to be carried out before graphite foam HEXs appear in the real vehicle cooling systems.

Chapter 6 Outlook for future work

Further investigations to be carried out based on this present work might be:

1) After comparing the graphite foam HEX with the aluminum HEX, other simulations might be included. Based on a single unit-cube with a spherical void, Yu et al. [39] gave an analytical expression for the effective thermal conductivity of carbon foams. Currently, most of the carbon/graphite foam studies are based on experiments. It is difficult to get the effective thermal conductivity, internal heat transfer coefficient, permeability, and the Forchheimer coefficient theoretically. If the graphite foam structures are reconstructed by building many unit-cubes with spherical voids at a microscopic scale, then the values of the effective thermal conductivity, permeability, and the Forchheimer coefficient can be obtained, and then the models and simulations can be improved.

2) Another important issue is the manufacturing process for the graphite foam heat exchanger. Muley et al. [78] presented a technology assessment for the metal foam heat exchanger. Several possible manufacturing processes have to be investigated for the graphite foam HEX. Thus, close contacts with heat exchanger industries are needed.

3) According to this study, it is found that the dimple fin presents low flow resistance. This is very attractive for the porous foam fin. Due to the weak mechanical properties of the graphite foam, the graphite foam dimple fin is very thick, which leads to a low compactness factor and a low power density. In order to increase the CF and PD values of HEXs, the aluminum foam dimple fin HEX will be considered in the vehicle cooling system in future.

Bibliography

[1] http://epp.eurostat.ec.europa.eu/tgm/table.do?tab=table&init=1&plugin=1&language=en&pcode=tsdpc320

[2] Davis S. C., Diegel S. W., and Boundy R. G., 2010, Transportation energy data book, 29th ed., http://cta.ornl.gov/data/index.shtml.

[3] LaGrandeur J., Crane D., Hung S., Mazar B., and Eder A., 2006, "Automotive waste heat conversion to electric power using Skutterudite, TAGS, PbTe and Bi Te", 2006 International Conference on Thermoelectrics, pp. 343-349.

[4] Smith K., and Thornton M., 2007, "Feasibility of thermoelectrics for waste heat recovery in hybrid vehicles", http://www.nrel.gov/docs/fy08osti/42256.pdf.

[5] Smith, K., and Wang, C. Y., 2006, "Power and thermal characterization of a lithium-ion battery pack for hybrid-electric vehicles", Journal of Power Sources, **160**, pp. 662-673.

[6] 2004, Fuel Cell Handbook. EG&G Technical Services, Inc.

[7] Torregrosa A. J., Broatch A., Olmeda P., and Romero C., 2008, "Assessment of the influence of different cooling system configurations on engine warm-up, emissions and fuel consumption", International Journal of Automotive Technology, **9**(4), pp. 447-458.

[8] Broatch A., Lujan J. M., Ruiz S., and Olmeda P., 2008, "Measurement of hydrocarbon and carbon monoxide emissions during the starting of automotive DI diesel engines", International Journal of Automotive Technology, **9**(2), pp. 129-140.

[9] Staunton N., Pickert V., and Maughan R., 2008, "Assessment of advanced thermal management systems for micro-hybrid trucks and heavy duty diesel vehicles", presented at IEEE Vehicle Power and Propulsion Conference (VPPC), Harbin, China, September 3-5, 2008.

[10] Cho H., Jung D., Filipi Z. S., Assanis D. N., Vanderslice J., and Bryzik W., 2007, "Application of controllable electric coolant pump for fuel economy and cooling performance improvement", ASME Journal of Engineering for Gas Turbines and Power, **129**, pp. 239-244.

[11] Li Q., 2004, "Investigation of enhanced heat transfer in nanofluids", Nanjing University of Science & Technology, PhD thesis (in Chinese).

[12] Leong K. Y., Saidur R., Kazi S. N., and Mamun A. H., 2010, "Performance investigation of an automotive car radiator operated with nanofluid-based coolants (nanofluid as a coolant in a radiator)", Applied Thermal Engineering, **30**, pp. 2685-2692.

[13] Kulkarni D. P., Vajjha R. S., Das D. K., and Oliva D., 2008, "Application of aluminum oxide nanofluids in diesel electric generator as jacket water coolant", Applied Thermal Engineering, **28**, pp. 1774-1781.

[14] Al-Hallaj S., Kizilel R., Lateef A., Sabbah R., Farid M., and Selman J. R., 2005, "Passive thermal management using phase change material (PCM) for EV and HEV Li-ion batteries", Vehicle Power and Propulsion, 2005 IEEE Conference, pp. 376-380.

[15] Sabbah R., Kizilel R., Selman J. R., and Al-Hallaj S., 2008, "Active (air-cooled) vs. passive (phase change material) thermal management of high power Lithium-ion packs: limitation of temperature rise and uniformity of temperature distribution", Journal of Power Sources, **182**, pp. 630-638.

[16] Kizilel, R., Sabbah, R., Selman, J. R., and Al-Hallaj, S., 2009, "An alternative cooling system to enhance the safety of li-ion battery packs", Journal of Power Sources, **194**, pp. 1105-1112.

[17] Kim K., Choi K., Kim Y., Lee K., and Lee K., 2010, "Feasibility study on a novel cooling technique using a phase change material in an automotive engine", Energy, **35**, pp. 478-484.

[18] Malvicino C., Mattiello F., Seccardini R., and Rostagno M., 2011, "Flat heat exchangers", presented at the Vehicle Thermal Management Systems Conference & Exhibition 10, Warwickshire, UK, May 15-19.

[19] Malvicino C., Sciullo F. D., Cuniberti M., Vestrelli F., and Beltramelli F., 2011, "Dual level vehicle heat rejection system", presented at the Vehicle Thermal Management Systems Conference & Exhibition 10, Warwickshire, UK, May 15-19.

[20] Peuvrier O., Iwasaki M., Hara J., and Mguriya Y., 2011, "Development of compact cooling system (SLIM)", presented at the Vehicle Thermal Management Systems Conference & Exhibition 10, Warwickshire, UK, May 15-19.

[21] Khaled M., Harambat F., Yammine A., and Peerhossaini H., 2010, "Optimization and active control of the underhood cooling system - a numerical analysis", presented at the ASME 2010 3rd Joint US-European Fluids Engineering Summer Meeting and 8th International Conference on Nanochannels, Microchannels, and Minichannels, Montreal (paper No. FEDSM-ICNMM2010-30865), Canada, August 1-5.

[22] Webb R. L., 1995, "Principles of enhanced heat transfer", pp: 3-88, John Wiley & Sons, Inc.

[23] Kays W. M., and London A. L., 1995, "Compact heat exchangers", 3rd edition, McGraw Hill Book.

[24] Oliet C., Oliva A., Castro J., and Perez-Segarra C. D., 2007, "Parametric studies on automotive radiators", Applied Thermal Engineering, **27**, pp. 2033-2043.

[25] Carluccio E., Starace G., Ficarella A., and Laforgia D., 2005, "Numerical analysis of a cross-flow compact heat exchanger for vehicle applications", Applied Thermal Engineering, **25**, pp. 1995-2013.

[26] Xie, G. N., Sundén, B., Zhang, W. H., 2011, "Comparisons of pins/dimples/protrusions cooling concepts for a turbine blade tip-wall at high Reynolds numbers," ASME Journal of Heat Transfer, **133**, 061902-(1-9).

[27] Lan, J. B., Xie, Y. H., Zhang, D., 2012, "Flow and heat transfer in microchannels with dimples and protrusions," ASME Journal of Heat Transfer, **134**, 021901-(1-9).

[28] Elyyan, M. A., Rozati, A., Tafti, D. K., 2008, "Investigation of dimpled fins for heat transfer enhancement in compact heat exchangers," International Journal of Heat and Mass Transfer, **51**, pp. 2950-2966.

[29] Doo, J. H., Yoon, H. S., Ha, M. Y., 2010, "Study on improvement of compactness of a plate heat exchanger using a newly designed primary surface," International Journal of Heat and Mass Transfer, **53**, pp. 5733-5746.

[30] Mahmood, G. I., Hill, M. L., Nelson, D. L., Ligrani, P. M., Moon, H. K., Glezer, B., 2001, "Local heat transfer and flow structure on and above a dimpled surface in a channel," ASME Journal of Turbomachinery, **123**, pp. 115-123.

[31] Mahmood, G. I., Sabbagh, M. Z., Ligrani, P. M., 2001, "Heat transfer in a channel with dimples and protrusions on opposite walls," AIAA Journal of Thermophysics and Heat Transfer, **15**(3), pp.275-283.

[32] Moon, H. K., O'Connell, T., Glezer, B., 2000, "Channel height effect on heat transfer and friction in a dimpled passage," ASME Journal of Engineering for Gas Turbines and Power, **122**, pp. 307-313.

[33] Burgess, N. K., Oliveira, M. M., Ligrani, P. M., 2003, "Nusselt number behavior on deep dimpled surfaces within a channel," ASME Journal of Heat Transfer, **125**, pp. 11-17.

[34] Won, S. Y., Zhang, Q., Ligrani, P. M., 2005, "Comparisons of flow structure above dimpled surfaces with different dimple depths in a channel," Physics of Fluids, **17**, 045105-(1-9).

[35] Ligrani, P. M., Mahmood, G. I., Harrison, J. H., Clayton, C. M., Nelson, D. L., 2001, "Flow structure and local Nusselt number variations in a channel with dimples and protrusions on opposite walls," International Journal of Heat and Mass Transfer, **44**, pp. 4413-4425.

[36] Mahmood, G. I., Ligrani, P. M., 2002, "Heat transfer in a dimpled channel: combined influences of aspect ratio, temperature ratio, Reynolds number, and flow structure," International Journal of Heat and Mass Transfer, **45**, pp. 2011-2020.

[37] Klett J. W., 2000, "Process for making carbon foam", US Patent 6033506.

[38] Klett J., Hardy R., Romine E., Walls C., and Burchell T., 2000, "High-thermal-conductivity, mescophase-pitch-derived carbon foams: effect of precursor on structure and properties", Carbon, **38**, pp. 953-973.

[39] Yu Q., Thompson B. E., and Straatman A. G., 2006, "A unit cube-based model for heat transfer and fluid flow in porous carbon foam", ASME Journal of Heat Transfer, **128**, pp. 352-360.

[40] Straatman A. G., Gallego N. C., Thompson B. E., and Hangan H., 2006, "Thermal characterization of porous carbon foam - convection in parallel flow", International Journal of Heat and Mass Transfer, **49**, pp. 1991-1998.

[41] Paek W. J., Kang H. B., Kim Y. S., and Hyum M. J., 2000, "Effective thermal conductivity and permeability of aluminum foam materials", International Journal of Thermophys, **21** (2), pp. 453-464.

[42] Klett J., Ott, R., and McMillan A., 2000, "Heat exchangers for heavy vehicles utilizing high thermal conductivity graphite foams", SAE Paper 2000-01-2207.

[43] Yu Q., Straatman A. G., and Thompson B. E., 2006, "Carbon-foam finned tubes in air-water heat exchangers", Applied Thermal Engineering, **26**, pp. 131-143.

[44] Garrity P. T., Klausner J. F., and Mei R., 2010, "Performance of aluminum and carbon foams for air side heat transfer augmentation", ASME Journal of Heat Transfer, **132**, 121901-(1-10).

[45] Straatman A. G., Gallego N. C., Yu Q., and Thompson B. E., 2007, "Characterization of porous carbon foam as a material for compact recuperators", ASME Journal of Engineering for Gas Turbines and Power, **129**, pp. 326-330.

[46] Gallego N. G., and Klett J. W., 2003, "Carbon foams for thermal management", Carbon, **41**, pp. 1461-1466.

[47] Leong K. C., Jin L. W., Li H. Y., and Chai J. C., 2008, "Forced convection air cooling in porous graphite foam for thermal management applications", 11th Intersociety Conference on Thermal and Thermomechanical Phenomena in Electronic Systems, pp. 57-64.

[48] Lin Y. R., Du J. H., Wu W., Chow L. C., and Notardonato W., 2010, "Experimental study on heat transfer and pressure drop of recuperative heat exchangers using carbon foam", Journal of Heat Transfer, **132**, 091902-(1-10).

[49] Pope S. B., 2000, "Turbulent flows", Cambridge University.

[50] 2011, "ANSYS FLUENT 14.0 - Theory guide", ANSYS, Inc.

[51] Menter, F. R., 1994, "Two-equation eddy-viscosity turbulence models for engineering applications," AIAA Journal, **32** (8), pp. 1598-1605.

[52] Vafai K., 2005, "Handbook of porous media", 2nd edition, Taylor & Francis Group LLC.

[53] Calmidi V. V., Mahajan R. L., 1999, "The effective thermal conductivity of high porosity fibrous metal foams", ASME Journal of Heat Transfer, **121**, pp. 466-471.

[54] Boomsma K., Poulikakos D., 2001, "On the effective thermal conductivity of a three-dimensionally structured fluid-saturated metal foam", International Journal of Heat and Mass Transfer, **44**, pp. 827-836, 2001.

[55] Bhattacharya A., Calmidi V. V., Mahajan R. L., 2002, "Thermophysical properties of high porosity metal foams", International Journal of Heat and Mass Transfer, **45**, pp. 1017-1031.

[56] Singh R., Kasana H. S., 2004, "Computational aspects of effective thermal conductivity of highly porous metal foams", Applied Thermal Engineering, **24**, pp. 1841-1849.

[57] Yang C., Nakayama A., 2010, "A synthesis of tortuosity and dispersion in effective thermal conductivity of porous media", International Journal of Heat and Mass Transfer, **53**, pp. 3222-3230.

[58] Kuwahara F., Yang C., Ando K., Nakayama A., 2011, "Exact solutions for a thermal nonequilibrium model of fluid saturated porous media based on an effective porosity", ASME Journal of Heat Transfer, **133**, pp. 112602-(1-9).

[59] Calmidi V. V., Mahajan R. L., 2000, "Forced convection in high porosity metal foams", ASME Journal of Heat Transfer, **122**, pp. 557-565.

[60] Hwang J. J., Hwang G. J., Yeh R. H., Chao C. H., 2002, "Measurement of interstitial convective heat transfer and frictional drag for flow across metal foams", ASME Journal of Heat Transfer, **124**, pp. 120-129.

[61] Garrity P. T., Klausner J. F., Mei R., 2010, "Performance of aluminum and carbon foams for air side heat transfer augmentation", ASME Journal of Heat Transfer, **132**, pp. 121901-(1-9).

[62] Hassell B., Ortega A., 2011, "Analysis of multilayer mini- and microchannel heat sinks in single-phase flow using one- and two equation porous media models", Heat Transfer Engineering, **32** (7-8), pp. 566-574.

[63] Lu W., Zhao C. Y., Tassou S. A., 2006, "Thermal analysis on metal-foam filled heat exchangers. Part I: Metal-foam filled pipes", International Journal of Heat and Mass Transfer, **49**, pp. 2751-2761.

[64] Zhao C. Y., Lu W., Tassou S. A., 2006, "Thermal analysis on metal-foam filled heat exchangers. Part II: Tube heat exchangers", International Journal of Heat and Mass Transfer, **49**, pp. 2762-2770.

[65] Xu H. J., Qu Z. G., Tao W. Q., 2011, "Analytical solution of forced convective heat transfer in tubes partially filled with metallic foam using the two-equation model", International Journal of Heat and Mass Transfer, **54**, pp. 3846-3855.

[66] Qu Z. G., Xu H. J., Tao W. Q., 2012, "Fully developed forced convective heat transfer in an annulus partially filled with metallic foams: An analytical solution", International Journal of Heat and Mass Transfer, **55**, pp. 7508-7519.

[67] Dai Z., Nawaz K., Park Y., Chen Q., Jacobi A. M., 2012, "A comparison of metal-foam heat exchangers to compact multilouver designs for air-side heat transfer applications", Heat Transfer Engineering, **33**(1), pp. 21-30.

[68] Amiri A., Vafai K., 1994, "Analysis of dispersion effects and non-thermal equilibrium, non-Darcian, variable porosity incompressible flow through porous media", International Journal of Heat and Mass Transfer, **37** (6), pp. 939-954.

[69] Lee D. Y., Vafai K., 1999, "Analytical characterization and conceptual assessment of solid and fluid temperature differentials in porous media", International Journal of Heat and Mass Transfer, **42**, pp. 423-435.

[70] Kim S. J., Kim D., Lee D. Y., 2000, "On the local thermal equilibrium in microchannel heat sinks", International Journal of Heat and Mass Transfer, **43**, pp. 1735-1748.

[71] Jeng T. M., Tzeng S. C., Hung Y. H., 2006, "An analytical study of local thermal equilibrium in porous heat sinks using fin theory", International Journal of Heat and Mass Transfer, **49**, pp. 1907-1914.

[72] Degroot C. T., Straatman A. G., 2012, "Numerical results for the effective flow and thermal properties of idealized graphite foam", ASME Journal of Heat Transfer, **134**, pp. 042603-1-10.

[73] Versteeg H. K., Malalasekera W., 2007, "An introduction to computational fluid dynamics", 2nd edition, Pearson Prentice Hall.

[74] Kreith F., 1973, "Principles of heat transfer", 3rd edition, Intext Press, Inc.

[75] Sundén, B., 2012, "Introduction to heat transfer", Southampton: WIT Press.

[76] Gee, D. L., Webb, R. L., 1980, "Forced convection heat transfer in helically rib-roughened tubes", International Journal of Heat and Mass Transfer, **23**, pp.1127-1136.

[77] Fan, J. F., Ding, W. K., Zhang, J. F., He, Y. L., Tao, W. Q., 2009, "A performance evaluation plot of enhanced heat transfer techniques oriented for energy-saving", International Journal of Heat and Mass Transfer, **52**, pp. 33-44.

[78] Muley, A., Kiser, C., Sundén, B., and K Shah, R., 2012, "Foam heat exchangers: A technology assessment", Heat Transfer Engineering, **33** (1), pp: 42-51.

Summary of papers

Paper 1
The number of vehicles in use is increasing from year to year. It causes more fuel/energy to be consumed, and more carbon dioxide or other exhaust gases are released to the environment. But the legislations on carbon dioxide emissions have become stricter than before. In the overall effort to achieve sustainability, advanced technological solutions have to be developed to reduce fuel consumption and carbon dioxide emissions from vehicles. More than half of the energy in vehicles is lost as heat to the different cooling systems (engine cooling system, air conditioning, frictional components cooling) and exhaust gas. Reducing the amount of energy lost in vehicle cooling systems will enhance the fuel efficiency of the vehicles. This paper presents a literature survey of different cooling systems in vehicles, which includes the engine cooling system, air conditioning of the compartment, the electronic cooling system and cooling of frictionally heated parts. The usage of exhaust gas in some cooling systems is also included. Some methods or factors are presented for these different cooling systems. Flow field and thermal management are important factors in designing the engine cooling system. Also the exhaust gas can be circulated back to the engine, or be used for driving air conditioning units. Reducing the thermal resistance can improve the electronic cooling performance. The flow field will affect the cooling of the frictional components. This literature survey is offering a starting point for future research in vehicle cooling systems.

Paper 2
Due to the increased power consumptions in equipment, the demand of effective cooling methods becomes crucial. Because of the small scale spherical pores, graphite foam has a huge specific surface area. Furthermore, the thermal conductivity of solid graphite is four times higher than that of copper. The density of graphite foam is only 20 % of that of aluminum. Thus, the graphite foam is considered as a novel highly - conductive porous material for high power equipment cooling applications. However, in the commercial market, aluminum and copper are still the preferred materials for thermal management nowadays. In order to promote the graphite foam as a thermal material for heat exchangers, an overall understanding of the graphite foam is needed. This paper describes the structure of the graphite foam. Based on the special structure, the thermal properties and the flow characteristics of graphite foam are outlined and discussed. Furthermore, the application of graphite foam as a thermal material for heat exchangers is highlighted for electronic packages and vehicle cooling systems. The physical problems and other aspects, which might block the development of graphite foam heat exchangers, are pointed out. Finally, several useful conclusions and suggestions are given to promote the development of graphite foam heat exchangers.

Paper 3

Due to the increasing cooling power and space limitation in vehicles, a new compact heat exchanger - graphite foam heat exchanger is proposed for vehicle cooling application. The graphite foam has high thermal conductivity (the effective thermal conductivity is 40-150 W/m K) and low density (0.2-0.6 g/cm^3), but it has high flow resistance which is a problem in heat exchanger applications. In order to find a graphite foam heat exchanger with low flow resistance, four different configurations (baffle, pin-finned, corrugated, and wavy corrugated) of graphite foam fins are analyzed in terms of thermal performance and pressure drop by using a computational fluid dynamics approach. The simulation results show that the wavy corrugated foam presents high thermal performance and low pressure drop. Moreover, a comparative study between the wavy corrugated foam heat exchanger and a conventional aluminum louver fin heat exchanger is carried out to evaluate the performance of graphite foam heat exchangers in terms of coefficient of performance (removed heat/air pumping loss), power density (removed heat/mass of heat exchangers), and compactness factor (removed heat/volume of heat exchangers). Finally, this paper concludes that graphite foam heat exchangers should be further developed in vehicles, and several recommendations are presented to promote such development.

Paper 4

Due to the increasing power requirement and the limited available space in vehicles, placing the heat exchanger at the roof or the underbody of vehicles might increase the possibility to handle the cooling requirement. A new configuration of the heat exchanger has to be developed to accommodate the position change. In this paper, a countercurrent heat exchanger is developed for position on the roof of the vehicle compartment. In order to find an appropriate configuration of fins with high thermal performance on the air side, the computational fluid dynamics approach is applied for a comparative study among louver fin, wavy fin, and pin fin by using the ANSYS FLUENT software. It is found that the louver fin has high thermal performance and low pressure drop. Thus, the louver fin is chosen to be the configuration of the countercurrent flow heat exchanger. It is also found that the countercurrent flow heat exchanger presents higher heat transfer coefficient than the cross flow heat exchanger. Furthermore, the overall size and the air pumping power of the countercurrent flow heat exchanger are lower than those in the cross flow heat exchanger. Several suggestions and recommendations are highlighted.

Paper 5

Due to the increasing power requirement and the limited available space in the vehicles, a countercurrent heat exchanger (HEX) is proposed for the position on the roof of the vehicle compartment. Furthermore, a new material, graphite foam with high thermal conductivity and low density, is a potential material for HEXs in vehicles. In order to evaluate the performance of the graphite foam HEX, the CFD computational fluid dynamics (CFD) approach is applied in a comparative study of the graphite foam and the aluminum HEXs at countercurrent flow condition. The analysis is conducted for the thermal performance (heat transfer coefficient) and the pressure loss. The simulation results show that the graphite foam HEX provides higher thermal performance than the

aluminum HEX. However, due to the high pressure loss in the graphite foam HEX, the coefficient of performance in the graphite foam HEX is much lower than that of the aluminum HEX. A specific case study is carried out to evaluate the performance of the graphite foam HEX as well. Useful recommendations are highlighted and provided to promote the development of the countercurrent flow HEXs in vehicles.

Paper 6

Graphite foam is a kind of favorable material in thermal engineering applications because of its high thermal conductivity and large specific surface area. However, there is an associated high flow resistance in the graphite foam resulting from the porous structure property. In order to reduce the flow resistance and enhance the heat transfer, dimpled fins could be applied in graphite foam heat exchangers. In this paper, the flow characteristics and thermal performance of graphite foam dimpled fin heat exchangers have been investigated numerically through three-dimensional simulations of fluid flow and heat transfer in graphite foam dimpled fin channels. The local thermal non-equilibrium model has been applied to analyze the thermal performance of the graphite foam dimple fin (porous zone), and the Forchheimer extended Darcy's law has been employed to consider the air pressure drop through the porous graphite foam. Moreover, the SST k-ω turbulence model has been used to capture the turbulent flow characteristics outside the graphite foam region. The details of the fluid flow and heat transfer over the dimple fin are presented. The results show that the graphite foam fin with two sides dimple presents the highest values of the normalized Nusselt number (between 2.4 and 4.6) and overall thermal performance factor. Furthermore, the graphite foam dimple fin provides higher effectiveness than the conventional aluminum offset fin, wavy fin and louver fin concerning energy saving.

Paper 7

Aluminum foams are favorable in modern thermal engineering applications because of the high thermal conductivity and the large specific surface area. The present study aims to investigate an application of porous aluminum foam by using the local thermal equilibrium (LTE) and local thermal non-equilibrium (LTNE) heat transfer models. Three-dimensional simulations of laminar flow (porous foam zone), turbulent flow (open zone) and heat transfer are performed by a computational fluid dynamics (CFD) approach. In addition, the Forchheimer extended Darcy's law is employed to evaluate the fluid characteristics. By comparing and analyzing the average and local Nusselt numbers, it is found that the LTNE and LTE models can reach the same Nusselt numbers inside the aluminum foam when the air velocity is high, meaning that the aluminum foam is in a thermal equilibrium state. Besides, a high interfacial heat transfer coefficient is required for the aluminum foam to reach a thermal equilibrium state as the height of the aluminum foam is reduced. This study suggests that the LTE model can be applied to predict the thermal performance at high fluid velocities or for the case with a large height of the foam.

Paper 1

SAE International™

Vehicle Cooling Systems for Reducing Fuel Consumption and Carbon Dioxide: Literature Survey	2010-01-1509 Published 05/05/2010

Wamei Lin and Bengt Sunden
Lund Univ.

ABSTRACT

The number of vehicles in use is increasing from year to year. It causes more fuel/energy to be consumed, and more carbon dioxide or other exhaust gases are released to the environment. But the legislations on carbon dioxide emissions have become stricter than before. In the overall effort to achieve sustainability, advanced technological solutions have to be developed to reduce fuel consumption and carbon dioxide emissions from vehicles. More than half of the energy in vehicles is lost as heat to the different cooling systems (engine cooling system, air conditioning, frictional components cooling) and exhaust gas. Reducing the amount of energy lost in vehicle cooling systems will enhance the fuel efficiency of the vehicles. This paper presents a literature survey of different cooling systems in vehicles, which includes the engine cooling system, air conditioning of the compartment, the electronic cooling system and cooling of frictionally heated parts. The usage of exhaust gas in some cooling systems is also included. Some methods or factors are presented for these different cooling systems. Flow field and thermal management are important factors in designing the engine cooling system. Whereas the exhaust gas can be circulated back to the engine, or used for driving air conditioning units. Reducing the thermal resistance can improve the electronic cooling performance. The flow field will affect the cooling of the frictional components. This literature survey is offering a starting point for future research in the vehicle cooling systems.

1. INTRODUCTION

In recent years the number of vehicles being used has constantly increased. Table 1 shows that the number of registered trucks and buses in selected countries increased from 179,498 to 266,236 in the years from 1998 to 2007. The increasing number of vehicles causes more energy/fuel to be consumed and more carbon dioxide and other exhaust gases to be released to the environment. Table 2 shows the highway transportation petroleum consumption. Table 3 presents the emission of carbon monoxide. Meanwhile the price of oil has also increased a lot. In 2008 the oil price was nearly 80 dollar per Barrel as shown in Fig. 1. In order to keep the sustainable development of vehicles, many different alternative fuels are used, as shown in Table 4. In addition, strong legislations on emissions are introduced. These force the manufacturers of vehicles to develop advanced technological solutions to satisfy the emission standards. According to the legislations in Europe, the average emission of new passenger cars registered in the European Union must not exceed 130 g CO_2/ km from 2012 onwards [1].

(See Table 1 after last section of paper.)

(See Table 2 after last section of paper.)

(See Table 3 after last section of paper.)

(See Figure 1 after last section of paper.)

(See Table 4 after last section of paper.)

A number of technical development has been introduced in order to meet the low fuel consumption and low carbon dioxide emission requirements for vehicles. In [3] some advanced engine technologies were discussed in view of reducing emissions. They included improving the combustion process, using a flexible fuel injection system, high rates of exhaust gas recirculation (EGR), improving the engine control systems, charge air and coolant temperature control, low friction, advanced exhaust gas aftertreatment system,

recuperation of energy contained in the exhaust gas stream and so on. More investigation about how to reduce vehicle emissions can be found in [4,5,6,7].

Concerning the energy distribution (as shown in Fig. 2) in the vehicle engine, only about one third of the total fuel energy finally becomes useful work, another one third of the total energy input is brought away by the coolant of engine cooling system, and the rest of the energy is lost to the exhaust gases. If one can reduce the energy wasted in the coolant or the exhaust gases, one can reduce the fuel consumption and the carbon dioxide emission, which is proportional to the fuel consumption. The engine cooling system has to make sure the engine works at its optimal temperature, which is about 80°C -90°C. If the engine cooling system can not bring away the heat quickly, the engine working temperature will increase. More fuel will be consumed and the life time of engine will reduce because of the high working temperature in the engine. If the cooling system brings away the heat too fast, this will lead to an unnecessary big radiator. In other words, the size and the weight of cooling system will increase. More fuel has to be used due to the increasing weight. On the other hand, a good engine cooling system can reduce the engine starting and warming up time, in which the engine reaches its working temperature [8]. A lot of hydrocarbon (HC) and carbon monoxide (CO) are produced in the starting and warming up period [9]. Thus it is important to study the vehicle engine cooling system.

(See Figure 2 after last section of paper.)

On the other hand, one third of the fuel energy is lost to the exhaust gas. Exhaust gas recirculation (EGR) no only can reduce the exhaust gas emission but also has some effect on saving the fuel energy. In the EGR process, a part of the exhaust gas goes back to the intake manifold. Before entering the intake manifold, the exhaust gas might be cooled by an EGR cooler to keep the combustion temperature below 1500°C. Then the reaction between nitrogen and oxygen that forms NO_x is reduced. The cooling extent of the exhaust gas depends on many factors. The temperature of the circulating exhaust gas can be higher than the ambient temperature. In this case, some energy is recovered from the high temperature exhaust gas in the EGR. Thus fuel energy can be saved by the EGR process. But if the EGR cooler has a high flow resistance, the combustion process will become bad and much fuel has to be consumed. Thus it is necessary to analyze EGR and EGR coolers.

The last thing to reduce fuel consumption is to optimize the energy which is converted into useful work. For this part of the energy, some is converted into the kinetic energy of vehicles. Another part is converted into thermal energy by the braking process or transmission (gearbox, bearing) process. In some vehicles, the compressor of the air conditioning in

the compartment is driven by the engine. If the air conditioning is optimized, the compressor will consume less power from the engine. That means the engine can save some energy. Considering reduction of fuel consumption, it is a good option to optimize the friction components (brake, retarder, gearbox, bearing) cooling system and the air conditioning system.

This paper summarizes some published results about the cooling systems in vehicles, which include engine cooling system, EGR cooler, air conditioning, the frictional components cooling system. Due to the contribution of electric/hybrid vehicles for reducing fuel consumption, the electronic equipment cooling system is also included. In this paper, we will introduce the engine cooling system, EGR/EGR coolers, air conditioning system, electronic cooling system and frictional components cooling system (including brakes, gearbox and bearings) in Sections 2, 3, 4, 5 and 6, separately. A summary is presented in the final section.

2. ENGINE COOLING SYSTEM

There are two major types of engine cooling systems. One is the air cooling system, the other one is the liquid cooling system. Nowadays the air cooling system is only used in older cars or some modern motorcycles. The liquid cooling system plays an important role in most automobiles. The liquid cooling system contains a coolant, a radiator or other forms of heat exchangers, a radiator cooling fan, one or more circulation pumps, a thermostat and so on. Figure 3 shows a standard liquid cooling system for the engine. The radiator is the heaviest equipment in the engine cooling system. It also occupies most space in the cooling system. Thus it has to be analyzed in detail during the optimization of the engine cooling system. The coolant is also considered here. Thus a clear comprehension of the cooling system can be given. In order to optimize the engine cooling system, some technology will be presented for the whole cooling system.

(See Figure 3 after last section of paper.)

2.1. DIFFERENT COMPONENTS ANALYSIS

2.1.1. Coolant

The engine coolant brings the excess heat from the engine, flows into the radiator where the heat is transferred to the ambient air. Then the coolant is circulated back into the engine for transporting away more heat. In order to ensure that the engine can work in cold weather, the coolant must have antifreezing capability. In this case, the coolant is a mixture of ethylene glycol and water with the ratio of 50%-50%. Debaun et al. [11] stated that the coolant should have corrosion protection and cavitation protection. Meanwhile it should be friendly to elastomer, seal, hose

compatibility. Because of the increasing power densities, the vehicle thermal loads had to increase. The coolant flow rates, turbulence and pressure drops also became serious. These conditions required improvements of the coolant quality. For the future, the extended life and extended service intervalled coolants would take the place of the conventional and traditional fully-formulated coolant. On the other hand, the nanotechnology would be used to improve the thermal conductivities of the coolant. In some case, the engine oil also dissipates heat from the engine. Abou-Ziyan [12] evaluated the thermal characteristics of five engine oils at subcooled boiling conditions. The experimental results showed that the thermal characteristic of engine oils was affected by the additive concentration in the engine oil. The oils with large concentrations of boron, magnesium, phosphorus and zinc provided good heat transfer properties.

2.1.2. Radiator or heat exchanger

If the coolant was the blood of the engine cooling system, then the radiator would be the heart of the engine cooling system. This is to illustrate that the radiator plays a very important role in the engine cooling system. Due to the space limitation in vehicles, a compact heat exchanger is a favorable type as radiators. Cowell et al. [13] introduced some common constraints for the radiator design. Compactness, low pressure drop, low weight, low cost and high volume were considered. The structure of radiators was described, in which there was an array of tubes to carry the hot engine coolant with a secondary surface attached to the outside of the tubes. Meanwhile some methods were presented to reduce the cost during the radiator manufacturing. For instance, the brazing process and the mechanical expansion were good for assembling a radiator.

Experimental or numerical methods are employed to investigate what kinds of radiator shapes are economic and efficient. Because of the high cost and the complexity of experiments, numerical methods are preferred by many researchers. Oliet et al. [14] used numerical methods to carry out parametric studies for automotive radiators. The influence of some geometrical parameters (fin spacing, louver angle and so on) and the importance of coolant flow lay-out on the radiator global performance were studied. The results showed that the air inlet temperature did not affect the overall heat transfer coefficient U_0 (as shown in Fig. 4). On the other hand the coolant flow regime (Re number) had a relationship with U_0 when coolant fluid or coolant flow arrangement varied. Fig. 5 shows that U_0 was increases with increasing Re, even under different flow arrangement (1 pass arrangement (I), 2 pass arrangement (U), 3 pass arrangement (U_{by-3})). When the flow regime was considered acceptable, the U (2 pass flow arrangement) -flow coolant arrangement was not as good as I (1 pass flow arrangement) -flow. Carluccio et al. [15] carried out a numerical study with a thermo-fluid-dynamic analysis for an air-oil compact cross

flow heat exchanger, which was used in ground vehicles. The fin configuration is shown in Fig. 6. For the oil side, the geometry of the offset fins did not cause a high level of turbulence, which can increase convective mass and heat transfer. It only increased the surface area. On the air side three different flow rates were used to estimate the influence of the air channel geometry. Based on a geometrical configuration study, it was found that the heat transfer of the suggested fins (as shown in Fig. 6) can be enhanced twice compared to the straight triangular fins.
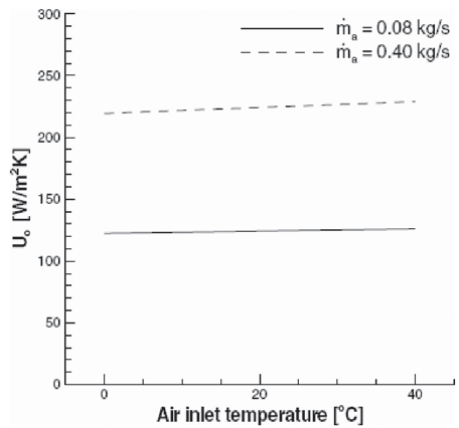

Fig. 4. Air inlet temperature influence on the overall heat transfer coefficient (U_0) [14].
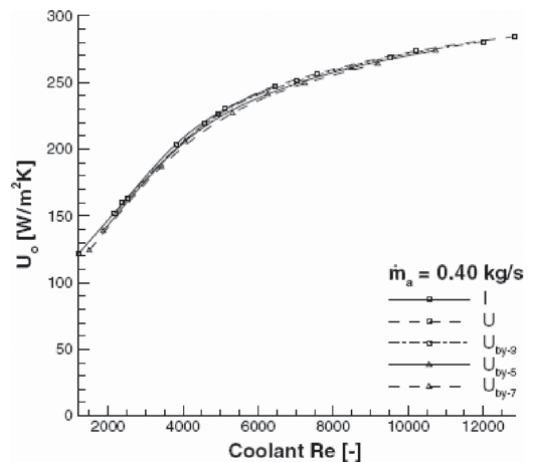

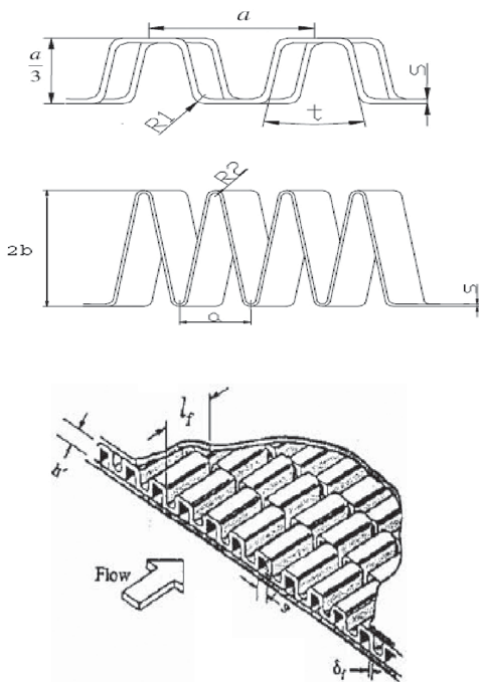**Fig. 5. Coolant lay-out influence on the U_0 [14].**

Fig. 6. The first one is the fin shape on the oil side, the second one is the fin shape on the air side, the last one is a typical offset strip fin core, for oil side [15].

The major material for a radiator is aluminum or copper, due to the high thermal conductivity. In 1997 Oak Ridge National Laboratory developed a new material (graphite foam) with very high thermal conductivity (1700 W/m.K) and high bulk apparent thermal conductivity (40-150 W/m.K). The weight of this foam is only about 1/5 that of aluminum. The open and interconnected void structure leads to a special surface area with 5000 and 50000 m^2/m^3. Klett et al. [16] reported the properties of carbon foams. Fig. 7 shows the photomicrographs of the foams. The bubble size affected the operating pressure. The bulk thermal conductivity was 150 W/m.K and the specific conductivity was six times that of copper. Klett et al. [17] suggested utilizing graphite foams for heat exchangers in heavy vehicles. Because of the high thermal conductivity and the low density (0.47 g/cm^3) of foam, this new heat exchanger was smaller and lighter than the one made by aluminum or copper. The overall heat transfer coefficient was 2500 W/m^2.K, which was much higher than the one of the standard automobile radiator (30 W/m^2.K). But there was a very high pressure drop inside a foam heat exchanger or heat sink, because of its alveolate structure. Leong et al. [18] analyzed four different shapes of a heat sink as shown in Fig. 8. Highest pressure drop (as shown

in Fig. 9) appeared for block and baffle foams. On the other hand, the high thermal conductivity capacity of foams only exists in a special direction. More information about foam thermal performance can be found in [19-20].

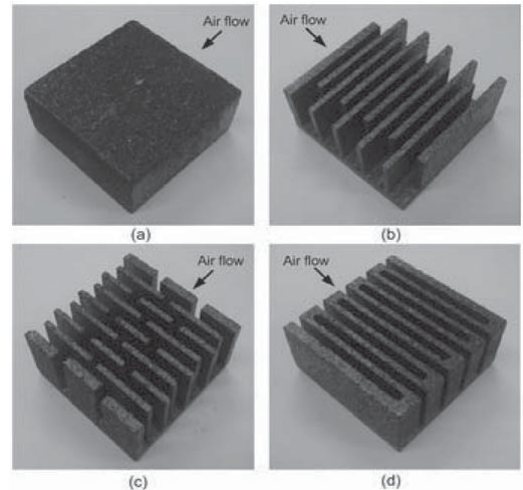(See Figure 7 after last section of paper.)

Fig. 8. Test graphite foam heat sinks of (a) block, (b) staggered, (c) baffle and (d) zigzag configurations [18].
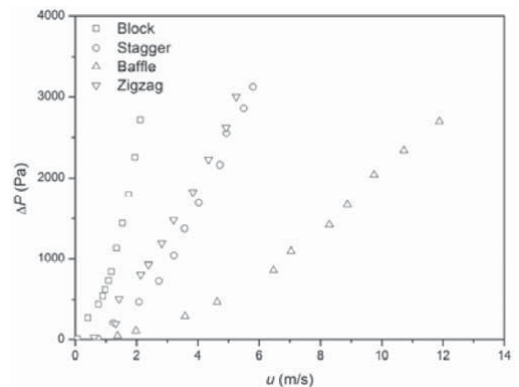

Fig. 9. Pressure drop versus inlet flow velocity of air flow through tested configurations [18].

For the radiator, it is very important to find a suitable manufacturing method, which can reduce the cost and improve the heat transfer performance. Witry et al. [21] introduced an aluminum roll-bonding technique for producing automotive radiators. Fig. 10 shows such an

aluminum roll-bonding design. This method was one of the cheapest methods for heat exchanger manufacturing. For this kind of radiator, the internal heat transfer increased because of the repeated impingement against the dimple obstructions. The heat transfer also increased for the external flow because of the wider and wavy nature of the surface area. As a whole, higher heat transfer levels, lower pressure drop levels, lower overall vehicle drag, smaller size radiators and cheaper manufacturing were the strengths of the roll-bonding heat exchanger design.
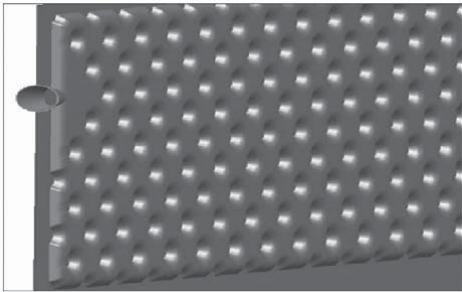

*Fig. 10. Partial dimple plate geometry [*21*].*

2.2. ANALYSIS OF THE WHOLE ENGINE COOLING SYSTEM

2.2.1. Engine cooling simulations

It is useful to analyze the different components of the engine cooling system separately. But an overall comprehensive investigation of the whole engine cooling system would have high possibility to identify the key factors that affect the fuel consumption. Computer simulation is a good tool to understand the cooling performance of a whole cooling system. Kim [22] developed a 3D CFD program to analyze the performance of the vehicle cooling system. Fig. 11 presents the simulation results of flow field around the vehicle. The simulated air speed in front of the radiator only deviated 7.9 % from the test data. The coolant inlet temperature had a linear relationship with the radiator performance. The partial displacement fan or the increased fan power at high speed had no impact on the coolant inlet temperature. Zheng et al. [23] introduced the finite-element method to calculate the thermal field so that the hot spot(s) can be found and the cooling system of the 4QT (a four-quadrant transducer) can be investigated. The result showed that the stator windings were mostly dependent on the water cooling system. However, the forced-air cooling had influence on the inner rotor winding temperature.
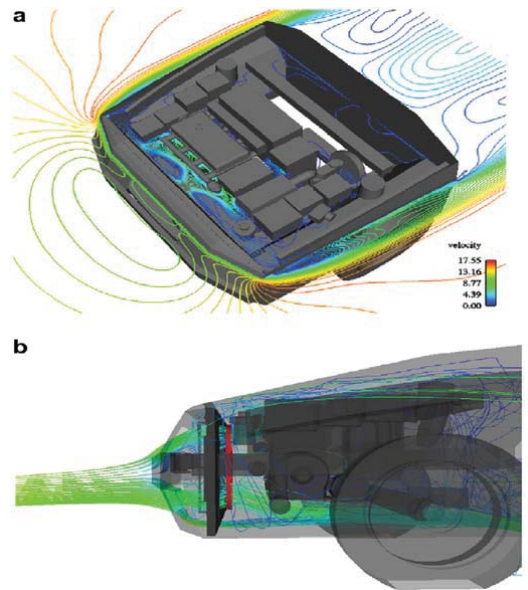

*Fig. 11. "a" shows the contours of the air velocity in the vehicle model, "b" shows the air particle traces through a vehicle model [*22*].*

2.2.2. Important aspects of the performance of engine cooling systems

Some aspects have great influence on the fuel consumption in vehicles. These include the flow field and the thermal management.

2.2.2.1. Flow field

The flow field caused by the movement of the vehicle affects the engine cooling performance. It also has influence on the fuel consumption by the mode of flow resistance. Jurng et al. [24] performed a two-dimensional simulation to analyze the characteristics of the cooling air through the radiator and the engine. The two-dimensional computation was not an excellent tool for predicting three-dimensional flow field. But it was a fast and efficient tool for predicting the flow rate of the cooling air through the radiator. Park et al. [25] also carried out a computer simulation to analyze the thermo-fluid performance of an engine cooling system. There was a good agreement between the simulation and experimental methods for predicting the radiator thermal performance, as shown in Fig. 12. On the other hand, Fig. 13 shows the different changing directions for the engine coolant temperature and the radiator downstream air temperature when the vehicle speed was changing.
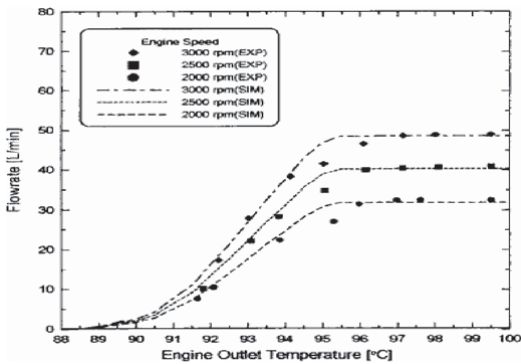
Fig. 12. Variation of coolant flowrate with engine outlet coolant temperature [25].
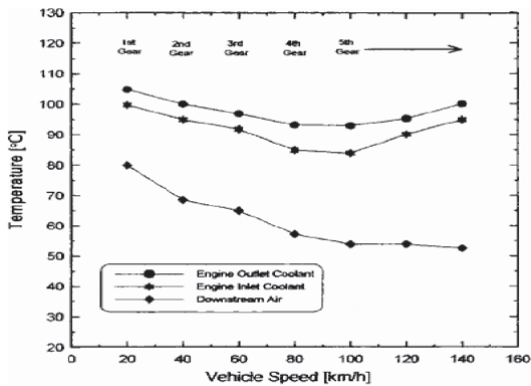

Fig. 13. Variation of coolant temperature with vehicle speed [25].

2.2.2.2. Thermal management

A good thermal management of the engine cooling system can extend the life of the engine and the life of the components in the engine cooling system. Also it has impact on the fuel consumption and carbon dioxide emissions. Electrical components in the engine cooling system have great importance in reducing the power consumption in vehicles, compared to the mechanical ones. Staunton et al. [26] carried out a study to compare several advanced thermal management systems topologies. Fig. 14 shows a thermal management system with an array of small electrical fans instead of one mechanical fan. The results showed that 17 kW power was saved in the micro-hybrid vehicle, when the engine cooling system was fully electrified. 14.5 kW was saved in the standard diesel vehicle. Cho et al. [27] studied the benefit of a controllable electric pump for the cooling performance and the pump operation. By using an electric

pump, the power consumption could be decreased more than 87 %, compared to a mechanical pump. Additionally, the radiator size could be reduced by more than 27 % as an electric pump was used. There are some other methods for thermal management. Staunton et al. [28] studied the difference in thermal loads for the parallel and series drivetrains. It was found that optimizing the cooling fan arrangement and duty cycle can save energy potentially. Salah et al. [29] used a set of servo-motors based cooling system components by a Lyapunov-based nonlinear-control technique. The engine block was maintained at the appointed temperature by the controller. At the same time the power consumption was minimized. According to thermodynamic principles and parameter identification techniques, Vermillion et al. [30] developed a dynamic model for the thermal management system involving heat exchangers and heaters.

(See Figure 14 after last section of paper.)

3. EGR/EGR COOLER

One third of the engine energy is lost to the exhaust gas. Reusing the exhaust gas has a great potential to reduce the fuel consumption. Thus EGR is a good option to achieve this goal. Hountalas et al. [31] used 3D multi-zone model to study the influence of the EGR temperature in a turbocharged DI diesel engine on performance and emissions. It was found that the EGR at high temperature had a negative influence on the brake specific fuel consumption and soot emission. However, EGR cooling had a positive influence on reducing NO_x and soot emission. At high EGR rates and low engine speed, the EGR cooling was more important. The cooler was very important for the performance of the EGR. Abu-Hamdeh [32] used spiral fin heat exchanger pipes for the EGR cooling. As shown in Fig. 15, some part of the exhaust gas was cooled by the heat exchanger pipes before it circulated back to the engine. The intake charge temperature was decreased by using heat exchanger pipes. Because of the heat exchange, the O_2 and CO_2 were reduced in the exhaust gases, while the CO was increased. The cooled EGR also reduced the percentage of NO_x. Huang et al. [33] carried out a numerical simulation to investigate the flow field and temperature distributions inside an EGR cooler. The improved cooler with a helical baffle in the cooling area not only extended the water flow path but also strengthened the swirl flow. Hendricks et al. [34-35] developed an analysis tool to integrate the heat exchanger/thermoelectric power system, so that the influence of heat exchanger and thermoelectric power generator performance would be studied in vehicle waste heat recovery applications. Chen et al. [36] proposed a CO_2 bottoming system to utilize the low-grade energy in the vehicle exhaust gas. About 20 % of the energy in the exhaust gas can be converted into useful work, when the gas heater pressure was 130 bars and the expansion

inlet temperature was 200 °C. As the gas heater pressure was increased to 300 bars, only 12 % of the exhaust gas energy was converted to useful work.

(See Figure 15 after last section of paper.)

4. AIR CONDITIONING

4.1. SIMULATIONS AND EXPERIMENTAL ANALYSIS

Air conditioning is an important system in a vehicle. It includes a laminated type evaporator, a swash plate type compressor, a parallel flow type condenser, a receiver driver and an externally equalized thermostatic expansion valve. The air conditioning offers comfortable environment for passengers or drivers, so that the passengers can enjoy their travelling or the drivers can focus on driving without interaction from the high or low ambient temperature.

Providing thermal comfort is the crucial function of the air conditioning system. Thus it is important to consider the thermal comfort during the optimization of the air conditioning system. Zhang et al. [37-38] used the FLUENT software to carry out a 3D simulation of temperature distributions and flow field in a compartment with or without passengers. Fig. 16 shows the simulated temperature and velocity distribution without passengers. Fig. 17 shows the simulation with four passengers (chest position). It was found that the thermal comfort was affected by the number of people in the compartment under given conditions. The results also showed that a better flow field can improve the uniformity of the temperature field inside the compartment. Saiz Jabardo et al. [39] developed a steady state computer simulation model for refrigeration circuits of automobile air conditioning systems. The evaporator return air temperature affected the refrigeration capacity greatly. On the other hand, the condensing and return air temperatures and compressor speed had a linear relationship with the refrigeration capacity, mass flow rate and coefficient of performance (COP). The deviations between the simulated results and the experimental data was about 10 %, the maximum value was 20 %. Lee et al. [40] carried out a performance study for different components in an automobile air conditioning system. The study showed that an overcharge of 10 % proved to have high COP under different operating conditions. But above 10 % overcharge, the COP dropped down. Trzebinski et al. [41] presented a thermodynamic analysis of a car air cooler. The decrease of the refrigerant charge caused a reduction of the COP. For the system with a thermostatic controlled expansion valve and a controlled compressor, the value of COP was reduced more than the one in non-controlled system.

(See Figure 16 after last section of paper.)

(See Figure 17 after last section of paper.)

Not only simulations but also some experimental analysis have been presented for the automotive air conditioning system. Ratts et al. [42] applied the second law of thermodynamics to quantify the thermodynamic losses in different components of an automotive vapor-compression refrigeration system. They found that compressor cycling and thermal dissipation in the condenser were the biggest sources of losses. By increasing the compressor cycling, the isentropic efficiency of the compressor decreased. Kaynak et al. [43] proved that the increase of the condenser temperature and compressor speed would cause an increase of the cooling capacity. Meanwhile the increase of the air inlet temperature in the evaporator would enhance the evaporator cooling capacity.

4.2. STRATEGIES TO REDUCE FUEL CONSUMPTION

Some vehicle engines not only provide the power for the vehicle movement, but also provide the power to drive the compressor of the air conditioning in compartment. It is a good option to consider the air conditioning together with engine cooling system. Qi et al. [44] combined the air conditioning system with the engine cooling system. A vehicle climate control system model was developed for different operational conditions. It was found that the air conditioning system was affected by the engine cooling system. The value of COP in the air conditioning system was reduced about 10 %, when the air conditioning was combined with the engine cooling system. Meanwhile due to the changes of heat duty of the air conditioning system, the exit temperature of the condenser was high. Kim et al. [45] considered the relationship between a fuel cell stack cooling and air conditioning. With the aid of air conditioning, the heat release from the fuel cell stack could be increased up to 36 % compared to a conventional radiator cooling system without cabin cooling.

Based on reuse of the exhaust gas energy which makes up nearly 30 % of the total vehicle energy consumption, an absorption cooling system was developed for the air conditioning in vehicles. Mostafavi et al. [46] established a thermodynamic model for a combination of a diesel and absorption refrigeration unit. Enough energy can be obtained from the exhaust gas to operate the absorption cooling system for the air conditioning. The cooling performance depended on the cycle configuration in terms of temperature ratio and pressure ratio. Zhang et al. [47] set up a new lumped parameter non-equilibrium model to study the dynamic performance of an absorption cooling system. The results showed that the specific cooling power (SCP) was more sensitive than COP, coefficient of waste heat recovery (WCOP) and coefficient of waste heat cooling (WCOE). In the current absorption cooling system, the requirement of

WCOP can be satisfied, but SCP was not satisfied. Talbi et al. [48] carried out a theoretical analysis for four different configurations of a combined turbocharged diesel engine and an absorption refrigeration unit. The diesel absorption with pre-inter cooling had a higher power output and a thermal efficiency compared to the other configurations. Zhang [49] described an experimental test for absorption cooling systems. The COP of the system was 0.38, and the SCP was 25.7 W/kg. Additional literature about the absorption cooling system driven by exhaust heat can be found in [50,51,52,53].

5. COOLING OF ELECTRONICS AND ELECTRIC EQUIPMENT

Considering saving energy and protecting the environment, many electric vehicles and hybrid electric vehicles (HEV) are used nowadays and their number will be increased in future. Some equipment need to be cooled in a hybrid vehicle. As shown in Fig. 18, the major electric equipment include inverters, batteries and motors. Because of the low working temperature of batteries (i.e., the working temperature of Li-ion battery is 55°C) and the high power density in inverters (about 150-200 W/cm^2), the cooling problems block the development of electric vehicles or hybrid electric vehicles. Thus the cooling electric equipment will play an important role in promoting the application of electric vehicles and hybrid electric vehicles, which are efficient in reducing fuel consumption and CO_2 emission.
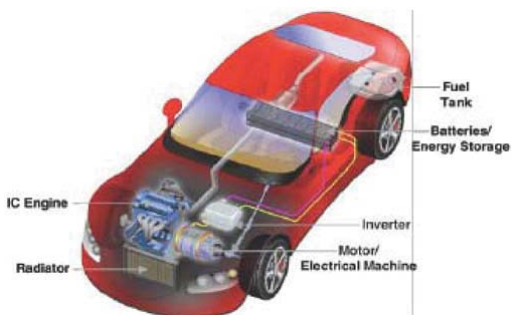

Fig. 18. Propulsion system components for a hybrid vehicle [54].

Advanced cooling techniques are used for electronics cooling in vehicles. Liang et al. [55] developed a direct cooling module for the inverter cooling, and compared it with the conventional water cooling module. The different structures of the direct cooling module and the conventional water cooling module are shown in Fig. 19. The thermal resistance between the inverter case and heat sink was reduced in the direct cooled module. A homogeneous temperature distribution was achieved on the chips. Meanwhile the temperature difference between different phase units was small. Buttay et al. [56] also approved that the direct cooling (i.e., without a heat spreader or base-plate) can reduce the total thermal resistance between junction and ambient up to 40 %, compared to the conventional module. A light and compact inverter can be achieved by the direct cooling method. Ayers et al. [57] used the refrigerant R- 134a as the cooling fluid for the electronic equipment in an HEV cooling system. This cooling fluid can be used in the air conditioning system separately. The volume of the inverters can be reduced more than 50 % and the power of the inverters was still kept at a high level. Sabbah et al. [58] compared the passive cooling by phase change materials (PCM) with the active (forced air) cooling for a compact Li-ion battery pack. The results showed that, when the current increased to 10 A and the ambient temperature was 45 °C, the active cooling did not keep the battery temperature below the working temperature of 55 °C, while the passive cooling had no problem to keep the battery temperature below 55 °C, as shown in Fig. 20. On the other hand, additional fan power was required for the active cooling. It was difficult to get uniform temperature on the battery by the active cooling. This affected the lifetime of battery. Additional literature on electronic cooling can be found in [59,60,61].
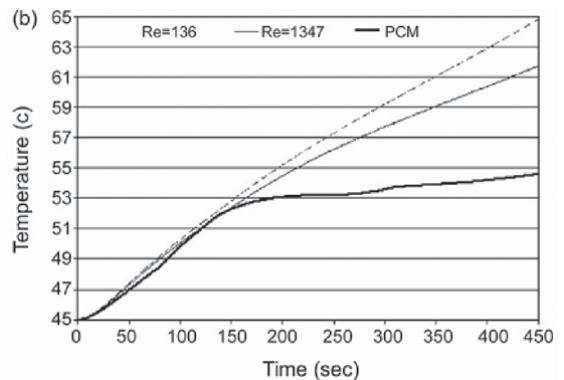
(See Figure 19 after last section of paper.)

Fig. 20. Comparision of cooling systems based on volume averaged cell temperature at 10 A, T_{amb} = 45°C [58].

6. COOLING SYSTEMS FOR FRICTIONAL COMPONENTS

There are some frictional components (i.e., brake rotor, retarder, bearings and gearbox) in a vehicle. Some part of the energy from the fuel consumption in a vehicle is lost to these components due to the action of friction. To reduce this energy loss, it is necessary to carry out a thermal analysis for these frictional parts in the vehicle.

With the rapid development of modern automobile technology and highway construction, vehicle speed is increasing and braking load of vehicles is larger than before. Thus a more powerful brake system is required to ensure the vehicle safety and reliability. The brake rotor generates an opposing torque to a shaft in order to decelerate the vehicle. During the braking process, kinetic energy is converted into thermal energy. Normally the air circulating through the brake rotor can provide the cooling function. McPhee et al. [62] studied a brake rotor in which there were radial fins between the braking surfaces. In this case, some passages were formed to facilitate the air flow for cooling. The detailed structure is shown in Fig. 21. Experimental and analytical methods were used to study the heat transfer and flow field of the brake rotor. It was found that the internal convection varied linearly with the rotor rotational speed. The volume flow rate varied also linearly with the speed. But there was no direct relationship between internal heat transfer coefficients and volume flow rate. Newcomb et al. [63] studied the thermal performance of oil-immersed brakes. The oil-immersed brakes extended the energy range and met the increasing cooling requirement which was caused by the increasing vehicle load and speeds. Kubota et al. [64] carried out a parametric study which included an analysis of the airflow through the ventilation holes and a thermal stress analysis as well as a vibration analysis during braking. A lightweight brake rotor was developed and improvements in all areas of the performance were gained. Much energy in the vehicle is lost due to the heat generating from the braking. If one understands well the thermal process taking place during braking, maybe one would find out how to reduce the energy lost in braking or reuse some energy from the braking. In the end one may enhance the vehicle fuel efficiency.
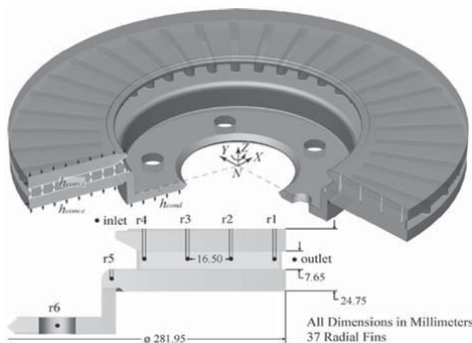

Fig. 21. Brake rotor geometry and thermocouple placement [62].

In cities or mountain area, the vehicles need to brake or reduce the speed frequently. This requirement is difficult to satisfy only by a brake rotor. Using a retarder can solve this problem. There are four types of retarders: exhaust type, engine type, hydraulic type and eddy current type. Lai et al. [65] presented a discussion of the structure and working principles of an eddy current retarder. Tan et al. [66] used an oil-water-exchanger for cooling a hydraulic retarder. The oil-water-exchanger can extract heat from the retarder in time, when the retarder is working. But there was one problem, if the oil-water-exchanger leaked, it would pollute the cooling system. Some patents about the retarder cooling were invented. Gazyakan et al. [67] invented a retarder system with a transmission oil circuit for lubrication and a retarder cooling circuit whose coolant was oil. Enlund et al. [68] invented a cooling system for a vehicle equipped with a retarder. The retarder cooling circuit, which was arranged in a circuit parallel with the radiator, incorporated a retarder cooler and an extra cooling medium pump.

There are some other frictional components in vehicles, for instance bearings and gears. Lubrication is important for these components, not only because of lubrication function but also due to the cooling functions. Henk et al. [69] investigated the fluid flow in gear lubrication in order to optimize the gear box design and explain the mechanism of heat dissipation and power losses. Michaelis et al. [70] analyzed the effect of geometric parameters on the friction losses and cooling oil requirement for bearings and gears. Gear geometry was developed and some of the lost energy was saved.

7. SUMMARY AND CONCLUDING REMARKS

About 70 % fuel energy in vehicles is lost to the cooling systems, which include the engine cooling system, the exhaust gas, other frictional components (i.e., brake rotor), and so on. To find out opportunities to reduce the fuel consumption and carbon dioxide emission in vehicles, a literature survey concerning different cooling systems was carried out. Some important/useful results are shown as follows:

(1). Engine cooling system keeps the engine work at an optimized temperature with minimized fuel consumption. A radiator is the most important component in the engine cooling system. Compactness, low pressure drop, low cost and new material should be considered in the radiator design.

(2). In 10-20 years, the combustion process still will be the major method for generating power in vehicles. Even though EGR has a little effect on reducing the fuel consumption, it plays an important role in reducing emissions. An EGR cooler promotes the EGR application due to the reduced NO_x emission.

(3). Absorption cooling is a good option for reusing the exhaust gas energy to drive the air conditioning system for

the compartment. However, the COP of the absorption cooling is very low.

(4). Electronic cooling system becomes important because of the electric/hybrid vehicles utilization. However, some electronic equipment have very low working temperature. For instance, the working temperature of a battery is about 55 °C. So some new cooling methods have to be used (i.e., using phase change material as a coolant in the battery cooling system).

(5). With increasing vehicle power, much heat is generated in the frictional components. The air around the frictional components can not supply enough cooling. A separate cooling system has to be developed to bring away the frictional heat.

The design of the engine cooling system will become more difficult because of the increasing power and the space limitation in vehicles. The radiator size will be increased so that more heat can be brought away from the engine. But the space inside a vehicle is limited. For future work, much consideration will be given to the radiator design and the arrangement. In addition, the EGR cooler will be studied too, because of the potential of reducing fuel consumption and emission in vehicles.

REFERENCES

1. http://ec.europa.eu/environment/air/transport/co2/co2_home.htm.

2. Davis, S. C., Diegel, S. W., and Boundy, R. G., Transportation Energy Data Book, 28th ed., http://cta.ornl.gov/data/Index.shtml.

3. Knecht, W., "Diesel Engine Development in View of Reduced Emission Standards," *Energy*, **33**: 264-271, 2008.

4. Favre, C., Bosteels, D., May, J., Souza, I. D., Beale, L., and Andersson, J., "An Emissions Performance Evaluation of State-of-the-art Motorcycles Euro 3 and WMTC Drive Cycles," http://www.aecc.eu/en/Publications/Publications.html.

5. Searles, R. A., Bosteels, D., Such, C. H., Nicol, A. J., Andersson, J. D., and Jemma, C. A., "Investigation of the Feasibility of Achieving Euro V Heavy- duty Emissions Limits with Advanced Emission Control Systems," http://www.aecc.eu/en/Publications/Publications.html.

6. May, J., Bosteels, D., Nicol, A., Andersson, J., and Such, C., "The Application of Emissions Control Technologies to a Low-emissions Engine to Evaluate the Capabilities of Future Systems for European and World-harmonised Regulations," http://www.aecc.eu/en/Publications/Publications.html.

7. Bertelsen, B. I., "Future US Motor Vehicle Emission Standards and the Role of Advanced Emission Control Technology in Meeting those Standards," *Topics in Catalysis* **16**(17): 15-22, 2001.

8. Torregrosa, A. J., Broatch, A., Olmeda, P., and Romero, C., "Assessment of the Influence of Different Cooling System Configurations on Engine Warm-up, Emissions and Fuel Consumption," *International Journal of Automotive Technology* **9**(4): 447-458, 2008.

9. Broatch, A., Lujan, J. M., Ruiz, S., and Olmeda, P., "Measurement of Hydrocarbon and Carbon Monoxide Emissions during the Starting of Automotive DI Diesel Engines," *International Journal of Automotive Technology* **9**(2): 129-140, 2008.

10. http://www.answers.com/topic/engine-cooling.

11. DeBaun, H. J., and Alverson, F. C., "Heavy Duty Diesel Engine Coolant Technology: Past, Present, and Future," *Journal of ASTM International* **4**(1): 8-16, 2007.

12. Abou-Ziyan, H. Z., "Heat Transfer Characteristics of Some Oils Used for Engine Cooling," *Energy Conversion and Management* **45**: 2553-2569, 2004.

13. Cowell, T., and Achaichia, N., "Compact Heat Exchangers in the Automobile Industry," presented at Compact Heat Exchangers for the Process Industries, Utah, June 22-27,1997.

14. Oliet, C., Oliva, A., Castro, J., and Perez-Segarra, C. D., "Parametric Studies on Automotive Radiators," *Applied Thermal Engineering* **27**: 2033-2043, 2007.

15. Carluccio, E., Starace, G., Ficarella, A., and Laforgia, D., "Numerical Analysis of a Cross-flow Compact Heat Exchanger for Vehicle Applications," *Applied Thermal Engineering* **25**: 1995-2013, 2005.

16. Klett, J., Hardy, R., Romine, E., Walls, C., and Burchell, T., "High-thermal-conductivity, Mesophase-pitch derived Carbon Foams: Effect of Precursor on Structure and Properties," *Carbon* **38**: 953-973, 2000.

17. Klett, J., Ott, R., and McMillan, A., "Heat Exchangers for Heavy Vehicles Utilizing High Thermal Conductivity Graphite Foams," SAE Technical Paper 2000-01-2207, 2000.

18. Leong, K. C., Jin, L. W., Li, H. Y., and Chai, J. C., "Forced Convection Air Cooling in Porous Graphite Foam for Thermal Management Applications," presented at 11th Intersociety Conference on Thermal and Thermomechanical Phenomena in Electronic Systems, 57-64, 2008.

19. Leong, K. C., Li, H. Y., Jin, L. W., and Chai, J. C., "Convective Heat Transfer in Graphite Foams with Complex Sturctures," presented at Thermal Issues in Emerging Technologies, ThETA 2, Cairo, Egypt, Dec 17-20, 2008.

20. Lafdi, K., Mesalhy, O., and Elgafy, A., "Graphite Foams Infiltrated with Phase Change Materials as Alternative Materials for Space and Terrestrial Thermal Energy Storage Applications," *Carbon* **46**: 159-168.

21. Witry, A., Al-Hajer, M. H., and Bondok, A. A., "Thermal Performance of Automotive Aluminium Plate

Radiator," *Applied Thermal Engineering* **25**: 1207-1218, 2005.

22. Kim, H. J., and Kim, C. J., "A Numerical Analysis for the Cooling Module Related to Automobile Air-conditioning System," *Applied Thermal Engineering* **28**: 1896-1905, 2008.

23. Zheng, P., Liu, R., Thelin, P., Nordlund, E., and Sadarangani, C., "Research on the Cooling System of a 4QT Prototype Machine Used for HEV," *IEEE Transactions on Energy Conversion* **23**(1): 61-67, 2008.

24. Jurng, J., Hur, N., Kim, K. H., and Lee, C. S., "Flow Analysis of Engine Cooling System for a Passenger Vehicle," *KSME Journal* **7**(4): 312-319, 1993.

25. Park, K. S., Won, J. P., and Heo, H. S., "Thermal Flow Analysis of Vehicle Engine Cooling System," *KSME Journal* **16**(7): 975-985, 2002.

26. Staunton, N., Pickert, V., and Maughan, R., "Assessment of Advanced Thermal Management Systems for Micro-hybrid Trucks and Heavy Duty Diesel Vehicles," presented at IEEE Vehicle Power and Propulsion Conference (VPPC), Harbin, China, September 3-5, 2008.

27. Cho, H., Jung, D., Filipi, Z. S., Assanis, D. N., Vanderslice, J., and Bryzik, W., "Application of Controllable Electric Coolant Pump for Fuel Economy and Cooling Performance Improvement," *Journal of Engineering for Gas Turbines and Power* **129**: 239-244, 2007.

28. Staunton, N., Maughan, R., and Pickert, V., "Controlled Cooling in Hybrid Electric Vehicles," *IET HEVC 2008 - Hybrid and Eco-Friendly Vehicle Conference*, 2008.

29. Salah, M. H., Mitchell, T. H., Wagner, J. R., and Dawson, D. M., "Nonlinear-control Strategy for Advanced Vehicle Thermal-management Systems," *IEEE Transactions on Vehicular Technology* **57**(1): 127-137, 2008.

30. Vermillion, C., Sun, J., Butts, K., and Hall, A., "Modeling and Analysis of a Thermal Management System for Engine Calibration," presented at Proceedings of the 2006 IEEE International Conference on Control Applications, Munich, Germany, October 4-6, 2006.

31. Hountalas, D. T., Mavropoulos, G. C., and Binder, K. B., "Effect of Exhaust Gas Recirculation (EGR) Temperature for Various EGR Rates on Heavy Duty DI Diesel Engine Performance and Emissions," *Energy* **33**: 272-283, 2008.

32. Abu-Hamdeh, N. H., "Effect of Cooling the Recirculated Exhaust Gases on Diesel Engine Emissions," *Energy Conversion and Management* **44**: 3113-3124, 2003.

33. Huang, Y. Q., Yu, X. L., and Lu, G. D., "Numerical Simulation and Optimization Design of the EGR Cooler in Vehicle," *Journal of Zhejiang University Science A* **9**(9): 1270-1276, 2008.

34. Hendricks, T. J., and Lustbader, J. A., "Advanced Thermoelectric Power System Investigations for Light-duty

and Heavy Duty Applications: Part I," presented at 21st International Conference on Thermoelectrics, pp. 381-386, 2002.

35. Hendricks, T. J., and Lustbader, J. A., "Advanced Thermoelectric Power System Investigations for Light-duty and Heavy Duty Applications: Part II," presented at 21st International Conference on Thermoelectrics, pp. 387-394, 2002.

36. Chen, Y., Lundqvist, P., and Platell, P., "Theoretical Research of Carbon Dioxide Power Cycle Application in Automobile Industry to Reduce Vehicle's Fuel Consumption," *Applied Thermal Engineering* **25**: 2041-2053, 2005.

37. Zhang, H. J., Dai, L., Xu, G. Q., Li, Y., Chen, W., and Tao, W. Q., "Studies of Air-flow and Temperature Fields Inside a Passenger Compartment for Improving Thermal Comfort and Saving Energy. Part I: Test/numerical Model and Validation," *Applied Thermal Engineering* **29**: 2022-2027, 2009.

38. Zhang, H. J., Dai, L., Xu, G. Q., Li, Y., Chen, W., and Tao, W. Q., "Studies of Air-flow and Temperature Fields Inside a Passenger Compartment for Improving Thermal Comfort and Saving Energy. Part II: Simulation Results and Discussion," *Applied Thermal Engineering* **29**: 2028-2036, 2009.

39. Saiz Jabardo, J. M., Gonzales Mamani, W., and Ianella, M. R., "Modeling and Experimental Evaluation of an Automotive Air Conditioning System with a Variable Capacity Compressor," *International Journal of Refrigeration* **25**: 1157-1172, 2002.

40. Lee, G. H., and Yoo, J. Y., "Performance Analysis and Simulation of Automobile Air Conditioning System," *International Journal of Refrigeration* **23**: 243-254, 2000.

41. Trzebinski, D., and Szczygiel, I., "Thermal Analysis of Car Air Cooler Unit," presented at 7th World Conference on Experimental Heat Transfer, Fluid Mechanics and Thermodynamics, Krakow, Poland, 28 June-03 July, 2009.

42. Ratts, E. B., and Steven, B. J., "An Experimental Analysis of Cycling in an Automotive Air Conditioning System," *Applied Thermal Engineering* **20**: 1039-1058, 2000.

43. Kaynakl, Ö., and Horuz, I., "An Experimental Analysis of Automotive Air Conditioning System," *Int. Comm. Heat Mass Transfer* **30**(2): 273-284, 2003.

44. Qi, Z. G., Chen, J. P., and Chen, Z. J., "Analysis and Simulation of Mobile Air Conditioning System Coupled with Engine Cooling System," *Energy Conversion and Management* **48**: 1176-11784, 2007.

45. Kim, S. C., Won, J. P., Park, Y. S., Lim, T. W., and Kim, M. S., "Performance Evaluation of a Stack Cooling System Using CO_2 Air Conditioner in Fuel Cell Vehicles," *International Journal of Refrigeration* **32**: 70-77, 2009.

46. Mostafavi, M., and Agnew, B., "Thermodynamic Analysis of Combined Diesel Engine and Absorption Refrigeration Unit-naturally Aspirated Diesel Engine," *Applied Thermal Engineering* **17**(5): 471-478, 1997.

47. Zhang, L. Z., and Wang, L., "Performance Estimation of an Adsorption Cooling System for Automobile Waste Heat Recovery," *Applied Thermal Engineering* **17**(12): 1127-1139, 1997.

48. Talbi, M., and Agnew, B., "Energy Recovery from Diesel Engine Exhaust Gases for Performance Enhancement and Air Conditioning," *Applied Thermal Engineering* **22**: 693-702, 2002.

49. Zhang, L. Z., "Design and Testing of an Automobile Waste Heat Adsorption Cooling System," *Applied Thermal Engineering* **20**: 103-114, 2000.

50. Suzuki, M., "Application of Adsorption Cooling Systems to Automobiles," *Heat Recovery Systems & CHP* **13**(4): 335-340, 1993.

51. Agnew, B., Talbi, M., and Mostafavi, M., "Combined Power and Cooling, an Analysis of the Combined Diesel-absorption Cycle," *Applied Thermal Engineering* **19**: 1097-1105, 1999.

52. Qin, F., Chen, J. P., Lu, M. Q., Chen, Z. J., Zhou, Y. M., and Yang, K., "Development of a Metal Hydride Refrigeration System as an Exhaust Gas-driven Automobile Air Conditioner," *Renewable Energy* **32**: 2034-2052, 2007.

53. Hilali, I., and Söylemez, M. S., "On the Optimum Sizing of Exhaust Gas-driven Automotive Absorption Cooling Systems," *Int. J. Energy Res.* **32**: 655-660, 2008.

54. Mudawar, I., "Two-phase Spray Cooling of Hybrid Vehicle Electronics," *IEEE Transactions on Components and Packaging Technologies* **32**: 501-512, 2009.

55. Liang, Z. H., and Li, L., "HybridPACK2-advanced Cooling Concept and Package Technology for Hybrid Electric Vehicles," presented at IEEE Vehicle Power and Propulsion Conference (VPPC), Harbin, China, September 3-5, 2008.

56. Buttay, C., Rashid, J., Johnson, C. M., Ireland, P., Udrea, F., Amaratunga, G., and Malhan, R. K., "High Performance Cooling System for Automotive Inverters," presented at 2007 European Conference on Power Electronics and Applications, pp. 1-9, 2007.

57. Ayers, C. W., Conklin, J. C., Hsu, J. S., and Lowe, K. T., "A Unique Approach to Power Electronics and Motor Cooling in a Hybrid Electric Vehicle Environment," presented at 2007 IEEE Vehicle Power and Propulsion Conference, pp. 102-106, 2007.

58. Sabbah, R., Kizilel, R., Selman, J. R., and Al-Hallaj, S., "Active (Air-Cooled) vs. Passive (Phase Change Material) Thermal Management of High Power Lithium-ion Pack: Limitation of Temperature Rise and Uniformity of Temperature Distribution," *Journal of Power Sources* **182**: 630-638, 2008.

59. Al-Hallaj, S., and Selman, J. R., "Thermal Modeling of Secondary Lithium Batteries for Electric Vehicle/hybrid Electric Vehicle Applications," *Journal of Power Sources* **110**: 341-348, 2002.

60. Zhang, L. H., Yang, X., Wang, F., and Wang, Z. A., "Pressure Contact Packaging for Hybrid Electric Vehicle Drive," presented at 2007 IEEE Power Electronics Specialists Conference, pp. 2228-2233, 2007.

61. Zhang, H. Y., Pinjala, D., and Teo, P. S., "Thermal Management of High Power Dissipation Electronic Packages: from Air Cooling to Liquid Cooling," presented at Electronics Packaging Technology, 2003 5th conference (EPTC 2003), pp. 620-625, 2003.

62. McPhee, A. D., and Johnson, D. A., "Experimental Heat Transfer and Flow Analysis of a Vented Brake Rotor," *International Journal of Thermal Sciences* **47**: 458-467, 2008.

63. Newcomb, T. P., and El-Sherbiny, M., "Liquid-cooled Disc Brakes," *Wear* **34**: 311-317, 1975.

64. Kubota, M., Hamabe, T., Nakazono, Y., Fukuda, M., and Doi, K., "Development of a Lightweight Brake Disc Rotor: a Design Approach for Achieving an Optimum Thermal, Vibration and Weight Balance," *JSAE Review* **21**: 349-355, 2000.

65. Lai, N. H., Wu, L. M., Wang, G. T., and Li, Z. G., "Research on Automotive Eddy Current Retarder and its Virtual Testing and Simulation," *ICEMI*: 166-169, 2007.

66. Tan, G., Guo, X., and Yang, T., "Simulation Based Heavy Truck Driveline Components Thermal Analysis System," presented at 9th International Conference on Electronic Measurement&Instruments, pp: 675-680, 2009.

67. Gazyakan, U., Baasch, D., and Altvater, R., "Retarder System," US Patent 6,817,455 B1, Nov. 16, 2004.

68. Enlund, B., Ångström, H., and Thoms, E., "Cooling System for a Vehicle Equipped with a Retarder", International Publication No.: WO95/01500, Jan. 12, 1995.

69. Li, L., Versteeg, H. K., Hargrave, G. K., Potter, T., and Halse, C., "A Study of Fluid Flow of Gear Lubrication in a Spur Gear Box," *VDI Berichte:* 133-146, 2008.

70. Michaelis, K., and Wimmer, A., "Gearboxes with Minimised Power Loss," *VDI Berichte:* 1451-1465, 2005.

CONTACT INFORMATION

Division of Heat Transfer, Department of Energy Sciences
Lund University
P.O.Box 118, S-22100, Lund, Sweden
Tel: 46-46-2228605
Fax: 46-46-2224717

Wamei.Lin@energy.lth.se
Bengt.Sunden@energy.1th.se

ACKNOWLEDGMENT

NOMENCLATURE

a

Fin pitch [m]

b

Half dimension triangular section [m]

h_{conve}

Convection heat transfer coefficienct [$W.m^{-2}.K^{-1}$]

h′

Plate spacing in offset strip fin [m]

I

1 pass flow arrangement

l_f

Fin length in offset strip fin [m]

$\dot{m}_a$

Air mass flow [$kg.s^{-1}$]

R

Radius [m]

Re

Reynolds number

R-134a

Refrigerant

s

Fin thickness [m]

t

Angle [rad]

T_{amb}

Ambient temperature [°C]

U

2 pass flow arrangement

u

Air velocity [$m.s^{-1}$]

U_{by-3}

3 pass flow arrangement

U_0

The overall heat transfer [$W.m^{-2}.K^{-1}$]

δ_f

Fin metal thickness in offset strip fin [m]

Δ P

Pressure drop [Pa]

Abbreviations

CO

Carbon monoxide

COP

The coefficient of performance

CO_2

Carbon dioxide

EGR

Exhaust gas recirculation

E85

A mixture of up to 85% denatured fuel ethanol and gasoline or other hydrocarbon by volume

GDP

Gross domestic product

HC

Hydrocarbon

HEV

Hybrid electric vehicle

IC

Internal combustion

J

Junctions

M

Microcracking

PCM

Phase change material

P2

Opening 2

SCP

The specific cooling power

WCOE

Coefficient of waste heat cooling

WCOP

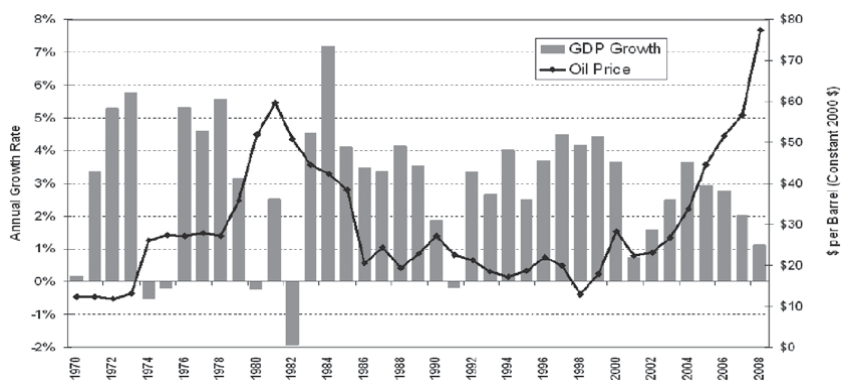Coefficient of waste heat recovery

Fig. 1. Oil price and economic growth, 1970-2008 [2].
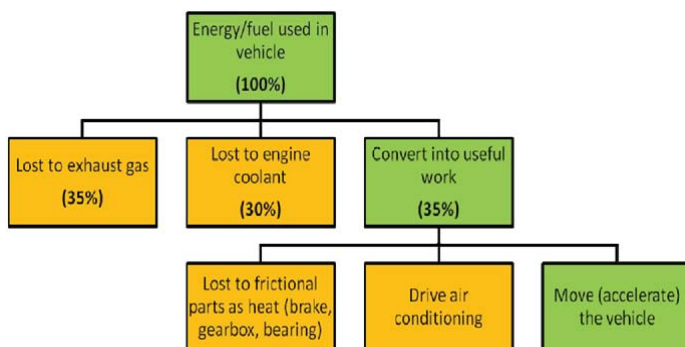

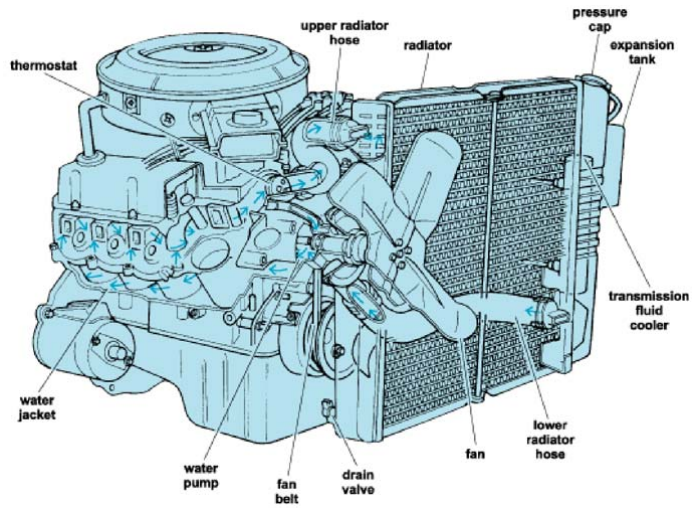*Fig. 2. Energy distribution in a vehicle*

*Fig. 3. Engine cooling system [*10*].*

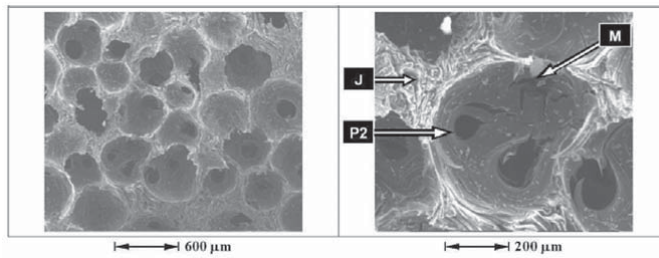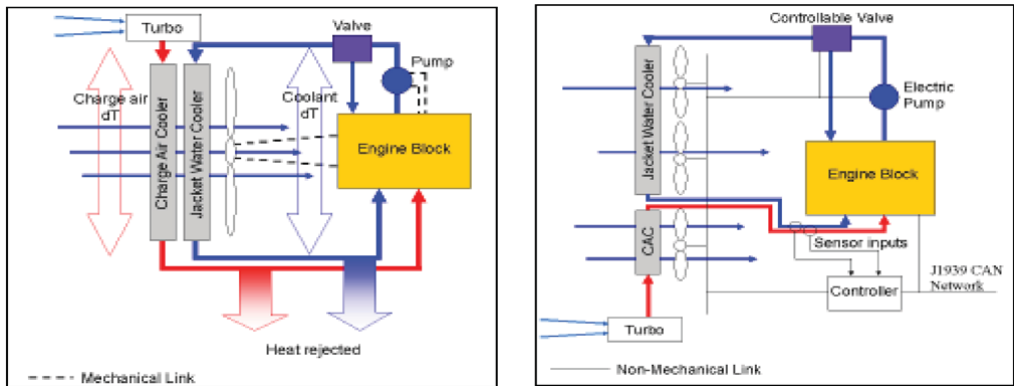*Fig. 7. Photomicrographs of the foams [*16*].*

Fig. 14. Left side shows a schematic of a standard diesel engine cooling system, right side shows a fully electric advanced thermal management systems [26].
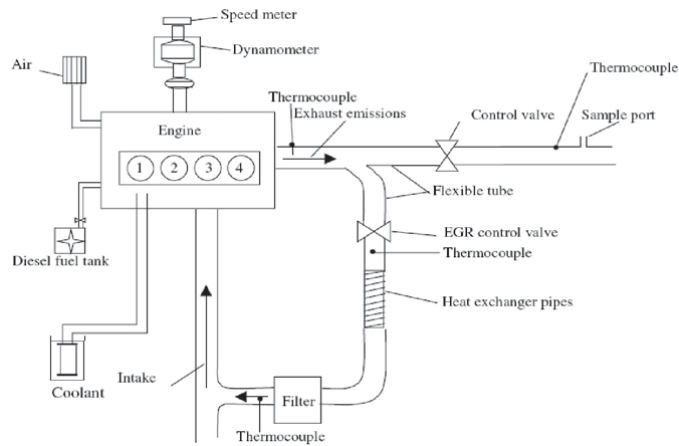

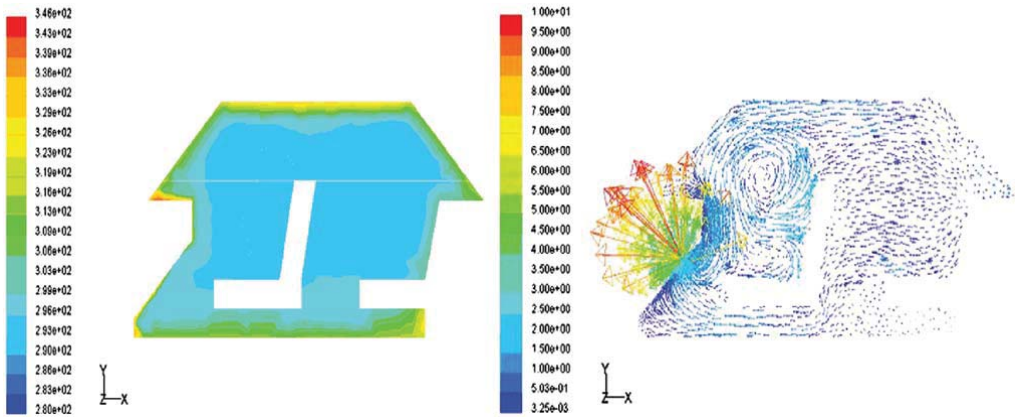*Fig. 15. Schematic arrangement of the cooled EGR system [32].*

Fig. 16. Left side shows the temperature distribution of the copilot side surface (z=-0.35 m), right side shows velocity distribution of the copilot side surface (z=-0.35 m) [38].
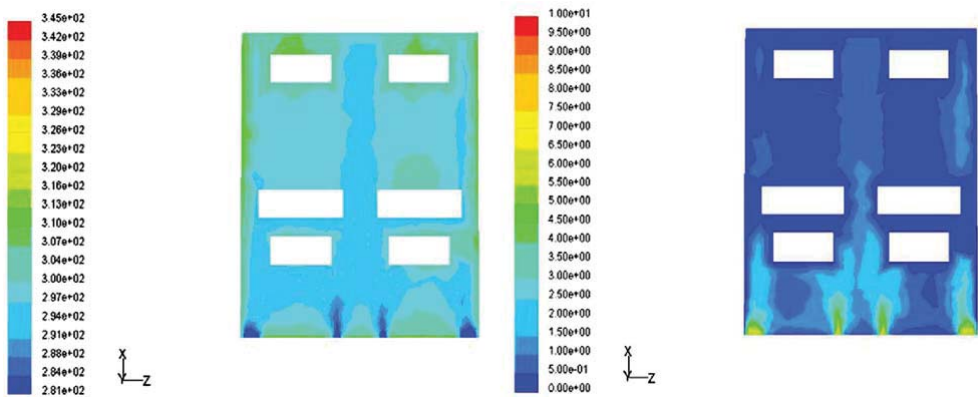

Fig. 17. Left side shows temperature distributions of chests (Y=-0.6 m) on horizontal plane, right side shows velocity distributions of chests (Y=-0.6 m) on horizontal plane [38].
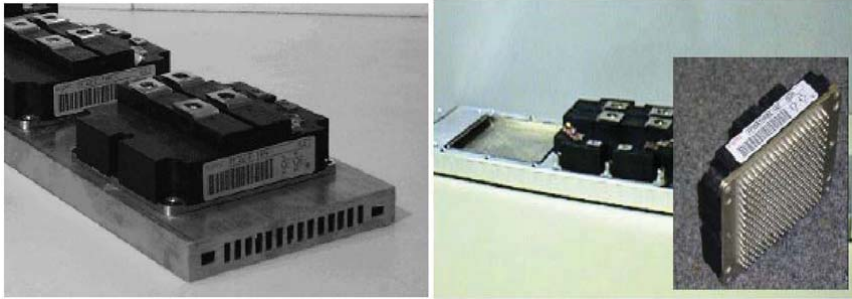
Fig. 19. Left side shows a conventional water cooling module, right side shows a direct cooled module [54].

Table 1. Truck and bus registrations for selected countries, 1998-2007 [2] (thousands)

Year	China	India	Japan	France	UK	Germany	Canada	USA	World total
1998	8313	2610	20919	5500	3169	4357	3694	79062	179498
1999	9400	3000	20559	5609	3392	3370	722	86640	188367
2000	9650	2390	20211	5753	3361	3534	739	85579	203273
2001	10212	2663	19985	5897	3412	3592	729	87969	207033
2002	10500	3535	17714	5984	3487	3568	724	91120	210776
2003	17222	4025	17312	6068	3569	3541	740	95262	223729
2004	19800	4190	17012	6139	3696	3540	745	98576	233537
2005	21750	4415	16734	6198	3943	3133	786	104788	245798
2006	24000	4850	16731	6230	4041	2766	841	109596	256222
2007	26336	5327	16505	6297	4164	2837	872	113477	266236
Average annual percentage change									
1998-2007	13.2%	7.1%	-2.6%	1.7%	1.3%	-0.9%	-11.9%	3.6%	3.3%

Table 2. Highway transportation petroleum consumption by mode, 1970-2007 [2] (thousands of barrels per day)

Year	Cars	Light trucks	Light vehicles subtotal	Motor-cycles	Buses	Heavy trucks	Highway subtotal	Total transportation
1997	4559	3222	7781	13	91	1949	9834	11777
1998	4677	3292	7969	13	93	2012	10086	12061
1999	4780	3448	8228	14	96	2212	10550	12639
2000	4766	3453	8219	14	98	2298	10630	12792
2001	4798	3491	8290	13	93	2295	10690	12672
2002	4923	3602	8525	12	91	2401	11029	12938
2003	4866	3963	8829	12	90	2334	11265	13108
2004	4919	4137	9055	13	92	2162	11323	13344
2005	5050	3840	8890	12	93	2426	11422	13537
2006	4893	3959	8852	14	94	2476	11436	13605
2007	4850	4032	8883	16	92	2515	11505	13710
Average annual percentage change								
1997-2007	0.6%	2.3%	1.3%	2.1%	0.1%	2.6%	1.6%	1.5%

Table 3. Emissions of carbon monoxide from highway vehicles, 1970-2005 [2] (million short tons)

Source category	1970	1980	1990	1995	2000	2005	Percent of total, 2005
Gasoline powered							
Light vehicles & motorcycles	119.4	98.21	67.24	46.54	36.40	24.19	50.2%
Light trucks	22.27	28.83	32.23	29.81	27.04	21.19	43.9%
Heavy vehicles	21.27	15.35	8.92	5.96	3.42	1.97	4.1%
Total	162.68	142.39	108.39	82.31	66.86	47.35	98.2%
Diesel powered							
Light vehicles	0.01	0.03	0.04	0.02	0.01	0.01	0.0%
Light trucks	0.06	0.05	0.03	0.02	0.01	0.01	0.0%
Heavy vehicles	0.49	1.36	1.81	1.53	1.19	0.85	1.8%
Total	0.56	1.43	1.87	1.57	1.20	0.87	1.6%
Total							
Highway vehicles total	**163.23**	**143.83**	**110.26**	**83.88**	**68.06**	**48.22**	**100.0%**
Percent diesel	0.3%	1.0%	1.7%	1.9%	1.8%	1.8%	

Table 4. Alternative fuel consumption, 2003-2007 [2] (thousand of gasoline-equivalent gallons)

	2003	2004	2005	2006	2007
Liquified petroleum gas	224697	211883	188171	173130	152360
Compressed natural gas	133222	158903	166878	172011	178585
Liquified natural gas	13503	20888	22409	23474	24594
E85[a]	26376	31581	38074	44041	54091
Electricity[b]	5141	5269	5219	5104	5037
Hydrogen	2	8	25	41	66
Biodiesel	18220	28244	91649	260606	c
Other	0	0	2	2	2
Total	**421161**	**456766**	**512427**	**678409**	**c**

a: Consumption includes gasoline portion of the mixture;
b: Vehicle consumption only, does not include power plant inputs;
c: Data are not available.

SAE *International*

Paper 2

Review on graphite foam as thermal material for heat exchangers

Wamei Lin, Jinliang Yuan, Bengt Sundén*

Department of Energy Sciences, Lund University, P.O.Box 118, SE-22100, Lund, Sweden
* Corresponding author. Tel: +46 46 2228605, Fax: +46 46 2224717, E-mail: bengt.sunden@energy.lth.se

Abstract: Due to the increased power consumptions in equipment, the demand of effective cooling methods becomes crucial. Because of the small scale spherical pores, graphite foam has huge specific surface area. Furthermore, the thermal conductivity of graphite foam is four times that of copper. The density of graphite foam is only 20 % of that of aluminum. Thus, the graphite foam is considered as a novel highly - conductive porous material for high power equipment cooling applications. However, in the commercial market, aluminum and copper are still the preferred materials for thermal management nowadays. In order to promote the graphite foam as a thermal material for heat exchangers, an overall understanding of the graphite foam is needed. This paper describes the structure of the graphite foam. Based on the special structure, the thermal properties and the flowing characteristics of graphite foam are outlined and discussed. Furthermore, the application of graphite foam as a thermal material for heat exchangers is highlighted for electronic packages and vehicle cooling systems. The physical problems and other aspects, which might block the development of graphite foam heat exchangers, are pointed out. Finally, several useful conclusions and suggestions are given to promote the development of graphite foam heat exchangers.

Keywords: Graphite foam, heat exchanger, thermal management

1. Introduction

Nowadays the power of equipment is increased. For instance, the power of computer chips is increased, and the power of vehicle engines is also increased. This increased power leads to a requirement of an effective cooling method. Currently the thermal management has focused on aluminum and copper heat exchangers, because of high thermal conductivity (180 W/(m.K) for aluminum 6061 and 400 W/(m.K) for copper). However, when the density is considered, the specific thermal conductivity of aluminum or copper (thermal conductivity divided by specific gravity) is only 54 and 45 W/(m.K), respectively. Thus, when the weight is a significant factor, it is necessary to introduce a thermal material with low density, high thermal conductivity and large specific surface area.

An efficient thermal management method is the utilization of microcellular foam materials such as metal or graphite foams, based on the enhancement of heat transfer by huge fluid-solid contact surface area and the fluid mixing. An example of graphite foam application was developed at Oak Ridge National Laboratory (ORNL) in 1997. Klett et al. [1] found that the thermal conductivity of the solid component of graphite was as high as 1700 W/(m.K), which was around four times that of copper. The effective thermal conductivity of graphite foam was more than 150 W/(m.K), which was higher than the value of aluminum foam (2 - 26 W/(m.K)). On the other hand, the density of graphite foam was 0.2 - 0.6 g/cm^3, which was only 1/5 of that of aluminum. The specific surface area was between 5000 and 50000 m^2/m^3.

Because of the high thermal conductivity, low density and large specific surface area, the graphite foam is recognized as an appropriate material for the thermal management. It is primarily focused on the electronic power heat sinks. A large number of studies have been carried out to analyze graphite foam heat exchangers. However, in the commercial market of heat exchangers, aluminum and copper are still the preferred thermal material. Thus, there are several problems blocking the development of graphite foam heat exchangers. Otherwise the graphite foam heat exchangers would be easily found in the market.

In order to promote the development of graphite foam as a thermal material for heat exchangers, this paper will present an overall view or conception about graphite foam heat exchangers. Firstly, the structure of graphite foam is introduced in Section 2. Based on the structure of graphite foam, the thermal properties and flow characteristics of graphite foam are explained in Section 2 as well. After that, the application of graphite foam heat exchangers is outlined in Section 3. In Section 4, potential problems blocking the development of graphite foam heat exchangers are pointed out. Based on the review and analysis, several useful conclusions and suggestions are highlighted in Section 5.

2. Structures and properties of graphite foam

2.1. Structures

Carbon foams were first developed in the late 1960s as reticulated vitreous (glassy) foam [2]. The initial carbon foams were made by pyrolysis of a thermosetting polymer foam to obtain a carbonaceous skeleton or reticulated vitreous carbon (RVC) foam. A blowing technique or pressure release is utilized to produce foam of the pitch precursor. Then the pitch foam is stabilized by heating in air or oxygen for many hours to cross-link the structure, and 'set' the pitch. In this case, the foam does not melt during the further heat treatment. However, stabilization can be a very time consuming and expensive process depending on the pore size. So ORNL [3] developed a new, little time consuming process to fabricate pitch - based graphitic foams without the traditional blowing and stabilization steps. This new foam is believed to be less expensive and easier to fabricate than the traditional foams.

Klett et al. [1] gave an overall view of the structure of the new graphite foam. The average pore diameter is from 275 to 350 μm in the ARA24 - derived foams. The scanning electron micrographs of fracture surfaces, which reveals the pore structure of the ARA24 - derived foams heat - treated at 1000 ℃, are shown in Fig. 1. Inside the foam, there are many spherical pores with small openings. These pores are three - dimensionally interconnected.
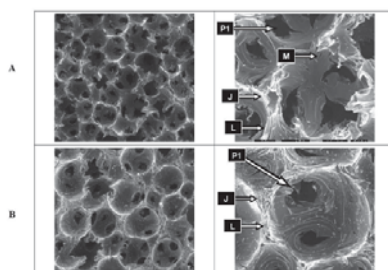

Fig. 1. Photomicrographs of the foams produced from Mitsubishi ARA 24 pitch at different densities A < B (P1: opening pore; M: microcrack; J: junction; L: ligament)[1].

2.2. Thermal properties of graphite foam

Because of the special structure of graphite foam, there are several prominent thermal properties in the graphite foam. The graphite foam made by the ORNL process exhibits high effective thermal conductivity (up to 182 W/(m.K)) and low density (0.2 -0.6 g/cm^3). The data in Table 1 show that the thermal conductivity in the z – plane is much larger than the one in the x – y plane. It implies that the high thermal conductivity of the graphite foam only exists in a certain direction. This is a disadvantage of the graphite foam. Klett et al. [4] found out that the heat inside the graphite lattice was transferred down the graphite lattice fast, because of the very stiff nature of the covalent bonds (as shown in Fig. 2). Moreover, the position and

vibration of atoms in the neighboring planes may impede the vibration of atoms in the plane of interest. The crystal perfection controls the thermal performance. In order to achieve high thermal conductivity in the graphite crystal, the structure must be comprised of aligned, straight grapheme planes, and so on.

Table 1. Properties of various graphite foams made by the ORNL method compared to Poco Foam[4].

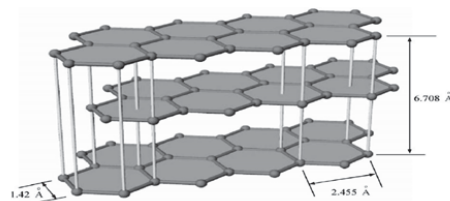|	Graphitiza-tion rate ($℃$/min)	Average bulk density (g/cm^3)	z -Plane thermal conductivity k_z (W/(m.K))	x-y Plane thermal conductivity k_{xy} (W/(m.K))
ORNL graphite foam (A)	10	0.45	125	41
ORNL graphite foam (B)	1	0.59	181	60
PocoFoam^{TM}	-	0.61	182	65

Fig. 2. Planar structure of hexagonal graphite [4].

On the other hand, Yu et al. [5] presented a model which was based on sphere - centered and interconnected unit cubes. The effective thermal conductivity was proved to be a function of the porosity of the graphite foam. Tee et al. [6] used a tapered, anisotropic strut model to predict the overall thermal conductivity of the porous graphite foam. When the size of the foam pores was increased, the convective heat transfer coefficient of the foam was reduced. By using graphite foams as the heat sinks, the enhancement of the convective heat transfer was not only because of its open and inter-connected pores, but also due to its high thermal conductivity and the extremely large surface areas. Furthermore, Straatman et al. [7] validated that the optimal thickness of graphite foam was 3 mm based on the thermal performance. Meanwhile the heat transfer increase was 28 % at low Reynolds numbers (150000). However, at high Reynolds number, the increase of the heat transfer was only 10 %.

2.3. Pressure drop of graphite foam

Graphite foam has a very high thermal conductivity, but it also has very high pressure drop, due to the large hydrodynamic loss associated with the open pores in the graphite foam [8]. Leong et al. [9] investigated pressure drop of four different configurations of graphite foams (as shown in Fig. 3). The pressure drops of these four configurations of graphite heat sinks are shown in Fig. 4. For the same inlet flow velocity, the block and baffle foams present the highest and the lowest pressure drop, respectively. On the other hand, Lin et al. [10] approved that the pressure drop through the corrugated passages could be reduced significantly while maintaining a high heat transfer coefficient. As shown in Fig. 5, for forced convection, the air is forced to go through a thin porous wall of graphite foam. Due to the short flow length inside the graphite foam, the pressure drop could be reduced greatly.

2.4. Advantages and disadvantages

Based on the special microscopic structures in graphite foams, the advantages of these materials can be summarized:

(1) High thermal conductivity (thermal conductivity of solid graphite is 1700 W/(m.K), and the effective thermal conductivity of graphite foam is more than 150 W/(m.K));
(2) Low density (0.2 to 0.6 g/cm^3);
(3) High specific surface area (5000 to 50000 m^2/m^3);

On the other hand, there are some disadvantages for the graphite foam materials:
(1) High thermal conductivity only exists in a certain direction;
(2) Due to the small scale pores and complex structures of the foam, the pressure drop through graphite foam is very high.
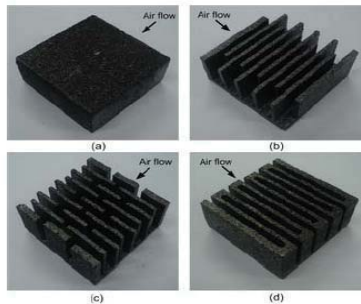

Fig. 3. Tested graphite foam heat sinks of (a) block, (b) staggered, (c) baffle and (d) corrugated configurations [9].
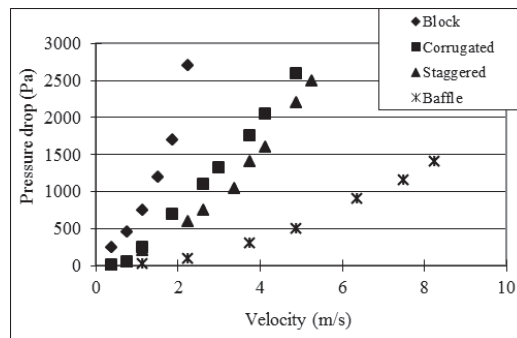
Fig. 4. Pressure drop versus inlet flow velocity of air flow through tested configuration [9].
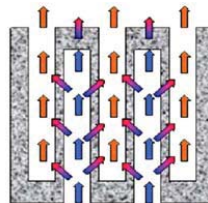
Fig. 5. Flow path inside the corrugated foam [10].

3. Applications of graphite foams

Due to the high thermal conductivity, low density and large specific surface area, the graphite foam is a good thermal material for heat exchangers or heat sinks. The major applications of graphite foam as materials for heat exchangers are: electronic package cooling, vehicle cooling systems, energy storage systems, and others.

3.1. *Electronic package cooling*

Because of the large internal interfaces and the high thermal conductivity, the usage of graphite foam is considered as an effective cooling method to dissipate the high heat flux in electronic equipment. Furthermore, the coolant of electronic equipment can be air instead of water, due to the high thermal conductivity of graphite foam. The removal of water can avoid shorting the circuitry of electronic equipment by water leakage.

Gallego et al. [11] demonstrated that the foam-based heat sink can be used to reduce the volume of the required cooling fluid or eliminate the water cooling system altogether. In terms of thermal performance, the graphite foam is much better than the aluminum. Meanwhile, the graphite foam heat sinks respond to transient loads faster than the traditional aluminum heat sinks. This response time may be crucial for the power electronics. Williams et al. [12] investigated several different channel - insert configurations as mini - heat exchangers by using both copper fins and graphite foams. The graphite foam was proved to have strong potential as a mini - heat exchanger.

On the other hand, the usage of thermosyphons in the thermal management of electronics is established and the methods for evaporator enhancement are of interest. Gandikota et al. [13] investigated the cooling performance of graphite foams for evaporator enhancement in thermosyphons and in pool boiling with FC-72 as the operating fluid. The exhibited thermal resistance was very low, averaging at about 0.024 K/W at low heat flux. The thermal resistance rose with increasing heat flux, but still remained very low. Lu et al. [14] used the graphite foam as a wick in a vapor chamber. With ethanol as the coolant, the vapor chamber (25 mm x 25 mm x 6 mm) had been demonstrated at a heat flux of 80 W/cm^2. The results showed that the performance of a vapor chamber using graphite foam was about twice that of one using a copper wick structure. Furthermore, Coursey et al. [15] found that 149 W heat load could be dissipated from a 1 cm^2 heated base at the operating temperature of 52 ℃, by usage of a graphite foam thermosyphon evaporator.

3.2. *Vehicle cooling systems*

Another important utilization of the graphite foam heat exchangers is in vehicle cooling systems. Because of the low density and large specific surface area, it might lead to a light and compact heat exchanger in vehicles. Meanwhile, graphite foam is considered as a potential material to solve critical heat rejection problems that must be solved before fuel cell and advanced power electronics technologies are introduced into automobiles.

The graphite foam could be utilized to produce a light and compact radiator in vehicles. In this case, the radiator might be placed away from the front of vehicles. If the size of the front of vehicles can be reduced, the vehicle does not push so much air in its forward motion. This implies less aerodynamic drag and increase of the fuel efficiency in vehicles. Kett et al. [16] designed a radiator (as shown in Fig. 6) with the carbon foam. Due to the increase of heat transfer coefficients, the number of coolant tubes in the radiator was reduced significantly. A typical automotive radiator with cross section of 48 cm x 69 cm might be reduced to 20 cm x 20 cm at the same heat removal rate. The reduced size will cut down the overall weight, cost, and volume of the cooling system. Thereby the fuel efficiency can be improved. Moreover, Yu et al. [17] compared a carbon foam fin - tube radiator with a conventional aluminum fin - tube radiator. The thermal performance of the carbon foam radiator was increased around 15 % without changing the frontal area or the air flow rate and pressure drop.
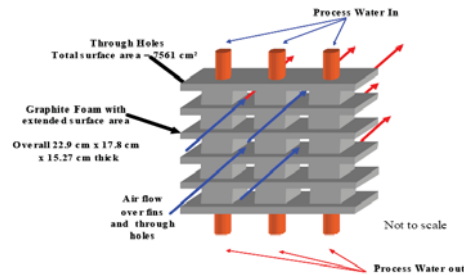
Fig. 6. Configuration of graphite foam radiator [16].

3.3. Energy storage system

Because of the high thermal conductivities in the graphite foam, the time used for heat transfer inside the material will be very short. This is a big advantage for energy storage applications. Lafdi et al. [18] investigated the thermal performance of graphite foams infiltrated with phase change materials for space and terrestrial energy storage systems. Because of the high thermal conductivity of graphite foams, the thermal performance of phase change material and foam system was improved significantly. In the phase change material related energy storage process, the higher thermal conductivity leads to a shorter time to charge or discharge, which implies better system performance.

4. Problems

Even though the graphite foam is an excellent thermal material, it is still very hard to find graphite foam heat exchangers in the commercial market. Thus, there are some problems blocking the development of graphite foam heat exchangers.

The most important problem facing the graphite foam heat exchanger is the high pressure drop. Because of the complex internal structure of the foam, the flow resistance inside the graphite foam is very high. This causes a high pressure drop through the graphite foam. Due to the high flow resistance, it is difficult for the cooling air to reach all the inter - faces and transfer the heat. Thus, the effective area of heat transfer is reduced greatly, which will result in a low thermal performance. Furthermore, the high pressure drop requires large input of pumping power to push the air through the graphite foam heat exchangers, which will cause a low coefficiency of performance (COP, the ratio of the removed heat to the input pumping power). Garrity et al. [19] proved that the graphite foam heat exchanger had lower COP than the aluminum multilouvered fin. In order to reduce the high pressure drop, it is important to adopt an appropriate configuration of the graphite foams, as discussed in [9-10].

The second problem is that the mechanical properties of the graphite foam are not as good as those of the metal foam. The tensile strength of graphite foam with porosity of 75 % is only 0.69 MPa [20]. However, the tensile strength of nickel foam with the same porosity is 18.44 MPa, which is much higher than the one of graphite foam [21]. In order to reinforce the mechanical properties of graphite foam, it might be useful to introduce some other material to the graphite foam. For instance, the compressive strength can increase ten times after the graphite foam has been mixed with epoxy resin. However, by changing the fabrication process to improve the foam's mechanical properties, the high thermal conductivity might sacrifice [22].

The third problem is the dust block. Most research of the graphite foam focus on the electronic equipment heat sinks. Little attention was put to the vehicle radiator applications. The major reason is the dust blocking problem. When the open pores in graphite foams are blocked by dust, the cold air can not reach all inter - faces and bring away the heat. Thus, the effective heat transfer area is reduced greatly and the thermal performance will decrease too. Due to the operating conditions, the dust block problem is more serious in vehicle radiators than in the electronic equipment heat sinks.

Due to these problems, the development of graphite foams is relatively slow and difficult. Much work has to be done before a mature graphite foam heat exchanger appears in the commercial market.

5. Conclusions and suggestions

The graphite foam has very high thermal conductivity, low density and large specific surface area. Because of these properties, the graphite foam is considered as a potential thermal material for heat exchangers. The graphite foam can be used as heat sinks to cool electronic packages. Also the graphite foam can be used as a radiator to cool the vehicle engines. Sometimes, the graphite foam can be used in energy storage applications.

However, due to the complex internal structure of the graphite foam, there is a very high pressure drop when the air flows through the graphite foams. There are also some other problems blocking the development of graphite foam, such as the low tensile strength, and the dust block. In order to promote the development of graphite foams as thermal material for heat exchangers, adopting an appropriate configuration might be useful to reduce the pressure drop through the graphite foam. On the other hand, mixing some other material with graphite foam might be helpful to reinforce the mechanical properties of graphite foam. Thus, much work has to be conducted before the graphite foam is accepted as a thermal material of heat exchangers.

6. Acknowledgments

References

[1] J. Klett, R. Hardy, E. Romine, C. Walls, and T. Burchell, High-thermal-conductivity, mesophase-pitch-derived carbon foams: effect of precursor on structure and properties, Carbon 38, 2000, pp. 953-973.

[2] W. Ford, Method of making cellular refractory thermal insulating material, 1964, US Patent 3121050.

[3] J. W. Klett, Process for making carbon foam, 2000, US Patent 6033506.

[4] J. W. Klett, A. D. Mcmillan, N. C. Gallego, and C. A. Walls, The role of structure on the thermal properties of graphite foams, Journal of Materials Science 39, 2004, pp. 3659-3676.

[5] Q. Yu, B. E. Thompson, A. G. Straatman, A unit cube-based model for heat transfer and fluid flow in porous carbon foam, Journal of Heat Transfer 128, 2006, pp. 354-360.

[6] C. C. Tee, N. Yu, and H. Li, Modeling the overall heat conductive and convective properties of open-cell graphite foam, Modelling Simulation Material Science Engineering 16, 2008, 075006.

[7] A. G. Straatman, N. C. Gallego, B. E. Thompson, H. Hangan, Thermal characterization of porous carbon foam - convection in parallel flow, International Journal of Heat and Mass Transfer 49, 2006, pp. 1991-1998.

[8] A. G. Straatman, N. G. Gallego, Q. Yu, and B. E. Thompson, Characterization of porous carbon foam as a material for compact recuperators, Journal of Engineering for Gas Turbines and Power 129, 2007, pp. 326-330.

[9] K. C. Leong, L. W. Jin, H. Y. Li, and J. C. Chai, Forced convection air cooling in porous graphite foam for thermal management application, 11th Intersociety Conference on Thermal and Thermomechanical Phenomena in Electronic Systems, 2008, pp. 57-64.

[10] Y. R. Lin, J. H. Du, W. Wu, L. C. Chow, W. Notardonato, Experimental study on heat transfer and pressure drop of recuperative heat exchangers using carbon foam, Journal of Heat Transfer 132, 2010, 091902-1.

[11] N. C. Gallego, and J. W. Klett, Carbon foams for thermal management, Carbon 41, 2003, pp. 1461-1466.

[12] Z. A. Williams, and J. A. Roux, Graphite foam thermal management of a high packing density array of power amplifiers, Journal of Electronic Packaging 128, 2006, pp. 456-465.

[13] V. Gandikota, and A. S. Fleischer, Experimental investigation of the thermal performance of graphite foam for evaporator enhancement in both boiling and an FC-72 thermosyphon, Heat Transfer Engineering 30(8), 2009, pp. 643-648.

[14] M. H. Lu, L. Mok, and R. J. Bezama, A graphite foams based vapor chamber for chip heat spreading, Journal of Electronic Packaging 128, 2006, pp. 427-431.

[15] J. S. Coursey, J. Kim, and P. J. Boudreaux, Performance of graphite foam evaporator for use in thermal management, Journal of Electronic Packaging 127, 2005, pp. 127-134.

[16] J. Klett, R. Ott, and A. McMillan, Heat exchangers for heavy vehicles utilizing high thermal conductivity graphite foams, SAE Technical Paper 2000-01-2207, 2000.

[17] Q. Yu, A. G. Straatman, B. E. Thompson, Carbon - foam finned tubes in air - water heat exchangers, Applied Thermal Engineering 26, 2006, pp. 131-143.

[18] K. Lafdi, O. Mesalhy, and A. Elgafy, Graphite foams infiltrated with phase change materials as alternative materials for space and terrestrial thermal energy storage applications, Carbon 46, 2008, pp. 15-168.

[19] P. T. Garrity, J. F. Klausner, R. Mei, Performance of aluminum and carbon foams for air side heat transfer augmentation, Journal of Heat Transfer 132, 2010, 121901-1.

[20] M. D. Haskell, Thermal resistance comparison of graphite foam, aluminum, and copper heat sinks, http://www.electronics-cooling.com/2006/02/thermal-resistance-comparison-of-graphite-foam-aluminum-and-copper-heat-sinks/.

[21] S. B. Zhao, Thought about the exponential item in formulas calculating tensile strength for high - porosity materials, Materials and Design 23, 2002, pp. 497-499.

[22] ORNL's graphite foam may aid transportation, http://www.ornl.gov/info/ornlreview/v33_3_00/foam.htm.

Paper 3

CrossMark

A performance analysis of porous graphite foam heat exchangers in vehicles

Wamei Lin, Bengt Sundén*, Jinliang Yuan

Department of Energy Sciences, Lund University, P.O. Box 118, Lund 22100, Sweden

HIGHLIGHTS

► Graphite foam wavy corrugated fins present good thermal and flow characteristics.
► The graphite foam wavy corrugated fin heat exchanger presents a high power density.
► A high compactness factor is provided by the graphite foam heat exchanger.
► The graphite foam heat exchanger has a low coefficient of performance (duty/pumping loss).
► Graphite foam heat exchangers have great potential in vehicle cooling applications.

ARTICLE INFO

ABSTRACT

Due to the increasing cooling power and space limitation in vehicles, a new compact heat exchanger – graphite foam heat exchanger is proposed for vehicle cooling application. The graphite foam has high thermal conductivity (the effective thermal conductivity is 40–150 W/m K) and low density (0.2–0.6 g/cm^3), but it has high flow resistance which is a problem in heat exchanger applications. In order to find a graphite foam heat exchanger with low flow resistance, four different configurations (baffle, pin-finned, corrugated, and wavy corrugated) of graphite foam fins are analyzed in terms of thermal performance and pressure drop by using a computational fluid dynamics approach. The simulation results show that the wavy corrugated foam presents high thermal performance and low pressure drop. Moreover, a comparative study between the wavy corrugated foam heat exchanger and a conventional aluminum louver fin heat exchanger is carried out to evaluate the performance of graphite foam heat exchangers in terms of coefficient of performance (removed heat/air pumping loss), power density (removed heat/mass of heat exchangers), and compactness factor (removed heat/volume of heat exchangers). Finally, this paper concludes that graphite foam heat exchangers should be further developed in vehicles, and presents several recommendations for how such development can be promoted.

© 2012 Elsevier Ltd. All rights reserved.

1. Introduction

Due to the high thermal conductivity of metal materials, aluminum or copper heat exchangers are very popular in vehicles. However, with the increased power production and reduced under-bonnet space, vehicle cooling becomes a more serious problem than before. In order to increase the thermal performance of heat exchangers in vehicles, it is important to apply extended surfaces on the air side to compensate for the low heat transfer coefficient. Thus, the cooling surface of heat exchangers has to be increased to dissipate the tremendous cooling power. However, because of space limitations in vehicles, there is not much available space to

increase the size of heat exchangers, which has led to an urgent need to develop a new compact heat exchanger with high thermal performance for vehicle cooling.

Due to its big specific surface area, a porous medium at a small size might be a good choice for the development of new compact heat exchangers. Compared to a metal foam [1–4], a graphite foam developed by Oak Ridge National Laboratory [5] has extremely high thermal conductivity. Several research studies on the characteristics of graphite foams have been carried out [6–8]. These studies show that the characteristics of graphite foams are as follows:

I. High thermal conductivity: The effective thermal conductivity of graphite foam, which is a weighted average of the solid material and the pores where a fluid is passing, is between 40 and 150 W/m K [8]. This is much higher than the

* Corresponding author. Tel.: +46 46 2228605.
  E-mail address: bengt.sunden@energy.lth.se (B. Sundén).

II. Low density: The density of graphite foam ranges from 200 to 600 kg/m^3, which is about 20% of that of aluminum.

III. Large specific surface area: Because of the open pores and inter-connected void structure, the specific surface area of graphite foam is between 5000 and 50,000 m^2/m^3 when the pore size is around from 500 μm to 10 μm respectively [8].

IV. Weak mechanical properties: The tensile strength of graphite foam is much less than that of a metal foam. The weak mechanical properties block the development of the graphite foam heat exchanger. Adding additional material into the graphite foam or changing the fabrication process might improve the foam's mechanical properties.

Based on these characteristics, the graphite foam has become a very promising material for heat exchangers. For example, Klett et al. [9] designed a radiator with carbon foam. In their study, the cross section of the automotive radiator was reduced from 48 cm × 69 cm to 20 cm × 20 cm. The reduced size enabled a substantial decrease of the overall weight, cost and volume of the cooling system. Furthermore, Yu et al. [10] proved that the thermal performance of a carbon foam finned tube radiator could be improved by 15% compared to a conventional aluminum finned tube radiator without changing the frontal area or the air flow rate or pressure drop. Also Garrity et al. [11] carried out an experimental comparison between a carbon foam heat exchanger and a multi-louvered fin heat exchanger. They found that the carbon foam samples brought away more heat than the multilouvered fin when the volume of the heat exchangers was the same.

Even though there is a huge heat transfer enhancement in the graphite foam, the graphite foam is still associated with other problems. The most important issue is that there is a high pressure drop due to the large hydrodynamic loss associated with the cell windows connecting the pores [12]. In a study concerning reduction of the pressure drop, Gallego and Klett [13] presented six different configurations of graphite foam heat exchangers. That study showed that the solid foam had the highest pressure drop while the finned configuration had the lowest pressure drop. In another study, Leong et al. [14] found that the baffle foam presented the lowest pressure drop among four configurations of graphite foams at the same heat transfer rate. Lin et al. [15] revealed that a corrugated foam could reduce the pressure drop while maintaining a high heat transfer coefficient compared to the solid foam. All together, these studies illustrate that the configuration has an important effect on the pressure drop through the graphite foam.

The present study concerns a computational fluid dynamics (CFD) analysis, with the aim to evaluate what graphite foam fin configuration is presenting the lowest pressure drop and highest thermal performance among baffle, pin-finned, corrugated and wavy corrugated graphite foam fins. Moreover, in order to predict the performance of graphite foam heat exchangers in vehicles, the graphite foam fin with low pressure drop and high thermal performance is compared with a conventional aluminum louver fin in terms of (1) coefficient of performance (COP, how much heat can be removed by a certain input pumping power), (2) power density (PD, how much heat can be removed by a certain mass of the fins), and (3) compactness factor (CF, how much heat can be removed in a certain volume).

2. Physical model and assumptions

2.1. Physical model

A simplified model of a plate-fin heat exchanger is shown in Fig. 1. Four different configurations (baffle, pin-finned, corrugated,

and wavy corrugated) of the graphite foam, which are equivalent fins, are placed between two water tubes. As shown in Fig. 1, the hot water flows inside the flat tubes, and the cold air flows through the porous carbon foam. The heat is transmitted through the tube wall and the graphite foam porous cell surface and finally it is dissipated to the air. There are many parameters to describe the configuration of the graphite foam heat exchanger. The overall size of the four configurations of the graphite foam core is 1.2 cm (z-direction) × 4.5 cm (y-direction) × 5 cm (x-direction). The details of the configurations and geometries are shown in Fig. 2. The important parameters of the graphite foam are described in Table 1, which is based on Ref. [12]. The fluid is assumed to be incompressible with constant properties and in steady-state. The water tubes are made of aluminum. Due to the large heat transfer coefficient between the hot water and the inner wall of the tube, as well as the high thermal conductivity of the pipe wall, the water tube is assumed to be at constant temperature. The connection between the tube wall and the graphite foam is assumed perfect without any air gap inside. Thus, the thermal resistance at the interface between the tube wall and the graphite foam is neglected.

2.2. Modeling assumptions

Before the numerical computations, a discussion of the computational model (laminar or turbulent) in adoption of the flow regime is carried out. In the comparison among the four configurations of the graphite foam, the inlet air speed is selected to be in the range from 12 m/s to 20 m/s based on the speed of vehicles. Correspondingly, the Reynolds number based on the frontal velocity and the hydraulic diameter (D_h) is ranging from 15,120 to 25,200. Thus turbulent flow prevails on the air side. However, inside the graphite foam the flow is laminar. This is so, because it is difficult to generate turbulent eddies in the small open pores of the foam.

The effect of turbulence on the flow field is implemented by the "renormalization group" (RNG) $k-\varepsilon$ turbulence model. On the other hand, due to the laminar flow inside the graphite foam, the RNG $k-\varepsilon$ turbulence model might be useful to take into account of low-Reynolds number effect near the foam walls.

2.3. Computational domain

In order to make sure the graphite foam fin is located in the fully developed flow region, the computational domain is extended upstream 1.5 times the graphite foam fin length to eliminate the entrance length effect. Similarly, the computational domain is extended downstream 5 times the length of the graphite foam fin to achieve the one-way coordinate assumption at the domain outlet. Thus, the whole stream length of the computational domain is 7.5 times the actual graphite foam fin length, as shown in Fig. 3.

3. Mathematical formulation and numerical method

3.1. Governing equations

According to the above presented assumptions, the governing equations for continuity, momentum and energy may be expressed as follows, see Refs. [16–18]:

3.1.1. Air zone governing equations (turbulent flow)
Continuity equation

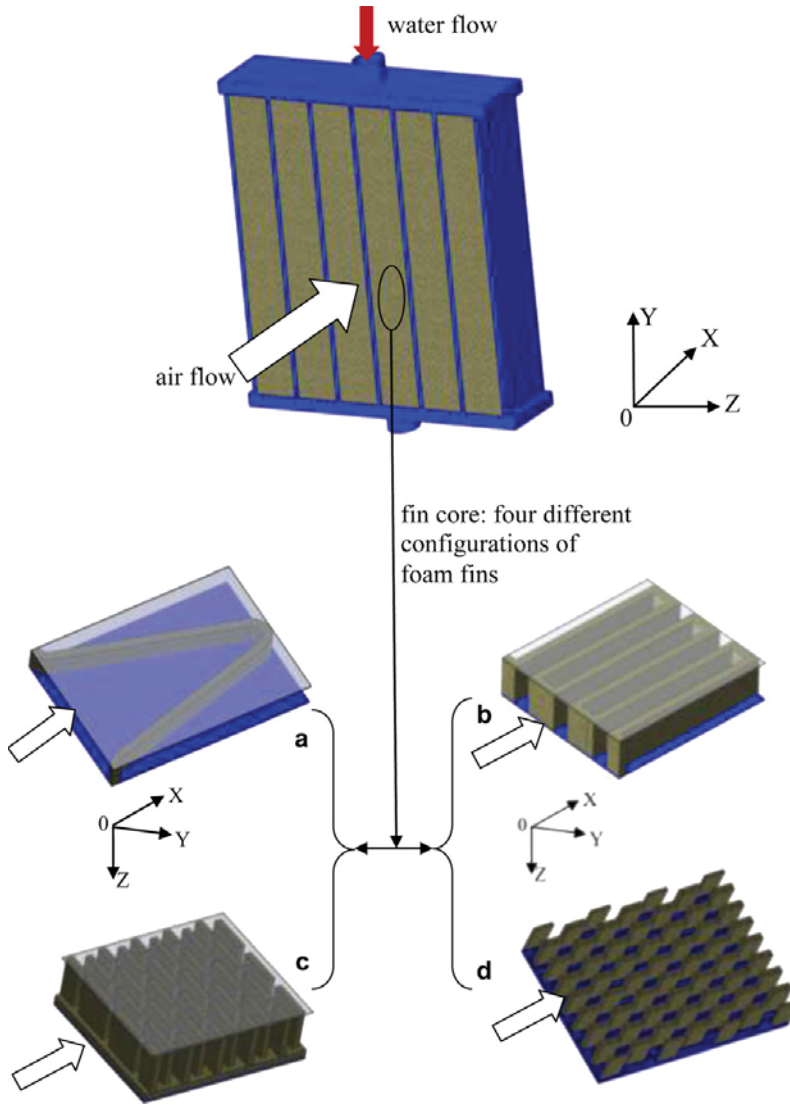$$\frac{\partial(\rho_{air}u_i)}{\partial x_i} = 0 \tag{1}$$

Fig. 1. Different configurations of graphite foam fins: (a) wavy corrugated; (b) corrugated; (c) baffle; (d) pin-finned.

Momentum equations

$$\frac{\partial(\rho_{air}u_iu_j)}{\partial x_j} = -\frac{\partial p}{\partial x_i} + \frac{\partial}{\partial x_j}\left((\mu_{air}+\mu_t)\left(\frac{\partial u_i}{\partial x_j}+\frac{\partial u_j}{\partial x_i}\right)\right) \tag{2}$$

Energy equation

$$\frac{\partial(\rho_{air}u_jT)}{\partial x_j} = \frac{\partial}{\partial x_j}\left(\left(\frac{\mu_{air}}{Pr_{air}}+\frac{\mu_t}{Pr_t}\right)\frac{\partial T}{\partial x_j}\right) \tag{3}$$

The equations for the turbulent kinetic energy k and the rate of energy dissipation ε corresponding to the RNG $k-\varepsilon$ turbulence model are:

Turbulent kinetic energy k equation:

$$u_j\frac{\partial k}{\partial x_j} = -\overline{u'_iu'_j}\frac{\partial u_i}{\partial x_j} + \frac{\partial}{\partial x_j}\left(\frac{K_m}{\sigma_k}\frac{\partial k}{\partial x_j}\right) - \varepsilon \tag{4}$$

Rate of energy dissipation ε equation:

$$u_j\frac{\partial \varepsilon}{\partial x_j} = -C_{\varepsilon 1}\frac{\varepsilon}{k}\overline{u'_iu'_j}\frac{\partial u_i}{\partial x_j} + \frac{\partial}{\partial x_j}\left(\frac{K_m}{\sigma_\varepsilon}\frac{\partial \varepsilon}{\partial x_j}\right) - C_{\varepsilon 2}\frac{\varepsilon^2}{k} - R \tag{5}$$
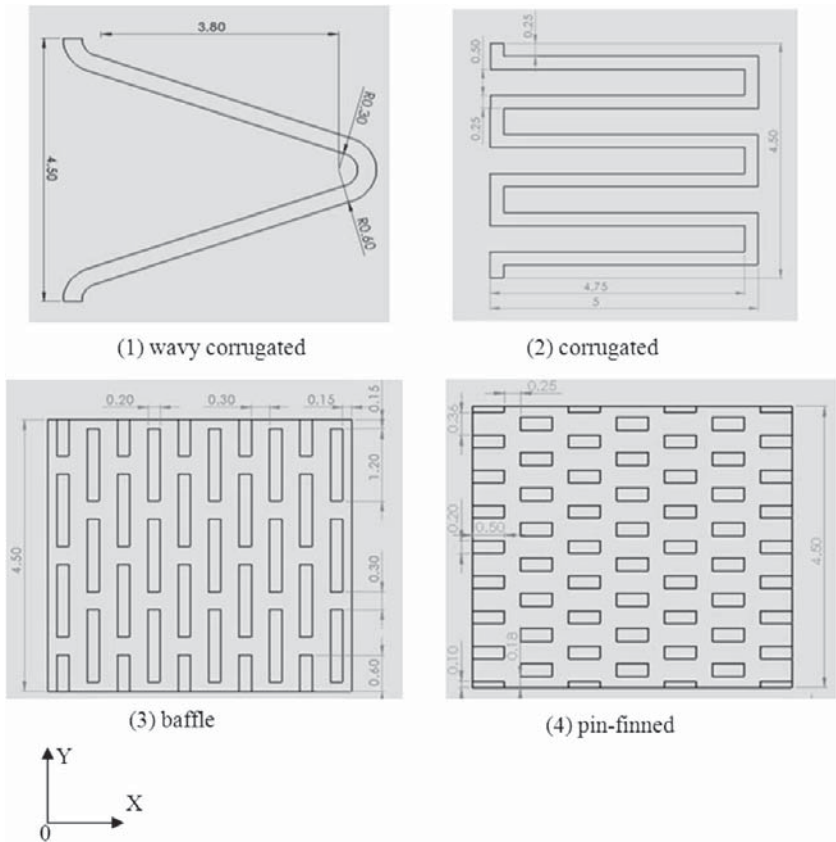
Fig. 2. Geometries of various graphite foam fins (cm).

where

$$R = \frac{C_\mu \eta^3 (1 - \eta\eta_0)\varepsilon^2}{(1 + \beta_0 \eta^3)k}, \quad \mu_t = \rho C_\mu \frac{k^2}{\varepsilon}$$

$$\eta = \frac{k}{\varepsilon}\left[\left(\frac{\partial u_i}{\partial x_j} + \frac{\partial u_j}{\partial x_i}\right)\frac{\partial u_i}{\partial x_j}\right]^{0.5},$$

$$K_m = \nu\left[1 + \left(\frac{C_\mu}{\nu}\right)^{0.5}\frac{k}{\varepsilon^{0.5}}\right]^2,$$

Table 1
Different parameters of graphite foam heat exchangers [12].

Graphite foam	Porosity (φ)	Pore diameter (D_p) (μm)	Effective thermal conductivity (λ_{eff}) (W/m K)	Permeability (α) (m^2)	Forchheimer coefficient (C_F)
POCO	0.82	500	120	6.13 × 10^{-10}	0.4457

and ν is the kinematic viscosity of air; u_i' are the fluctuations of the mean velocity u_i.

The values of the constants are as follows:

$$C_\mu = 0.0845; \quad \sigma_k = 0.7179; \quad \sigma_\varepsilon = 0.7179$$

$$C_{\varepsilon 1} = 1.42; \quad C_{\varepsilon 2} = 1.68; \quad \beta_0 = 0.012; \quad \eta_0 = 4.377$$

3.1.2. Graphite foam zone governing equations (laminar flow)

Because the graphite foam is a porous medium, the Forchheimer extended Darcy's law has been applied for the air pressure drop through the graphite foam. However, there are two major models for the heat transfer of the graphite foam. One is the thermal equilibrium model, in which the effective thermal conductivity of the porous media is significant. Another one is the non-thermal equilibrium model (two-equation model), in which the interfacial heat transfer coefficient has to be specified to connect the energy transport between the solid part and the fluid part. However, there is only little data available about the interfacial heat transfer coefficient h_{fs} for graphite foams in the literature. In order to keep the accuracy of the simulation, the thermal equilibrium model is used in this study. In the present study, the effective thermal conductivity of the graphite foam (λ_{eff}) is based on experimental results found in the literature [12]. Thus, the governing equations for the graphite foam are as follow:
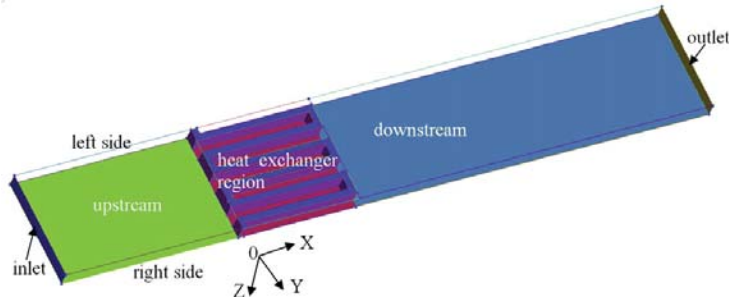
Fig. 3. Computational domain.

Continuity equation:

$$\frac{\partial(\rho_{\text{air}} u_i)}{\partial x_i} = 0 \tag{6}$$

Momentum equations:

$$\frac{\partial(\rho_{\text{air}} u_i u_j)}{\partial x_j} = -\varphi \frac{\partial p}{\partial x_i} + \frac{\partial}{\partial x_j}\left(\mu_{\text{air}}\left(\frac{\partial u_i}{\partial x_j} + \frac{\partial u_j}{\partial x_i}\right)\right) - \varphi\left(\frac{\mu_{\text{air}}}{\alpha} u_i\right.$$
$$\left. + \frac{\rho_{\text{air}} C_{\text{F}}}{\sqrt{\alpha}} |u| u_i\right) \tag{7}$$

Energy equation:

$$\varphi \frac{\partial(\rho_{\text{air}} c_{p,\text{air}} u_j T)}{\partial x_j} = \lambda_{\text{eff}} \frac{\partial}{\partial x_j}\left(\frac{\partial T}{\partial x_j}\right) \tag{8}$$

where φ is the porosity of the porous graphite foam; α the permeability of the porous graphite foam (m^2); C_{F} the Forchheimer coefficient.

3.2. Boundary conditions

The momentum and energy transports are calculated simultaneously for the air and porous graphite foam zones. The boundary conditions on the graphite foam "walls" are set up as "interior surface". Thus, the solutions for the momentum and energy transports on the interfaces between air and porous graphite foam zones are not required. The necessary boundary conditions are as follows:

(1) For the upstream extended region (domain inlet)
    At the inlet:

$$u = \text{const}; \ T = \text{const}; \ v = w = 0$$

At the upper and lower boundaries:

$$\frac{\partial u}{\partial z} = \frac{\partial v}{\partial z} = 0, \ w = 0, \ \frac{\partial T}{\partial z} = 0$$

At the right and left sides:

$$\frac{\partial u}{\partial y} = \frac{\partial w}{\partial y} = 0, \ v = 0, \ \frac{\partial T}{\partial y} = 0$$

(2) For the downstream extended region (domain outlet)
    At the upper and lower boundaries:

$$\frac{\partial u}{\partial z} = \frac{\partial v}{\partial z} = 0, \ w = 0, \ \frac{\partial T}{\partial z} = 0$$

At the right and left sides:

$$\frac{\partial u}{\partial y} = \frac{\partial w}{\partial y} = 0, \ v = 0, \ \frac{\partial T}{\partial y} = 0$$

At the outlet boundary:

$$\frac{\partial u}{\partial x} = \frac{\partial v}{\partial x} = \frac{\partial w}{\partial x} = \frac{\partial T}{\partial x} = 0$$

(3) For the graphite foam region (middle part)
    At the right and left sides:

$$\frac{\partial u}{\partial y} = \frac{\partial w}{\partial y} = 0, \ v = 0, \ \frac{\partial T}{\partial y} = 0$$

At the upper and lower boundaries:

$$u = v = w = 0, \ T_{\text{w}} = \text{const}$$

3.3. Numerical method

The commercial code ANSYS FLUENT 12.0 is used for the numerical solution. A control-volume-based technique is adopted to convert the governing equations to algebraic equations so that these can be solved numerically [19]. The Semi-Implicit Method for Pressure Linked Equations (SIMPLE) algorithm is used to couple pressure and velocity. A second-order upwind scheme is used for the space discretization of the momentum and energy equations in the simulations. The residual of the continuity, components of velocity is set to be below 10^{-3}, while for energy it is below 10^{-6}.

A hexagon mesh is generated by using the blocking technique in ICEM software. The heat exchanger region (as shown in Fig. 4) occupies most of the cells (60–70% of the whole computational domain). In order to control the grid independence, several sets of mesh size were studied. For instance, three sets of mesh size ($11 \times 81 \times 49$, $11 \times 81 \times 75$, $19 \times 81 \times 75$) were selected for the heat exchanger region to find out the grid independence of the corrugated foam fin. It is found that the variation of pressure drop is between 0.3 and 2.2%, and the variation of Nusselt number is between 1.4 and 3.0%. Based on this, a mesh size of $11 \times 81 \times 75$ was adopted for the corrugated foam fin simulation. The same method was adopted to find out the grid independence of the other foam configurations (the mesh size of wavy corrugated, pin-finned and baffle are $21 \times 139 \times 100$, $19 \times 93 \times 79$, $17 \times 99 \times 83$, respectively).
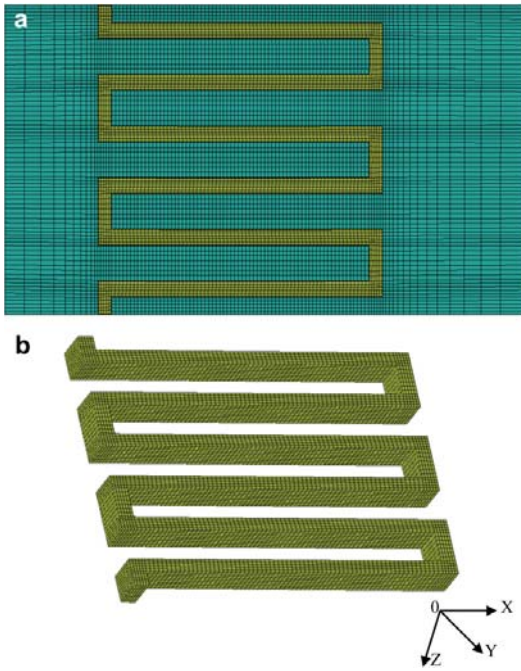
Fig. 4. Meshing for the computations: (a) 2-D cross-sectional view; (b) 3-D on fin surfaces.

3.4. Evaluation of performance parameters

For given conditions, the thermal performance of the graphite foam can be characterized by the Nusselt number (Nu).

$$Nu = \frac{hD}{\lambda_f} = \frac{DQ_{removed}}{\lambda_f A \Delta T} \tag{9}$$

In Eq. (9), D is the length scale based on either the equivalent particle diameter of the foam or the hydraulic diameter of the channel. A is the area which is the effective heat transfer surface or the heated base area of the foam. In order to simplify Eq. (9), D is defined as the hydraulic diameter of the channel D_h, A the heated base area A_b, and ΔT is the mean temperature difference between the heated base and the fluid inlet. Thus Eq. (9) can be written as:

$$Nu = \frac{D_h Q_{removed}}{\lambda_f A_b \Delta T} \tag{10}$$

4. Results and discussion

4.1. Validation of simulation model

Before presenting the results of the four configurations of the foam, it is necessary to validate the simulation model of the graphite foam. In order to set up the same conditions as in the experiment [12], a block graphite foam with a size of 0.6 cm (width) × 5 cm (height) × 5 cm (length) was adopted, and the coolant through the graphite foam block is water instead of air (in order to compare with the experimental results). In addition, a constant temperature is specified at the base of the graphite foam

Table 2
Deviation between the simulation and the experimental data.

Frontal velocity (m/s)	Nu number in Ref. [12]	Nu number predicted in this study	Δp in Ref. [12] (kPa)	Δp predicted (kPa)
0.009	40	38 (5%)	1.0	1.029 (2.9%)
0.03	100	101.9 (1.9%)	3.5	3.41 (2.6%)
0.048	122	130 (6.5%)	7.0	6.9 (1.4%)
0.069	140	150 (7.1%)	11.2	10.9 (2.7%)

block. The pressure drop (Δp) and Nu number are calculated and compared with the experimental results in Ref. [12], as shown in Table 2. It is found that the largest deviation of the Nusselt number between the simulation (laminar flow: the frontal velocity was chosen based on the one in the experimental work [12]) and the experimental result is less than 7.1%, and the lowest deviation is around 1.9%. The deviation of the pressure drops between the simulation and the experimental data is less than 3%. It should be noted that no information on experimental uncertainty of the Nu number was supplied in the experimental work [12]. Based on the maximum deviation (7.1% in the Nusselt number, 3% in the pressure drop), it is believed that the present model is satisfactory and can be applied further to estimate the graphite foam pressure drop and the thermal performance.

4.2. Comparison between four configurations of graphite foam

4.2.1. Pressure loss

The pressure loss through the graphite foam is predicted based on the Forchheimer extended Darcy's equation. As expected, the pressure drop through the graphite foam is increased with increasing frontal velocity as shown in Fig. 5. However, the pressure drop through the baffle graphite foam increases faster than the other cases. The major factors affecting the pressure drop through the graphite foam are the flowing length inside the foam and the air path.

All the air has to pass through the corrugated and the wavy corrugated foams. However, due to the short flow length (the flow length inside the corrugated foam is 2.5 mm, the one inside the wavy corrugated foam 3 mm), the pressure drop through the wavy corrugated foam fin or the corrugated foam fin is low. On the other hand, the major amount of air bypasses the foam instead of passing through the baffle and the pin-finned foams. Because the flow path around the pin-fins (in Fig. 6(a)) is much smoother than the one
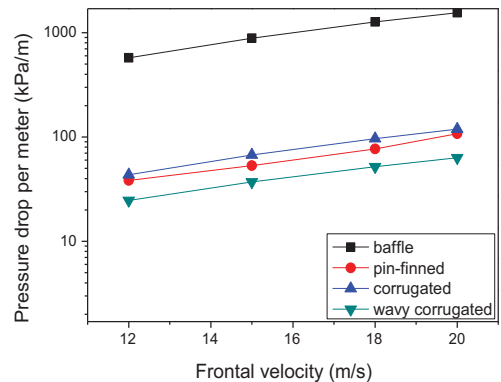

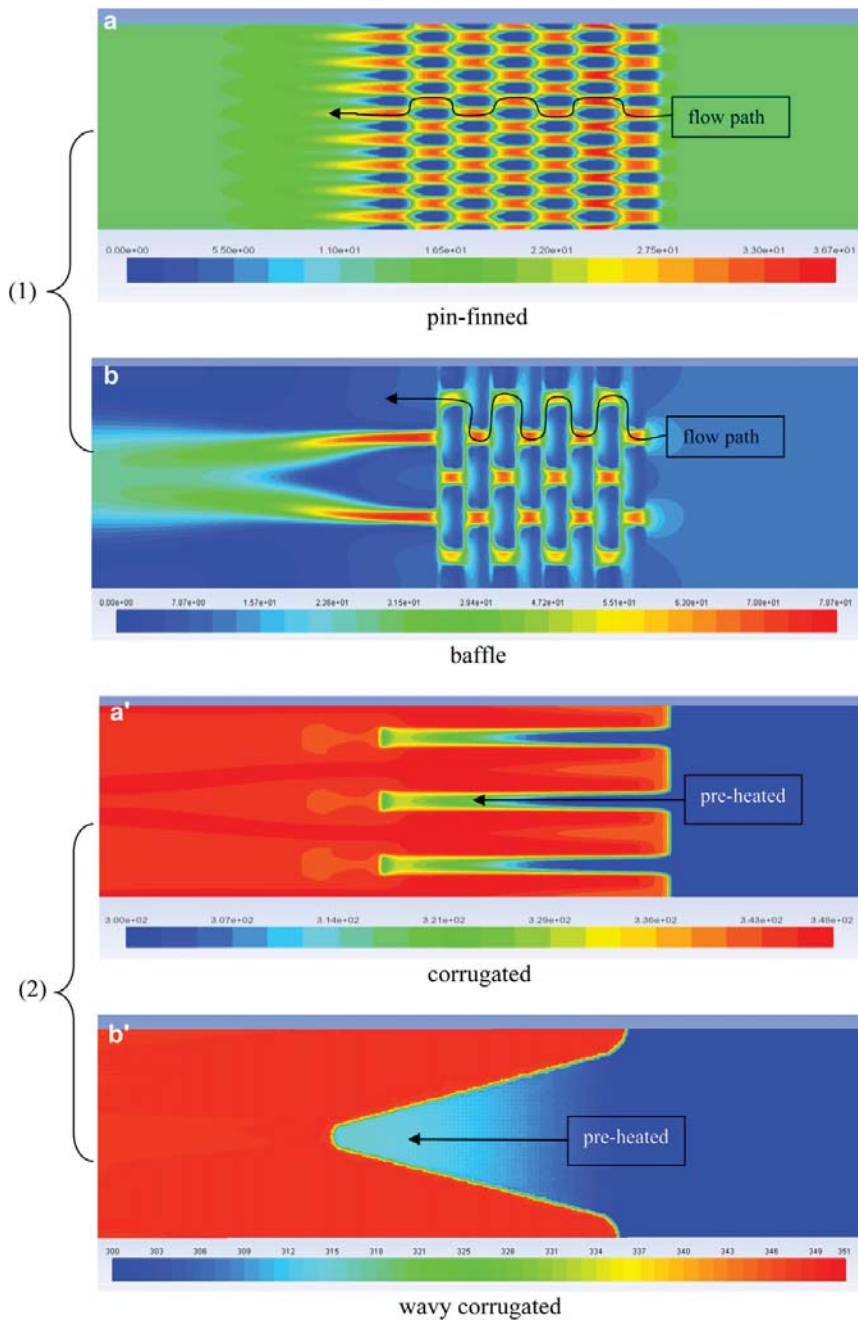**Fig. 5.** Pressure drop through four configurations of foam.

Fig. 6. (1) Velocity distribution contours at 12 m/s inlet velocity (m/s) and (2) temperature distribution (K).

around the baffle fins (in Fig. 6(b)), the pressure drop of the pin-finned foam is much less than that for the baffle fins. Furthermore, due to the complex air flow path of the baffle fins, a large amount of air is forced to pass through the baffle graphite foam fins. Thus, a high flow resistance is produced in the baffle fins, compared to the other configurations of the graphite foam fins. In other words, the baffle fin presents the highest pressure drop among the considered four configurations.

4.2.2. Thermal performance

The heat transfer coefficients predicted for the four configurations of graphite foam fins are shown in Fig. 7. The heat transfer coefficient is correlated with the frontal velocity of air. Among these four configurations, the wavy corrugated fin provides a much higher heat transfer coefficient than the other configurations. In addition, the heat transfer coefficient is increased much faster in the wavy corrugated fin than the other cases, as the air frontal velocity increases.

By taking into account Fig. 6, an in-depth understanding of the thermal performance among these four graphite foam fins may be obtained. Fig. 6(a′) and (b′) shows that the fresh air is pre-heated before it reaches the graphite foam fin due to the heat transported from the nearby fins. The space between two adjacent fins is much larger in the wavy corrugated fin than in the corrugated fin. Thus, the pre-heating effect is minor in the wavy corrugated fin compared to that in the corrugated fin. Due to the pre-heating effect, the temperature difference between the fin and the air is reduced in the corrugated fin. The reduced temperature difference decreases the thermal performance of the corrugated fin. Thus, the heat transfer coefficient inside the corrugated fin is much lower than that of the wavy corrugated fin.

On the other hand, due to the different flow path appearing in the pin-finned and the baffle-finned foams (see Fig. 6(a) and (b)), the air is mixed better in the baffle-finned foam than in the pin-finned foam. Thus, the thermal performance of the baffle foam is a little better than that of the pin-finned foam. However, there is a higher flow resistance in the baffle foam than in the wavy corrugated foam, as discussed previously. The high flow resistance leads to less cold air reaching the inner surface of the baffle foam. This means that the effective surface for heat transfer is substantially reduced in the baffle foams compared to the wavy corrugated foam. Overall it seems that the thermal performance of the wavy corrugated foam is the best, see Fig. 7.
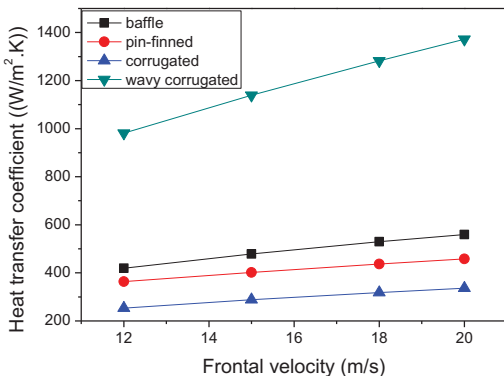
4.3. Comparison between graphite foam fin and aluminum louver fin

According to the comparison among the four configurations of graphite foam fins, the wavy corrugated fin presents lower pressure drop and higher thermal performance than the corrugated, pin-finned and the baffle fins. However, it is still not sure whether the graphite foam wavy corrugated fin would reach better performance than the conventional aluminum louver fin or not. In order to clarify this, a comparison between the graphite foam wavy corrugated fin and the aluminum louver fin is carried out. The aim of the comparison is based on: (1) coefficient of performance (COP, how much heat can be removed by a certain input pumping power), (2) power density (PD, how much heat can be removed by a certain mass of fins), and (3) compactness factor (CF, how much heat can be removed in a certain volume). These parameters are defined as follows:

$$\text{COP} = \frac{Q_{\text{removed}}}{P_{\text{pump}}} = \frac{Q_{\text{removed}}}{u_{\text{in}} A_{\text{in}} \Delta p} \tag{11}$$

$$\text{PD} = \frac{Q_{\text{removed}}}{1000 \cdot m_{\text{HEX}}} \tag{12}$$

$$\text{CF} = \frac{Q_{\text{removed}}}{1000 \cdot V_{\text{HEX}}} \tag{13}$$

where Q_{removed} is the amount of heat dissipated by the heat exchanger (W); P_{pump} the input power of the air fan (W); u_{in} the bulk velocity at the inlet of the heat exchanger (m/s); A_{in} the cross section area at the inlet (m^2); Δp the pressure drop through the heat exchanger (Pa); m_{HEX} the mass of the heat exchanger (kg); V_{HEX} the volume of the heat exchanger (m^3).

The major parameters of the louver fin are: (1) louver pitch is 1 mm; (2) the louver angle is 29°; (3) fin pitch is 2.5 mm. According to the experimental research on louver fin heat exchangers [20–23], the heat removed by the aluminum louver fin heat exchanger can be evaluated in this paper by using the heat transfer correlation in [20], which was based on 91 samples of louver fin heat exchangers at a mean deviation of 7.55%. The pressure drop also can be evaluated by the friction correlation in [21], which showed a deviation of 9.21% for the 91 samples. The comparison results of COP, PD, and CF between the graphite foam wavy
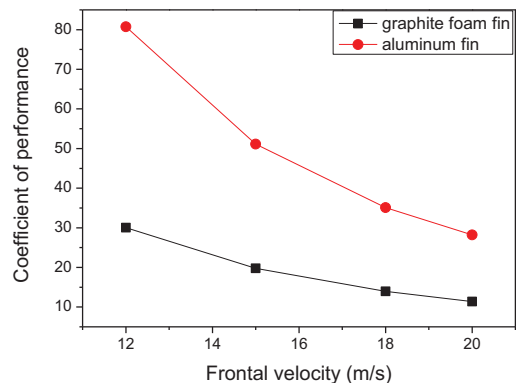

Fig. 7. Heat transfer coefficient of four configurations of foam.

Fig. 8. Coefficient of performance of graphite foam wavy corrugated fin and aluminum louver fin.
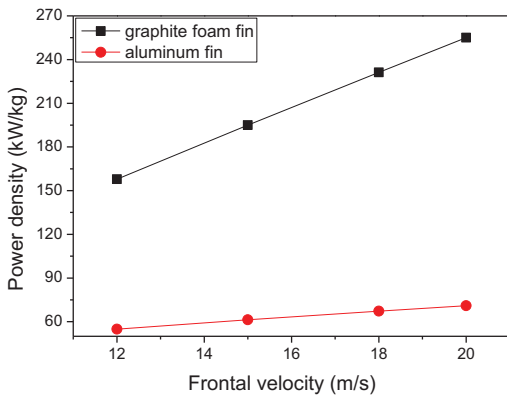
Fig. 9. Power density of graphite foam wavy corrugated fin and aluminum louver fin.

corrugated fin and the aluminum louver fin heat exchangers are shown in Figs. 8–10, respectively.

The COP values predicted for the graphite foam heat exchanger and the aluminum heat exchanger are shown in Fig. 8. Even though the wavy corrugated graphite foam fin presents a high heat transfer coefficient, its COP is lower than that of the aluminum heat exchanger, mainly due to the high flow resistance in the graphite foam. The low COP in the graphite foam implies that the air fan pumping power is much larger for the graphite foam heat exchanger than for the aluminum heat exchanger at the same dissipated heat condition.

It should be noted that the COP of the aluminum louver fin reduces faster than that of the graphite foam fin as the air velocity increases. Thus, the aluminum louver fin has less superiority in COP compared to the graphite foam wavy corrugated fin at high velocities. However, if the graphite foam heat exchanger reaches the same COP value as the aluminum heat exchanger, then the velocity of air will be supersonic according to the prediction from Fig. 8. Thus, it is not feasible for the graphite foam heat exchanger to achieve the same COP as the aluminum heat exchanger only by increasing the air velocity. Other methods, like different configurations of the foam fins or different structures of the foam, have to be considered to increase the COP value of the graphite foam heat exchanger.
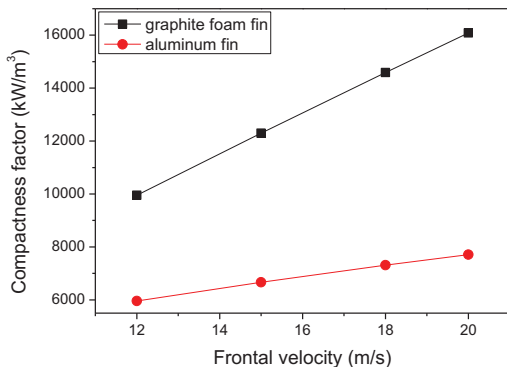

Fig. 10. Compactness factor of graphite foam wavy corrugated fin and aluminum louver fin.

Fig. 9 reveals that the PD of the graphite foam wavy corrugated fin is much higher than that of the aluminum louver fin. Moreover, the PD of the graphite foam wavy corrugated fin becomes big with increasing velocity. The high PD value for the graphite foam heat exchanger is mainly due to the small density of the graphite foam. Furthermore, the high heat transfer coefficient and the large specific surface area inside the graphite foam also contribute to the high PD, which means that the graphite foam heat exchanger is lighter than the louver fin heat exchanger when the removed heat is the same.

The predicted CF behaves similarly to the PD performance for both the graphite foam wavy corrugated fin and the aluminum louver fin, as shown in Fig. 10. The graphite foam wavy corrugated fin presents higher CF value than the aluminum louver fin. This means that the graphite foam can dissipate more heat than the aluminum louver fin at the same volume of the heat exchangers. This is so because of the large specific surface area attributed by many open pores in the graphite foam. Thus, the graphite foam can provide much larger heat transfer surface than the aluminum louver fin within the same volume. In other words, the compactness of the graphite foam wavy corrugated fin heat exchanger is much higher than that of the aluminum louver fin heat exchanger. This highly compact heat exchanger is favorable for application in vehicle cooling systems because of the space limitation in vehicles. Thus, it can be concluded that the graphite foam heat exchanger has a high potential in the vehicle cooling systems.

5. Conclusions and recommendations

Due to the high thermal conductivity, the graphite foam is considered as a potential candidate material for heat exchangers in vehicles. However, the high pressure drop is a major issue blocking the development of graphite foam heat exchangers. In order to reduce the pressure drop, this paper presented a computational analysis of four different configurations (baffle, pin-finned, corrugated, and wavy corrugated) of graphite foam. A low pressure drop and high thermal performance were achieved by the wavy corrugated fin configuration.

By comparison with a conventional aluminum louver fin heat exchanger, it is found that the graphite foam wavy corrugated fin heat exchanger presents higher power density (PD) and compactness factor (CF). This result means that the graphite foam can reduce the weight and size of the heat exchangers significantly, which has a great potential in the vehicle cooling application. However, the coefficient of performance (COP) is lower for the graphite foam heat exchanger compared to the aluminum heat exchanger, i.e., a large input air pumping power is required for the graphite foam heat exchanger, which may reduce the feasibility of the graphite foam in the vehicle cooling application. In order to promote the development of the graphite foam heat exchanger in the vehicle cooling, the problem of high flow resistance in the graphite foam has to be resolved by optimizing the structure or the configurations of the graphite foam fins, which is left for further work.

Acknowledgements

Nomenclature

A	area (m^2)
A_b	heated base area (m^2)
c_p	specific heat (J/kg K)
C_F	Forchheimer coefficient

CF   compactness factor (kW/m^3)
COP   coefficient of performance
D length scale (m)
D_h hydraulic diameter (m)
D_p pore diameter (μm)
h heat transfer coefficient (W/m^2 K)
k turbulent kinetic energy (m^2/s^2)
m mass (kg)
Nu Nusselt number
p pressure (Pa)
PD   power density (kW/kg)
P_{pump} the input power of pump (W)
Pr Prandtl number
$Q_{removed}$ removed heat (W)
T temperature (K)
u, v, w velocity components in x, y and z directions, respectively (m s)
u_i' fluctuation from the mean velocity u_i (m/s)
V volume (m^3)
Δp pressure drop (Pa)
ΔT temperature difference (K)

Greek symbols
α permeability (m^2)
ε rate of energy dissipation
λ thermal conductivity (W/m K)
μ dynamic viscosity (Pa s)
ρ density (kg/m^3)
φ porosity

Subscripts
air   air
eff   effective
f   fluid
HEX   heat exchanger
in   inlet
i, j coordinate indices
s   solid
t   turbulence

References

[1] W.J. Paek, H.B. Kang, Y.S. Kim, M.J. Hyum, Effective thermal conductivity and permeability of aluminum foam materials, International Journal of Thermophysics 21 (2) (2000) 453–464.

[2] M. Odabaee, K. Hooman, Metal foam heat exchangers for heat transfer augmentation from a tube bank, Applied Thermal Engineering 36 (2012) 456–463.
[3] S. Mancin, C. Zilio, L. Rossetto, A. Cavallini, Foam height effects on heat transfer performance of 20 ppi aluminum foams, Applied Thermal Engineering 49 (2012) 55–60.
[4] S. Mavridou, G.C. Mavropoulos, D. Bouris, D.T. Hountalas, G. Bergeles, Comparative design study of a diesel exhaust gas heat exchanger for truck applications with conventional and state of the art heat transfer enhancements, Applied Thermal Engineering 30 (2010) 935–947.
[5] J.W. Klett, Process for making carbon foam, US Patent 6033506, 2000.
[6] Q. Yu, B.E. Thompson, A.G. Straatman, A unit cube-based model for heat transfer and fluid flow in porous carbon foam, ASME Journal of Heat Transfer 128 (2006) 352–360.
[7] A.G. Straatman, N.C. Gallego, B.E. Thompson, H. Hangan, Thermal characterization of porous carbon foam − convection in parallel flow, International Journal of Heat and Mass Transfer 49 (2006) 1991–1998.
[8] J. Klett, R. Hardy, E. Romine, C. Walls, T. Burchell, High-thermal-conductivity, mescophase-pitch-derived carbon foams: effect of precursor on structure and properties, Carbon 38 (2000) 953–973.
[9] J. Klett, R. Ott, A. McMillan, Heat exchangers for heavy vehicles utilizing high thermal conductivity graphite foams, SAE Paper 2000-01-2207, 2000.
[10] Q. Yu, A.G. Straatman, B.E. Thompson, Carbon-foam finned tubes in air−water heat exchangers, Applied Thermal Engineering 26 (2006) 131–143.
[11] P.T. Garrity, J.F. Klausner, R. Mei, Performance of aluminum and carbon foams for air side heat transfer augmentation, ASME Journal of Heat Transfer 132 (2010) 121901-1–121901-10.
[12] A.G. Straatman, N.C. Gallego, Q. Yu, B.E. Thompson, Characterization of porous carbon foam as a material for compact recuperators, Journal of Engineering for Gas Turbines and Power 129 (2007) 326–330.
[13] N.G. Gallego, J.W. Klett, Carbon foams for thermal management, Carbon 41 (2003) 1461–1466.
[14] K.C. Leong, L.W. Jin, H.Y. Li, J.C. Chai, Forced convection air cooling in porous graphite foam for thermal management applications, in: 11th Intersociety Conference on Thermal and Thermomechanical Phenomena in Electronic Systems, 2008, pp. 57–64.
[15] Y.R. Lin, J.H. Du, W. Wu, L.C. Chow, W. Notardonato, Experimental study on heat transfer and pressure drop of recuperative heat exchangers using carbon foam, ASME Journal of Heat Transfer 132 (2010) 091902-1–091902-10.
[16] J. Yuan, Y. Huang, B. Sundén, W. Wang, Analysis of parameter effects on chemical reaction coupled transport phenomena in SOFC anodes, Heat and Mass Transfer 45 (2009) 471–484.
[17] W. Lu, C.Y. Zhao, S.A. Tassou, Thermal analysis on metal-foam filled heat exchangers. Part I: metal-foam filled pipes, International Journal of Heat and Mass Transfer 49 (2006) 2751–2761.
[18] S.B. Pope, Turbulent Flows, Cambridge University, UK, 2000.
[19] H.K. Versteeg, W. Malalasekera, An Introduction to Computational Fluid Dynamics, second ed., Pearson Prentice Hall, UK, 2007.
[20] Y. Chang, C. Wang, A generalized heat transfer correlation for louver fin geometry, International Journal of Heat and Mass Transfer 40 (1997) 533–544.
[21] Y. Chang, K. Hsu, Y. Lin, C. Wang, A generalized friction correlation for louver fin geometry, International Journal of Heat and Mass Transfer 43 (2000) 2237–2243.
[22] A. Achaichia, T.A. Cowell, Heat transfer and pressure drop characteristics of flat tube and louvered plate fin surfaces, Experimental Thermal and Fluid Science 1 (1988) 147–157.
[23] J. Dong, J. Chen, Z. Chen, W. Zhang, Y. Zhou, Heat transfer and pressure drop correlations for the multi-louvered fin compact heat exchangers, Energy Conversion and Management 48 (2007) 1506–1515.

Paper 4

Performance Analysis of a Countercurrent Flow Heat Exchanger Placed on the Truck Compartment Roof

Wamei Lin

Jinliang Yuan

Bengt Sundén[1]
e-mail: bengt.sunden@energy.lth.se

Department of Energy Sciences,
Lund University,
P. O. Box 118,
S-221 00 Lund, Sweden

Due to the increasing power requirement and the limited available space in vehicles, placing the heat exchanger at the roof or the underbody of vehicles might increase the possibility to handle the cooling requirement. A new configuration of the heat exchanger has to be developed to accommodate with the position change. In this paper, a countercurrent heat exchanger is developed for position on the roof of the vehicle compartment. In order to find an appropriate configuration of fins with high thermal performance on the air side, the computational fluid dynamics approach is applied for a comparative study among louver fin, wavy fin, and pin fin by using ANSYS FLUENT software. It is found that the louver fin performs high thermal performance and low pressure drop. Thus, the louver fin is chosen to be the configuration of the countercurrent flow heat exchanger. It is also found that the countercurrent flow heat exchanger presents higher heat transfer coefficient than the cross flow heat exchanger. Furthermore, the overall size and the air pumping power of the countercurrent flow heat exchanger are lower than those in the cross flow heat exchanger. Several suggestions and recommendations are highlighted. [DOI: 10.1115/1.4007438]

Keywords: thermal performance, pressure drop, countercurrent flow, heat exchanger, roof of vehicles

1 Introduction

Low fuel consumption, low carbon dioxide emission, and low noise emission become much more important than before in the vehicle industry. These requirements lead to a number of technical developments, e.g., new concept on primary missions control like homogeneous charge compression ignition engines, after treatment like exhaust gas recirculation valves [1], and noise shields within the engine compartment. All these efforts increase the operating temperature in the engine compartment. In order to keep the engine working at its optimal conditions, a huge amount of heat has to be released from the engine to the ambient. In modern heavy vehicles, this heat is so huge that a conventional heat exchanger (HEX) cannot handle it easily. In addition, more and more electric powertrain is introduced to heavy vehicles. Because the operating temperature of electric equipment (battery: $\sim$55 °C) is much lower than that of a combustion engine (combustion engine: $\sim$90 °C) [2], larger cooling surface area has to be used for the battery cooling than the one for the combustion engine cooling. However, there is space limitation in vehicles. It is impossible to increase the size of the radiator to dissipate the huge amount of heat from the vehicle. All these factors lead to a revolution of the radiator design in vehicles.

An idea of new HEXs suggested some time ago is to place HEXs at the underbody of vehicles [3–5]. For instance, most public buses have the engine radiator at the underbody. This is mostly due to the engine position (at the rear of the bus). Recently, the Centro Ricerche Fiat [5] used some parts of the vehicle body panels as HEXs to reduce the radiator size in light duty vehicles. Two

roll bond HEXs were installed on the engine hood and below the engine, respectively. These could dissipate 60% of heat from the engine for all the test conditions. In addition, two levels of cooling systems (high temperature and low temperature systems) were introduced to a car in Ref. [6]. The condenser and the intercooler were cooled by liquid instead of air. Thus, the condenser and the intercooler could be relocated from the front of the vehicle to other more suitable places. The rearrangement of HEXs position led to 4% reduction of fuel consumption in the vehicle. Previous studies have shown that the cooling power could be increased and the fuel consumption would be reduced by rearranging the position of HEXs in vehicles [4].

The conventional radiator of the heavy duty vehicles is placed in the front of the vehicle, as shown in Fig. 1. A possible position for placing the radiator is the roof of driver compartment. If the radiator is placed on the roof (as shown in Fig. 1), the coolant flow direction and the air flow direction would be opposite. This is typical principle of a countercurrent flow HEX [7]. However, the engine radiator is normally a cross flow HEX in vehicles. Based on the HEX design theory, generally a countercurrent flow HEX has better thermal performance than does a cross flow HEX, see Ref. [7]. Thus, the option of placing a countercurrent flow HEX on the roof of the truck driver compartment might be a good idea to the engine radiator revolution.

In order to evaluate the performance of the countercurrent flow HEX on the roof of the truck driver compartment, various configurations of fins in HEX are evaluated to choose an appropriate one in this paper. Based on Ref. [8], three configurations of fins (louver-, wavy-, and pin fin) are adopted and analyzed by the ANSYS FLUENT software on the air side of a countercurrent flow HEX. The one presenting high thermal performance and low pressure drop will be selected to compare with a conventional cross flow HEX (louver fin is on the air side and flat tube on the
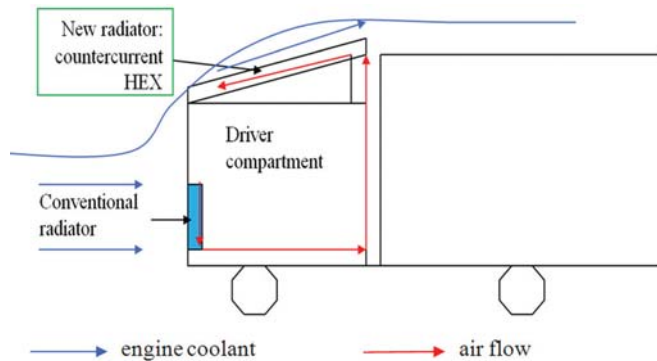

Fig. 1 Schematics of the positions of a radiator in trucks

water side), in terms of thermal performance. Several advantages and disadvantages of the countercurrent flow HEX are outlined and discussed based on a specific case study at the end of the paper.

2 Description of Physical Model and Assumptions

A simplified model of the countercurrent flow HEX is shown in Fig. 2. The engine coolant flows in the negative direction of x-axis. However, the air flow direction (the positive direction of x-axis) is opposite to the direction of engine coolant, as shown in Fig. 2(a). Three different configurations of fins (louver-, wavy-, and pin fin) are placed on the air side of HEX, as shown in Figs. 2(b)–2(d), respectively. The fluid is assumed to be incompressible with constant properties and in steady-state. The engine coolant is assumed to be water. The countercurrent flow HEX is made of aluminum. The thermal resistance between the water tubes and the fins is neglected. In order to simplify the simulation model and save computational time, only a core of the HEX is adopted, as shown in Fig. 2. The overall size of the core is 2.31 mm × 6.85 mm × 70.00 mm (W × H × L). The parameters of the fins are presented in Table 1.

3 Mathematical Formulation and Numerical Method

3.1 Adoption of Flow Model.
Based on the European law, the maximum velocity of heavy vehicles is 80 km/h. Thus, the air inlet velocity in the simulation is ranging from 50 to 70 km/h. In this case, the Reynolds number on the air side is from 2400 to 5000. Thus, low Reynolds number turbulent flow prevails on the air side. In order to capture the low Reynolds number turbulent flow, the "renormalization group" (RNG) k-ε turbulence model is adopted [9,10]. However, laminar flow is used on the water side, in order to simplify the simulation model (the inlet velocity of water is assumed to be less than 2 m/s).

3.2 Governing Equations.
The governing equations for continuity, momentum, and energy can be expressed as follows [11]:

Continuity equation

$$\frac{\partial(\rho u_i)}{\partial x_i} = 0 \qquad (1)$$

Momentum equations

$$\frac{\partial(\rho u_i u_j)}{\partial x_j} = -\frac{\partial p}{\partial x_i} + \frac{\partial}{\partial x_j}\left(\left(\mu + \delta\mu_t\right)\left(\frac{\partial u_i}{\partial x_j} + \frac{\partial u_j}{\partial x_i}\right)\right) \qquad (2)$$
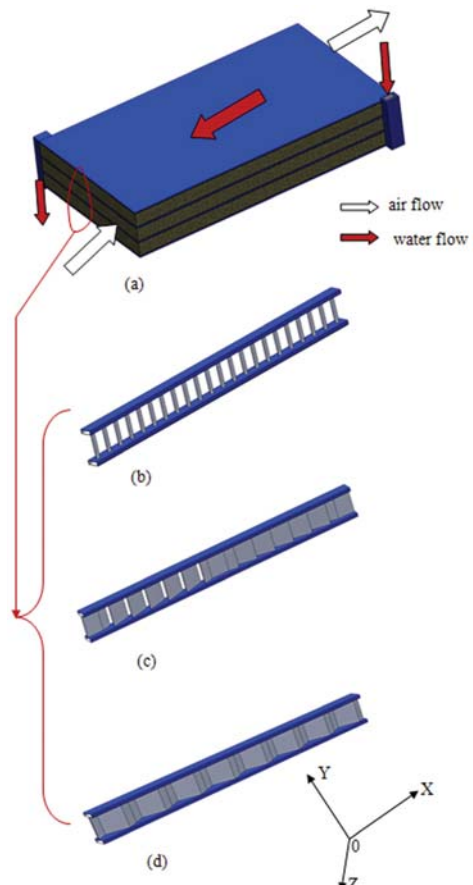

Fig. 2 (a) Schematics of the countercurrent flow HEX, with (b) louver, (c) wavy, and (d) pin fin core

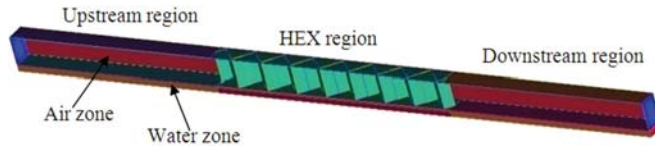| Louver fin [8]	Fin pitch	Fin thickness	Louver spacing	Louver angle (deg)
	2.31	0.152	4.76	17.06
Wavy fin	Fin pitch	Fin thickness	Wave length	Wave amplitude
	2.23	0.152	8.9	1
Pin fin	Pin pattern	Pin diameter	Transverse spacing	Longitudinal spacing
	In-line	0.79	2.3	3.18

Fig. 3   Computational domain

Energy equation

$$\frac{\partial(\rho \mu_j T)}{\partial x_j} = \frac{\partial}{\partial x_j}\left(\left(\frac{\mu}{Pr} + \delta\frac{\mu_t}{Pr_t}\right)\frac{\partial T}{\partial x_j}\right) \qquad (3)$$

When laminar flow (the water side) prevails, $\delta = 0$; when turbulent flow (the air side) prevails, $\delta = 1$. The equations of turbulent kinetic energy k and the rate of energy dissipation ε corresponding to the RNG k-ε turbulence model are

Turbulent kinetic energy k equation

$$\frac{\partial}{\partial x_i}(\rho k u_i) = \frac{\partial}{\partial x_j}\left(\left(\mu + \frac{\mu_t}{\sigma_k}\right)\frac{\partial k}{\partial x_j}\right) + P_k - \rho\varepsilon \qquad (4)$$

Rate of energy dissipation ε equation

$$\frac{\partial}{\partial x_i}(\rho\varepsilon u_i) = \frac{\partial}{\partial x_j}\left(\left(\mu + \frac{\mu_t}{\sigma_\varepsilon}\right)\frac{\partial \varepsilon}{\partial x_j}\right) + C_{1s}\frac{\varepsilon}{k}p_k - C_{2s}^*\rho\frac{\varepsilon^2}{k} \qquad (5)$$

where

$$C_{2s}^* = C_{2s} + \frac{c_\mu\eta^3(1 - \eta/\eta_0)}{1 + \beta\eta^3}, \quad \mu_t = \rho C_\mu\frac{k^2}{s},$$

$$\eta = sk/\varepsilon, \quad \text{and} \quad s = (2s_{ij}s_{ij})^{1/2}$$

The values of all of the constants are as follows (see Ref. [12]):

$$C_\mu = 0.0845; \quad \sigma_k = 0.7194; \quad \sigma_\varepsilon = 0.7194;$$

$$C_{\varepsilon 1} = 1.42; \quad C_{\varepsilon 2} = 1.68; \quad \eta_0 = 4.38; \quad \beta = 0.012$$

3.3 Computational Domain and Boundary Conditions. The louver-, wavy-, and pin fins are symmetrical in the height direction. Thus, only half of the fin height is simulated. The water tube is also simulated by using half height. On the other hand, in order to eliminate the effect of the entrance, the computational domain is extended upstream by an additional length of the HEX. Meanwhile, the computational domain is also extended downstream with the length of the HEX to eliminate the effect of outlet on the flow inside the HEX. Thus, the whole length of the computational domain is three times of the length of the HEX, as shown in Fig. 3.

Because there are air and water zones in the simulation, the boundary conditions should be specified in different zones separately.

1. Air zone
   (a) Upstream region: top-, front-, and back sides are symmetry surfaces; left side is the velocity inlet.

   (b) Downstream region: top-, front-, and back sides are symmetry surfaces; right side is the outlet.
   (c) HEX region: top side is symmetry surface; front side and back side are periodic (as the geometry of louver fin or wavy fin is not symmetry).

2. Water zone
   (a) Upstream region: bottom-, front-, and back sides are symmetry surfaces; left side is the outlet.
   (b) Downstream region: bottom-, front-, and back sides are symmetry surfaces; right side is the velocity inlet (the temperature difference between the air inlet and the water inlet is set to 50 °C).
   (c) HEX region: bottom-, front-, and back sides are symmetry surfaces.

3.4 Numerical Method. The commercial code ANSYS FLUENT 12.0 is used for the numerical solution. A finite volume method is adopted to convert the governing equations to algebraic equations so that they can be solved numerically [12]. The SIMPLE algorithm is used to couple pressure and velocity. A second-order upwind scheme is introduced to the space discretization of the momentum, energy, and turbulence equations in the simulations. The convergence criterion for continuity, momentum, k, and ε equations is below 10^{-3}. However, in order to ensure an energy balance between the water zone and the air zone under the countercurrent flow condition, the convergence criterion of energy is below 10^{-8}.

The mesh generation is carried out by the ICEM software. In order to check the grid independence, three sets of mesh size (coarse: $20 \times 28 \times 250$; middle: $22 \times 34 \times 340$; fine: $26 \times 38 \times 368$) are chosen to be compared in the wavy fin (HEX region in the air zone). The predicted pressure drop and Nusselt number from these three sets of mesh are shown in Table 2. It is found that the deviation of the pressure drop and Nusselt number between the middle case and the fine case is 2.5% and 4.6%, respectively. In order to save computational time and keep the accuracy of the simulation, the middle mesh size ($22 \times 34 \times 340$) is chosen for the wavy fin. The same method was also adopted to check the grid independence of the louver fin and the pin fin.

4 Results and Discussion

4.1 Parameter Definitions. Before analyzing and comparing the fluid flow and heat transfer characteristics for three different configurations of countercurrent flow HEX (louver-, wavy-, and pin fin), the definitions of Nusselt (Nu) number, Stanton (St) number, and friction factor (f) are presented. First, the Nusselt number and Stanton number are calculated as

Table 2 Grid independence study for wavy fin (Re = 3700)

	Coarse (20 × 28 × 250)	Middle (22 × 34 × 340)	Fine (26 × 38 × 368)
$\triangle P$ (Pa)	1350 (19%)	1155 (2.5%)	1126 (base)
Nu	34.2 (54.5%)	23.16 (4.6%)	22.13 (base)

Table 3 Deviation between the simulation model and the experiment

Re	$StPr^{2/3}$ in Ref. [8]	Simulation $StPr^{2/3}$	f in Ref. [8]	Simulation f
2837	0.0092	0.0097 (5.4%)	0.0435	0.044 (1.1%)
3392	0.0087	0.0086 (1.2%)	0.041	0.04 (2.4%)
3769	0.0082	0.0081 (1.2%)	0.0398	0.0382 (4.1%)

$$Re = \frac{\rho_f \cdot u_{max} \cdot D_h}{\mu} \qquad (6)$$

$$h_f = \frac{Q}{A_0 \Delta T} \qquad (7)$$

$$Nu = h_f \cdot \frac{D_h}{\lambda_f} \qquad (8)$$

$$St = \frac{h_f}{\rho_f \cdot u_{max} \cdot C_p} \qquad (9)$$

where, Q is the total amount of heat dissipated to air (W), A_0 the fin surface area (m^2), $\triangle T$ the logarithmic mean temperature difference, i.e., LMTD (K) and D_h the hydraulic diameter (m). These are defined as follows:

$$Q = m \cdot c_p \cdot (T_{out} - T_{in}) \qquad (10)$$

$$\Delta T = \frac{(\Delta T_{max} - \Delta T_{min})}{ln \dfrac{\Delta T_{max}}{\Delta T_{min}}} \qquad (11)$$

$$\Delta T_{max} = \max(T'_{out} - T_{in}, T'_{in} - T_{out}) \qquad (12)$$

$$\Delta T_{min} = \min(T'_{out} - T_{in}, T'_{in} - T_{out}) \qquad (13)$$

$$D_h = \frac{4A_c}{P} \qquad (14)$$

The friction factor (f) is defined as

$$f = \frac{A_c}{A_0} \cdot \frac{2\Delta P}{\rho_f (u_{max})^2} \qquad (15)$$

where, A_c is the minimum free-flow area; u_{max} is the maximum velocity.

4.2 Model Validation. Prior to presenting the simulation results, it is important to validate the computational model. In order to compare the simulation results of the louver fin with the experimental results [8], which were obtained under the cross flow condition, the water zone in the simulation is assumed to be at a constant temperature. The comparison between the simulation and the experimental results is shown in Table 3. The deviation of the $StPr^{2/3}$ between the simulations by the RNG k-ε turbulence model and the experimental data are less than 5.4%, and the deviation of the friction factor f between the simulation and the experimental results less than 4.1%. Thus, there is a good agreement between the simulation and the experiment, in terms of thermal performance and the pressure loss.

4.3 Performance Comparison Among Three Configurations of HEX. The thermal performance and the pressure loss are two important factors in the heat exchanger design. In order to
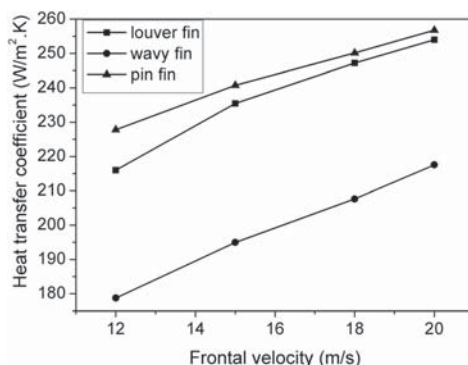
Fig. 4 Heat transfer coefficient versus frontal velocity
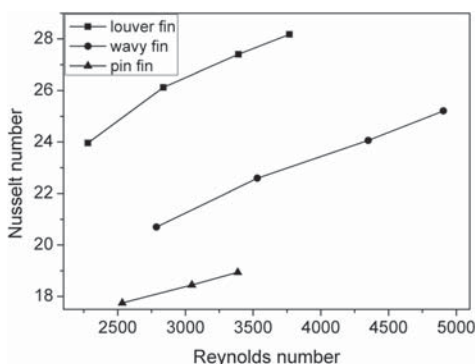
Fig. 5 Nusselt number versus Reynolds number

develop a high performance countercurrent flow HEX, three different configurations of fins (louver-, wavy-, and pin fin) are simulated. The thermal performance and the pressure loss are obtained by using ANSYS FLUENT.

4.3.1 Thermal Performance. The heat transfer coefficients predicted for three configurations of fins are correlated with the frontal velocity, as shown in Fig. 4. Among these three configurations of fins, the cases with louver and pin fins reach higher heat transfer coefficients than does the wavy fin. The main reason causing the different heat transfer coefficients is probably the thermal boundary layers on the different configurations of the fins. For the louver fin, the boundary layer is developed along the louver, but it is broken at the end of the fin. The boundary layer cannot become thick due to the short louver length. This relatively thin boundary layer on the louver fin is the major factor to produce the high thermal performance. In addition, because the boundary layer separates around the pin fin, a high thermal performance is achieved as well. However, the thickness of the boundary layer on the wavy fin is kept constant, because the thickness is reduced on one side and increased on the other side at the same location. Due to the constant thickness boundary layer, the thermal performance of the wavy fin is not as good as that of the louver fin and the pin fin.

On the other hand, in order to remove the effect of different size of fin, the dimensionless parameters (Nu number and Re number) are introduced to analyze the thermal performance. Figure 5 illuminates the relationship between the Nu number and the Re number. The louver fin presents higher Nu number than do
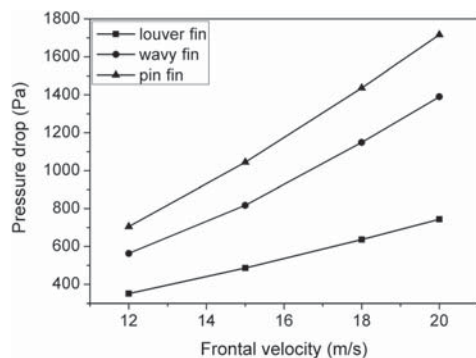
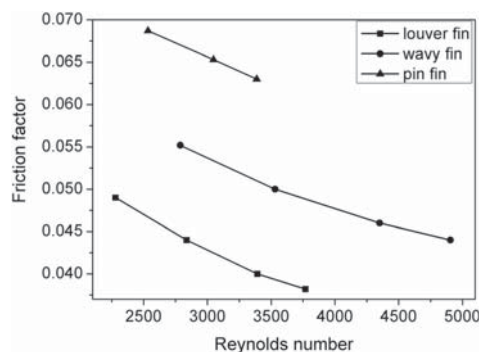**Fig. 6 Pressure drop versus frontal velocity**

Fig. 7 Friction factor versus Reynolds number

the wavy fin and the pin fin at the same Re number. Even though the heat transfer coefficient is similar between the pin fin and the louver fin, due to the in-line fin pattern and the small hydraulic diameter in the pin fin, the Nu number is much lower in the pin fin than the one in the louver fin. Based on Figs. 4 and 5, it is revealed that the louver fin presents better thermal performance than the other cases.

4.3.2 Pressure Loss. Figure 6 illuminates the pressure drop through the three configurations of fins (louver-, wavy-, and pin fin) as a function of frontal air velocity. As expected, the pressure drops increase with increasing air velocity. The louver fin presents the lowest pressure drop among the three configurations. This result might appear because the flow through the louver fins becomes parallel to the louvers at high speed. In this case, the louver fins act like a flat plate, and the air flow path is smooth due to similarity with a "flat plate" boundary layer flow. However, the flow path might change its direction along the fins due to the structure of the wavy fin and pin fin. The smooth flow path along the louver fin might be the main reason causing the flow resistance in the louver fin to be lower than those of the wavy fin and the pin fin. The low flow resistance on the louver fin is also shown in Fig. 7. By considering the dimensionless parameter–friction factor (*f*), the louver fin has lower friction factor than the one in the wavy fin or the pin fin at the same Reynolds number.

4.4 Performance Comparison Between a Countercurrent Flow HEX and a Cross Flow HEX. Based on the analysis of thermal performance and pressure loss among the louver-, wavy-, and pin fins, it is proved that the louver fin presents higher thermal
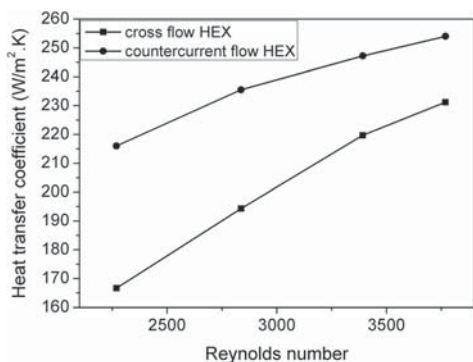

Fig. 8 Heat transfer coefficient in cross flow HEX and in countercurrent flow HEX

Table 4 Assumed operating data of a truck

Cooling power (kW)	200	
Truck speed (km/h)	65	
Radiator (water side)	$T_{in} = 90\ °C$	$T_{out} = 85\ °C$
Radiator (air side)	$T_{in} = 30\ °C$	$T_{out} = 55\ °C$

performance and lower pressure drop than do the wavy fin and the pin fin. Thus, the louver fin is chosen as the configuration of fin on the air side for the countercurrent flow HEX. In order to evaluate the performance of the countercurrent flow HEX, a conventional aluminum louver fin cross flow HEX is adopted for comparison. Due to the fact that the same louver fin is used in the countercurrent and cross flow HEXs, the flow resistance on the air side is the same for both cases. Thus, the pressure loss is not considered here.

The thermal performance comparison between the cross flow HEX and the countercurrent flow HEX is shown in Fig. 8. The countercurrent flow HEX has higher heat transfer coefficient than does the cross flow HEX. This result is mainly because the countercurrent flow arrangement could maximize the temperature difference between two fluids to transfer more heat than does the cross flow arrangement. When the Reynolds number varies from 2800 to 3800, the heat transfer coefficient of the countercurrent flow HEX is 21% to 9.8%, respectively, higher than the one in the cross flow HEX. This high heat transfer coefficient is beneficial to reduce the size of the countercurrent flow HEX compared to the cross flow HEX.

Furthermore, a specific case study (a typical truck with 200 kW cooling power) is carried out to analyze the performance of the countercurrent flow HEX. The operating data are shown in Table 4.

Based on this specific case, the different results between the countercurrent flow and the cross flow HEXs are shown in Table 5. Due to the high heat transfer coefficient performance in the countercurrent flow HEX, the total cooling surface area (air side) is reduced by 11.2% compared to the cross flow HEX. The overall size of the cross flow HEX could be designed as $1000 \times 337 \times 70$ mm (W × H × L). Meanwhile, the overall size of the countercurrent flow HEX could be designed as $1000 \times 300 \times 70$ mm (W × H × L). Because the cross-section area of the countercurrent flow HEX (1000 mm × 300 mm) is 11% less than that of the cross flow HEX (1000 mm × 337 mm), there is 11% reduction in power for pushing air through the countercurrent flow HEX.

However, due to the height of countercurrent flow HEX (300 mm), the streamline of flow field of the heavy vehicle might be destroyed, and a huge flow resistance might be presented to the vehicle. In order to reduce the flow resistance and optimize the performance of the countercurrent flow HEX, the countercurrent flow HEX

Table 5 Comparison between the cross flow HEX and the countercurrent flow HEX

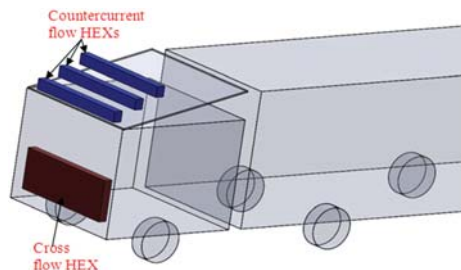|	Cross flow HEX	Countercurrent flow HEX
Air side cooling surface area (m²)	19.3	17.1 (11.2% reduction)
Overall size (W × H × L) (mm × mm × mm)	1000 × 337 × 70	1000 × 300 × 70
Total volume (m³)	0.0236	0.021 (11% reduction)
Power for pushing air through HEX (W)	3858	3434 (11% reduction)

Fig. 9 Countercurrent flow HEX and cross flow HEX in a heavy duty truck

($1000 \times 300 \times 70$ mm) is divided into three smaller countercurrent flow HEXs (the size of each one is $1000 \times 100 \times 70$ mm). These three countercurrent flow HEXs are placed on the gradient roof of vehicle as like a staircase, as shown in Fig. 9.

After the analysis of the specific cases, several advantages and disadvantages of countercurrent flow HEX could be summarized as follows:

- Advantages:

  (1) The heat transfer coefficient is higher in the countercurrent flow HEX than the one in the cross flow HEX.
  (2) The overall size of the countercurrent flow HEX is smaller than that of the cross flow HEX, when the removed heat is the same.
  (3) The pressure loss is lower in the countercurrent flow HEX than the one in the cross flow HEX, because of the reduction of size in the countercurrent flow HEX.
  (4) The high heat transfer coefficient and low pressure loss lead to a high coefficient of performance in the countercurrent flow HEX.

- Disadvantages:

  1. The countercurrent flow HEX placed on the roof of the vehicle might destroy the streamline flow field of the vehicle. The collocation of countercurrent flow HEX should be optimized.
  2. The cooling air through the countercurrent flow HEX is driven by the movement of vehicles. When the vehicle climbs on a mountain, the speed of the vehicle is low. However, the engine cooling power is high at the same time. Thus, this problem should be analyzed in future work.

5 Conclusion and Recommendation

Due to the increasing cooling power and the space limitation in vehicles, it is impossible to increase the size of the radiator to dissipate the increasing amount of heat from the engine. Placing the radiator at the underbody of the vehicle or on the roof of the driver compartment might be a good method to handle the increasing cooling power. In this paper, a radiator is designed to be placed on the roof of the truck compartment. Due to the radiator position change, a countercurrent flow heat exchanger is accordingly proposed. The major results are as follows:

1. Compared to the wavy and the pin fins, the louver fin design presents high thermal performance and low pressure drop in the countercurrent flow HEX.
2. The heat transfer coefficient in the louver fin countercurrent flow HEX is 21%–9.8% higher than the one in the louver fin cross flow HEX when Reynolds number varies between 2800 and 3800.
3. For the specific case in this paper, the total cooling surface area of the countercurrent flow HEX could be reduced by 11.2% compared to the cross flow HEX. Moreover, the power for pushing air through the countercurrent flow HEX is 11% lower than that of the cross flow HEX.

Thus, placing a countercurrent flow HEX on the roof of the truck driver compartment is a useful method to dissipate the increasing cooling power in vehicles. However, there are still several problems facing the application of countercurrent flow HEX in vehicles. Thus, much effort (the collocation of HEX, air supply to HEX without fans, or the available place for a fan) has to be conducted for the development of countercurrent flow HEXs in vehicles.

Nomenclature

A_c = minimum free-flow area on the air side, m²
A_0 = total heat transfer surface area on the air side, m²
c_p = air specific heat, J·kg⁻¹·K⁻¹
D_h = hydraulic diameter, m
f = Fanning friction factor, dimensionless
h = heat transfer coefficient, W·m⁻²·K⁻¹
H = height of fin, m
k = turbulent kinetic energy, m²·s⁻²
L = length of fin, m
m = air mass flow, kg·s⁻¹
Nu = Nusselt number, dimensionless
P = wetted perimeter of passages on the air side, m
P_k = production of turbulent kinetic energy
Pr = Prandtl number, dimensionless
Q = total amount of heat dissipating to air side, W
Re = Reynolds number, dimensionless
St = Stanton number, dimensionless
T_in = air inlet temperature, K
T_out = air outlet temperature, K
T'_in = water inlet temperature, K
T'_out = water outlet temperature, K
u = air velocity, m·s⁻¹
W = width of fin, m
ΔP = pressure drop through fins, Pa
ΔT = logarithmic mean temperature difference, K
ε = rate of energy dissipation
λ = thermal conductivity, W·m⁻¹·K⁻¹
ρ = density of fluid, kg·m⁻³
μ = dynamic viscosity of air, Pa s

Subscripts

f = air fluid
max = maximum
min = minimum
t = turbulent

References

[1] Hountalas, D. T., Mavropoulos, G. C., and Binder, K. B., 2008, "Effect of Exhaust Gas Recirculation (EGR) Temperature for Various EGR Rates on Heavy Duty DI Diesel Engine Performance and Emissions," Energy, **33**, pp. 272–283.

[2] Doughty, D. H., Butler, P. C., Jungst, R. G., and Roth, E. P., 2002, "Lithium Battery Thermal Models," J. Power Sources, **110**, pp. 357–363.

[3] Khaled, M., Harambat, F., and Peerhossaini, H., 2010, "Underhood Thermal Management: Temperature and Heat Flux Measurements and Physical Analysis," Appl. Therm. Eng., **30**, pp. 590–598.

[4] Larsson, L., Wiklund, T., and Löfdahl, L., 2011, "Cooling Performance Investigation of a Rear Mounted Cooling Package for Heavy Vehicles," SAE Technical Paper No. 2011-01-0174.

[5] Malvicino, C., Mattiello, F., and Seccardini, R., 2011, "Flat Heat Exchangers," Proceedings of the 10th Vehicle Thermal Management Systems Conference and Exhibition, Gaydon, Warwickshire, UK, pp. 91–98.

[6] Malvicino, C., Sciullo, F. D., Cuniberti, M., Vestrelli, F., and Beltramelli, F., 2011, "Dual Level Vehicle Heat Rejection System," Proceedings of the 10th Vehicle Thermal Management Systems Conference & Exhibition, Gaydon, Warwickshire, UK, pp. 473–480.

[7] Shah, R. K., and Sekulic, D. P., 2003, *Fundamentals of Heat Exchanger Design*, John Wiley & Sons, New York.

[8] Kays, W. M., and London, A. L., 1995, *Compact Heat Exchangers*, 3rd ed., McGraw-Hill, New York.

[9] Pope, S. B., 2000, *Turbulent Flows*, Cambridge University, Cambridge, England.

[10] ANSYS, Inc., 2009, ANSYS FLUENT 12.0—Theory Guide.

[11] Tannehill, J. C., Anderson, D. A., and Pletcher, R. H., 1997, *Computational Fluid Mechanics and Heat Transfer*, 2nd ed., Taylor & Francis, London.

[12] Versteeg, H. K., and Malalasekera, W., 2007, *An Introduction to Computational Fluid Dynamics*, 2nd ed., Pearson Prentice-Hall, Englewood Cliffs, NJ.

Paper 5

Heat Transfer Engineering

Performance Analysis of Aluminum and Graphite Foam Heat Exchangers Under Countercurrent Arrangement

Wamei Lin [a] , Jinliang Yuan [a] & Bengt Sundén [a]

[a] Department of Energy Sciences , Lund University , Lund , Sweden
Accepted author version posted online: 06 Sep 2013.Published online: 25 Nov 2013.

PLEASE SCROLL DOWN FOR ARTICLE

Taylor & Francis
Taylor & Francis Group

Performance Analysis of Aluminum and Graphite Foam Heat Exchangers Under Countercurrent Arrangement

WAMEI LIN, JINLIANG YUAN, and BENGT SUNDÉN

Department of Energy Sciences, Lund University, Lund, Sweden

Due to the increasing power requirement and the limited available space in the vehicles, a countercurrent heat exchanger (HEX) is proposed for the position on the roof of the vehicle compartment. Furthermore, a new material, graphite foam with high thermal conductivity and low density, is a potential material for HEXs in vehicles. In order to evaluate the performance of the graphite foam HEX, the CFD computational fluid dynamics (CFD) approach is applied in a comparative study between the graphite foam and the aluminum HEXs under countercurrent flow condition. The analysis is conducted for the thermal performance (heat transfer coefficient) and the pressure loss. The simulation results show that the graphite foam HEX proves higher thermal performance than the aluminum HEX. However, due to the high pressure loss in the graphite foam HEX, the coefficient of performance in the graphite foam HEX is much lower than that of the aluminum HEX. A specific case study is carried out to evaluate the performance of graphite foam HEX as well. Useful recommendations are highlighted and provided to promote the development of the countercurrent flow HEXs in vehicles.

INTRODUCTION

Due to the increasing need for power production and the limited available space in vehicles, it is extremely difficult to increase the size of the radiators placed in the front of vehicles. The position of countercurrent heat exchangers (HEXs) in vehicles has to be rearranged in an effective way to dissipate the huge cooling power. Recently, Malvicino et al. [1] used some parts of the vehicle body panels as HEXs to reduce the radiator size in light-duty vehicles. Two roll bond HEXs installed on the engine hood and below the engine could dissipate 60% of heat from the engine in all the test conditions. In reference [2] two levels of cooling systems (high-temperature and low-temperature systems) were introduced to a car. The condenser and the intercooler were cooled by liquid instead of air. Thus, the condenser and intercooler could be relocated from the front of the vehicle to other suitable places. The rearrangement of HEXs' positions led to 4% reduction of fuel consumption in the vehicle. Moreover, the thickness of the cooling package (including a radiator,

a condenser, and a subradiator) was reduced by placing the subradiator on the top (instead of in the front) of the condenser. Due to the slim cooling package, the cooling fan power was smaller and fuel consumption was reduced by 3–5% [3].

Previous studies have shown that cooling power could be increased and fuel consumption would be reduced by rearranging the position of HEXs in vehicles. The conventional radiator of the heavy-duty vehicles is always placed in the front of the vehicle, as shown in Figure 1. If the radiator were placed at the underbody or on the roof of the vehicle, it might increase the possibility of meeting the critical cooling requirement. A new configuration of the heat exchangers has to be developed to accommodate the position change. As shown in Figure 1, the engine coolant and the airflow directions are opposite, as the radiator is placed on the roof of the driver compartment. This is a typical principle of a countercurrent-flow HEX [4]. In the vehicle industry, the engine radiator is mostly a cross-flow HEX. However, a countercurrent-flow HEX generally has better thermal performance than does a cross-flow HEX [5]. Thus, placing a countercurrent-flow HEX on the roof of the truck driver compartment might be a good option for the engine radiator.

On the other hand, the thermal performance of the aluminum radiator is limited, because the radiator has nearly reached its peak compactness nowadays. One useful method to increase the compactness or thermal performance of the HEX is to use
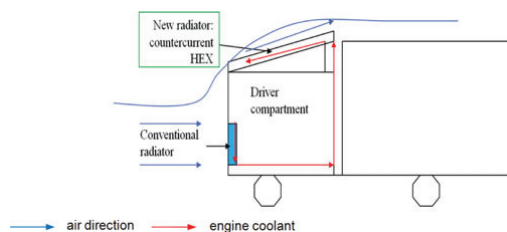
Figure 1 Schematics of the positions of a radiator in truck. (Color figure available online.)

microcellular foam materials. A lot of research has been focused on the aluminum foam HEX [6–13]. However, the porous aluminum only presented a thermal performance similar to that of the conventional louvered fin design. Meanwhile, the pressure drop was higher in the aluminum foam than in the louvered fin design [7]. Another interesting foam material is graphite foam, whose effective thermal conductivity (40 to 150 W/(m-K)) [14] is much higher than that of the aluminum foam (2 to 26 W/(m-K)) [8]. Besides that, the graphite foam has low density (0.2 to 0.6 g/cm^3) and large specific surface area (5000 to 50000 m^2/m^3) [15, 16].

The graphite foam is a potential material for heat exchangers, due to its high thermal performance. Klett et al. [17] designed a radiator with carbon foam. The cross section of the automotive radiator was reduced from 48 cm × 69 cm to 20 cm × 20 cm. The reduced size can decrease the overall weight, cost, and volume of the system. Yu et al. [18] proved that the thermal performance of a carbon foam finned tube radiator could be improved by 15%, compared to a conventional aluminum finned tube radiator, without changing the frontal area, or the airflow rate and pressure drop. Furthermore, Garrity et al. [19] found that the carbon foam samples took away more heat than the multilouvered fin when the volume of the heat exchangers was the same.

However, there is high pressure drop through the graphite foam, due to the large hydrodynamic loss associated with the small open pores in the graphite foam [20]. An appropriate configuration of the foam can reduce the pressure drop [21]. For instance, Lin et al. [22] proved that corrugated foam could reduce the pressure drop and maintain a high heat transfer coefficient. However, the coefficient of performance (COP, a ratio of the removed heat to the input pumping power) of the corrugated foam is lower than that of the aluminum louver fin [23].

In order to develop a new HEX to resolve the cooling problems in the vehicle, a countercurrent-flow HEX might be introduced and placed on the roof of a heavy-duty vehicle. The HEX might be made of graphite foam. To reduce the pressure drop of graphite foam HEX, a triangular corrugated configuration is applied here to the foam on the air side of the HEX. Furthermore, a comparison between the graphite foam and the aluminum heat exchangers under the countercurrent flow is carried out by computational fluid dynamics (CFD), to evaluate the thermal performance and the flow characteristics. Finally, the
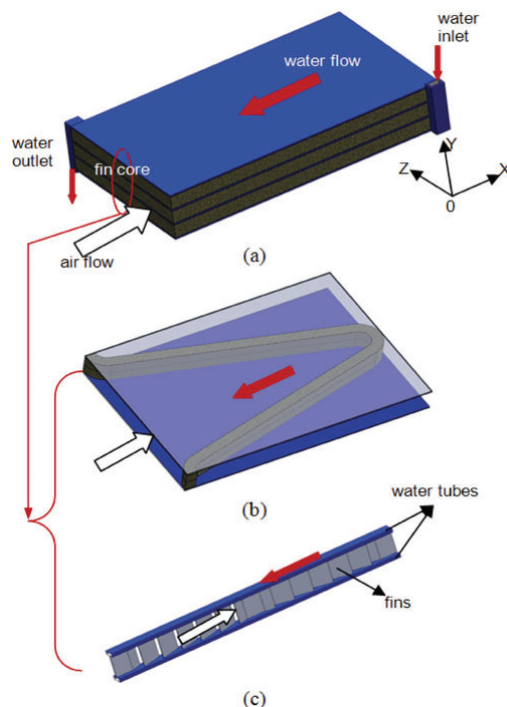
Figure 2 (a) Schematics of the countercurrent flow HEX, with (b) graphite foam fin and (c) aluminum louver fin core. (Color figure available online.)

coefficient of performance (COP, a ratio of the removed heat to the input pumping power) is analyzed.

PHYSICAL MODEL

A simplified configuration of the countercurrent-flow HEX is shown in Figure 2. The hot water is separated and distributed into different water tubes after entering from the inlet collector of the HEX. Then the water flows along the negative direction of the X-axis inside the water tubes and dissipates heat through the tubes and fins to the ambient air. Finally it leaves the HEX through the outlet collector. However, the air flows through the fins along the positive direction of the X-axis, which is opposite to the flow direction of water, to bring away the dissipated heat from the water, as shown in Figure 2a. In order to simplify the simulation model and save computational time, only a core of the HEX is adopted. This is shown in Figures 2b and 2c, respectively, for the graphite foam fin and aluminum louver fin. The overall size of the core of the graphite foam fin is 49.70 mm × 6.85 mm × 70.00 mm (W × H × L). The size of the aluminum louver fin is: 2.31 mm × 6.85 mm × 70.00 mm (W × H × L). The detailed configuration parameters are shown in Table 1. Furthermore, the parameters of graphite foam material are presented in Table 2.

Table 1 Sizes of aluminum louver fin and graphite foam fin

Aluminum louver fin [30]	Fin pitch (mm), 2.31	Fin thickness (mm), 0.152	Louver spacing (mm), 4.76	Louver angle (°), 17.06
Graphite foam fin	Fin height (mm), 6.75	Fin thickness (mm), 3	Wave length (mm), 49.7	Double wave amplitude (mm), 70

On the other hand, the fluid is assumed to be incompressible with constant properties, and the flow is steady-state. The thermal resistance between the water tubes and the fins is neglected.

MATHEMATICAL FORMULATION AND NUMERICAL METHOD

Adoption of Flow Model

Based on the velocity of heavy vehicles, the air inlet velocity of the countercurrent-flow HEX in the simulation ranges from 50 to 70 km/h. In this case, the Reynolds number on the air side ranges from 2400 to 5000. Thus, low-Reynolds-number turbulent flow prevails on the air side. In order to capture the low Reynolds characteristics in the turbulent flow, the "renormalization group" (RNG) k-ε turbulence model is adopted [24, 25] on the air side. However, laminar flow prevails inside the graphite foam. This is so because it is difficult to generate turbulent eddies in the small open cells of the graphite foam. Furthermore, laminar flow is considered on the water side as well, in order to simplify the simulation model (the inlet velocity of water is assumed to be less than 2 m/s).

Mathematical Formulation

Based on the already-mentioned assumptions, the governing equations for continuity, momentum, and energy can be expressed as follows [26–28]:

Continuity equation:

$$\frac{\partial(\rho_f u_i)}{\partial x_i} = 0 \qquad (1)$$

Momentum equations:

$$\frac{\partial(\rho_f u_i u_j)}{\partial x_j} = -\varphi \frac{\partial p}{\partial x_i} + \frac{\partial}{\partial x_j}\left((\mu_f + \delta\mu_t)\left(\frac{\partial u_i}{\partial x_j} + \frac{\partial u_j}{\partial x_i}\right)\right)$$
$$+ \varphi S_i \qquad (2)$$

Energy equation:

$$\frac{\partial(\rho_f u_i T)}{\partial x_i} = \frac{\partial}{\partial x_i}\left(\left(\frac{\mu_f}{\Pr_f} + \delta\frac{\mu_t}{\Pr_t}\right)\frac{\partial T}{\partial x_i}\right) \qquad (3)$$

The heat transfer in porous media (graphite foam zone) is under the assumption of a local thermal equilibrium between fluid and solid phases. The different terms in the governing equations are defined differently in the air zone, water zone, and graphite foam zone, as shown in Table 3.

For the air side, the equations of turbulent kinetic energy k and the rate of energy dissipation ε corresponding to the RNG k-ε turbulence model are:

Turbulent kinetic energy k equation:

$$\frac{\partial}{\partial x_i}(\rho k u_i) = \frac{\partial}{\partial x_j}\left(\left(\mu + \frac{\mu_t}{\sigma_k}\right)\frac{\partial k}{\partial x_j}\right) + P_k - \rho\varepsilon \qquad (4)$$

Rate of energy dissipation ε equation:

$$\frac{\partial}{\partial x_i}(\rho\varepsilon u_i) = \frac{\partial}{\partial x_j}\left(\left(\mu + \frac{\mu_t}{\sigma_\varepsilon}\right)\frac{\partial\varepsilon}{\partial x_j}\right) + C_{\varepsilon 1}\frac{\varepsilon}{K}P_k - C_{\varepsilon 2}^*\rho\frac{\varepsilon^2}{k}$$
$$(5)$$

where

$$C_{\varepsilon 2}^* = C_{\varepsilon 2} + \frac{c_\mu \eta^3(1 - \eta/\eta_0)}{1 + \beta\eta^3}, \quad \mu_t = \rho C_\mu \frac{k^2}{\varepsilon}$$

and

$$\eta = Sk/\varepsilon \text{ and } S = (2S_{ij}S_{ij})^{0.5}$$

The values of the constants are as follows:

$$C_\mu = 0.0845; \sigma_k = 0.7194; \sigma_\varepsilon = 0.7194;$$

$$C_{\varepsilon 1} = 1.42; C_{\varepsilon 2} = 1.68; \eta_0 = 4.38; \beta = 0.012.$$

Computational Domain and Boundary Conditions

Only half of the fin height is simulated, due to the symmetry in the fin height direction. The water tube is also simulated for a half height. Moreover, in order to eliminate the effect of the entrance on the flow inside the HEX, the computational domain is extended upstream by two times of the length of the HEX. The downstream region of the HEX is also extended by two times of the HEX length, to eliminate the effect of outlet on the flow inside the HEX. Thus the total length of the computational domain is five times of the length of the HEX, as shown in Figure 3.

Table 2 Parameters of graphite foam [20]

Porosity	Effective thermal conductivity (W/(m-K))	Density (kg/m³)	Area to volume ratio (m²/m³)	Permeability (m²)	Forchheimer coefficient
0.82	120	500	5420	6.13×10^{-10}	0.4457

Table 3 Parameters definition in different zones

Parameter	Air zone	Water zone	Graphite foam zone
ρ_f	ρ_{air}	ρ_{water}	ρ_{air}
μ_f	μ_{air}	μ_{water}	μ_{air}
Pr_f	Pr_{air}	Pr_{water}	$\frac{\mu_{air}^c p_{eff}}{k_{eff}}$ where $c_{p.eff} = \varphi c_{p.air}$
S_i	0	0	$-(\frac{\mu_{air}}{\alpha} u_i + \frac{\rho_{air} c_F}{\sqrt{\alpha}} \lvert u \rvert u_i)$ (based on Forchheimer extended Darcy's equation)
δ	1	0	0
φ	1	1	0.82

Because there are air and water zones in this simulation, the boundary conditions should be specified in the different zones separately.

1. Air zone:
   a) Upstream region: top, front, and back sides are symmetry surfaces; left side is the velocity inlet.
   b) Downstream region: top, front, and back sides are symmetry surfaces; right side is the outlet.
   c) HEX region: top side is a symmetry surface; front side and back side are periodic for louver fin (due to the geometry of louver fin being not symmetry). However, front and back side are symmetry surfaces for the graphite foam fin.

2. Water zone:
   a) Upstream region: bottom, front, and back sides are symmetry surfaces; left side is the outlet.
   b) Downstream region: bottom, front, and back sides are symmetry surfaces; right side is the velocity inlet (the temperature difference between the air and the water inlets is set to 50°C).
   c) HEX region: bottom, front, and back sides are symmetry surfaces.

Numerical Method

The commercial code ANSYS FLUENT 12.0 is used for the numerical solution. A finite-volume method (FVM) is adopted to convert the governing equations to algebraic equations so that they can be solved numerically [29]. The SIMPLE algorithm is

Figure 3 Computational domain of graphite foam fin. (Color figure available online.)

used to couple pressure and velocity. A second-order upwind scheme is used for the space discretization of the momentum, energy and turbulence equations in the simulations. The convergence criterion for continuity, momentum, k, and ε equations is below 10^{-3}. However, the convergence criterion for energy is below 10^{-8}, in order to ensure the energy balance between the air zone and the water zone under countercurrent flow.

The mesh generation is carried out by the commercial software ICEM. In order to achieve grid independence, three sets of mesh size ($150 \times 21 \times 100$; $139 \times 21 \times 100$; $139 \times 15 \times 100$) are built for the graphite foam HEX region in the air zone. Other mesh sizes ($150 \times 5 \times 100$, $139 \times 5 \times 100$, $139 \times 3 \times 100$) are applied for the HEX region in the water zone. The comparison of pressure drop and heat transfer coefficient among the three sets of mesh sizes shows that the variation of pressure drop is between 1.5% and 2.2% in the graphite foam HEX region of the air zone, and between 0.013% and 0.35% in the HEX region of the water zone. The variation of heat transfer coefficient is between 0.25% and 0.05% in the graphite foam HEX region of the air zone, and between 0.064% and 0.33% in the HEX region of the water zone (when the air inlet velocity is 18 m/s and the water inlet speed is 1.5 m/s). Thus, the mesh size of $139 \times 21 \times 100$ is adopted for the graphite foam fin in the air zone, and $139 \times 5 \times 100$ is adopted for the water zone core. Moreover, the same method is adopted to check the grid independence of the aluminum louver fin simulation.

RESULTS AND DISCUSSION

Parameter Definitions

Before presenting the simulation results, some parameters have to be defined. The first one is the heat transfer coefficient, which reads:

$$h = \frac{Q}{A_0 \Delta T} \qquad (6)$$

where

$$Q = m_f c_p (T_{out} - T_{in}) \qquad (7)$$

$$\Delta T = \frac{\Delta T_{max} - \Delta T_{min}}{\ln \frac{\Delta T_{max}}{\Delta T_{min}}} \qquad (8)$$

$$\Delta T_{max} = \max(T_{out.water} - T_{in.air}, T_{in.water} - T_{out.air}) \qquad (9)$$

$$\Delta T_{min} = \min(T_{out.water} - T_{in.air}, T_{in.water} - T_{out.air}) \qquad (10)$$

where A_0 is the fin surface area (m²). In the graphite foam, $A_0 = \gamma V$ (γ is the area to volume ratio, m²/m³; V is the volume of graphite foam, m³).

On the other hand, the coefficient of performance (COP) is the ratio between the removed heat and the required pumping power,

$$COP = \frac{Q}{P_{pum}} = \frac{Q}{u_{in.air} A_{in} \Delta p} \qquad (11)$$
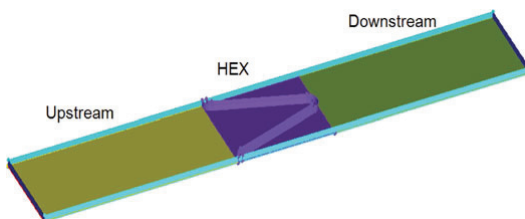
Table 4 Deviation between the simulation results and the experimental data (aluminum louver fin)

Re	StPr$^{2/3}$ in [30]	Simulation StPr$^{2/3}$	f in [30]	Simulation f
2837	0.0092	0.0097 (5.4%)	0.0435	0.044 (1.1%)
3392	0.0087	0.0086 (1.2%)	0.041	0.04 (2.4%)
3769	0.0082	0.0081 (1.2%)	0.0398	0.0382 (4.1%)

where Δp is the air pressure drop through the countercurrent-flow HEX (Pa).

Model Validation

Prior to any further simulation, the validation of the model has to be carried out. There are two simulation models in this paper. One is the graphite foam fin model, and there is another one for the aluminum louver fin. The validation of the graphite foam model was carried out and presented in reference [23]. It was shown that the simulated pressure drop and the thermal performance of the graphite foam agreed satisfactorily with the experimental data. On the other hand, the aluminum louver fin model was validated by comparing with experimental results in reference [30]. The deviation between the simulation and the experimental results is shown in Table 4. The StPr$^{2/3}$ predicted by the RNG k-ε turbulence model deviated less than 5.4% from the experimental results. Moreover, the deviation of the friction factor f between the simulation and the experimental results is less than 4.1%. Thus, there is a good agreement as well for the aluminum louver fin, in terms of thermal performance and pressure drop.

Performance Comparison Between the Graphite Foam Fin and the Aluminum Louver Fin

The thermal performance and pressure loss are two important factors in the heat exchanger design. In order to compare the performance of the graphite foam fin and the aluminum louver fin, the heat transfer coefficient is considered in the thermal performance. The pressure drop is used to analyze the flow characteristics. Finally, a composite parameter COP is presented.

Thermal Performance

The heat transfer coefficients predicted for the graphite foam fin and the aluminum louver fin are shown in Figure 4. The heat transfer coefficients increase with the frontal velocity. Furthermore, the heat transfer coefficient in the graphite foam fin is increased more rapdily than the one in the aluminum louver fin. Figure 4 also shows that the heat transfer coefficient of the graphite foam fin is much higher than that of the aluminum louver fin. Thus, there is a high thermal performance in the graphite foam fin. This is mostly because of the special structure of the graphite foam, in which there are many opening pores connected together. The air changes its direction very frequently by the inducement of the foam structure. In this case, the air can
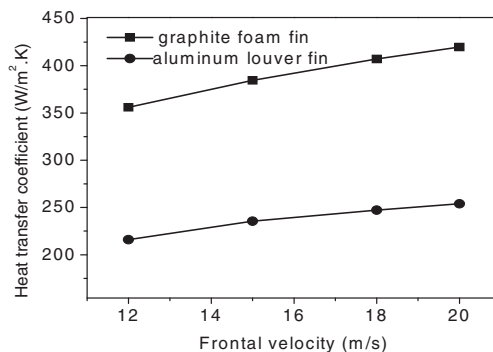
Figure 4 Heat transfer coefficients at different velocity.

be mixed sufficiently in the graphite foam to increase the heat transfer coefficient. Meanwhile, there is an extremely high thermal conductivity in the graphite foam. The heat transfer inside the solid foam is so fast that there is big temperature difference between the air and fin wall. All these factors contribute to the high thermal performance of the graphite foam fin.

Pressure Loss

The pressure loss through the graphite foam is based on the Forchheimer extended Darcy's equation (the source term in Eq. (2)). Figure 5 illuminates the pressure drop through the graphite foam fin and the aluminum louver fin as a function of frontal air velocity. It is clear that the pressure drop increases with the frontal velocity. However, the pressure drop through the graphite foam is much higher than that through the aluminum louver fin. Meanwhile, the pressure drop is increasing extremely more rapidly in the graphite foam than the one in the aluminum louver fin. The high pressure drop implies that there is a high flow resistance in the graphite foam, which is associated with a big number of small-size open pores in the graphite foam. Due to the scrambling of the open pores, the air changes its flow direction very frequently inside the foam, which causes a high
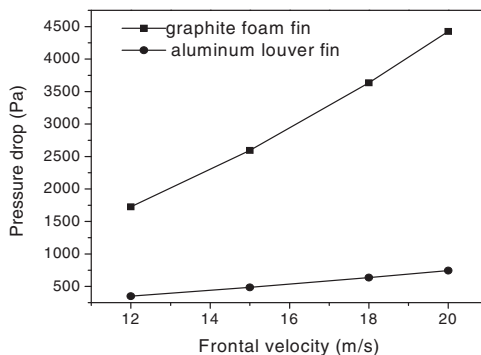
Figure 5 Pressure drops at different velocity.

Figure 6   Coefficient of performance (COP) at different velocity.

Table 6   Comparison between the graphite foam HEX and aluminum louver fin HEX under countercurrent flow
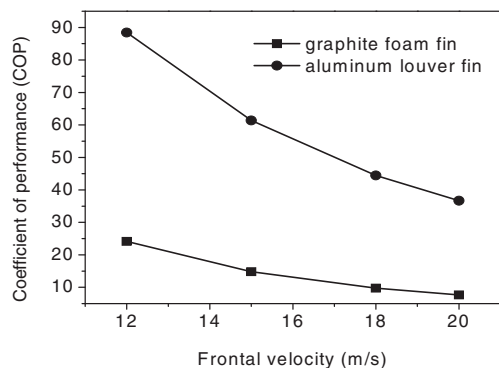
	Graphite foam HEX	Aluminum louver fin HEX
Cooling surface area (m^2)	11.75	17.1
Overall size (W × H × L) (mm × mm × mm)	1000 × 163 × 70	1000 × 300 × 70
Total volume (m^3)	0.0114	0.021
Weight of fins in air side (kg)	1.12	3.58
Power for forcing air through HEX (W)	7610	3434

hydrodynamic loss. Moreover, the large specific surface area in the graphite foam also increases the hydrodynamic loss. It is a fact that the high flow resistance in the graphite foam fin is the major concern for any further applications, compared to the aluminum louver fin.

Coefficient of Performance (COP)

There is a high heat transfer coefficient in the graphite foam fin (as shown in Figure 4), together with a high pressure drop as in Figure 5. In order to compare the graphite foam fin with the aluminum louver fin in an appropriate manner, the coefficient of performance (COP) is usually adopted. The definition of COP is shown in Eq. (11). The simulation results of COP are shown in Figure 6. Even though there is high thermal performance in the graphite foam fin, the COP of graphite foam is lower than that in the aluminum louver fin, due to the extremely high flow resistance in the graphite foam. The low COP of graphite foam implies that more pumping power of air is required for the graphite foam HEX than for the aluminum louver fin HEX under the same dissipated heat condition.

On the other hand, the COP values are reduced when the velocity is increased. The COP of the aluminum louver fin is reduced more rapidly than the one in the graphite foam fin. By increasing the velocity, the difference of COP between the graphite foam fin and the aluminum louver fin is reduced. However, if graphite foam fin reaches the same COP value as the aluminum louver fin, and then the velocity of air might be supersonic, based on Figure 6. Thus, increasing the air velocity to achieve the same COP as the aluminum louver fin is not feasible for the graphite foam fin.

Table 5   Assumed operating data for a truck

Cooling power (kW)		200	
Truck speed (km/h)		65	
Radiator (water side)	$T_{in} = 90°C$		$T_{out} = 85°C$
Radiator (air side)	$T_{in} = 30°C$		$T_{out} = 55°C$

A Comparison Study Between a Graphite Foam HEX and an Aluminum Louver Fin HEX Under Countercurrent Flow

In order to evaluate the performance difference between a graphite foam HEX and an aluminum louver fin HEX under countercurrent flow, a case study (a truck with 200 kW cooling power) is carried out. The operating data of this case are shown in Table 5.

After analyzing this case, the total cooling surface required for the aluminum louver fin HEX is 17.1 m^2, and 11.75 m^2 for the graphite foam HEX (as shown in Table 6). The total volume of the graphite foam HEX is 0.0114 m^3, which is 45.6% less than the one of the aluminum louver fin HEX (0.021 m^3). Moreover, the weight of the graphite foam HEX is 1.12 kg, which is 65% lower than that of the aluminum louver fin HEX (only considering the fin weight in the air side). Thus, a light and compact HEX could be achieved by using the graphite foam fin. However, due to the high flow resistance in the graphite foam, the power for forcing air through the HEX is much higher in the graphite foam HEX than in the aluminum louver fin, when the removed heat is the same.

CONCLUSIONS AND RECOMMENDATIONS

Because of the increased cooling requirement in vehicles, an advanced heat exchanger has to be developed in the vehicle industry. Placing the heat exchanger at a new place on vehicles or using new material for heat exchanger might favor the design of advanced heat exchangers. In this paper, a countercurrent-flow graphite foam HEX is presented for placement on the roof of the driver compartment. Furthermore, a performance comparison between the graphite foam HEX and the aluminum louver fin HEX is carried out under countercurrent flow. The major results are as follows:

1. The graphite foam fin design has higher heat transfer coefficient than does the aluminum louver fin. However, the pressure drop through the graphite foam is much higher than that through the aluminum louver fin.
2. The coefficient of performance (COP) in the graphite foam fin is lower than in the aluminum louver fin, due to the large hydrodynamic losses in the graphite foam,

3. For the case considered in this paper, the volume of the graphite foam HEX is 45.6% less than that of the aluminum louver fin, and the weight of the graphite foam HEX is 65% less than that of the aluminum louver fin, under the countercurrent-flow condition.

Thus, a light and compact heat exchanger would be achieved by using the graphite foam. However, there are still several problems facing the application of graphite foam HEX in vehicles.

1. It requires large input pumping power for the graphite foam HEX. Thus, an appropriate configuration of graphite foam has to be developed to reduce the pressure drop.
2. The manufacturing methods of graphite foam HEX are not mature, compared to the aluminum HEX.

Thus, there is still much effort needed for the development of new heat exchangers in the vehicle industry.

NOMENCLATURE

A	area [m^2]
A_0	fin surface area [m^2]
C_F	Forchheimer coefficient
c_p	specific heat [J kg^{-1} K^{-1}]
f	friction factor
h	heat transfer coefficient [W m^2 K^{-1}]
k	turbulent kinetic energy
m	mass [kg]
P_k	turbulence production term
P_{pum}	pumping power [W]
Pr	Prandtl number
p	pressure [Pa]
Q	amount of heat energy [W]
S_i	source term
St	Stanton number
T	temperature [K]
u	velocity [m s^{-1}]
V	volume [m^3]

Greek Symbols

α	permeability [m^2]
Δp	pressure drop [Pa]
ΔT	logarithmic mean temperature difference [K]
δ	turbulent index (turbulent $\delta = 1$; laminar $\delta = 0$)
ε	rate of energy dissipation
ϕ	porosity
γ	area to volume ratio [m^2 m^{-3}]
μ	dynamic viscosity [Pa-s]
ρ	density [kg m^{-3}]

Subscripts

air	air
eff	effective
f	fluid
in	inlet
max	maximum
min	minimum
out	outlet
t	turbulent
water	water

REFERENCES

[1] Malvicino, C., Mattiello, F., Seccardini, R., and Rostagno, M., Flat Heat Exchangers, *Proc. 10th Vehicle Thermal Management Systems Conference & Exhibition*, Gaydon, Warwickshire, UK, pp. 91–98, 2011.

[2] Malvicino, C., Sciullo, F. D., Cuniberti, M., Vestrelli, F., and Beltramelli, F., Dual Level Vehicle Heat Rejection System, *Proc. 10th Vehicle Thermal Management Systems Conference & Exhibition*, Gaydon, Warwickshire, UK, pp. 473–480, 2011.

[3] Peuvrier, O., Iwasaki, M., Hara, J., and Mguriya, Y., Development of Compact Cooling System (SLIM), *Proc. 10th Vehicle Thermal Management Systems Conference & Exhibition*, Gaydon, Warwickshire, UK, pp. 481–490, 2011.

[4] Shah, R. K., and Sekulic, D. P., *Fundamentals of Heat Exchanger Design*, John Wiley & Sons, New York, NY, pp. 56–64, 2003.

[5] Lin, W. M., Yuan, J. L., and Sundén, B., Performance Analysis of a Countercurrent Flow Heat Exchanger Placed on the Truck Compartment Roof, *Proc. of IMECE 2011*, Denver, CO, Paper No. IMECE 2011-62520, 2011

[6] Calmidi, V. V., and Mahajan, R. L., The Effective Thermal Conductivity of High Porosity Fibrous Metal Foams, *Journal of Heat Transfer*, vol. 121, pp. 466–471, 1999.

[7] Kim, S. Y., Paek, J. W., and Kang, B. H., Flow and Heat Transfer Correlations for Porous Fin in a Plate-fin Heat Exchanger, *Journal of Heat Transfer*, vol. 122, pp. 572–578, 2000.

[8] Paek, J. W., Kang, B. H., Kim, S. Y., and Hyum, J. M., Effective Thermal Conductivity and Permeability of Aluminum Foam Materials, *International Journal of Thermophys*, vol. 21, no. 2, pp. 453–464, 2000.

[9] Boomsma, K., and Poulikakos, D., On the Effective Thermal Conductivity of a Three-Dimensionally Structured Fluid-Saturated Metal Foam, *International Journal of Heat and Mass Transfer*, vol. 44, pp. 827–836, 2001.

[10] Bhattacharya, A., Calmidi, V. V., and Mahajan, R. L., Thermophysical Properties of High Porosity Metal Foams, *International Journal of Heat and Mass Transfer*, vol. 45, pp. 1017–1031, 2002.

[11] Mahjoob, S., and Vafai, K., A Synthesis of Fluid and Thermal Transport Models for Metal Foam Heat Exchangers, *International Journal of Heat and Mass Transfer*, vol. 51, pp. 3701–3711, 2008.

[12] Dai, Z., Nawaz, K., Park, Y., Chen, Q., and Jacobi, A. M., A Comparison of Metal-Foam Heat Exchangers to

Compact Multilouver Designs for Air-Side Heat Transfer Applications, *Heat Transfer Engineering*, vol. 33, no. 1, pp. 21–30, 2012.

[13] Muley, A., Kiser, C., Sundén, B., and Shah, R. K., Foam Heat Exchangers: A Technology Assessment, *Heat Transfer Engineering*, vol. 33, no. 1, pp. 42–51, 2012.

[14] Klett, J., Hardy, R., Romine, E., Walls, C., and Burchell, T., High-Thermal-Conductivity Mescophase-Pitch-Derived Carbon Foams: Effect of Precursor on Structure and Properties, *Carbon*, vol. 38, pp. 953–973, 2000.

[15] Yu, Q., Thompson, B. E., and Straatman, A. G., A Unit Cube-Based Model for Heat Transfer and Fluid Flow in Porous Carbon Foam, *Journal of Heat Transfer*, vol. 128, pp. 352–360, 2006.

[16] Straatman, A. G., Gallego, N. G., Thompson, B. E., and Hangan, H., Thermal Characterization of Porous Carbon Foam-Convection in Parallel Flow, *International Journal of Heat and Mass Transfer*, vol. 49, pp. 1991–1998, 2006.

[17] Klett, J., Ott, R., and McMillan, A., Heat Exchangers for Heavy Vehicles Utilizing High Thermal Conductivity Graphite Foams, SAE Paper 2000-01-2207, 2000.

[18] Yu, Q., Straatman, A. G., and Thompson, B. E., Carbon-foam Finned Tubes in Air-water Heat Exchangers, *Applied Thermal Engineering*, vol. 26, pp. 131–143, 2006.

[19] Garrity, P. T., Klausner, J. F., and Mei, R., Performance of Aluminum and Carbon Foams for Air Side Heat Transfer Augmentation, *Journal of Heat Transfer*, vol. 132, 121901, 2010.

[20] Straatman, A. G., Gallego, N. C., Yu, Q., and Thompson, B. E., Characterization of Porous Carbon Foam as a Material for Compact Recuperators, *Journal of Engineering for Gas Turbines and Power*, vol. 129, pp. 326–330, 2007.

[21] Gallego, N. G., and Klett, J. W., Carbon Foams for Thermal Management, *Carbon*, vol. 41, pp. 1461–1466, 2003.

[22] Lin, Y. R., Du, J. H., Wu, W., Chow, L. C., and Notardonato, W., Experimental Study on Heat Transfer and Pressure Drop of Recuperative Heat Exchangers Using Carbon Foam, *Journal of Heat Transfer*, vol. 132, 091902, 2010.

[23] Lin, W. M., and Sundén, B., Graphite Foam Heat Exchanger for Vehicles, *Proc. 10th Vehicle Thermal Management Systems Conference & Exhibition*, Gaydon, Warwickshire, UK, pp. 81–90, 2011.

[24] Pope, S. B., *Turbulent Flows*, Cambridge University, New York, NY, pp. 358–385, 2000.

[25] *ANSYS FLUENT 12.0—Therory Guide*, ANSYS, Inc., Lebanon, New Hampshire, USA, pp. 112–125, 2009.

[26] Tannehill, J. C., Anderson, D. A., and Pletcher, R. H., *Computational Fluid Mechanics and Heat Transfer*, 2nd ed., Taylor & Francis, Boca Raton, FL, pp. 249–320, 1997.

[27] Yuan, J., Huang, Y., Sundén, B., and Wang, W., Analysis of Parameter Effects on Chemical Reaction Couple Transport Phenomena in SOFC Anodes, *Heat Mass Transfer*, vol. 45, pp. 471–484, 2009.

[28] Lu, W., Zhao, C. Y., and Tassou, S. A., Thermal Analysis on Metal-Foam Filled Heat Exchangers. Part I: Metal-Foam Filled Pipes, *International Journal of Heat and Mass Transfer*, vol. 49, pp. 2751–2761, 2006.

[29] Versteeg, H. K., and Malalasekera, W., *An Introduction to Computational Fluid Dynamics*, Longman Scientific & Technical, London, UK, pp. 85–133, 1995.

[30] Kays, W. M., and London, A. L., *Compact Heat Exchangers*, 3rd ed., McGraw-Hill, New York, NY, pp. 156–185, 1995.

Wamei Lin is a Ph.D. student in heat transfer at Lund University in Sweden. Her research concerns heat exchangers in future transportation systems. CFD analysis of various heat exchanger configurations including metal foams is the major task. She received the licentiate of engineering degree in 2011 and is expected to present her Ph.D. thesis in 2014.

Jinliang Yuan is a professor at the Department of Energy Sciences, Lund University in Sweden. His research concerns analysis of heat and mass transfer and other transport phenomena in fuel cells and associated heat exchangers, as well as fuel reformers. He has worked as a project leader or/and senior researcher in projects and also as a supervisor of Ph.D. students, and is actively involved as a teacher in the undergraduate and postgraduate courses. He is a member of the editorial board for several journals. His current research interests are focused on comprehensive analysis of catalytic chemical reactions and effects of nano-/microstructured porous material on various transport processes in the components of advanced energy systems.

Bengt Sundén received his M.Sc. in mechanical engineering 1973, Ph.D. in applied thermodynamics and fluid mechanics 1979, and became docent in applied thermodynamics and fluid mechanics in 1980, all from Chalmers University of Technology, Gothenburg, Sweden. He was appointed Professor of Heat Transfer at Lund University, Lund, Sweden, in 1992 and has served as Department Head of Energy Sciences, Lund University, since 1995. His research activities include compact heat exchangers, enhancement of heat transfer, gas turbine heat transfer, combustion-related heat transfer, CFD methods for laminar and turbulent fluid flow and heat transfer, liquid crystal thermography, microscale heat transfer, transport phenomena in fuel cells, computational modeling and analysis of multiphysics, and multiscale phenomena for fuel cells. Dr. Sundén established and was first editor-in-chief of *IJHEX—International Journal of Heat Exchangers* (R. T. Edwards, Inc., USA), 1999–2008, was an associate editor of *ASME Journal of Heat Transfer*, 2005–2008, and has been editor-in-chief of a book series, Developments in Heat Transfer (WIT Press, UK), since 1995. He has published more than 500 papers in journals, books, and proceedings. He has edited 25 books and authored three textbooks. He has supervised 170 M.Sc. theses, 40 licentiate of engineering theses, and 37 Ph.D. theses. He is a fellow of the ASME, honorary professor of Xian Jiaotong University, China, a regional editor of *Journal of Enhanced Heat Transfer* since 2007, an associate editor of *Heat Transfer Research* since 2011, and an associate editor *ASME Journal of Thermal Science, Engineering and Applications*, 2010–2013. He was a recipient of the ASME Heat Transfer Memorial Award, 2011.

Paper 6

FLOW AND THERMAL PERFORMANCE OF GRAPHITE FOAM DIMPLED FIN HEAT EXCHANGERS

Wamei Lin[1], Gongnan Xie[2], Bengt Sundén[1*], Qiuwang Wang[3]

[1]Department of Energy Sciences, Lund University, Box 118, Lund 22100, Sweden
[2]School of Mechanical Engineering, Northwestern Polytechnical University, P.O.Box 552, Xi'an, Shaanxi 710072, China
[3]Key Laboratory of Thermo-Fluid Science and Engineering, MOE, Xi'an Jiaotong University, Shaanxi, 710049, China

ABSTRACT

Graphite foam is one kind of favorable materials in thermal engineering applications because of its high thermal conductivity and large specific surface area. However, there is an associated high flow resistance in the graphite foam resulting from the porous structure property. In order to reduce the flow resistance and enhance the heat transfer, dimpled fins could be applied in graphite foam heat exchangers. In this paper, the flow characteristics and thermal performance of graphite foam dimpled fin heat exchangers have been investigated numerically through three-dimensional simulations of fluid flow and heat transfer in graphite foam dimpled fin channels. The local thermal non-equilibrium model has been applied to analyze the thermal performance of the graphite foam dimple fin (porous zone), and the Forchheimer extended Darcy's law has been employed to consider the air pressure drop through the porous graphite foam. Moreover, the SST k-ω turbulence model has been used to capture the turbulent flow characteristics outside the graphite foam region. The details of the fluid flow and heat transfer over the dimple fin are presented. The results show that the graphite foam fin with two sides dimple presents the highest values of the normalized Nusselt number (between 2.4 and 4 .6) and overall thermal performance factor. Furthermore, the graphite foam dimple fin provides higher effectiveness than the conventional aluminum offset fin, wavy fin and louver fin concerning energy saving.

KEY WORDS: Graphite foam heat exchanger, Dimpled fin, Heat transfer enhancement, Turbulent mixing, Thermal performance, Computational methods.

1. INTRODUCTION

Because of the high thermal conductivity (the solid phase thermal conductivity is 1500-2000 W/(m·K), and the effective thermal conductivity is varied with density from 40 to 150 W/(m·K)) and the large specific surface area (5000-50,000 m^2/m^3) [1], graphite foam is a kind of favorable materials in thermal engineering applications such as electronic cooling systems, vehicle cooling systems, energy storage systems, high temperature heat exchangers and so on. Review works about the graphite foam used in thermal engineering applications can be found in [2-3].

A lot of research works has been carried out to analyze the thermal performance of the graphite foam heat exchangers. Klett et al. [4] used the graphite foam to design a radiator. The cross section of the automotive radiator was reduced from 48 cm × 69 cm to 20 cm × 20 cm because of the graphite foam. The overall weight, cost and the volume of the cooling system were reduced as well. On the other hand, Yu et al. [5] proved that the thermal performance of a carbon foam finned tube radiator could be improved by 15 % compared to a conventional aluminum finned tube radiator without changing the frontal area, or the air flow rate, or pressure

---

drop. Based on an experimental work, Garrity et al. [6] found that the carbon foam samples brought away more heat than the multilouvered fin when the volume of the heat exchangers was kept the same. Furthermore, Lin et al. [7] found that the graphite foam wavy corrugated fin heat exchanger presents higher power density and compactness factor than an aluminum louver fin heat exchanger.

Even though there is a substantial heat transfer enhancement in the graphite foam, the graphite foam is still associated with other problems. One of the most important issues is the high pressure drop due to the large hydrodynamic loss associated with the cell windows connecting the pores [8]. In a study concerning reduction of the pressure drop, Gallego et al. [9] presented six different configurations of graphite foam heat exchangers. That study showed that the solid foam had the highest pressure drop while the finned configuration had the lowest pressure drop. In another study, Leong et al. [10] found that the baffle foam presented the lowest pressure drop among four configurations of graphite foams at the same heat transfer rate. Lin et al. [11] revealed that the corrugated fin could reduce the pressure drop while maintaining a high heat transfer coefficient compared to the solid foam. All together, these studies illustrate that the configuration has an important effect on the pressure drop through the graphite foam.

In order to find an appropriate fin type for the graphite foam heat exchanger, many different structures of aluminum fins (wavy fin, louver fin, offset fin, dimple fin, and so on) are considered in terms of thermal performance and pressure loss. It was found that the dimple could be an attractive fin shape due to its high heat transfer performance and low flow resistance [12-15]. Mahmood et al. [16] experimentally tested the local heat transfer and flow characteristics above a dimpled surface in a channel. The heat transfer was enhanced by the vortex pairs and vertical fluid near the dimple. However, different parameters would affect the thermal performance of dimple surfaces [17-20]. When the ratio of dimple depth to dimple print diameter was reduced, the vortex pairs became stronger and the local Nusselt number was increased [17]. Furthermore, Moon et al. [18] analyzed the thermal performance in the dimple passage under different channel height. The heat transfer could be enhanced by around 2.1 times compared to the channel without dimples. On the other hand, Ligrani et al. [21] found that the dimple with protrusions on opposite walls led to additional vertical, secondary flow and strong flow mixing compared to the one with flat surface. The heat transfer enhancement could be achieved by adding the protrusion in the dimple channel, but the friction factors were also increased 2.0-2.7 times compared to one in a channel with dimples and flat top surface. Combining the increased form drag and channel friction factors, the thermal performance factors in the channel with dimples and protrusion top surface were lower than those in the flat top surface channel [22].

From the above literature review, it is evident that the dimple technology may enhance the heat transfer in a channel or in a heat exchanger. However, the available research is limited concerning the dimple technology used in the porous graphite foam, which is a very good potential material for compact heat exchangers. So in order to take advantage of the graphite foam, high thermal conductivity and low density, at the meantime to reduce the flow resistance of graphite foam, the fins with one-side dimples or two-side dimples are designed into the graphite foam heat exchanger in this paper. The main objective of the present study is to investigate the heat transfer enhancement of graphite foam dimple fin, and the flow characteristics caused by the porous graphite foam dimple fin. The local thermal non-equilibrium model was applied to analyze the thermal performance of the graphite foam dimple fin, and the Forchheimer extended Darcy's law was employed to consider the air pressure drop through the porous graphite foam. The SST k-ω turbulence model was validated to capture the turbulent flow characteristics outside the graphite foam region. The detail fluid flow and heat transfer over the dimple fin are presented. In addition, the overall performance of the graphite foam dimpled fin is compared with conventional aluminum offset fin, wavy fin, and louver fin. Some fin structures are evaluated in terms of energy saving.

2. PHYSICAL MODEL

A schematic diagram of the physical model (plate-fin heat exchanger) in this study is shown in Fig. 1. The hot water flows inside the flat tubes, and the cold air flows through the porous graphite foam fins. The heat is transmitted through the tube wall to the graphite foam fins and finally dissipated to the air. The properties of the graphite foam are listed in Table 1. Three cases of graphite foam fins are analysed: rectangular fin

without dimple (Case 1); rectangular fin with one-side dimples (Case 2); rectangular fin with two-side dimples (Case 3). Note that the fin thickness of the three cases is kept the same. According to research work about the graphite foam fin [23], the optimal thickness of graphite foam fin is between 3 mm to 5 mm in terms of thermal performance. Accordingly, the thickness of graphite foam fin is selected to be 5 mm in this study. The pitch of fins in the height direction (z-direction) is 15 mm, and the width of fins is 64 mm. The assumptions in this study are as follows:

(1) The air is assumed to be incompressible with constant properties and in steady-state.
(2) The connection between the tube wall and the graphite foam fin is assumed perfect without any air gap inside. Thus, the thermal resistance at the interface between the tube wall and the graphite foam is neglected.
(3) The porosity through the graphite foam dimple fin is constant.
(4) The thermal conductivity of graphite foam is assumed to be isotropic.

Table 1 Properties of the graphite foam considered in this study [8].

Specimen	Porosity (φ)	Average void diameter (D_p) (μm)	Special surface area (a) (m^2/m^3)	Permeability (α) (m^2)	Forchheimer coefficient (C_F)	Effective thermal conductivity (λ_{eff}) (W/m K)
POCO	0.82	500	5240	6.13×10^{-10}	0.4457	120
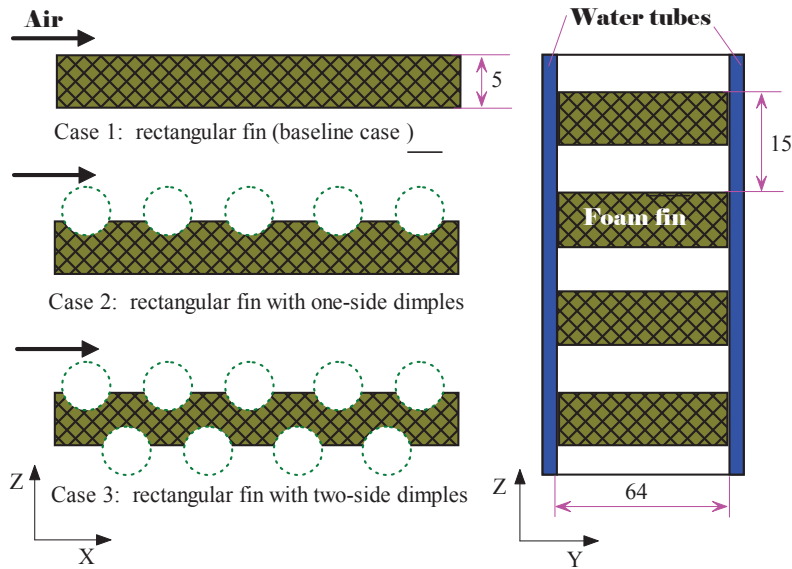
Fig. 1 Schematic pictures of physical model: plate fin heat exchangers (dimensions are given in mm).

The detailed geometry of the dimple fin is shown in Fig. 2. An array of circular dimples is positioned on the surface in a staggered arrangement, as shown in Fig. 2 (a). The spacing of adjacent dimple rows (S) is 8 mm, and the spacing of every other dimple row (P) is 16 mm. The dimple print diameter (D) is 5.08 mm, and the dimple depth (δ) is 1.02 mm. Due to the periodic structure, a core of graphite foam fin is chosen with only two rows of dimples (x-direction) and half of the fin width, the overall size of the core is: 16mm×32mm×15 mm (x×y×z), as shown in Fig. 2 (c). A periodic condition is applied to the flow inlet and flow outlet.

Fig. 2 Schematic figures of dimple fin geometry. All dimensions are given in mm.

3. NUMERICAL METHOD

3.1 Flow Modeling Selection

A detailed discussion of the computational model (laminar or turbulent) of the flow regime has to be presented before the numerical computations. Because the porous structure and high flow resistance in the graphite foam region, the air velocity inside the foam is very low. The Reynolds number based on the pore diameter and the air velocity inside the pore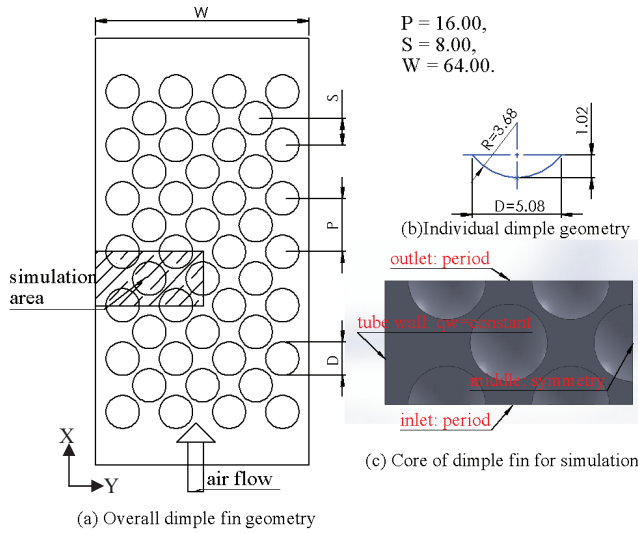 is lower than 10, which is lower than the transition region value of 100. So laminar flow is considered inside the graphite foam region. However, the Reynolds number based on the channel hydraulic diameter and the air mean velocity is ranging from 2700 to 9000 outside the foam region, and thus turbulent flow prevails on the air zone.

Furthermore, it is very important to select an appropriate turbulence model for a specific simulation. In order to capture the effect of the vortex pairs and vertical fluid near the dimple, the k-ω turbulent model is considered in the near the dimple walls to predict the location of flow separation and the displacement effect associated with it. However, the k-ω model has a very strong sensitivity to the free stream outside the boundary layer, and the k-ω model can not accurately represent the k and ε distribution in agreement with direct numerical simulation (DNS) data. So in the free stream far from the boundary walls, the k-ε turbulent model is used, due to its good agreement with DNS data by employing different damping functions. Therefore in this study the shear-stress transport (SST) k-ω model, combining the effect of k-ω model and the k-ε model, has been applied to capture the turbulent flow characteristics [24].

3.2 Governing Equations

Based on the above mentioned assumptions, the governing equations for continuity, momentum and energy can be expressed as follows [24-27]:

3.2.1 Air zone governing equations
Continuity equation:

4

$$\frac{\partial\left(\rho_{air}u_i\right)}{\partial x_i}=0 \tag{1}$$

Momentum equations:

$$\frac{\partial\left(\rho_{air}u_iu_j\right)}{\partial x_j}=-\frac{\partial p}{\partial x_i}+\frac{\partial}{\partial x_j}\left(\left(\mu_{air}+\mu_t\right)\left(\frac{\partial u_i}{\partial x_j}+\frac{\partial u_j}{\partial x_i}\right)\right) \tag{2}$$

Energy equation:

$$\frac{\partial\left(\rho_{air}u_jT\right)}{\partial x_j}=\frac{\partial}{\partial x_j}\left(\left(\frac{\mu_{air}}{\mathrm{Pr}_{air}}+\frac{\mu_t}{\mathrm{Pr}_t}\right)\frac{\partial T}{\partial x_j}\right) \tag{3}$$

The equations for the turbulent kinetic energy k and the specific dissipation rate ω corresponding to the SST k-ω turbulence model are:

Turbulent kinetic energy k:

$$\frac{\partial\left(\rho_{air}u_jk\right)}{\partial x_j}=\frac{\partial}{\partial x_j}\left[\left(\mu_{air}+\frac{\mu_t}{\sigma_k}\right)\frac{\partial k}{\partial x_j}\right]+G_k-\rho_{air}\beta^*k\omega \tag{4}$$

Specific dissipation rate ω:

$$\frac{\partial\left(\rho_{air}u_j\omega\right)}{\partial x_j}=\frac{\partial}{\partial x_j}\left[\left(\mu+\frac{\mu_t}{\sigma_\omega}\right)\frac{\partial\omega}{\partial x_j}\right]+\frac{\eta}{v_t}G_k-\rho_{air}\beta_t\omega^2+2\left(1-F_1\right)\rho_{air}\sigma_{\omega2}\frac{1}{\omega}\frac{\partial k}{\partial x_j}\frac{\partial\omega}{\partial x_j} \tag{5}$$

where, G_k is generation of turbulent kinetic energy, F_1 blending function, β^*=0.09, σ_ω=0.5, $\sigma_{\omega2}$=0.856, β_t=0.0828.

3.2.2 Graphite foam zone governing equations

Due to the porous structure of the graphite foam, the Forchheimer extended Darcy's law is applied to consider the air pressure drop through the graphite foam. On the other hand, concerning the heat transfer in the porous media, there are two major models: (1) the local thermal equilibrium model; (2) the local thermal non-equilibrium model. Because of the large difference of thermal conductivity between the air and the graphite foam, the local thermal non-equilibrium model is employed to analyze the heat transfer performance of the graphite foam, but the thermal dissipation is neglected in the energy equation. Based on this, the governing equations for the graphite foam are as follows:

Continuity equation:

$$\frac{\partial\left(\rho_{air}u_i\right)}{\partial x_i}=0 \tag{6}$$

Momentum equations:

$$\frac{\partial\left(\rho_{air}u_iu_j\right)}{\partial x_j}=-\varphi\frac{\partial p}{\partial x_i}+\frac{\partial}{\partial x_j}\left(\mu_{air}\left(\frac{\partial u_i}{\partial x_j}+\frac{\partial u_j}{\partial x_i}\right)\right)-\varphi\left(\frac{\mu_{air}}{\alpha}u_i+\frac{\rho_{air}C_F}{\sqrt{\alpha}}|u|u_i\right) \tag{7}$$

Energy equations:

1. *Air phase:*

$$\varphi\frac{\partial\left(\rho_{air}c_{p.air}u_jT_f\right)}{\partial x_j}=\lambda_{air.eff}\frac{\partial}{\partial x_j}\left(\frac{\partial T_{air}}{\partial x_j}\right)+h_{s.air}a_{s.air}\left(T_s-T_{air}\right) \tag{8}$$

2. *Solid phase:*

$$0=\lambda_{s.eff}\frac{\partial}{\partial x_j}\left(\frac{\partial T_s}{\partial x_j}\right)-h_{s.air}a_{s.air}\left(T_s-T_{air}\right) \tag{9}$$

where $\lambda_{eff} = \lambda_{s.eff} + \lambda_{air.eff} = \lambda_{s.eff} + \varphi\lambda_{air}$. λ_{eff} is taken from experimental data [8] and then the value of $\lambda_{s.eff}$ can be obtained. The value of the interfacial heat transfer coefficient ($h_{s.air}$) needs to be specified for the energy equations. There are many different empirical formulas of $h_{s.air}$, which are based on experimental or theoretical works. After a comparison of the different formulas, the following one is used in this study [34]:

$$Nu_{s.air} = a_{s.air}h_{s.air}D_p^2 / \lambda_{air} \tag{10}$$

$$(1)\ Pe_d \prec 40,\ Nu_{s.air} = (33.3 + 0.51Pe_d^{0.85})(1-\varphi)^{0.42} \tag{11}$$

$$(2)\ Pe_d \succ 40,\ Nu_{s.air} = (32.0\,\mathrm{Pr}_{air}^{0.077} + 1.18\,\mathrm{Re}_d^{0.68}\,\mathrm{Pr}_{air}^{0.38})(1-\varphi)^{0.42} \tag{12}$$

where, $Pe_d = \mathrm{Re}_d\,\mathrm{Pr}_{air} = \dfrac{u_p D_p}{v_{air}}\mathrm{Pr}_{air}$

3.3 Boundary Conditions

The momentum and energy transports are calculated simultaneously in the air and the graphite foam zones. The boundaries on the graphite foam walls of the fluid phase are set up as "interior surfaces" or interfaces, and the ones of the solid phase are "walls". Thus, the solution in the momentum and energy transports on the interfaces between the air and graphite foam zones are not required. The necessary boundary conditions are shown in Fig. 3. The boundary conditions are as follows:

    (1) X=0 and X=P (16 mm): periodic inlet and periodic outlet. The length of the period is P (16 mm). Only the rate of flow in x-direction is set up.

    (2) Y=0: constant heat flux is given; Y= W/2 (32 mm): symmetric boundary condition.

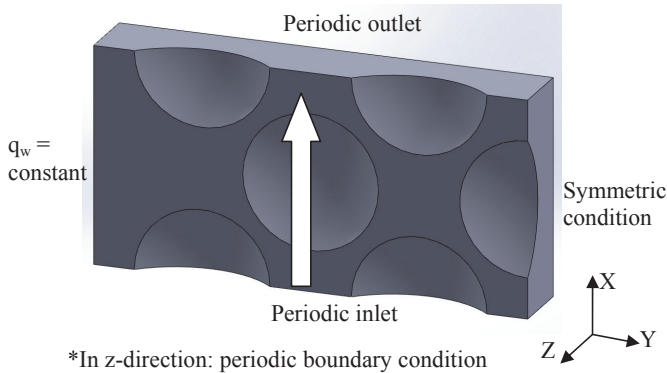   (3) Z=0 and Z=H (15 mm): periodic boundary conditions.

Fig. 3 Boundary conditions of the core of graphite foam dimple fin (Case 2)

3.4 Parameters Definition

In order to compare the thermal performance, the averaged Nusselt number of the dimple fin is employed. The definition is as follow:

$$\overline{Nu} = \frac{D_h q_w}{\lambda_{air}(T_w - T_{air})} \tag{13}$$

6

where, $\overline{T_w} = \dfrac{\int_{A_w} T_w dA}{A_w}$, and $\overline{T_{air}} = \dfrac{\int_{V_{air}} T_{air} dV}{V_{air}}$. On the other hand, the flow characteristics are presented by the

Fanning friction factor f:

$$f = \frac{\Delta p D_h}{2 L \rho_{air} u_b^2} \tag{14}$$

Another method to evaluate the performance of the graphite foam dimple fin is to normalize the averaged Nusselt number and the friction factor with the corresponding values in a fully developed rectangular channel flow without any fin enhancement. The values for $\overline{Nu}_0$ and f_0 for fully developed channel flow are defined as follows [28]:

$$\overline{Nu}_0 = \frac{(f_0 / 2)(\mathrm{Re}_D - 1000)\mathrm{Pr}_{air}}{1.0 + 12.7\sqrt{f_0 / 2}\left(\mathrm{Pr}_{air}^{2/3} - 1\right)} \tag{15}$$

$$f_0 = \left(0.79 \ln \mathrm{Re}_D - 1.64\right)^{-2} / 4 \tag{16}$$

3.5 Numerical Method and Grid Dependence Test

The commercial code ANSYS FLUENT 14.0 is used for the numerical simulations. A control-volume-based technique is adopted to convert the governing equations to algebraic equations so that these can be solved numerically [29]. The Semi-Implicit Method for Pressure Linked Equations (SIMPLE) algorithm is used to couple pressure and velocity. A second-order upwind scheme is used for the space discretization of the momentum and energy equations in the simulations. The residual of the continuity, components of velocity, k, and ω is set to be below 10^{-4}, while for the energy it is below 10^{-7}. On the other hand, the pressure drop gradient was monitored as well.

Due to the complex geometries, an unstructured grid is employed by using the ICEM software, as shown in Fig. 4. To ensure accuracy and validity of the numerical results, grid independence has to be validated by using different sets of mesh size. In this study, four sets of mesh size (Mesh 1: 225000, Mesh 2: 696000, Mesh 3: 1177000, Mesh 4: 2000000) were tested in the Case 2 at Reynolds number of 8,536. The averaged Nusselt number and the friction factor from these four grid systems are listed in Table 2. It is found that the relative deviations of Nusselt number and friction factor between Mesh 3 and base line (Mesh 4) is 1.68 % and 1.85 %, respectively. Therefore considering the numerical accuracy and computational time, the Mesh 3 is chosen for the Case 2. The same method is employed to check the grid independence of Case 1, and Case 3. The grid with 630000 elements is chosen for Case 1. However, due to the complex geometry, a huge grid with many small elements has to be employed in Case 3. Accordingly, a grid with 1250000 elements is chosen for Case 3. On the other hand, by checking the value of y^+ near the wall, it is found that the y^+ is from 0.2 to 0.7 among the three cases. This indicates that the grid is fine enough (y^+<1) near the wall to capture the boundary layer flow characteristics.
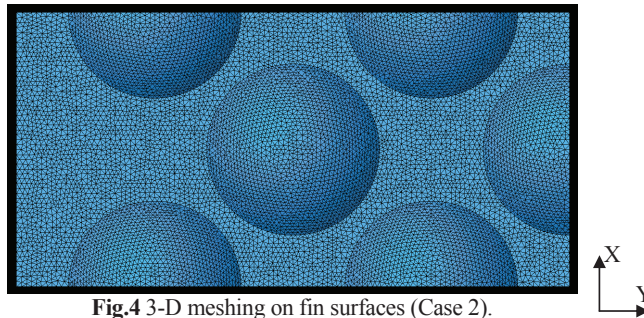

Fig.4 3-D meshing on fin surfaces (Case 2).

Table 2 Grid independence test (Re = 8,536).

	Mesh 1:	Mesh 2	Mesh 3	Mesh 4
$\overline{Nu}$	74.72	66.67	64.60	63.53
f	0.02108	0.02025	0.01979	0.01943
$|\Delta \overline{Nu}|$	17.61 %	4.94 %	1.68 %	Base line
$|\Delta f|$	8.49 %	4.22 %	1.85 %	Base line

4. RESULTS AND DISCUSSION

4.1 Model Validation

Before presenting the simulation results, a validation of the simulation model has to be carried out. There are two simulation models to be validated in this study: the graphite foam porous model and the dimple fin model. The graphite foam porous model has been validated in [7, 30], and is not repeated here.

In order to validate the dimple fin model, the numerical results of the dimple fin case from the SST k-ω and the realizable k-ε turbulence models were compared with the experimental data of Mahmood et al. [17]. The comparison results are listed in Table 3. The same dimensions and boundary conditions as in the experimental work were applied in the validation. As shown in the table, the numerical results from the SST k-ω turbulence model were in good agreement with the experimental data, with a maximum error of 7.32 % in the normalized friction factor f/f_0 and 3.15 % in the normalized averaged Nusselt number $\overline{Nu} / \overline{Nu}_0$, respectively. However, the simulation results from the realizable k-ε turbulence model were quite far away from the experimental data (the deviations of f/f_0 and $\overline{Nu} / \overline{Nu}_0$ are from 22.93 % to 46.87 % and from 10.36 % to 38.70 %, respectively). This is mostly because the k-ε model is weak in capturing the boundary layer characteristics near the dimple (flow separation, vortex pairs etc.). The SST k-ω model complements this and takes advantage of the k-ε model in the free shear layers. Thus the SST k-ω turbulence model is employed to predict the thermal performance and the flow characteristics of the dimple fin model in this study.

Table 3 Validation of two turbulence models for the dimple fin model.

	Re_H	f/f_0	f/f_0 [17]	$|\Delta f/f_0|$	$\overline{Nu} / \overline{Nu}_0$	$\overline{Nu} / \overline{Nu}_0$ [17]	$|\Delta \overline{Nu} / \overline{Nu}_0|$
SST k-ω model	5000	4.40	4.10	7.32 %	2.31	2.30	0.43 %
	10000	3.13	3.20	2.19 %	2.23	2.24	0.46 %
	15000	3.25	3.10	4.84 %	2.15	2.22	3.15 %
Realizable k-ε model	5000	5.04	4.10	22.93 %	3.19	2.30	38.70 %
	10000	4.70	3.20	46.87 %	2.69	2.24	20.09 %
	15000	4.03	3.10	30 %	2.45	2.22	10.36 %

4.2 Velocity and Temperature Fields

In order to provide a better understanding of the flow characteristics and heat transfer performance inside the graphite foam dimple fin, the velocity vectors and the temperature distribution near the dimple (only Case 2 at Reynolds number of 5,687 is analyzed) are presented in Figs. 5 and 6, respectively. When the fluid flows through the dimple, because of the sudden expansion of the cross section of the flow channel, there is a negative pressure area upstream of the dimple. This negative pressure causes a recirculating flow inside the dimple, as shown in Fig. 5. The recirculating flow leads to a low heat transfer performance. The fluid temperature in the recirculating zone is higher than in the downstream region, as shown in Fig. 6. This indicates that the thermal boundary layer is thicker in the flow recirculating zone than in the downstream region. The thicker the thermal boundary layer is, the poorer the heat transfer performance is. After the recirculating zone, the shear layer reattaches near the downstream edge of the dimples where high heat transfer is accordingly attained.

Furthermore, due to the pressure difference between the dimple side and the flat side on the graphite foam fin, the heat transfer is enhanced further in the graphite foam fin.
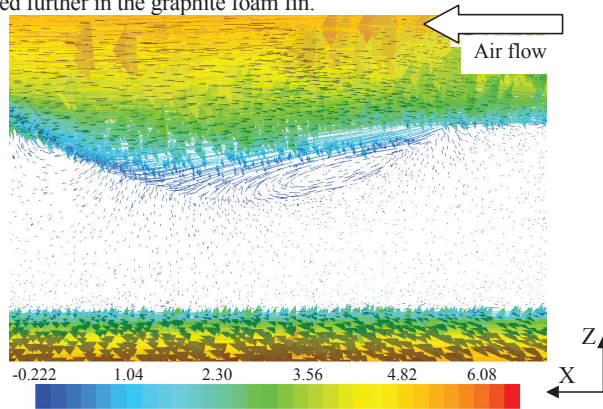
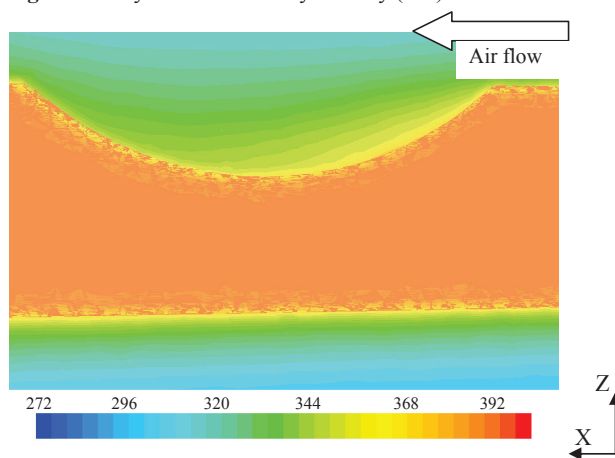**Fig. 5** Velocity vector colored by velocity (m/s) at Re=5687.

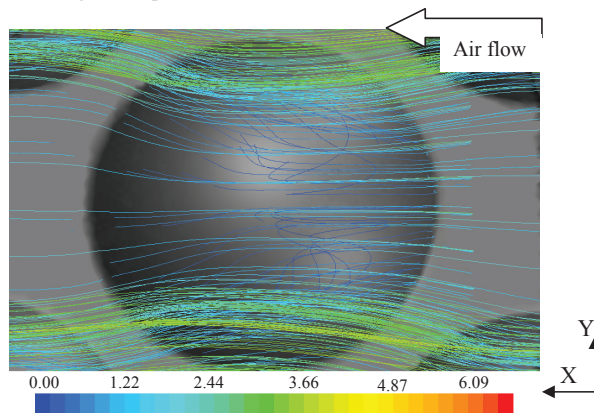**Fig.6** Temperature distribution (K) at Re=5687.

Fig.7 Stream line colored by velocity (m/s) at Re=5687.

9

The details of the flow streamlines inside the dimple are shown in Fig. 7. The recirculating flow is a three-dimensional phenomenon. The recirculating flow occurs upstream of the dimple. Due to the strong reattachment of the shear layer, some part of the recirculating flow traverses the side of the dimple, loses its momentum and is ejected along the side rim of dimples.

4.3 Heat Transfer Performance and Flow Characteristics

In order to evaluate the heat transfer performance of the graphite foam, the surface averaged Nusselt number is considered. Figure 8(a) shows that the averaged Nusselt numbers in the graphite foam fin with one side dimple or with two sides dimple are higher than for the graphite foam fin without dimple. This is because the dimple can enhance heat transfer by effect of vortex pairs, vertical fluid, secondary flow and strong flow mixing. This effect is much clearer on the fin with two sides dimple. Moreover, as the flow structure is different between the two sides of the fin, some part of the fluid penetrates through the graphite foam. This penetration process also increases the heat transfer. Because of these two main reasons, the averaged Nusselt number in the graphite foam fin with one side dimple is around 1.5 times higher than the one in the graphite foam flat fin, and the one in the graphite foam fin with two sides dimple is around 2 times higher than the one in the flat fin.

The flow characteristics are expressed by the pressure drop, as shown in Fig. 8(b). The pressure drop of the fin with one side dimple is around 1.5 times higher than that of the flat fin, while the fin with two sides dimple produces about 2.2 times higher pressure drop than the flat fin. This is mostly because of strong flow mixing inside the dimple and the penetration through the graphite foam. The flow mixing inside the dimple becomes more intensive as the Reynolds number is increasing. Based on this reason, the pressure drops of the fin with one or two sides dimple are increased faster than that of the flat fin. Compared to the flat fin, the pressure drop of the fin with one or two sides dimple is 1.9 and 2.8 times higher, at the high Reynolds number, respectively.

(a) Averaged Nusselt numbers   (b) Pressure drop (Pa/m)
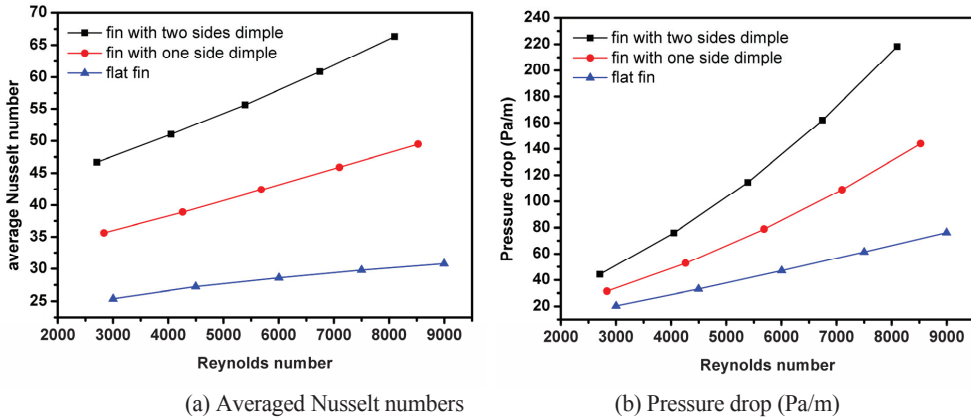
Fig. 8 Heat transfer and pressure drop performance through the graphite foam fins.

Another method to evaluate the performance of the graphite foam dimple fin is to normalize the averaged Nusselt number and the friction factor with the corresponding values in fully developed rectangular channel without any fin enhancement. The values for $\overline{Nu_0}$ and f_0 of fully developed channel flow without any fin enhancement are defined by Eqs.15 and 16 already.

Figure 9 shows that the values of $\overline{Nu}/\overline{Nu_0}$ and f/f_0 are decreasing by increasing Reynolds number. Due to the effect of graphite foam fin, there is heat transfer enhancement based on the values of $\overline{Nu}/\overline{Nu_0}$ (larger than 1.0). The heat transfer enhancement of graphite foam fin with two sides dimple is best among the three cases based on the values of $\overline{Nu}/\overline{Nu_0}$, which is between 4.6 and 2.4. On the other hand, Due to the high flow resistance inside

the graphite foam, more and more fluid prefers to flow through the empty channel instead of penetrating through the graphite foam as the Reynolds number is increasing. Accordingly, the effect of porous graphite foam is slowly eliminated as the Reynolds number is increased. This is the reason that the heat transfer enhancement of the graphite foam flat fin compared to the fully-developed channel flow is reduced from 2.5 to 1.14 (nearly 1.0) as the Reynolds number is increased, and the friction factor increase in the flat fin is also reduced closed to 1 at high Reynolds number. Furthermore, due to the weakening of the porous graphite foam as the increasing of Reynolds number, the reduction ratios of $\overline{Nu} / \overline{Nu_0}$ and f/f_0 are similar for all three cases.

(a) Normalized Nusselt number (b) Normalized friction factor
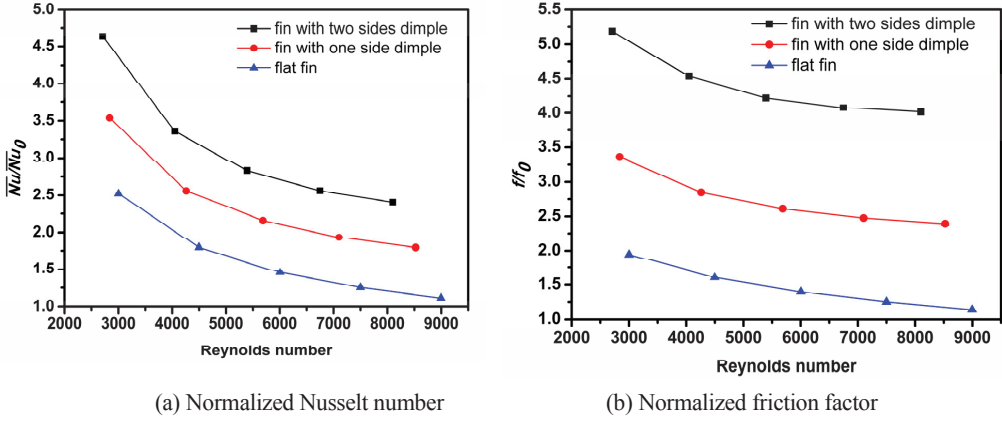
Fig. 9 Normalized Nusselt number and friction factor over the fully-developed flow case.

4.4 Overall Performance

From the foregoing analysis of the computed results, it is found that the heat transfer enhancement is the best in the graphite foam fin with two sides dimple. However, this case also presents the highest flow resistance. In order to combine the heat transfer performance and the flow characteristics, the overall performance of the graphite foam fin is presented.

Fig. 10 Overall thermal performances of the three foam fins

The first overall performance criterion is the value of $\overline{Nu} / \overline{Nu_0} /(f/f_0)^{1/3}$, which was proposed by Gee et al. [31]. This performance parameter provides a heat transfer augmentation quantity under a certain input pumping power

and a certain heat transfer duty condition. This parameter considers both the heat transfer augmentation and the friction loss increase. Figure 10 shows among the three cases, the graphite foam fin with two sides dimple provides the highest value of $\overline{Nu}\,/\,\overli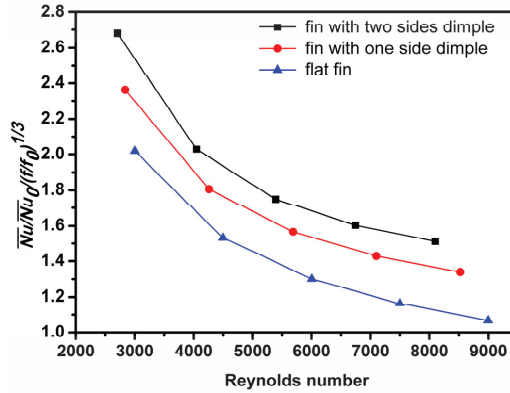ne{Nu_0}\,/(f\!/\!f_0)^{1/3}$, which is between 1.5 and 2.7. This implies that the graphite foam fin with two sides dimple can enhance the heat transfer by maximum 2.7 times under the same input pumping power and the same heat transfer duty compared with the other two cases. Therefore, the graphite foam fin with two sides dimple exhibits good overall performance.

After the comparison among the three cases of the graphite foam fin, another overall performance criterion is concerned to compare the graphite foam fin and the aluminum fin. The criterion is based on energy saving to compare the effectiveness of the different enhancement techniques [32]. The ratios of heat transfer enhancement ($\overline{Nu}\,/\,\overline{Nu_0}$) and friction factor increase ($f\!/\!f_0$) are employed as the coordinates in this criterion. When the two coordinates are both greater than 1.0, the plot is divided into four different regions based on the energy saving effect, as shown in Fig. 11. If a working point of an enhancement technique is located in Region 1, the consumption of one unit pumping power will lead to less heat transfer rate compared with that of the reference case. Thus for energy-saving purposes the working point should be located outside Region 1.
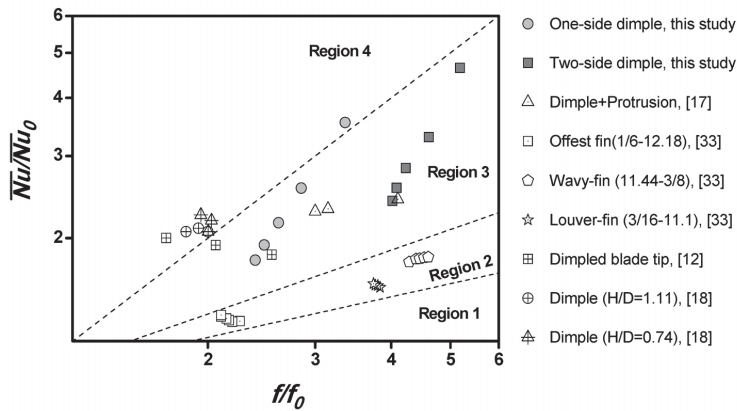

Fig. 11 Energy saving performance among the graphite foam fins and the aluminum fins.

The reference data of the aluminum offset fin, wavy fin and louver fin comes from the experimental data in Kays and London's book [33]. Moreover, other reference data concerning a channel with dimples from the research work [12, 17, 18] is also included in Fig. 11. All of the working points are for turbulent flow condition. It is found that the working points of the aluminum offset fin, wavy fin and louver fin are all located in Region 2, in which heat transfer is enhanced based on identical pumping power but deteriorated based on identical pressure drop. The working points of the dimple cases are all in Region 3. This means that heat transfer is enhanced based on identical pressure drop but the increase in friction factor is larger than the enhancement of heat transfer at identical flow rate. From the energy saving point of view, the dimple cases are better than the aluminum offset fin, wavy fin and louver fin. On the other hand, based on the line slope of one side dimple (graphite foam fin), two sides dimple (graphite foam fin) and other channel with dimple in Fig. 11, it is shown that the slope of one side dimple (graphite foam fin) is very large among these cases. The larger the basic line slope of a working point is, the better its energy-saving effectiveness is. From the foregoing analysis of Fig. 11, the graphite foam fin with one side dimple is effective in terms of energy saving.

6. CONCLUSIONS

Flow characteristics and heat transfer performances were studied in graphite foam fin with three cases at Reynolds number of 2700 – 9000: flat fin (Case 1), fin with one side dimple (Case 2), and fin with two sides

dimple (Case 3). Based on the present study, it can be concluded that the graphite foam fin with dimple has the potential to enhance the heat transfer. The main findings from this study are summarized as follows.

(1) The dimples lead to strong flow mixing along the graphite foam fin, and enhance the heat transfer. Meanwhile due to the penetration and high thermal conduction of the graphite foam, the heat transfer was enhanced more deeply.

(2) Compared with the fully developed rectangular channel without any fin enhancement, among the three cases in this study, the graphite foam fin with two sides dimple (Case 3) presents the highest value of $\overline{Nu} / \overline{Nu_0}$, which is between 4.6 and 2.4. This indicates that the heat transfer enhancement in Case 3 is a factor of up to 4.6. However, due to the porous structure of the graphite foam, the normalized friction factor f/f_0 is between 5.2 and 4.0.

(3) Combining the enhanced heat transfer and pressure drop increase, the overall performance criterion of $\overline{Nu} / \overline{Nu_0} /(f/f_0)^{1/3}$ is analyzed among the three cases. It is found that the graphite foam fin with two sides dimple provides the highest value of $\overline{Nu} / \overline{Nu_0} /(f/f_0)^{1/3}$ which is ranging from 1.5 to 2.7.

(4) In terms of energy saving, the graphite foam fin with one side or two sides dimple provides higher performance than the conventional aluminum offset fin, wavy fin and louver fin. Furthermore, the graphite foam fin with one side dimple presents higher effectiveness in the energy saving than one with two sides dimple.

ACKNOWLEDGMENT

NOMENCLATURE

Nomenclature

a	specific surface area	(1/m)
C_F	Forchheimer coefficient	(-)
D	dimple print diameter	(m)
D_p	pore average diameter	(m)
F_1	blending function	
G_k	generation of turbulent kinetic energy	(m^2/s^2)
k	turbulent kinetic energy	(m^2/s^2)
P	spacing of every other dimple rows	(m)
S	spacing of adjacent dimple rows	(m)

Greek Symbols

α	permeability	(m^2)
β	constant for turbulent dissipation	
δ	dimple depth	(m)
ε	rate of energy dissipation	

η	coefficient for generation of specific dissipation rate	
λ	thermal conductivity	(W/m.K)
σ	temperature gradient	(K/m)
ω	specific dissipation rate	(1/s)
$\omega_{1.2}$	weighting factor	

Subscripts

air	air
d	pore diameter
D	channel hydraulic diameter
eff	effective
h	hydraulic
H	channel height
t	turbulence
0	referenced channel

REFERENCES

[1] Klett, J., Hardy, R., Romine, E., Walls, C., Burchell, T., "High-thermal-conductivity, mesophase-pitch-derived carbon foams: effect of precursor on structure and properties," *Carbon*, 38, pp.953-973, (2000).

[2] Lin, W. M., Yuan, J. L., Sundén, B., "Review on graphite foam as thermal material for heat exchangers," *Proceedings of World Renewable Energy Congress 2011*, WREC 2011- 0263EEE, pp. 1-8, (2011).

[3] Wang, Q., Han, X. H., Sommers, A., Park, Y., Joen, C. T., Jacobi, A., "A review on application of carbonaceous materials and carbon matrix composites for heat exchangers and heat sinks," *International Journal of Refrigeration*, 35, pp.7-26, (2012).

[4] Klett, J., Ott, R., McMillan, A., "Heat exchangers for heavy vehicles utilizing high thermal conductivity graphite foams," SAE Paper 2000-01-2207, 2000.

[5] Yu, Q., Straatman, A. G., Thompson, B. E., "Carbon-foam finned tubes in air-water heat exchangers," *Applied Thermal Engineering*, 26, pp.131-143, (2006).

[6] Garrity, P. T., Klausner, J. F., Mei, R., "Performance of aluminum and carbon foams for air side heat transfer augmentation," *ASME Journal of Heat Transfer*, 132, pp.121901-(1-10), (2010).

[7] Lin, W. M., Sundén, B., Yuan, J. L., "A performance analysis of porous graphite foam heat exchangers in vehicles," *Applied Thermal Engineering*, 50, pp.1201-1210, (2013).

[8] Straatman, A. G., Gallego, N. C., Yu, Q., Thompson, B. E., "Characterization of porous carbon foam as a material for compact recuperators," *ASME Journal of Engineering for Gas Turbines and Power*, 129, pp.326-330, (2007).

[9] Gallego, N. G., Klett, J. W., "Carbon foams for thermal management," *Carbon*, 41, pp.1461-1466, (2003).

[10] Leong, K. C., Jin, L. W., Li, H. Y., Chai, J. C., "Forced convection air cooling in porous graphite foam for thermal management applications," *Proceedings of 11th Intersociety Conference on Thermal and Thermomechanical Phenomena in Electronic Systems*, pp: 57-64, 2008.

[11] Lin, Y. R.,   Du, J. H., Wu, W., Chow, L. C., Notardonato, W., "Experimental study on heat transfer and pressure drop of recuperative heat exchangers using carbon foam," *ASME Journal of Heat Transfer*, 132, pp.091902-(1-10), (2010).

[12] Xie, G. N., Sundén, B., Zhang, W. H., "Comparisons of pins/dimples/protrusions cooling concepts for a turbine blade tip-wall at high Reynolds numbers," *ASME Journal of Heat Transfer*, 133, 061902-(1-9), (2011).

[13] Lan, J. B., Xie, Y. H., Zhang, D., "Flow and heat transfer in microchannels with dimples and protrusions," *ASME Journal of Heat Transfer*, 134, 021901-(1-9), (2012).

[14] Elyyan, M. A., Rozati, A., Tafti, D. K., "Investigation of dimpled fins for heat transfer enhancement in compact heat exchangers," *International Journal of Heat and Mass Transfer*, 51, pp.2950-2966, (2008).

[15] Doo, J. H., Yoon, H. S., Ha, M. Y., "Study on improvement of compactness of a plate heat exchanger using a newly designed primary surface," *International Journal of Heat and Mass Transfer*, 53, pp.5733-5746, (2010).

[16] Mahmood, G. I., Hill, M. L., Nelson, D. L., Ligrani, P. M., Moon, H. K., Glezer, B., "Local heat transfer and flow structure on and above a dimpled surface in a channel," *ASME Journal of Turbomachinery*, 123, pp.115-123, (2001).

[17] Mahmood, G. I., Sabbagh, M. Z., Ligrani, P. M., "Heat transfer in a channel with dimples and protrusions on opposite walls," *AIAA Journal of Thermophysics and Heat Transfer*, 15(3), pp.275-283, (2001).

[18] Moon, H. K., O'Connell, T., Glezer, B., "Channel height effect on heat transfer and friction in a dimpled passage," *ASME Journal of Engineering for Gas Turbines and Power*, 122, pp.307-313, (2000).

[19] Burgess, N. K., Oliveira, M. M., Ligrani, P. M., "Nusselt number behavior on deep dimpled surfaces within a channel," *ASME Journal of Heat Transfer*, 125, pp.11-17, (2003).

[20] Won, S. Y., Zhang, Q., Ligrani, P. M., "Comparisons of flow structure above dimpled surfaces with different dimple depths in a channel," *Physics of Fluids*, 17, 045105-(1-9), (2005).

[21] Ligrani, P. M., Mahmood, G. I., Harrison, J. H., Clayton, C. M., Nelson, D. L., "Flow structure and local Nusselt number variations in a channel with dimples and protrusions on opposite walls," *International Journal of Heat and Mass Transfer*, 44, pp.4413-4425, (2001).

[22] Mahmood, G. I., Ligrani, P. M., "Heat transfer in a dimpled channel: combined influences of aspect ratio, temperature ratio, Reynolds number, and flow structure," *International Journal of Heat and Mass Transfer*, 45, pp.2011-2020, (2002).

[23] Straatman, A. G., Gallego, N. C., Thompson, B. E., Hangan, H., "Thermal characterization of porous carbon foam – convection in parallel flow," *International Journal of Heat and Mass Transfer*, 49, pp.1991-1998, (2006).

[24] Menter, F. R., "Two-equation eddy-viscosity turbulence models for engineering applications," *AIAA Journal*, 32 (8), pp.1598-1605, (1994).

[25] Vafai, K., *Handbook of Porous Media,* 2nd Edition, Boca Raton: Taylor & Francis Group. LLC, (2005).

[26] Pope, S. B., *Turbulent Flows*, London: Cambridge University, (2000).

[27] Tannehill, J. C., Anderson, D. A., Pletcher, R. H., *Computational Fluid Mechanics and Heat Transfer*, 2nd Edition, Washington: Taylor & Francis Group. LLC, (1997).

[28] Sundén, B., *Introduction to Heat Transfer*, Southampton: WIT Press, (2012).

[29] Versteeg, H. K., Malalasekera, W., *An Introduction to Computational Fluid Dynamics*, second edition, Pearson Prentice Hall, UK, 2007.

[30] Lin, W. M., Xie, G. N., Yuan, J. L., Sundén, B., "Comparison and analysis of heat transfer in a porous aluminum foam using local thermal equilibrium and local thermal non-equilibrium models," *Proc. of 2nd International Workshop on Heat Transfer Advances for Energy Conservation and Pollution Control*, IWHT 2013-067, pp. 1-8, (2013).

[31] Gee, D. L., Webb, R. L., "Forced convection heat transfer in helically rib-roughened tubes," *International Journal of Heat and Mass Transfer*, 23, pp.1127-1136, (1980).

[32] Fan, J. F., Ding, W. K., Zhang, J. F., He, Y. L., Tao, W. Q., "A performance evaluation plot of enhanced heat transfer techniques oriented for energy-saving," *International Journal of Heat and Mass Transfer*, 52, pp. 33-44, (2009).

[33] Kays, W. M., London, A. L., *Compact Heat Exchangers*, 3rd Edition, Florida: Krieger, (1998).

[34] Degroot, C. T., Straatman, A. G., "Numerical results for the effective flow and thermal properties of idealized graphite foam," *ASME Journal of Heat Transfer*, 134, pp. 042603-1-10, (2012).

Paper 7

Comparison and Analysis of Heat Transfer in Aluminum Foam using Local Thermal Equilibrium or Non-equilibrium Model

Wamei Lin[1], Gongnan Xie[2], Jinliang Yuan[1], Bengt Sundén[1*]

[1]Department of Energy Sciences, Lund University, P. O. Box 118, Lund, 22100, Sweden

[2]School of Mechanical Engineering, Northwestern Polytechnical University, P.O. Box 552, Xi'an, Shaanxi 710072, China

ABSTRACT

Aluminum foams are favorable in modern thermal engineering applications because of the high thermal conductivity and the large specific surface area. The present study aims to investigate an application of porous aluminum foam by using the local thermal equilibrium (LTE) and local thermal non-equilibrium (LTNE) heat transfer models. Three-dimensional simulations of laminar flow (porous foam zone), turbulent flow (open zone) and heat transfer are performed by a computational fluid dynamics (CFD) approach. In addition, the Forchheimer extended Darcy's law is employed to evaluate the fluid characteristics. By comparing and analyzing the average and local Nusselt numbers, it is found that the LTNE and LTE models can reach the same Nusselt numbers inside the aluminum foam when the air velocity is high, meaning that the aluminum foam is in a thermal equilibrium state. Besides, a high interfacial heat transfer coefficient is required for the aluminum foam to reach a thermal equilibrium state as the height of the aluminum foam is reduced. This study suggests that the LTE model can be applied to predict the thermal performance at high fluid velocities or for the case with a large height.

Address correspondence to Professor Bengt Sundén, P. O. Box 118, Department of Energy Sciences, Lund University, 22100 Lund, Sweden.
E-mail: bengt.sunden@energy.lth.se
Phone Number: 0046-46-2228605, Fax Number: 0046-46-2224717

INTRODUCTION

Due to the large specific surface area, the porous structure of aluminum foams can enlarge the surface available for heat transfer. Meanwhile, the irregular structure induces a tortuous flow and breaks up the thermal boundary to produce high thermal performance. Thus, the porous aluminum foams are favorable in modern thermal engineering applications [1-2], such as electronic cooling, thermal energy absorbers, and so on.

There are two major simulation models to analyze the heat transfer performance of porous media: (1) the local thermal equilibrium (LTE) model, in which the fluid phase and solid phase are assumed to be at the same temperature. The effective thermal conductivity (λ_{eff}) of the porous media is used to consider the combined effect of the fluid and solid thermal conductivity. Due to the effect of the curly thermal path (thermal tortuosity) and the different structures of the porous materials, there are many different formulas for λ_{eff} based on experimental work or theoretical analyses [3-8]. (2) the local thermal non-equilibrium (LTNE) model, in which there is a temperature difference between the fluid phase and the solid phase. An interfacial heat transfer coefficient (h_{sf}) has to be specified to connect the thermal energy transport between the solid part and the fluid part. There exist various correlations to estimate the h_{sf} in different porous structures [9-11].

A temperature difference between the solid phase and the fluid phase is assumed because of the large difference of the thermal conductivity between the solid phase and fluid phase inside the porous foam [12]. This is the main reason why there are several research works on metal foams using the LTNE model to analyze the heat transfer inside aluminum foams [13-17]. Furthermore, some researchers tried to evaluate the accuracy of the LTNE model by comparing it with the LTE model. Aniri et al. [18] presented the validity of the LTE condition, and presented comprehensive error maps of the LTE based on the numerical results. Lee et al. [19] also investigated the validity of the LTE model, and presented a conceptual assessment of solid and fluid temperature differences. The error by using the LTE model was increased when the difference of the thermal conductivity between the solid phase and fluid phase was increased. In addition, Calmidi et al. [9] used experimental and numerical methods to quantify the thermal non-equilibrium effects in metal foams.

However, due to the high interfacial heat transfer coefficient and the large specific surface area, the metal foam and the fluid could be in a near "thermal equilibrium" state when the fluid velocity is very high. According to [11], it was found that the solid and fluid phases inside the metal foam were in near thermal equilibrium when the air mean velocity was larger than 3 m/s. On the other hand, Kim et al. [20] obtained analytical solutions of the temperature distribution in a microchannel heat sink (whose characteristics of fluid and thermal fields were similar to those in a porous media) by using both the LTE and LTNE model. It was shown that the LTE model could be practically used in microchannel heat sinks with high porosity. Futhermore, Jeng et al. [21] applied the fin theory and the concept of thermal network to estimate the heat transfer of a porous heat sink. Based on the results, local thermal equilibrium could occur at a large height of the porous heat sink and high Reynolds number.

Based on a literature review, it is found that the LTE model is much simpler than the LTNE model in solving one equation and defining few parameters (no interfacial heat transfer coefficient (h_{sf}) and no specific surface area (a_{sf})). Furthermore, the simple LTE model is able to estimate as accurately as the LTNE model in some thermal applications. Accordingly, the present study aims to investigate the thermal performance of a porous aluminum foam by using the LTE and LTNE heat transfer models, and exploring deeply in which engineering

applications the LTE model can be used instead of the LTNE model. In addition, to capture the fluid characteristics, the Forchheimer extended Darcy's law is employed. The average Nusselt numbers calculated by the LTNE and LTE model are compared. It is found that the LTE model can predict the heat transfer performance of the aluminum foam as accurately as the LTNE model at high fluid velocities.

PHYSICAL MODEL

A simplified configuration of the porous aluminum foam is shown in Fig. 1. The aluminum foam with a uniform porosity is placed in a rectangular channel, and the foam is heated at its top and bottom surfaces symmetrically. Thus, only half height of the channel is analyzed in this study. The overall size of the core of the aluminum foam is: 15.24 cm × 5.08 cm × 15.24 cm (W×H×L). The fluid is assumed to be incompressible with constant properties, and the flow is at steady-state. The parameters of the porous aluminum foam are listed in Table 1.

Table 1. The properties of the studied aluminum foam [11]

Foam sample	α (m^2)	C_F	φ	D_p (m)	λ_{se} (W/m K)	a (m^{-1})
40 PPI	6.98×10^{-9}	0.02	0.918	5.08×10^{-4}	9.78	2760

MATHEMATICAL FORMULATION AND NUMERICAL METHOD

Computational domain

In order to ensure that the aluminum foam is located in the fully developed flow region, the computational domain is extended upstream 1.5 times the aluminum foam sample length to eliminate the entrance length effect [22]. Similarly, the computational domain is extended downstream 5 times the length of the aluminum foam sample to achieve the one-way coordinate assumption at the domain outlet. Thus, the whole length of the computational domain is 7.5 times the actual aluminum foam length, as shown in Fig. 1.
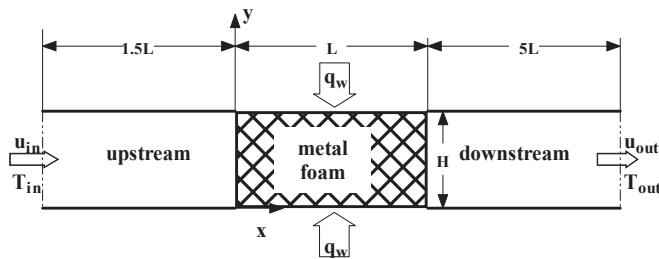
Figure 1 Schematic of a 2D model configuration for the porous foam

Adoption of flow models

In this study, the air inlet velocity of the upstream channel is ranging from 0.7 to 5 m/s with the corresponding Reynolds number on the air side ranging from 3387 to 24190. Due to the critical Reynolds number for transition from laminar flow to turbulent flow is 2300 for channel flow [22], low Reynolds number turbulent flow prevails in the channel. On the other

hand, the Reynolds number inside the aluminum foam is ranging from 19 to 130, which is based on the pore diameter and the mean velocity inside the pore. However, turbulent flow prevails inside the porous media only when the Reynolds number is larger than 150, see [23]. Thus in this study, laminar flow is considered inside the aluminum foam. In order to capture the low Reynolds number characteristics of the turbulent flow in the upstream channel, the "renormalization group" (RNG) k-ε turbulence model is adopted [24-25] on the air side.

Mathematical formulation

According to the above presented assumptions, the governing equations for continuity, momentum and thermal energy may be expressed as follows:

Air zone governing equations (turbulent flow)

Continuity equation

$$\frac{\partial \left(\rho_f u_i \right)}{\partial x_i} = 0 \tag{1}$$

Momentum equations

$$\frac{\partial \left(\rho_f u_i u_j \right)}{\partial x_j} = -\frac{\partial p}{\partial x_i} + \frac{\partial}{\partial x_j}\left(\left(\mu_f + \mu_t \right)\left(\frac{\partial u_i}{\partial x_j} + \frac{\partial u_j}{\partial x_i} \right) \right) \tag{2}$$

Energy equation

$$\frac{\partial \left(\rho_f u_j T \right)}{\partial x_j} = \frac{\partial}{\partial x_j}\left(\left(\frac{\mu_f}{\mathrm{Pr}_f} + \frac{\mu_t}{\mathrm{Pr}_t} \right)\frac{\partial T}{\partial x_j} \right) \tag{3}$$

The equations of the turbulent kinetic energy k and the rate of energy dissipation ε corresponding to the RNG k- ε turbulence model are as follows:

Turbulent kinetic energy k equation:

$$u_j \frac{\partial k}{\partial x_j} = -\overline{u_i' u_j'}\frac{\partial u_i}{\partial x_j} + \frac{\partial}{\partial x_j}\left(\frac{K_m}{\sigma_k}\frac{\partial k}{\partial x_j} \right) - \varepsilon \tag{4}$$

Rate of energy dissipation ε equation:

$$u_j \frac{\partial \varepsilon}{\partial x_j} = -C_{\varepsilon 1}\frac{\varepsilon}{k}\overline{u_i' u_j'}\frac{\partial u_i}{\partial x_j} + \frac{\partial}{\partial x_j}\left(\frac{K_m}{\sigma_\varepsilon}\frac{\partial \varepsilon}{\partial x_j} \right) - C_{\varepsilon 2}\frac{\varepsilon^2}{k} - R \tag{5}$$

where, $R = \dfrac{C_\mu \eta^3 \left(1 - \eta \eta_0 \right)\varepsilon^2}{\left(1 + \beta_0 \eta^3 \right)k}$, $\mu_t = \rho C_\mu \dfrac{k^2}{\varepsilon}$,

$$\eta = \frac{k}{\varepsilon}\left[\left(\frac{\partial u_i}{\partial x_j} + \frac{\partial u_j}{\partial x_i}\right)\frac{\partial u_i}{\partial x_j}\right]^{0.5}, \quad K_m = v\left[1+\left(\frac{C_\mu}{v}\right)^{0.5}\frac{k}{\varepsilon^{0.5}}\right]^2,$$

and v is the kinematic viscosity of air; u_i' represents the fluctuations of the time-averaged velocity u_i.

The values of the constants are as follows:

$C_\mu = 0.0845; \sigma_k = 0.7179; \sigma_\varepsilon = 0.7179; C_{\varepsilon 1} = 1.42; C_{\varepsilon 2} = 1.68; \beta_0 = 0.012; \eta_0 = 4.377.$

Aluminum foam zone governing equations (laminar flow)

Because the aluminum foam is a porous medium, the Forchheimer extended Darcy's law has been applied for the air pressure drop through the aluminum foam [23]. Due to the porous structure, the thermal length inside the aluminum foam has to be modified by the tortuosity of the foam, which is the ratio of the actual flow path length average (L_e) to the length (L) of the porous medium in the direction of the macroscopic flow, $\tau = L_e / L$ [26]. On the other hand, because the effective thermal conductivity of the porous foam is dominated by the thermal conductivity of aluminum, the thermal dispersion is ignored in the energy equation. Thus, the governing equations for the aluminum foam are as follows:

Continuity equation:

$$\frac{\partial\left(\rho_f u_i\right)}{\partial x_i . \varphi} = 0 \tag{6}$$

Momentum equations:

$$\frac{\partial\left(\rho_f u_i u_j\right)}{\partial x_j} = -\varphi\frac{\partial p}{\partial x_i} + \frac{\partial}{\partial x_j}\left(\mu_f\left(\frac{\partial u_i}{\partial x_j} + \frac{\partial u_j}{\partial x_i}\right)\right) - \varphi\left(\frac{\mu_f}{\alpha}u_i + \frac{\rho_f C_F}{\sqrt{\alpha}}|u|u_i\right) \tag{7}$$

Energy equation:

a. LTE case

$$\varphi\frac{\partial\left(\rho_f c_{p.f} u_j T\right)}{\partial x_j} = \lambda_{eff}\frac{\partial}{\partial x_j}\left(\frac{\partial T}{\partial x_j}\right) \tag{8}$$

b. LTNE case
   i. for fluid:

$$\varphi\frac{\partial\left(\rho_f c_{p.f} u_j T_f\right)}{\partial x_j} = \lambda_{fe}\frac{\partial}{\partial x_j}\left(\frac{\partial T_f}{\partial x_j}\right) + h_{sf}a_{sf}(T_s - T_f) \tag{9}$$

   ii. for solid:

$$0 = \lambda_{se}\frac{\partial}{\partial x_j}\left(\frac{\partial T_s}{\partial x_j}\right) - h_{sf}a_{sf}(T_s - T_f) \tag{10}$$

where, $\lambda_{fe} = \lambda_f\varphi, \lambda_{se} = \lambda_s(1-\varphi)/\tau, \lambda_{eff} = \lambda_{fe} + \lambda_{se}$, see [15] . The internal heat transfer coefficient h_{sf} is calculated by $h_{sf}\sqrt{\alpha}\lambda_f = \frac{d_p}{\sqrt{\alpha}}(\frac{u_m\sqrt{\alpha}}{v_f}\frac{1}{4887} - 0.01)$, see [11]. The values of τ and a_{sf} are adopted from the experimental work in [11]. φ is the porosity of the porous aluminum foam; α the permeability of the porous aluminum foam (m^2); C_F the Forchheimer coefficient.

Boundary conditions

The momentum and energy transports are calculated simultaneously for the air and porous aluminum foam zones. The boundaries on the aluminum foam left- and right walls are set up as "interior surfaces" or interfaces. Thus, the solutions for the momentum and energy transports on the interfaces between upstream/downstream air and porous aluminum foam zones are not required. The necessary boundary conditions are as follows:

(1) For the upstream extended region ($-1.5L \leqslant x < 0$)

At the inlet (x=-1.5L): $u = const$, $T = const$, $v = w = 0$

At the upper and lower boundaries (y=0, y=H): $\dfrac{\partial u}{\partial y} = \dfrac{\partial w}{\partial y} = 0$, $v = 0$, $\dfrac{\partial T}{\partial y} = 0$

At the sides of z=0 and z=W: $\dfrac{\partial u}{\partial z} = \dfrac{\partial v}{\partial z} = 0$, $w = 0$, $\dfrac{\partial T}{\partial z} = 0$

(2) For the downstream extended region ($L < x \leqslant 6L$)

At the upper and lower boundaries (y=0, y=H): $\dfrac{\partial u}{\partial y} = \dfrac{\partial w}{\partial y} = 0$, $v = 0$, $\dfrac{\partial T}{\partial y} = 0$

At the sides of z=0 and z=W: $\dfrac{\partial u}{\partial z} = \dfrac{\partial v}{\partial z} = 0$, $w = 0$, $\dfrac{\partial T}{\partial z} = 0$

At the outlet boundary (x=6L): $\dfrac{\partial u}{\partial x} = \dfrac{\partial v}{\partial x} = \dfrac{\partial w}{\partial x} = \dfrac{\partial T}{\partial x} = 0$

(3) For the aluminum foam region ($0 \leqslant x \leqslant L$)

At the sides of z=0 and z=W: $\dfrac{\partial u}{\partial z} = \dfrac{\partial v}{\partial z} = 0$, $w = 0$, $\dfrac{\partial T}{\partial z} = 0$

At the upper boundary (y=H): $\dfrac{\partial u}{\partial y} = \dfrac{\partial w}{\partial y} = 0$, $v = 0$, $\dfrac{\partial T}{\partial y} = 0$

At the lower boundary (y=0): $u = v = w = 0$, $q_w = const$

Evaluation of performance parameters

In order to compare the thermal performance difference of the LTE and LTNE models, an average Nusselt number (Nu) for the solid wall (y = 0) is defined to characterize the thermal performance of the aluminum foam.

$$Nu = \frac{hD_h}{\lambda_f} = \frac{D_h Q_{removed}}{\lambda_f A_b \Delta T} = \frac{D_h q_w}{\lambda_f \Delta T} = \frac{D_h q_w}{\lambda_f (\overline{T_w} - (\overline{T_{in}} + \overline{T_{out}})/2)} \tag{11}$$

where D is the length scale based on either the equivalent particle diameter of the foam or the hydraulic diameter of the channel. A is the effective heat transfer surface area or the heated base area of the foam. In this study, D is defined as the hydraulic diameter of the channel D_h, A the heated base area A_b, and ΔT is the mean temperature difference between the heated base temperature and the fluid mean temperature.

Another important parameter is the local Nusselt number (Nu_x), which is defined as:

$$Nu_x = \frac{D_h q_w}{\lambda_f (T_{w.x} - \overline{T_x})} \tag{12}$$

Numerical method and grid independence test

The commercial code ANSYS FLUENT 14.0 is used for the numerical solution. A control-volume-based technique is adopted to convert the governing equations to algebraic equations so that these can be solved numerically [25]. The Semi-Implicit Method for Pressure Linked Equations (SIMPLE) algorithm is used to couple the pressure and velocity. A second-order upwind scheme is used for the space discretization of the momentum, energy and turbulence equations in the simulations. A second-order scheme is applied to the space discretization of pressure as well. The residual of the continuity equation, components of velocity, k and ε is set to be below 10^{-3}, while for the energy equation it is below 10^{-6}.

A hexagonal mesh is generated by using the blocking technique in the ICEM software, as shown in Fig. 2. In order to control the grid independence, three sets of mesh size (Mesh I: 80×20×60; Mesh II: 120×30×80; Mesh III: 200×50×120 (W×H×L)) were selected for the aluminum foam region to find out the grid dependence. It was found that the deviation of the pressure drop is between 0.07 - 0.35%, and the deviation of the Nusselt number is between 0.12 - 0.65 %, as shown in Table 2. On the other hand, the value of y^+ near the wall ranges from 5 to 7 which falls within the transitional region. Based on these results, a mesh size of 120×30×80 was adopted in the final simulations.

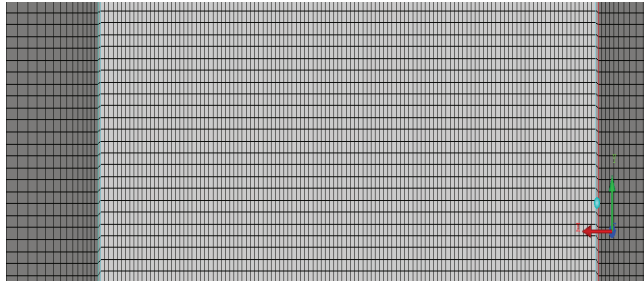**Figure 2** Typical hexagonal meshes for the computations

Table 2. Grid independence test (u=1.2 m/s)

	Mesh I 80×20×60	Mesh II 120×30×80	Mesh III 120×30×80
Δp (Pa)	1427	1433	1432
Nu	3413	3387	3391
$|\Delta p|$ deviation	0.35 %	0.07%	base line
|Nu| deviation	0.65 %	0.12%	base line

RESULTS AND DISCUSSION

Validation of simulation model

Before presenting the simulation results, it is necessary to validate the current simulation model of the aluminum foam. The validation of the LTE model has been presented in [27]. Only the LTNE model will be validated here. The pressure drop (Δp) and the top surface (x = 0.5 H) temperature are calculated and compared with the experimental data [11]. Figure 3 shows the pressure drop of the simulation results and the experimental data. The maximum pressure drop deviation between the simulation and the experimental data is less than 0.9 %. Thus, this simulation model is satisfactory by taking into account the fluid characteristics.
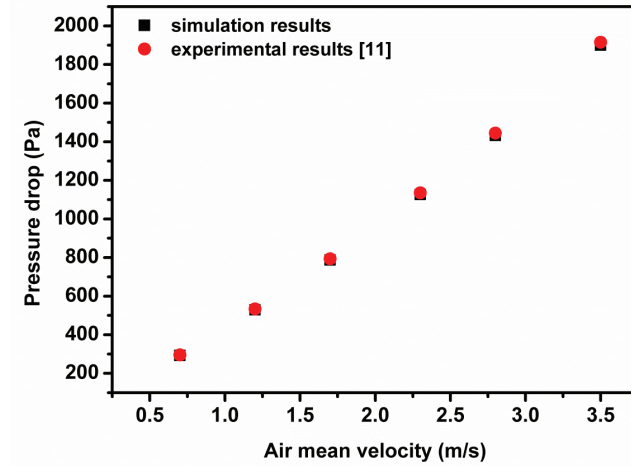
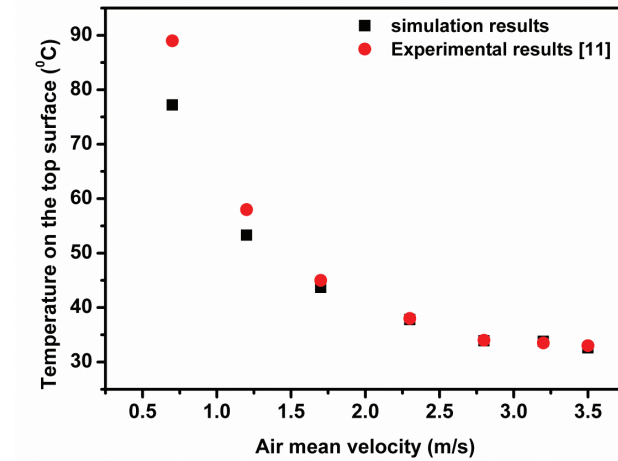**Figure 3** Pressure drop through the porous aluminum foam (L=0.1524m)

Figure 4 The temperature of the top surface (0.5 H) of aluminum foam

A comparison of the top surface temperature on the porous aluminum foam is shown in Fig. 4. There is a relatively large deviation between the simulation results and the experimental ones

at a low velocity, i.e., 0.7 m/s. However, the deviation is gradually reduced as the air velocity is increased. Typically quite good agreement between the simulation results and the experimental data is obtained when the air velocity is larger than 1 m/s. Thus, it is believed that the present model is satisfactory and can be applied further to estimate the pressure drop and the thermal performance of the porous aluminum foam.

Temperature distribution of aluminum foam

Because the Forchheimer extended Darcy's law has been applied together with the LTE heat transfer model or the LTNE model, the present study will only focus on the difference in heat transfer performance between the LTE and the LTNE models.

Figure 5 shows the air temperature distribution inside the aluminum foam. The maximum temperature in Figs. 5 (a) and (b) is higher than the one in Fig. 5 (c). This is because the air velocity is increased in Fig. 5 (c), and a higher air velocity means that more heat can be dissipated or a lower temperature is revealed. On the other hand, when the air velocity is 2.3 m/s, the air temperature near the foam inlet surface (x = 0) is somewhat lower for the LTE model than for the LTNE model. This means that the heat is predicted to be dissipated more efficiently by the LTE model than the LTNE model near the foam inlet surface. In other words, the thermal performance near the foam inlet surface is predicted to be higher by the LTE model than by the LTNE model. However, the temperature distribution becomes similar as the length of the foam is increased.
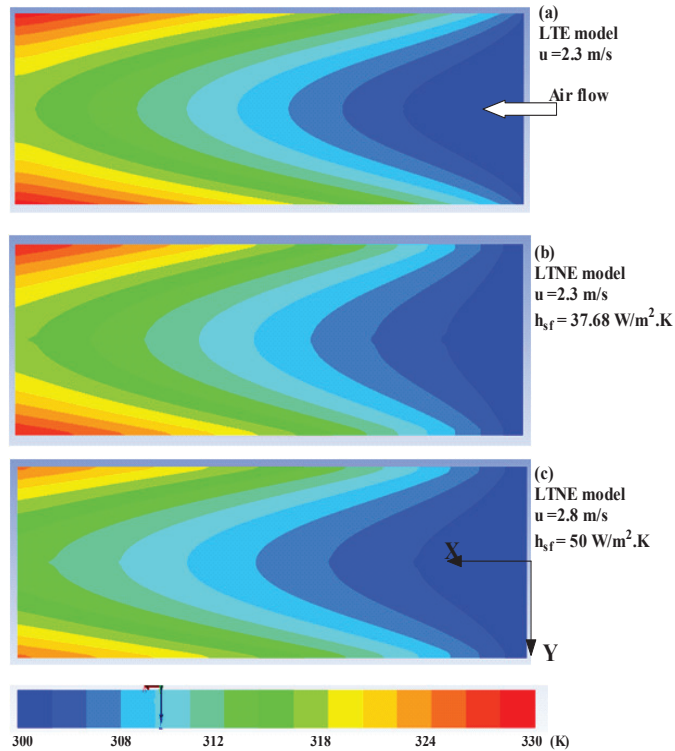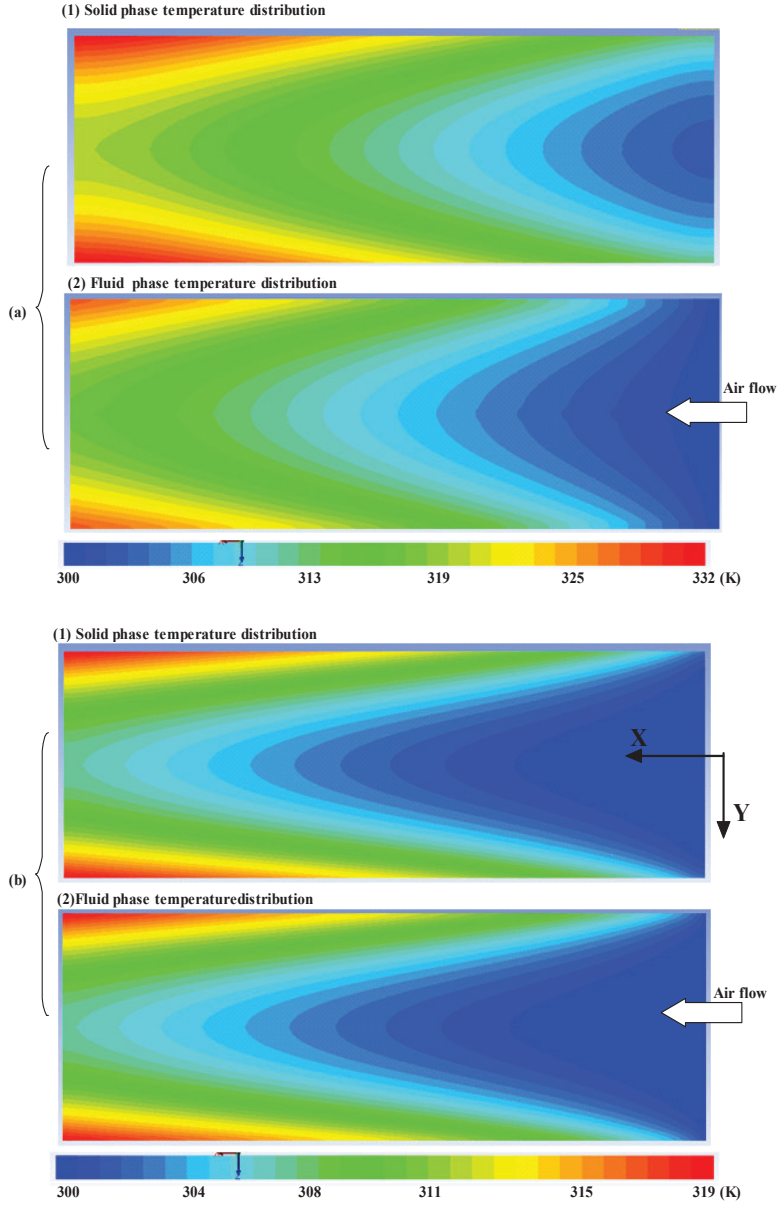

Figure 5 Air temperature distributions in the aluminum foam

(1) Solid phase temperature distribution

(2) Fluid phase temperature distribution

(a)

Air flow

| 300 | 306 | 313 | 319 | 325 | 332 (K) |

(1) Solid phase temperature distribution

X

Y

(b)

(2)Fluid phase temperaturedistribution

Air flow

| 300 | 304 | 308 | 311 | 315 | 319 (K) |

*(a) u = 2.3 m/s, h_{sf} = 37.68 W/m^2.K; (b) u = 4.5 m/s, h_{sf} = 68 W/m^2.K

Figure 6 Solid and fluid temperature distribution inside the aluminum foam by LTNE model: (a) u = 2.3 m/s; (b) u = 4.5 m/s

The solid phase and the fluid phase temperature distributions inside the aluminum foam are shown in Fig. 6. By applying the LTNE model, the temperature difference between the solid phase and the fluid phase can easily be seen as the air velocity is 2.3 m/s, as shown in Fig. 6 (a). This means that the aluminum foam is in a local thermal non-equilibrium state when the air velocity is 2.3 m/s. Moreover, as the thermal resistance in the solid phase is smaller than

the one in the fluid phase, the temperature of the solid phase is higher than that in the fluid phase. However, as the air velocity is increased to 4.5 m/s, the temperature distribution in the solid phase becomes similar to the one in the fluid phase, as shown in Fig. 6 (b). This is mostly because the high air velocity leads to a high interfacial heat transfer coefficient, which can reduce the thermal resistance in the fluid phase. Thus, the temperature difference between the solid phase and the fluid phase is very small. In this case, the aluminum foam is in a near local thermal equilibrium state. It is suggested that the LTE model can be applied for the high velocity case.

Nusselt number by LTNE and LTE models

In order to compare the heat transfer performance by using the LTNE model and LTE models, the average Nusselt number (Nu) is analyzed. Figure 7 shows that the average Nu predicted by both models is increased as the air velocity is increased. When the air velocity is low, the average Nu by the LTE model is higher than that by the LTNE model at a fixed velocity. This means that the LTE model over-predicts the heat transfer performance compared to the LTNE model at low velocity. However, the difference in average Nu is gradually reduced as the air velocity is increased. When the velocity is larger than 4 m/s, the average Nu by the LTE model is similar to that by the LTNE model. This indicates that the aluminum foam is predicted to have a similar heat transfer performance for the LTNE and LTE models at high velocity. In other words, the aluminum foam is in a near thermal equilibrium state at high velocities. This is mostly because the high velocity produces high convective effects, and thereby the thermal resistance in the fluid phase is of the same order as that of the solid phase. In this sense, the fluid phase and the solid phase might have a similar temperature distribution when the fluid velocity is sufficiently high.
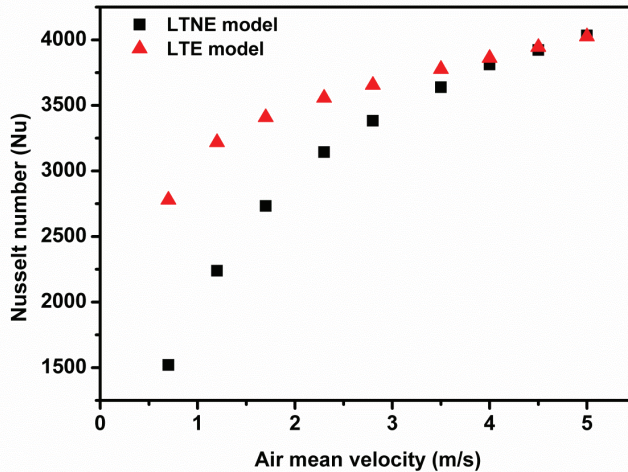
*In LTNE model, the value of h_{sf} is changed by the air velocity.
Figure 7 Average Nusselt number between LTNE and LTE model

Figure 8 shows the local Nusselt number (Nu_x) profiles along the bottom length of the aluminum foam. The local Nu_x calculated by the LTE model is higher than that obtained by the LTNE model at an air velocity of 1.2 m/s, as observed in Fig. 8 (a). This means that the aluminum foam is in a thermal non-equilibrium state along the length as the air velocity is low. However, when the air velocity is increased to 4 m/s, the local Nu_x calculated by the LTE model approaches that by the LTNE model along the length of the aluminum foam, as

shown in Fig. 8 (b). Accordingly, as the air velocity is high, the aluminum foam is in a "thermal equilibrium" state not only from an overall performance point of view (Fig. 7), but also along its whole length (Fig. 8 (b)).
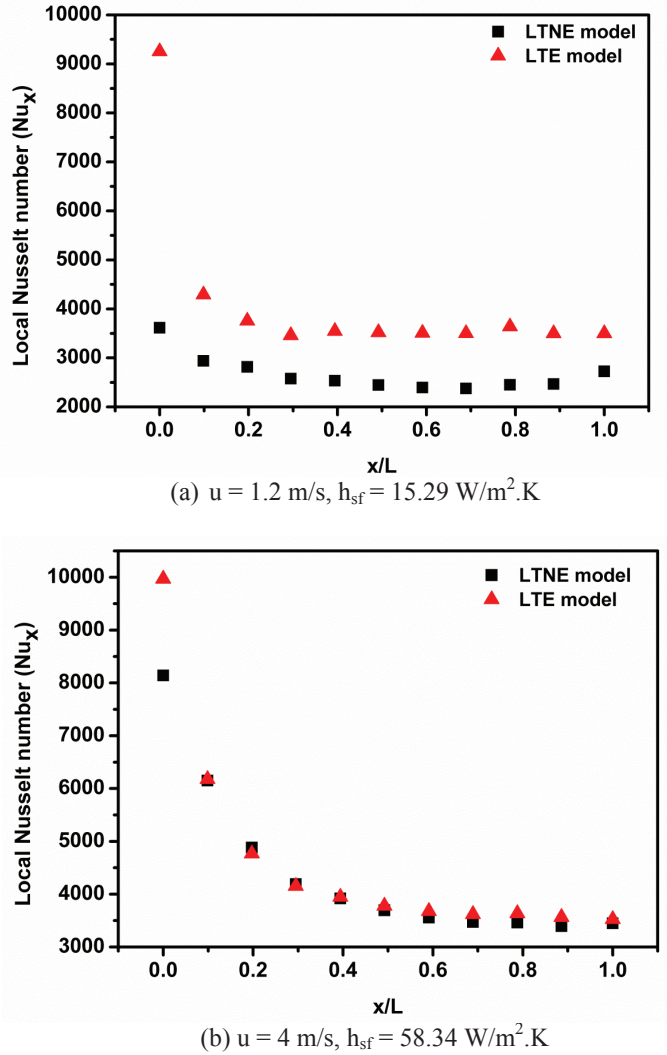

(a) u = 1.2 m/s, h_{sf} = 15.29 W/m^2.K

(b) u = 4 m/s, h_{sf} = 58.34 W/m^2.K

Figure 8 Local Nusselt number along the length under different air velocity

Effect of parameters on the LTE state of porous media

The parameters affecting the porous media, regardless of the LTNE state or the LTE state, are λ_{se}, λ_{fe}, H, and φ. When the difference between λ_{se} and λ_{fe} is large, a high interfacial heat transfer coefficient h_{sf} is required for the porous media to reach a thermal equilibrium state. On the other hand, if the height (H) of the porous media is reduced, a high value of h_{sf} is required for the porous media to reach a thermal equilibrium state as well. A high value of h_{sf} requires a high air velocity. As shown in Fig. 9, when the height of the aluminum foam is reduced to 0.5H, the Nu of the LTNE model is close to the one of the LTE model only at an

air velocity of around 7 m/s, which is higher than the one in the aluminum foam at the height of 1H (as shown in Fig. 7 around 4 m/s). The reason for this is that the heat transferring length from the heated base surface becomes shorter as the height of the aluminum foam is reduced. In this case, the thermal resistance of the solid phase is smaller than for other cases. Thus, the thermal resistance in the fluid phase has to be smaller to achieve a thermal equilibrium state. Accordingly, the air velocity has to be increased to reduce the thermal resistance in the fluid phase.
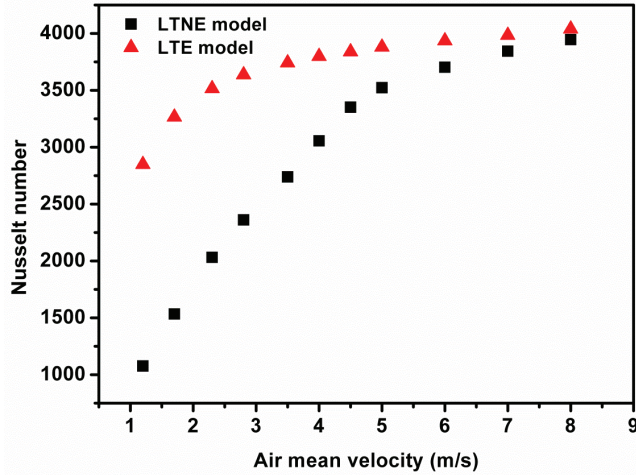
*In LTNE model, the value of h_{sf} is changed by the air velocity.
Figure 9 Comparison of Nusselt number between LTNE and LTE models (0.5H)

CONCLUSIONS

The present study investigated the thermal performance of a porous aluminum foam by using the LTE and LTNE models. Three-dimensional flow and heat transfer were studied by a computational fluid dynamics approach. This research aims to evaluate the probable applications of the LTE model and the LTNE model for specific engineering problems. Through detailed comparisons and analysis, the major conclusions are as follows:

(1) By comparing the average Nusselt numbers, it is found that the LTE model results in the same average Nusselt numbers inside the aluminum foam as the LTNE model when the air velocity is high. It is suggested that the LTE model is used to predict the heat transfer performance of aluminum foam at high flow velocities, in which the aluminum foam is considered to be in thermal equilibrium state.

(2) As the aluminum foam is in the thermal equilibrium state, the value of the interfacial heat transfer coefficient does not have any effect at all on the thermal performance.

(3) When the difference between λ_{se} and λ_{fe} is large or the height of the porous media is reduced, a high flow velocity is required to increase the thermal convection in the porous media to reach thermal equilibrium state.

(4) Even though the LTNE model is a more accurate for simulation in predicting the thermal performance of aluminum foams, the LTE model can be used at high flow velocity cases or if the aluminum foam has a large height.

ACKNOWLEDGMENTS

NOMENCLATURE

a	specific surface area, m^{-1}
A	area, m^2
c_p	specific heat, $J.kg^{-1}.K^{-1}$
C_F	Forchheimer coefficient
D	diameter, m
h	heat transfer coefficient, $W.m^{-2}.K^{-1}$
H	height, m
k	turbulent kinetic energy, $m^2.s^{-2}$
L	length, m
Nu	Nusselt number
p	pressure, Pa
Pr	Prandtl number
PPI	pores per inch
q	heat flux, $W.m^{-2}$
Q	disspated heat, W
T	temperature, K
u, v, w	velocity components in x, y and z directions, $m.s^{-1}$
u_i'	fluctuation in the mean velocity u_i, $m.s^{-1}$
W	width, m
Δp	pressure drop, Pa
$\triangle T$	temperature difference, K
$\overline{T}$	average temperature, K

Greek Symbols

α	permeability, m^2
ε	rate of energy dissipation
λ	thermal conductivity, $W.m^{-1}.K^{-1}$
μ	dynamic viscosity, Pa.s
ρ	density, $kg.m^{-3}$
τ	tortuosity
φ	porosity

Subscripts

b	base
eff, e	effective
f	fluid
h	hydraulic
in	inlet
i, j	coordinate indices
out	outlet
p	pore
s	solid
t	turbulence

w   wall

REFERENCES

[1] Muley A., Kiser C., Sundén B., Shah R. K., Foam heat exchangers: a technology assessment, *Heat Transfer Engineering*, vol. 33 (1), pp. 42-51, 2012.

[2] Han X., Wang Q., Park Y., T'Joen C., Sommers A., Jacobi A., A review of metal foam and metal matrix composites for heat exchangers and heat sinks, *Heat Transfer Engineering*, vol. 33 (12), pp. 991-1009, 2012.

[3] Calmidi V. V., Mahajan R. L., The effective thermal conductivity of high porosity fibrous metal foams, *ASME Journal of Heat Transfer*, vol.121, pp. 466-471, 1999.

[4] Boomsma K., Poulikakos D., On the effective thermal conductivity of a three-dimensionally structured fluid-saturated metal foam, *International Journal of Heat and Mass Transfer*, vol. 44, pp. 827-836, 2001.

[5] Bhattacharya A., Calmidi V. V., Mahajan R. L., Thermophysical properties of high porosity metal foams, *International Journal of Heat and Mass Transfer*, vol. 45, pp. 1017-1031, 2002.

[6] Singh R., Kasana H. S., Computational aspects of effective thermal conductivity of highly porous metal foams, *Applied Thermal Engineering*, vol. 24, pp. 1841-1849, 2004.

[7] Yang C., Nakayama A., A synthesis of tortuosity and dispersion in effective thermal conductivity of porous media, *International Journal of Heat and Mass Transfer*, vol. 53, pp. 3222-3230, 2010.

[8] Kuwahara F., Yang C., Ando K., Nakayama A., Exact solutions for a thermal nonequilibrium model of fluid saturated porous media based on an effective porosity, *ASME Journal of Heat Transfer*, vol. 133, pp. 112602-(1-9), 2011.

[9] Calmidi V. V., Mahajan R. L., Forced convection in high porosity metal foams, *ASME Journal of Heat Transfer*, vol. 122, pp. 557-565, 2000.

[10] Hwang J. J., Hwang G. J., Yeh R. H., Chao C. H., Measurement of interstitial convective heat transfer and frictional drag for flow across metal foams, *ASME Journal of Heat Transfer*, vol. 124, pp. 120-129, 2002.

[11] Garrity P. T., Klausner J. F., Mei R., Performance of aluminum and carbon foams for air side heat transfer augmentation, *ASME Journal of Heat Transfer*, vol. 132, pp. 121901-(1-9), 2010.

[12] Hassell B., Ortega A., Analysis of multilayer mini- and microchannel heat sinks in single-phase flow using one- and two equation porous media models, *Heat Transfer Engineering*, vol. 32 (7-8), pp. 566-574, 2011.

[13] Lu W., Zhao C. Y., Tassou S. A., Thermal analysis on metal-foam filled heat exchangers. Part I: Metal-foam filled pipes, *International Journal of Heat and Mass Transfer*, vol. 49, pp. 2751-2761, 2006.

[14] Zhao C. Y., Lu W., Tassou S. A., Thermal analysis on metal-foam filled heat exchangers. Part II: Tube heat exchangers, *International Journal of Heat and Mass Transfer*, vol. 49, pp. 2762-2770, 2006.

[15] Xu H. J., Qu Z. G., Tao W. Q., Analytical solution of forced convective heat transfer in tubes partially filled with metallic foam using the two-equation model, *International Journal of Heat and Mass Transfer*, vol. 54, pp. 3846-3855, 2011.

[16] Qu Z. G., Xu H. J., Tao W. Q., Fully developed forced convective heat transfer in an annulus partially filled with metallic foams: An analytical solution, *International Journal of Heat and Mass Transfer*, vol. 55, pp. 7508-7519, 2012.

[17] Dai Z., Nawaz K., Park Y., Chen Q., Jacobi A. M., A comparison of metal-foam heat

exchangers to compact multilouver designs for air-side heat transfer applications, *Heat Transfer Engineering*, vol. 33(1), pp. 21-30, 2012.

[18] Amiri A., Vafai K., Analysis of dispersion effects and non-thermal equilibrium, non-Darcian, variable porosity incompressible flow through porous media, *International Journal of Heat and Mass Transfer*, vol. 37 (6), pp. 939-954, 1994.

[19] Lee D. Y., Vafai K., Analytical characterization and conceptual assessment of solid and fluid temperature differentials in porous media, *International Journal of Heat and Mass Transfer*, vol. 42, pp. 423-435, 1999.

[20] Kim S. J., Kim D., Lee D. Y., On the local thermal equilibrium in microchannel heat sinks, *International Journal of Heat and Mass Transfer*, vol. 43, pp. 1735-1748, 2000.

[21] Jeng T. M., Tzeng S. C., Hung Y. H., An analytical study of local thermal equilibrium in porous heat sinks using fin theory, *International Journal of Heat and Mass Transfer*, vol. 49, pp. 1907-1914, 2006.

[22] Sundén B., Introduction to Heat Transfer, WIT Press, 2012.

[23] Nield D. A., Bejan A., Convection in Porous Media, 3rd edition, Springer, 2005.

[24] Pope S. B., Turbulent Flows, Cambridge University, 2000.

[25] Versteeg H. K., Malalasekera W., An Introduction to Computational Fluid Dynamics, second edition, Pearson Prentice Hall, UK, 2007.

[26] Vallabh R., Banks-Lee P., Seyam A., New approach for determining tortuosity in fibrous porous media, *Journal of Engineered Fibers and Fabrics*, vol. 3 (5), pp. 7-15, 2010.

[27] Lin W. M., Sundén B., Yuan J., A performance analysis of porous graphite foam heat exchangers in vehicles, *Applied Thermal Engineering*, vol. 50, pp. 1201-1210, 2013.

Wamei Lin is a Ph.D. student at the Department of Energy Sciences Lund University in Sweden from 2009. She received the licentiate of engineering degree in 2011 and is expected to present her Ph.D. thesis in June 2014. Before the Ph.D. studies in Lund, she was working as a thermal engineer on electronic cooling for one year in Shanghai, China. Her research concerns new heat exchangers (porous graphite foam or metal foam heat exchangers) in future transportation systems; electronic cooling: heat pipes, heat sinks, or cooling plates design; refrigeration/cryogenics and air-condition; numerical heat transfer and computational fluid dynamics; optimization and design of energy network system; computational intelligence (evolutionary algorithm).

Gongnan Xie is an Associate Professor of Mechanical Engineering at Northwestern Polytechnical University, Xi'an, China, also an Affiliated Research Professor of Energy Sciences Department at Lund University, Lund, Sweden. He received his Ph.D. degree in Engineering Thermophysics from Xi'an Jiaotong University in 2007, Xi'an, China. He was a postdoctoral fellow at Lund University 2008 and 2009. His main interests are computational heat transfer, gas turbine heat transfer, thermal protection, microchannel heat sinks, heat exchangers and optimization design. He has published more than 60 international journal papers and more than 20 ASME conference papers. He is a member of ASME. He serves as an editorial board member for some international journals. He is currently a Guest Editor of two special issues of ASME Journal of Heat Transfer and ASME Journal of Electronic Packaging.

	Jinliang Yuan is a professor at the Department of Energy Sciences, Lund University in Sweden. His research concerns analysis of heat and mass transfer and other transport phenomena in fuel cells and associated heat exchangers as well as fuel reformers. He has worked as a project leader or/and senior researcher in projects and also as a supervisor of Ph.D. students, and is involved as a teacher in graduate courses. He is a member of the editorial board for some journals. His current research interests are focused on comprehensive analysis of catalytic chemical reactions and effects of nano-/micro-structured porous material on transport processes in the components of advanced energy systems.
	Bengt Sundén received his M.Sc. in Mechanical Engineering 1973, Ph.D. in Applied Thermodynamics and Fluid Mechanics 1979, and became Docent in Applied Thermodynamics and Fluid Mechanics 1980, all from Chalmers University of Technology, Gothenburg, Sweden. He was appointed Professor of Heat Transfer at Lund University, Lund, Sweden in 1992 and has served as Department Head of Energy Sciences, Lund University, Lund, Sweden since 1995. The research activities include compact heat exchangers, enhancement of heat transfer, gas turbine heat transfer, combustion-related heat transfer, CFD-methods for laminar and turbulent fluid flow and heat transfer, liquid crystal thermography, microscale heat transfer, transport phenomena in fuel cells, computational modeling and analysis of multiphysics and multiscale phenomena for fuel cells. Dr. Sunden established and was first editor-in-chief of IJHEX – International Journal of Heat Exchangers (R.T. Edwards Inc., USA) 1999-2008, an associate editor of ASME J. Heat Transfer 2005-2008, editor-in-chief of a Book Series – Developments in Heat Transfer (WIT Press, UK) since 1995. He has published more than 600 papers in journals, books and proceedings. He has edited 25 books and authored three text books. He has supervised 170 M.Sc. theses, 43 Licentiate of Engineering theses, 39 PhD-theses. He is a Fellow of ASME, Honorary Professor of Xian Jiaotong University, China, Guest Professor at Northwestern Polytechnical University, Xi'an, China, a regional editor Journal of Enhanced Heat Transfer since 2007, an associate editor of Heat Transfer Research since 2011, an associate editor ASME J. Thermal Science, Engineering and Applications 2010-2013, 2013-2016. He was a recipient of the ASME Heat Transfer Memorial Award 2011. He received the ASME HTD 75th Anniversary Medal 2013.